

Dissertation zur Erlangung des Doktorgrades
der Fakultät für Chemie und Pharmazie
der Ludwig-Maximilians-Universität München

**Paving Nitridophosphate-Based Phosphors' Way
to Industrial Application**

Sebastian Wendl

aus

Kötzting, j. Bad Kötzting

Deutschland

2022

Erklärung

Diese Dissertation wurde im Sinne von § 7 der Promotionsordnung vom 28. November 2011 von Herrn Prof. Dr. Wolfgang Schnick betreut.

Eidesstattliche Versicherung

Diese Dissertation wurde eigenständig und ohne unerlaubte Hilfe erarbeitet.

München, den 09.04.2022

.....

Sebastian Wendl

Dissertation eingereicht am:	07.02.2022
1. Gutachter:	Prof. Dr. Wolfgang Schnick
2. Gutachter:	Prof. Dr. Hubert Huppertz
Mündliche Prüfung am:	21.03.2022

Für meine Familie

Phantasie ist wichtiger als Wissen, denn Wissen ist begrenzt.

Albert Einstein (1879-1955)

Danksagung

Mein ganz besonderer Dank gilt Herrn Prof. Dr. Wolfgang Schnick für die Aufnahme in seine Arbeitsgruppe und die Betreuung meiner Dissertation. Die zur Verfügung stehenden Mittel und die damit einhergehenden hervorragenden Arbeitsbedingungen haben den Grundstein für den Erfolg meiner Promotion gelegt. Darüber hinaus bedanke ich mich für die zahlreichen fachlichen Diskussionen und Anregungen sowie die große Freiheit bei der Gestaltung des überaus spannenden Themas.

Bei Herrn Prof. Dr. Hubert Huppertz bedanke ich mich ganz herzlich für die Übernahme des Koreferats dieser Arbeit.

Ich danke außerdem Herrn PD Dr. Constantin Hoch, Herrn Prof. Dr. Stefan Schwarzer, Herrn Prof. Dr. Konstantin Karaghiosoff und Frau Prof. Dr. Lena Daumann für die bereitwillige Teilnahme als Prüfer an meinem Rigorosum.

Großer Dank geht des Weiteren an Prof. Dr. Oliver Oeckler, Dr. Peter Schmidt, Dr. Philipp Strobel, Dr. Jonathan P. Wright, Lucien Eisenburger, Daniel Günther und Dr. Mathias Mallmann, die im Rahmen interner und externer Kooperationen wesentlich zum Erfolg der Projekte beigetragen haben.

Besonders möchte ich mich bei meinem thematischen Vorgänger Dr. Alexey Marchuk bedanken. Durch seine Forderung und Förderung wurde ich während meiner Bachelor- und Masterarbeit bestens in die Thematik der Nitridophosphate eingearbeitet. Seine Erfahrungen und besonderen Kniffe haben mir den Einstieg in das wissenschaftliche Arbeiten ungemein erleichtert.

Bei Dr. Thomas Bräuniger, Dr. Otto Zeman und Christian Minke bedanke ich mich für die Durchführung von NMR Experimenten und interessante Gespräche, bei denen ich viel lernen konnte. Priv.-Doz. Constantin Hoch, Dr. Peter Mayer sowie Dr. Arthur Haffner danke ich für die Messung einer Vielzahl von Kristallen. Außerdem danke ich Dr. Fabian Kessler und Marion Sokoll für die Aufnahme von FTIR-Spektren.

Bedanken möchte ich mich außerdem bei Lisa Gamperl und Christian Minke für die schier unendlichen Stunden am Rasterelektronenmikroskop, bei Thomas Miller und Dieter Rau für die

Betreuung der Röntgendiffraktometer und ihr Bemühen um die Arbeitssicherheit, bei Wolfgang Wünschheim für die Unterstützung bei technischen Problemen jeder Art und bei Olga Lorenz für ihre unschätzbare wertvolle Arbeit zu allen organisatorischen Fragen.

Für die großartige Unterstützung und Expertise bei Arbeiten mit Autoklaven und der HIP danke ich Dr. Mathias Mallmann, Eugenia Elzer, Lisa Gamperl, Tobias Giftthaler und Reinhard Pritzl.

Meinen Praktikanten Sara Mardazad, Reinhard Pritzl, Patrick Schüler, Lisa Seidl und Mirjam Zipkat danke ich für ihre zuverlässige und engagierte Unterstützung bei meinen Forschungsprojekten.

Meinen ehemaligen und aktuellen Kollegen aus D2.110 und dessen erweitertem Kreis danke ich ganz herzlich für das angenehme Arbeitsumfeld. Statt Konkurrenz stand hier immer die Zusammenarbeit an erster Stelle. Diesbezüglich möchte ich meinen Dank ganz besonders an Dr. Eva-Maria Bertschler, Dr. Philipp Bielec, Dr. Simon Kloß, Dr. Christian Maak, Dr. Mathias Mallmann, Dr. Sebastian Vogel, Dr. Matthias Wörsching, Sebastian Ambach, Tobias Giftthaler, Reinhard Pritzl, Dr. Tobias Rackl und Stefanie Schneider aussprechen. Danke für die vielen fachlichen Diskussionen, interessanten Ideen und nicht zuletzt die geselligen und immer witzigen Laborabende.

Ich danke natürlich auch allen bisher nicht namentlich genannten Mitgliedern der Arbeitskreise Schnick, Hoch, Johrendt und Lotsch für die stets großartige Stimmung im zweiten Stock.

Neben meiner fachlichen Ausbildung während der Zeit als Student und Doktorand durfte ich mich auch persönlich weiterentwickeln. Ganz herzlich möchte ich mich hierfür bei meinen engsten Freunden in München, im bayerischen Wald und im Allgäu bedanken. Besonders hervorheben möchte ich hier die „Pura-Vidaner“ um Dr. Niels Weidmann, Annemarie Breu, Anton Breu, Julia Fleißner, Markus Mühlbauer und Julia Weidmann. Vielen lieben Dank für die tolle Zeit und die gemeinsamen Erinnerungen. Sehr wichtig für meine persönliche Entwicklung, den regen Kontakt in die Heimat und den gesunden Ausgleich zum Alltag waren und sind auch die „Grün-Weißen Jungen“ vom SV Thenried. Euch danke ich ganz besonders für die vielen schönen Momente, Ausflüge und Feiern sowie den unvergleichlichen Zusammenhalt in Sieg und Niederlage.

Abschließend und überhaupt am allermeisten möchte ich mich noch bei all denjenigen bedanken, die ich zu meiner Familie zähle. Liebe Lisa, lieber Ewald, vielen Dank, dass ihr mich so herzlich in den Familienkreis aufgenommen und mich und Beatrix zu jeder Zeit unterstützt habt. Bei dir, Bea, kann ich mich gar nicht genug bedanken. Selbst in den stressigsten und schwierigsten Momenten hast du es immer verstanden mich mit deiner guten Laune und deinem Lachen anzustecken. Die vielen schönen Stunden Zuhause, auf unseren gemeinsamen Reisen und sogar auf den langen Autofahrten bereiten mir unendlich viel Vorfreude auf all das, was uns und unsere kleine Sophia in Zukunft noch erwartet.

Zu guter Letzt: Danke, Mama, Papa und Christian! Danke, dass ich euch zu jeder Zeit hinter mir wusste. Ohne eure Unterstützung wäre ich nicht der, der ich heute bin. Dafür werde ich euch immer dankbar sein!

Sebastian Wendl

Table of Contents

1	Introduction	1
1.1	Chemistry as the Hero in Everyday Life and the Necessity of Change.....	1
1.2	Challenging Synthesis of Nitridophosphates.....	3
1.3	Structural chemistry and applications of nitridophosphates.....	10
1.4	Scope of this Thesis.....	13
1.5	References.....	16
2	BaP₆N₁₀NH:Eu²⁺ as a Case Study – An Imidonitridophosphate Showing Luminescence	
	<i>illuminating Imidonitrides: Imidonitridophosphates in particular and imidonitrides in general are completely uncharted compound classes with regard to any physical and optical properties. Highly-condensed BaP₆N₁₀NH was prepared through high-pressure high-temperature synthesis starting from Ba(N₃)₂, P₃N₅, and NH₄Cl. Eu²⁺-doped samples of BaP₆N₁₀NH were used for a case study on the first luminescent imidonitridophosphates.....</i>	<i>27</i>
2.1	Introduction	29
2.2	Results and Discussion.....	30
2.3	Conclusions	39
2.4	Experimental Section.....	40
2.5	Acknowledgements	44
2.6	References	45
3	Nitridophosphate-Based Ultra-Narrow-Band Blue-Emitters: Luminescence Properties of AEP₈N₁₄:Eu²⁺ (AE = Ca, Sr, Ba)	
	<i>Ultra-narrow-band blue-emitters: Ternary alkaline earth metal nitridophosphates AEP₈N₁₄ (AE = Ca, Sr, Ba) were prepared under HP/HT conditions starting from P₃N₅, and the respective alkaline earth metal azides AE(N₃)₂. AEP₈N₁₄ shows the hitherto highest degree of condensation ($\kappa \approx 0.57$) among AE/P/N compounds. Excitation with UV to blue light rendered CaP₈N₁₄:Eu²⁺ and SrP₈N₁₄:Eu²⁺ the first P/N-based ultra-narrow-band blue-emitters.....</i>	<i>49</i>
3.1	Introduction	51
3.2	Results and Discussion.....	52
3.3	Conclusions	59
3.4	Experimental Section.....	60
3.5	Acknowledgements	64
3.6	References	65

4	Crystalline Nitridophosphates by Ammonothermal Synthesis.....	
	<i>Ammonothermal Synthesis:</i> P/N-based model compounds with different degrees of condensation, namely α - $\text{Li}_{10}\text{P}_4\text{N}_{10}$, β - $\text{Li}_{10}\text{P}_4\text{N}_{10}$, $\text{Li}_{18}\text{P}_6\text{N}_{16}$, Ca_2PN_3 , $\text{SrP}_8\text{N}_{14}$, and LiPN_2 , were synthesized applying the ammonothermal technique. The applicability of the presented approach on group-, chain-, layer-, and network-type structures demonstrates its great potential.	69
4.1	Introduction	71
4.2	Results and Discussion.....	73
4.3	Conclusions	79
4.4	Experimental Section.....	79
4.5	Acknowledgements	83
4.6	References.....	84
5	Ammonothermal Synthesis of $\text{Ba}_2\text{PO}_3\text{N}$ – An Oxonitridophosphate with Non-Condensed PO_3N Tetrahedra	
	<i>Ortho-oxonitridophosphate:</i> $\text{Ba}_2\text{PO}_3\text{N}$ was synthesized in a high-temperature autoclave starting from red phosphorus P_{red} , BaO , NaN_3 and KOH . $\text{Ba}_2\text{PO}_3\text{N}$ extends the range for accessible degrees of condensation of (oxo-)nitridophosphates to $\kappa = 1/4$ and represents the first nitridophosphate with non-condensed tetrahedra synthesized by ammonothermal technique.	89
5.1	Introduction	91
5.2	Results and Discussion.....	92
5.3	Conclusions	100
5.4	Experimental Section.....	101
5.5	Acknowledgements	104
5.6	References.....	105
6	$\text{Sr}_3\text{P}_3\text{N}_7$: Complementary Approach of Ammonothermal and High-Pressure Methods	
	<i>Collaborating methods:</i> $\text{Sr}_3\text{P}_3\text{N}_7$ was prepared by ammonothermal and multianvil syntheses. The combination of medium- and high-pressure methods with their respective benefits enabled fast structure elucidation, as well as, phase pure synthesis and studies on luminescence properties of Eu^{2+} -doped samples. $\text{Sr}_3\text{P}_3\text{N}_7$ exhibits infinite dreier double chains and extends the class of ternary alkaline earth nitridophosphates by the degree of condensation of $\kappa = 3/7$	111
6.1	Introduction	113
6.2	Results and Discussion.....	114
6.3	Conclusions	122
6.4	Experimental Section.....	123
6.5	Acknowledgements	127
6.6	References.....	128

7	HIP to be Square: Simplifying Nitridophosphate Synthesis in a Hot Isostatic Press	133
	<i>Hot Isostatic Press: Ca_2PN_3 was prepared as model compound for nitridophosphate synthesis in a hot isostatic press. After following literature known protocols, the use of red phosphorus was adapted from ammonothermal syntheses. The presented far-reaching proof-of-principle demonstrates the general applicability of HIP methods for nitridophosphate synthesis.</i>	133
7.1	Introduction with Results and Discussions	135
7.2	Acknowledgements	141
7.3	References	142
8	Synthesis of Nitride Zeolites in a Hot Isostatic Press	147
	<i>Nitride Zeolites: $\text{AE}_3\text{P}_5\text{N}_{10}\text{X}$ ($\text{AE} = \text{Sr}, \text{Ba}, \text{X} = \text{Cl}, \text{Br}$) were synthesized in a hot isostatic press starting from the respective alkaline earth metal azides and halides, as well as, P_3N_5 or P_{red}. Therefore, the broad applicability of HIPs for nitridophosphate synthesis is demonstrated by extending the accessible degree to $\kappa = 0.5$. The preparation of the introduced strontium compounds suggests the existence of phases being exclusively accessible under medium-pressure conditions.....</i>	147
8.1	Introduction with Results and Discussions	149
8.2	Acknowledgements	155
8.3	References	156
9	Post-Synthetic Modification: Systematic Study on a Simple Access to Nitridophosphates	161
	<i>Reactions with Halides: First systematic studies on a top-down strategy for nitridophosphate synthesis are presented. Therefore, pre-synthesized compounds were reacted with halides of lighter homologues under medium- or high-pressure conditions. A multifaceted reaction behavior was observed investigating chain-, layer-, and framework-type nitridophosphates.</i>	161
9.1	Introduction with Results and Discussions	163
9.2	Acknowledgements	170
9.3	References	171
10	Summary	175
11	Discussion and Outlook.....	187
11.1	Nitridophosphates as Promising Aspirants for Solid-State Lighting	187
11.2	Progress in Nitridophosphate Synthesis	192
11.3	Concluding Remarks	198
11.4	References	199
A	Supporting Information for Chapter 2	203
A.1	Results and Discussions	204
A.2	Author Contributions.....	211

B	Supporting Information for Chapter 3	213
B.1	Results and Discussions	214
B.2	Author Contributions	228
B.3	References	228
C	Supporting Information for Chapter 4	229
C.1	Results and Discussions	230
C.2	Author Contributions	240
C.3	References	241
D	Supporting Information for Chapter 5	243
D.1	Results and Discussions	244
D.2	Author Contributions	249
D.3	References	250
E	Supporting Information for Chapter 6	251
E.1	Results and Discussions	252
E.2	Author Contributions	258
F	Supporting Information for Chapter 7	259
F.1	Experimental	260
F.2	Results and Discussion	264
F.3	Author Contributions	270
F.4	References	271
G	Supporting Information for Chapter 8	273
G.1	Experimental	274
G.2	Results and Discussion	278
G.3	Author Contributions	292
G.4	References	293
H	Supporting Information for Chapter 9	295
H.1	Experimental	296
H.2	Results and Discussion	299
H.3	Author Contributions	311
H.4	References	312
I	Miscellaneous	313
I.1	List of Publications	314

I.2	List of Publications beyond this Thesis	318
I.3	Fundings.....	320
I.4	Conference Contributions and Presentations	321
I.5	Deposited Crystallographic Data	323
I.6	Curriculum Vitae	324

1 Introduction

1.1 Chemistry as the Hero in Everyday Life and the Necessity of Change

“Every aspect of the world today – even politics and international relations – is affected by chemistry.”^[1] With these words Linus Pauling summed it up in 1984 and underlined the essential role of chemistry in everyday life. More than 35 years later this quote is still true, as chemistry appears more essential than ever and is omnipresent in daily routines. Starting with care and cosmetic products in the morning, chemistry accompanies us as plastics, adhesives, dyes or components of electronic devices during the day, before evenings are prolonged by artificial illumination. But why has this branch of science lost none of its topicality?

The continuing importance of chemistry over the last decades is closely associated with constantly growing and changing demands of consumers. While, for example, in the early days of globalization the focus was exclusively on productivity and cost-reduction – keeping with the principle: higher, faster, further – priorities have changed considerably in recent years as a result of rising environmental awareness. Nowadays, especially CO₂ balances and energy savings are among the most important issues regarding large-scale production and materials properties in order to help with the realization of the 17 sustainable development goals established.^[2] In this context, chemists and materials scientists are repeatedly faced with new challenges, as the worldwide overall energy consumption increases with global population and progressing industrialization. For instance, first projections published in the *International Energy Outlook 2019* predict a nearly 50% increase of the global energy demand by 2050.^[3] To reconcile society’s rising demands with booming energy requirements, steady development is mandatory. But is this research effort still worthwhile in view of today’s highly advanced technologies? How much savings potential is there at all hidden in the largest energy-consuming sectors (process/room heat, mechanical energy, lighting, etc.) and what is basic research able to contribute to a solution at all?

Due to the complexity of these questions it is almost impossible to give an all-encompassing answer. It is a fact, however, that with the enormous amounts of energy consumed, even smallest

progress can have a major influence. In order to get at least a rough insight into the existing potential at this point, the following two aspects should be examined exemplary:

- Savings potential in the sector of artificial lighting
- Infinite versatility of basic research

Even though individual regions and states, such as the European Union (EU), have already banned the sale of incandescent light bulbs in the early 2010s, light-emitting diodes (LEDs) have not completely penetrated the global market of artificial illumination by 2020.^[4] Such policy measures could reduce the worldwide annual energy consumption for lighting by approximately 25% (640 TWh) in 2030 according to a report of the United Nations (UN).^[5] This equals a saving of 390 million metric tons of CO₂ per year and avoids a total of 3.3 gigatonnes CO₂ in the period from 2015 to 2030.^[5] Analyses of the U.S. Department of Energy (DOE) go even further and assume savings of up to 60% (130 TWh) in the USA compared to a non-solid-state lighting (SSL) scenario, estimating the market penetration for LEDs in lumen-hour sales to more than 90% in 2030.^[6] Although these forecasts from the sector of artificial illumination already indicate a huge progress, further innovations could help to achieve the stated goals faster and reduce the remaining potential for energy savings.

However, such development processes are lengthy and complicated, as the existing state of research and currently used materials are obviously insufficient to meet the highly ambitious aims. Therefore, two different strategies take effect in order to achieve the stated goals. On the one hand there is applied research, which deals mostly with improvement and optimization of established processes and materials. On the other hand, basic research focuses on the development of scarcely known or even novel substance classes and techniques. To accomplish significant advances, basically a successful collaboration of these two disciplines is required. But, while optimization processes concerning extensively studied compounds and methods often result in minor progresses, investigations on hitherto neglected methods and (almost) unexplored substance classes seem to represent the by far greater potential with its sheer endless possibilities of element combinations. With an overall number of 10^{80} – 10^{90} hypothetical compounds, chemical intuition, proper synthesis planning and the selection of suitable starting points are essential to handle this plethora of possibilities.^[7] Especially, the inspiration of desired materials by natural products may play an important role and contribute to the discovery of new promising substance classes. As example for

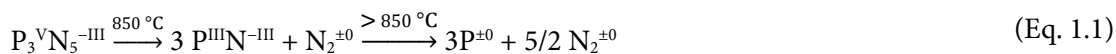
successful implementation of these points, the above-mentioned field of SSL may be given. Here, almost purely synthetically accessible nitrides (N^{3-}), which are reminiscent to oxides (O^{2-}), have led to a revolution in lighting. Next to already applied nitridosilicates and nitridoaluminates, promising potential has been observed among nitridophosphate-based host lattices (i.e. $M/P/N$ compounds with anionic P/N structures).^[8-15]

Despite these findings and the accompanying increased interest, the characteristics of nitrogen, nitride compounds in general and nitridophosphates in particular still present chemists and material scientists with difficulties in their synthesis. In the following section, these issues and existing solutions will be explained in more detail on the basis of nitridophosphates and phosphorus nitrides, focusing especially on alkaline earth metal compounds.

1.2 Challenging Synthesis of Nitridophosphates

In order to understand nitrides as almost purely synthetic materials and the associated challenging preparation, physical and chemical properties of the elemental forms of oxygen and nitrogen have to be considered. While molecular oxygen O_2 can be formulated as diradical (nominal double bond) with a bonding energy of $498 \text{ kJ}\cdot\text{mol}^{-1}$, molecular nitrogen N_2 can rather be classified unreactive or even inert, featuring an exceptional stable triple bond ($941 \text{ kJ}\cdot\text{mol}^{-1}$).^[16] Furthermore, oxygen exhibits a high redox potential ($E^0 = +1.229 \text{ V}$; $\text{O}_{2(\text{g})}$, $\text{H}^+/\text{H}_2\text{O}_{(\text{l})}$) and is known as a strong oxidizer, while nitrogen features a negative redox potential ($E^0 = -0.736 \text{ V}$; $\text{N}_{2(\text{g})}$, NH_3/OH^-).^[16, 17] In accordance therewith and with its electron affinity (-1.46 eV), oxygen can easily be reduced to O^{2-} .^[16] In contrast, the reduction of nitrogen to the oxidation state -III of nitride ions is strongly unfavored due to its positive electron affinity ($+0.07 \text{ eV}$).^[16] As a consequence the absolute exclusion of oxygen and moisture is a mandatory prerequisite for successful synthesis of pure nitrides. The above outlined characteristics of nitrogen and the relative stability of the $\text{N}\equiv\text{N}$ triple bond additionally cause a considerable vulnerability of nitride ions N^{3-} to oxidation and increase the complexity of nitride synthesis.^[16] Hence, targeted nitridophosphates/phosphorus nitrides may be prone to thermal decomposition and elimination of N_2 . This issue can probably be best explained by the binary parent compound P_3N_5 , which starts to decompose at temperatures above $850 \text{ }^\circ\text{C}$ (Equation 1.1).^[18] Here,

phosphorus +V serves as redox partner for the nitride ion, forming elemental nitrogen, amorphous phosphorus(III) nitride and even elemental phosphorus (± 0).



Opposed to the thermal instability, the cleavage and reformation of chemical bonds in numerous solid-state compounds are only enabled at temperatures of $> 1000^\circ\text{C}$. Thus, successful synthesis of P/N compounds is quite challenging since it would require the crystallization temperature to be lower than the decomposition temperature of essential starting materials and desired products. To overcome this obstacle, different synthetic strategies have been developed by either decreasing the crystallization temperature (Figure 1.1, blue) or increasing the decomposition temperature (Figure 1.1, brown).^[19]

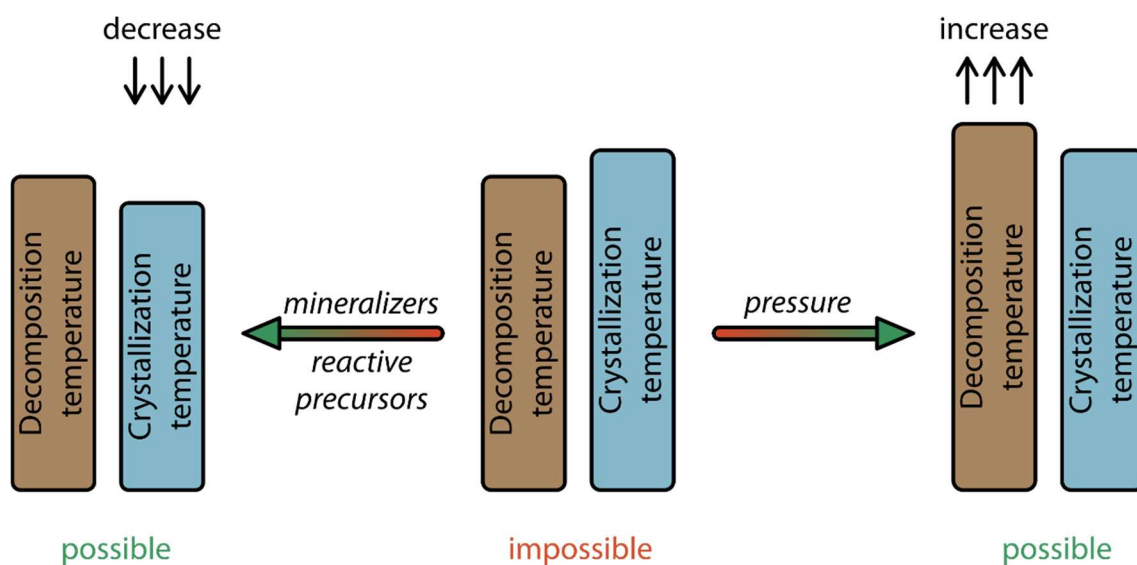


Figure 1.1. Middle: Illustration of the central problem of nitridophosphate/phosphorus nitride synthesis: The crystallization temperature (blue) exceeds the decomposition temperature (brown) at ambient pressure. This issue can be circumvented by either using mineralizers or reactive precursors (left: decreasing crystallization temperature) or applying medium-/high-pressure methods (right: increasing decomposition temperature).

To simplify the overview of the available laboratory methods so far, they are categorized according to their reaction conditions as ambient (AP), medium- (MP), and high-pressure (HP) methods. Since the boundaries between these pressure ranges are blurred and not precisely defined, they are methodically separated from each other in the course of this work. In this context, large volume

presses that can operate at reaction pressures in a gigapascal (1 GPa = 10^9 Pa $\hat{=}$ 10000 bar) range from 1–20 GPa are classified as HP methods (Figure 1.2, brown). MP methods cover a range from several bar to 1 GPa (Figure 1.2, blue and red colors). The lower limit separates conventional ampoule reactions from synthesis in pressure ampoules in which gaseous species are formed *in situ*. The upper limit serves to distinguish autoclave techniques ($p < 6 \cdot 10^8$ Pa) from large volume presses. Ampoules and tube furnace techniques with a maximum practicable reaction temperature of ca. 850 °C are designated as AP methods (Figure 1.2, green).

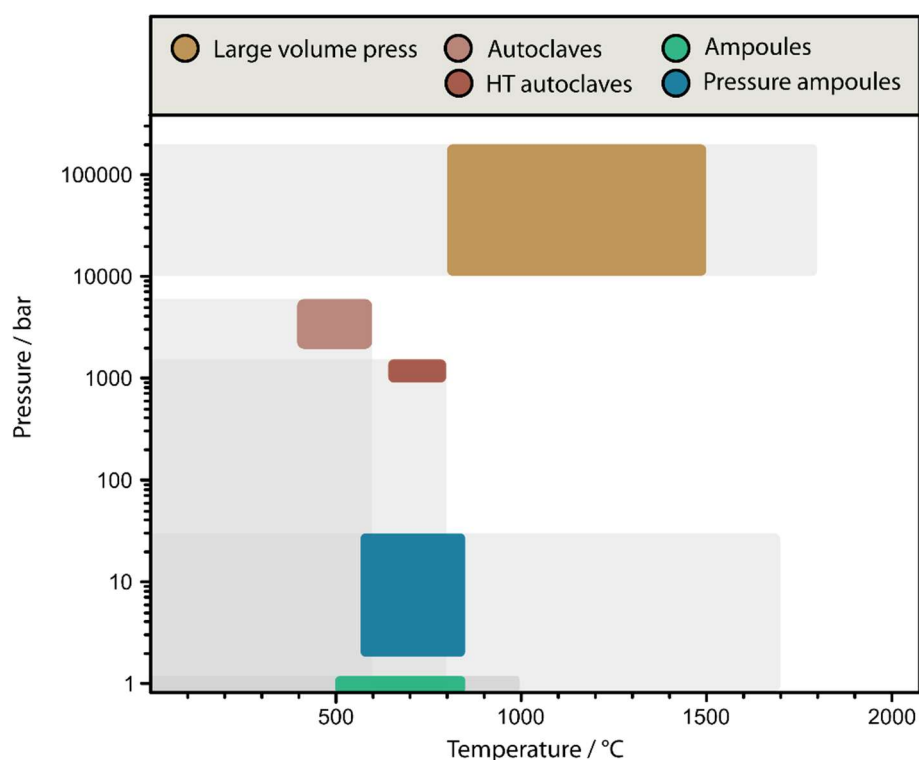


Figure 1.2. Visualization of the practically implemented conditions of established techniques for nitridophosphate/phosphorus nitride syntheses. Brown: large volume presses (1–20 GPa; 800–1500 °C); light red: autoclaves (2000–6000 bar; 400–600 °C); dark red: HT autoclaves (1000–1700 bar; 650–800 °C); blue: pressure ampoules (< 30 bar; 580–850 °C); green: ampoules (AP; 500–850 °C). Gray sections around each colored area indicate the potential pressure and temperature ranges of the respective method. The ordinate is plotted logarithmically.

Some of the latter AP techniques originate from molecule chemistry and represent the earliest approaches in solid-state P/N research. Thereby molecular precursors are used, while the critical temperature of 850 °C is not surpassed during synthesis. For instance, disordered phosphorus(V) nitride P_3N_5 has been prepared by ammonolysis of P_4S_{10} at the beginning of the 20th century.^[20]

Further AP ammonolysis and condensation reactions have enabled the synthesis of crystalline α - P_3N_5 , PON, P_4N_6O , and $SiPN_3$.^[21-24]

In addition to the solid-gas reactions listed, syntheses that work through combination of P_3N_5 with metal nitrides under Ar atmosphere at ambient pressure have been introduced. Due to the high reactivity and the low melting point of Li_3N (814 °C under N_2 atmosphere)^[25] this pathway has proven to be particularly suitable for syntheses of lithium nitridophosphates, like $LiPN_2$, Li_7PN_4 , $Li_{12}P_3N_9$, α/β - $Li_{10}P_4N_{10}$, $Li_{13}P_4N_{10}X_3$ ($X = Cl, Br$), and $Li_{47}B_3P_{14}N_{42}$.^[26-31] Analogous long-term solid-solid/solid-liquid reactions have enabled the preparation of the first alkaline earth metal nitridophosphates Mg_2PN_3 and Ca_2PN_3 (Equation 1.2).^[32, 33]



Closely related pressure ampoules are considered the simplest way to realize MP conditions. In contrast to AP methods, gaseous *in situ* formed (intermediate) products (e.g. NH_3) are not released but used to generate slightly increased reaction pressures. However, the role of the gas can differ fundamentally in individual reactions. Ammonia may either be a byproduct during condensation reactions of molecular precursors like $(NH_2)_2P(S)NP(NH_2)_3$ or used as reactant for subsequent ammonolysis of further starting materials like P_3N_5 .^[34, 35] Applying such synthesis strategies, crystalline phosphorus nitride imides α - HP_4N_7 and α - HPN_2 have been obtained, for instance.^[34, 35]

However, a notable disadvantage of this approach is the limited availability of P/N containing precursors with appropriate P/N ratios. Therefore, more versatile multicomponent reactant systems have been introduced using a combination of $OP(NH_2)_3$ and $SP(NH_2)_3$. Under elevated temperatures these (thio)phosphoryl triamides eliminate gaseous species and lead formally to (pseudo-)binary P/(O/)N compounds (Equations 1.3 and 1.4).^[36-40]



Adding metal halides and sulfides to the starting mixture has enabled the first successful MP syntheses of alkaline earth metal oxonitridophosphates, like SrP_3N_5O and $Ba_6P_{12}N_{17}O_9Br_3$.^[36, 37] Furthermore, two unprecedented nitridophosphate based zeolite structures, so-called NPO (*Nitridophosphate One*, $Li_xH_{12-x-y+z}[P_{12}O_yN_{24-y}]X_z$, $X = Cl, Br$) and NPT (*Nitridophosphate Two*, $Ba_{19}P_{36}O_{6+x}N_{66-x}Cl_{8+x}$) have been synthesized following this multicomponent approach.^[38-40]

Another MP sector deals with the preparation of P/N compounds in autoclaves. These can be seen as pressure vessels, in which amides have initially been added to P_3N_5 at low temperatures between 400 and 600 °C. Starting from alkali metal amides MNH_2 ($M = Na, Rb, Cs$) the nitridophosphate imide amides $Rb_8[P_4N_6(NH)_4](NH_2)_2$, $Na_{10}(P_4(NH)_6N_4)(NH_2)_6(NH_3)_{0.5}$, and $Cs_5[P(NH)_2](NH_2)_2$ have been obtained.^[41-43] Autoclaves can also be used for ammonothermal syntheses (adopted from the hydrothermal method) as shown for HPN_2/DPN_2 and $K_3P_6N_{11}$, where supercritical NH_3 is used as solvent.^[44, 45] Despite the provision of large sample quantities, this technique has been neglected for more than 20 years. Only recently, the ammonothermal approach has been reconsidered for nitridophosphate synthesis enabling the formation of Mg_2PN_3 and Zn_2PN_3 starting from P_3N_5 and metal powders in advanced custom-built autoclaves.^[46] Adding mineralizers, like alkali metal azides MN_3 ($M = Na, K$), to the starting materials leads to the formation of amides and other intermediates, which contribute to better solubility and crystal growth.^[46, 47]

An alternative MP approach that plays an important role within the course of this thesis is the synthesis in a hot isostatic press (HIP). Although this process is already applied on a large-scale for nitridosilicate synthesis and diverse sintering and annealing processes in ceramics production, it has previously been completely neglected for synthetic P/N chemistry so far.^[48-53]

Despite all the approaches listed above and recent developments in autoclave technology, high-pressure (HP) methods offer the most versatile access to nitridophosphates and phosphorus nitrides to date.^[19] A major advantage of these high-pressure methods is that the decomposition of P/N compounds is shifted to higher temperatures, according to Le Chatelier's principle. Basically, P/N research has been significantly facilitated due to the applied harsh reaction conditions, since more accessible but less reactive starting materials can be used. While initially, belt modules have been used to reach the high-pressure high-temperature (HP/HT) conditions, nowadays the multianvil approach is considered state-of-the-art.^[54] Here, a well-thought setup of steel wedges and WC cubes with truncated edges deflects the provided uniaxial pressure of the hydraulic press in several directions resulting in quasi-hydrostatic conditions.^[55-59]

Within this technique as standard method for nitridophosphate synthesis, various approaches have been established.^[19] Even though an overall great elemental and structural diversity has been realized (see Figure 1.3 and Chapter 1.4), each individual route is limited to a certain group of nitridophosphates.

H																	He
Li	Be										B	C	N	O	F		Ne
Na	Mg										Al	Si	P	S	Cl		Ar
K	Ca	Sc	Ti	V	Cr	Mn	Fe	Co	Ni	Cu	Zn	Ga	Ge	As	Se	Br	Kr
Rb	Sr	Y	Zr	Nb	Mo	Tc	Ru	Rh	Pd	Ag	Cd	In	Sn	Sb	Te	I	Xe
Cs	Ba	La	Hf	Ta	W	Re	Os	Ir	Pt	Au	Hg	Tl	Pb	Bi	Po	At	Rn
Fr	Ra	Ac															

Ce	Pr	Nd	Pm	Sm	Eu	Gd	Tb	Dy	Ho	Er	Tm	Yb	Lu
Th	Pa	U	Np	Pu	Am	Cm	Bk	Cf	Es	Fm	Md	No	Lr

Figure 1.3. Periodic Table of the Elements with all electropositive elements colored in light blue that have already been incorporated in (oxo/imido)nitridophosphates. Halides Cl, Br, and I are highlighted in ochre since they may occur as additional counter ions in zeolite-like (oxo/imido)nitridophosphates. As a generic sum formula $M_x[P_vN_x(O/NH)_y]X_z$ may be given. Color coding: P brown; tetrahedra vertices N, and O: dark blue; incorporated counter cations: light blue; incorporated counter anions: ochre.

For instance, the Li_3N self-flux approach has been introduced as promising access to Li/P/N compounds under HP/HT conditions.^[19] The excess of Li_3N required for this route can either be added directly or be formed *in situ* by using a surplus of Li_7PN_4 in combination with $LiPN_2$.^[28, 60, 61] Based on such known Li/P/N phases high-pressure metathesis, which grants a simple and systematic access to rare-earth and transition metal nitridophosphates, has been developed.^[62-68] In general, the ingenuity of this route can be broken down to the reaction of $LiPN_2$ with metal halides instead of using alternative nitrogen sources, which are often hard to come by or difficult to handle. Following the basic concept of metathesis reactions, the formation of thermodynamically more stable lithium halides, is utilized to generate the necessary driving force.

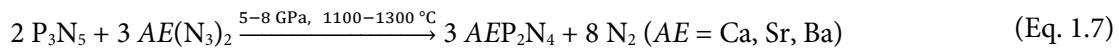
Recently, a mineralizer-assisted route has been established to synthesize BP_3N_6 and SiP_3N_5NH by the activation of refractory h-BN or Si_3N_4 .^[69, 70] Here, $(PNCl_2)_3$ is used in combination with NH_4N_3 since conventional P and N containing precursors (e.g. azides, nitrides, HPN_2 , or P_3N_5) are not capable to activate such inert compounds under HP/HT conditions.^[69, 70] In this context, hydrochloric acid is discussed as a catalyst for reversible cleavage and reformation of P–N bonds.^[18, 71] Another approach, which has been classified as a variant of mineralizer routes much earlier, is

based on adding non-stoichiometric amounts of NH_4Cl to the starting mixture.^[13, 72-75] This strategy is actually adapted from ambient pressure methods, as well-crystallized samples of SiPN_3 have only been obtained in presence of catalytic NH_4Cl .^[24] Accordingly, $\beta\text{-HPN}_2$, AEP_2N_4 ($\text{AE} = \text{Ca}, \text{Sr}, \text{Ba}$), $\text{AEH}_4\text{P}_6\text{N}_{12}$ ($\text{AE} = \text{Mg}, \text{Ca}, \text{Sr}$), and $\text{SrP}_3\text{N}_5\text{NH}$ have been prepared using this technique.^[13, 72-75]

Although the mineralizer route has facilitated the elucidation of some alkaline earth metal (imido)nitridophosphates, the most straightforward access to EA/P/N compounds is the reaction of P_3N_5 with corresponding metal nitrides. Whereas the nitride route is limited to chain-like AE_2PN_3 ($\text{AE} = \text{Mg}, \text{Ca}$) under AP, more densely packed structure types can be obtained under HP/HT conditions (Equation 1.5).^[32, 33, 76]



However, a striking disadvantage of this pathway is the unavailability of some binary nitrides. In the context of this work, especially “ Sr_3N_2 ” and “ Ba_3N_2 ” have to be mentioned. For this purpose, an alternative synthetic approach had to be developed. Thinking about other appropriate P and N containing precursors, alkaline earth metal azides $\text{AE}(\text{N}_3)_2$ have led to the implementation of the so-called azide route.^[13-15, 19] Next to a higher reactivity of the starting materials, the disproportionation of the azide ion N_3^- into nitride ions N^{3-} and nitrogen N_2 contributes to a further increased reaction pressure within the assembly shifting the reaction equilibrium to the nitride side (Equations 1.6 and 1.7).



Recapitulating this chapter, which provides an overview of all synthesis routes available to date, it has to be noted that a precise assignment of products to a single approach is not always trivial. Especially, the preparations of quaternary compounds, such as (oxo/imido) nitridophosphates ($\text{AEH}_4\text{P}_6\text{N}_{12}$ ($\text{AE} = \text{Mg}, \text{Ca}, \text{Sr}$), $\text{SrP}_3\text{N}_5\text{NH}$, $\text{AE}_3\text{P}_6\text{O}_6\text{N}_8$ ($\text{AE} = \text{Sr}, \text{Ba}$)) and nitridophosphate halides ($\text{Ba}_3\text{P}_5\text{N}_{10}\text{X}$ ($\text{X} = \text{Cl}, \text{Br}, \text{I}$)) make use of combinations of the available pathways by adding amorphous HPN_2 , PON , or BaX_2 halides, respectively.^[14, 15, 73-75, 77, 78] Moreover, it is noticeable that there is no approach to this day that combines all the advantages of the individual methods. Instead, every strategy has its notable drawbacks that prevent an acceleration of nitridophosphate research. Certainly (pressure)ampoules and autoclave techniques fall back on gentle conditions and provide

large sample quantities, but require long-term reactions and specially prepared precursors. Recently, reconsidered ammonothermal synthesis has so far only found niche applications and has to deal with scaling issues, as operations in supercritical ammonia are necessary. Most widely used multianvil method yields only very small sample quantities, but often offers well-crystallized samples that facilitate structure elucidation revealing a great structural diversity for nitridophosphates, as shown in section 1.3.

1.3 Structural chemistry and applications of nitridophosphates

Despite all synthetic possibilities and a three-decade long research, the number of known nitridophosphates and related compounds is still rather limited (< 100 compounds).^[79] Nevertheless, nitridophosphates are considered a vast class of compounds, which has developed into one of the best studied nitride classes over the years. Their structural diversity can be derived directly from the close relationship to oxosilicates, since the element combinations Si/O and P/N are isoelectronic. Moreover, SiO_4 or P(N/O)_4 tetrahedra, respectively, can be found as fundamental building units for both compound classes, leading to the observation of several homeotypic or isotypic structure types. The similarity is further underlined by various polymorphs of SiO_2 and the corresponding analogues of pseudo-binary HPN_2 and PON (e.g. α -/ β -cristobalite, moganite, α -quartz, coesite and post coesite structure types).^[22, 35, 72, 80-84] However, the structural diversity of nitridophosphates and phosphorus nitrides even exceeds that of oxosilicates in some points. Next to edge-sharing tetrahedra, which have been solely discussed for fibrous silica but are observed in α - P_3N_5 , α - HP_4N_7 , $\text{P}_4\text{N}_6\text{O}$, and α - BP_3N_6 even complete structure types can be realized in P/N compounds (δ -PON, NPO, and the nitridic clathrate), which have so far only been predicted for silicates.^[21, 23, 34, 38, 39, 69, 84-89]

A measure that easily and quickly reveals the even greater structural diversity of nitridophosphates than can exist for silicates at all, is the degree of condensation κ . This parameter represents the atomic ratio of the respective tetrahedra centers to tetrahedra vertices (e.g. $n(\text{Si/P}):n(\text{O/N})$) and covers an individual range for each class of tetrahedra-based substances. While all of them have in common that the lower end of the scale is constrained to $\kappa = 1/4$ representing non-condensed tetrahedra, the upper limit is marked by the degree of condensation of the binary

parent compounds (e.g. SiO_2 : 1/2, P_3N_5 : 3/5). With increasing values for the degree of condensation the connectivity of tetrahedra rises, as well, forming tetrahedra groups, chains, layers, or frameworks. Important benchmarks within the achievable range of κ for alkaline earth metal (oxo/imido)nitridophosphates are 1/4 ($\text{AE}_2\text{PO}_3\text{N}$: non-condensed tetrahedra), 1/3 (Ca_2PN_3 : chains), and 3/7 ($\text{AE}_3\text{P}_6\text{O}_6\text{N}_8$: layers), for instance (Figure 1.4).^[32, 33, 77, 78, 90] Framework structure types with all-side vertex-sharing tetrahedra, like observed for BaP_2N_4 , require the degree of condensation to be at least 1/2 and are therefore referred to as highly-condensed networks.^[91]

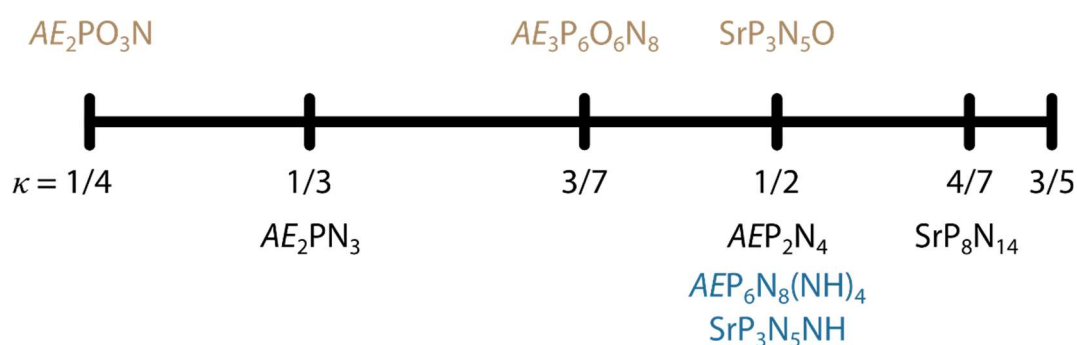


Figure 1.4. Hitherto realized degrees of condensation κ for (pseudo)ternary (oxo/imido)nitridophosphates. Nitridophosphates are colored black, imidonitridophosphates in blue, and oxonitridophosphates in brown.

However, this rule does not apply strictly the other way round for nitridophosphates. This means that with a degree of condensation of $\kappa \geq 1/2$ a framework structure type with all-side vertex-sharing tetrahedra is not obligatory, as shown for layered $\text{SrH}_4\text{P}_6\text{N}_{12}$.^[74] Even the so far highest degree of condensation among ternary nitridophosphates $\kappa = 4/7$ has been obtained for related layer-type $\text{SrP}_8\text{N}_{14}$.^[74] In order to realize such structure types and values of $\kappa \geq 1/2$, in general, triply bridging vertices have to be implemented.

Thereby, mandatory $N^{[3]}$ atoms* can be achieved in different ways, by either three solely vertex-sharing tetrahedra (e.g. β - HP_4N_7 , $K_3P_6N_{11}$, SrP_8N_{14}) or two edge-sharing tetrahedra in combination with a third vertex-sharing one (e.g. α - P_3N_5 , α - HP_4N_7 , P_4N_6O).^[45, 74, 92-94] Beyond that, high-pressure polymorphs γ - P_3N_5 and γ - HP_4N_7 exhibit $N^{[3]}$ vertices by connecting a tetrahedron with two edge-sharing PN_5 square pyramids or trigonal bipyramids, respectively.^[95, 96] Reasons for the more frequent observation of such rare structural motifs among nitridophosphates might be the higher valence of nitrogen and the reduced electrostatic repulsion in nitridophosphates due to the high covalent character of P–N bonds.^[97]

Concomitant with the development of a manifold elementary and structural diversity in nitridophosphates by basic research, various fields of application have opened up, as well. Among the microporous materials the nitridic clathrate $P_4N_4(NH)_4(NH_3)$ in particular has been discussed with regard to its potential use in catalysis or as a separate membrane or gas storage medium.^[98] Crystalline Li/P/N compounds have repeatedly been validated as Li^+ ion conductors, while amorphous LiPON has already found application in thin film batteries.^[30, 60, 99, 100] Moreover, phosphorus nitride P_3N_5 is used as a flame retardant and has previously been employed as a getter material in the fabrication of incandescent lamps and similar devices.^[101-103] Additional examinations on the optical and dielectric properties of thin films of P_3N_5 were conducted in the 1970s paving the way for electronic applications.^[104, 105] The wide band gap of P_3N_5 , which is specified with values from 5.1 to 5.9 eV, allows for application as intermediate gate insulator material, for instance.^[104, 106-108] For this purpose, photo-CVD (chemical vapor deposition) grown films are prepared on InP substrates to produce high performance MIS (metal-insulator semiconductor) devices like field effect transistors or solar cells.^[106, 109-111] Assuming a comparable high band gap for ternary and multinary nitridophosphates, they are also well suited as host lattices for the development of new phosphor materials. Here, especially alkaline earth metal compounds have emerged as promising candidates, since activators such as Eu^{2+} can be easily introduced due to identical ion charges. Their great potential as high-performance luminescence materials is underlined by recently published zeolites

* This nomenclature was introduced by Niggli and further developed by Lima-de-Faria et al..^[87, 88] The number given in superscripted square brackets for a certain atom illustrates its respective coordination number. Thus, $N^{[3]}$ refers to a triply bridging N atom. This formalism can be used to express complete structures. For instance, the systematic term $\infty^3[P^{[4]}_3N^{[2]}_3N^{[3]}_2]$ describes the P/N network of P_3N_5 . The superscripted number of dimensions expressed in how many direction the network extends infinitively and gives the dimensionality (here: $\infty^3[...]$).

$\text{Ba}_3\text{P}_5\text{N}_{10}\text{X}$ ($X = \text{Cl}, \text{Br}, \text{I}$), which have been discussed as natural-white-light single emitter for $X = \text{Br}$. $\text{MP}_2\text{N}_4:\text{Eu}^{2+}$ ($M = \text{Ca}, \text{Sr}, \text{Ba}$) and $\text{BaSr}_2\text{P}_6\text{N}_{12}:\text{Eu}^{2+}$ show that a wide range of the visible spectrum can be covered with phosphors based on P/N chemistry.^[13-15]

1.4 Scope of this Thesis

Especially in the last five years, research on nitridophosphates gained considerable momentum leading to fundamental progress in basic and applied research. Besides the structural elucidation of numerous new compounds and the introduction of novel structural motifs, nitridophosphates have particularly attracted attention as potential host lattices for luminescent materials. The broad coverage of the spectral range with only a few compounds and the zeolite $\text{Ba}_3\text{P}_5\text{N}_{10}\text{Br}:\text{Eu}^{2+}$, which is being discussed as a natural-white-light single emitter, brought the alkaline earth metal nitridophosphates into focus.^[13-15] Despite their interesting properties, however, these phosphors have been considered unsuitable for commercial production due to the use of specifically prepared starting materials and the lack of a simple method to prepare them in sufficient quantities. This is where this thesis ties on, following the motto “paving P/N-based phosphors’ way to industrial application”.

To substantiate the legitimacy and the need of this novel view on the subject, the first part of this thesis deals with the synthesis and characterization of further promising nitridophosphate-based phosphors using conventional HP methods. This is primarily intended to show that the mentioned intriguing properties investigated so far are no exceptions, but that a broad interest in this material class is also justified from an application-oriented point of view. Therefore not only ternary nitridophosphates, but also related imidonitridophosphates are investigated, as their luminescence properties had been completely unexplored prior to this work. $\text{BaP}_6\text{N}_{10}\text{NH}:\text{Eu}^{2+}$ is investigated as a case study for luminescent imidonitridophosphates in Chapter 2. Chapter 3 introduces the syntheses of $\text{AEP}_8\text{N}_{14}:\text{Eu}^{2+}$ ($\text{AE} = \text{Ca}, \text{Sr}, \text{Ba}$), which represent the first nitridophosphate-based ultra-narrow-band blue-emitters that can compete with other (oxo)nitridoberyllate and -silicate phosphors.^[112-116]

The second part of this thesis focuses on extending the application of already established MP methods. Even if there is no doubt that elevated pressures are essential to suppress thermal

decomposition, the minimum and actually required reaction pressure is still unknown. In Chapter 4 the ammonothermal technique, which has so far only found niche applications for the synthesis of nitridophosphates, is discussed as a promising preparative access. Through continuous development of autoclave techniques and materials, systematic studies have led to the successful reproduction of nitridophosphates covering a wide range of the degree of condensation ($1/3 \leq \kappa \leq 4/7$). In addition to the provision of larger sample quantities, Chapter 4 also aims to facilitate synthesis by dispensing with not readily available starting materials (e.g. P_3N_5) and establishing red phosphorus instead. The successful implementation of this strategy is expanded in Chapter 5. For this purpose, the previously unknown oxonitridophosphate Ba_2PO_3N is prepared enlarging the accessible degree of condensation by $\kappa = 1/4$. Supplementary, Eu^{2+} doping of the title compound demonstrates that suitable host lattices for activator ions can be synthesized starting from red phosphorus at MP conditions. In Chapter 6 a complementary approach of ammonothermal and multianvil syntheses is presented, which can be seen as a powerful package for a simplified and fast method for detailed characterization of nitridophosphates granting a comprehensive analysis of $Sr_3P_3N_7:Eu^{2+}$.

The third part of the presented dissertation strives for the investigation of hitherto neglected synthesis strategies in the context of P/N chemistry. Of course, the focus here is on further simplification of nitridophosphate synthesis, taking both application-oriented and basic research into account. In addition to the targeted elaboration of an approach for the large-scale production of nitridophosphates, systematic studies on an innovative strategy for improved synthesis planning and control are carried out. Meeting the application-oriented aspect, Chapter 7 introduces the hot isostatic press as an alternative MP synthetic tool for nitridophosphates using Ca_2PN_3 as model compound. Next to significantly shortened reaction times compared to previously described synthesis, red phosphorus is established as starting material, as well. Furthermore, large and well-defined crystals enable the structure elucidation of Ca_2PN_3 by means of single-crystal X-ray diffraction for the first time and luminescence properties of Eu^{2+} -doped samples are examined. Chapter 8 describes the preparation of literature known $Ba_3P_5N_{10}X:Eu^{2+}$ ($X = Cl, Br$) by HIP synthesis, demonstrating that this synthesis concept can be easily transferred to highly-condensed compounds. In addition, structural and physical properties of unprecedented $Sr_3P_5N_{10}X:Eu^{2+}$ ($X = Cl, Br$) are described.

Chapter 9 covers the basic research area of interest within this part. Applying HIP synthesis and multianvil techniques an explorative top-down strategy is investigated. Motivated by the fact that all previous routes, with only one exception, work through direct combination of the starting materials, the introduced approach is inspired by the ion exchange recently introduced for nitridosilicates.^[117-122] For this purpose, pre-synthesized framework-, layered-, and chain-like nitridophosphates are reacted with alkaline earth metal halides. The results of this substantial overview with a diverse observed reaction behavior are presented in Chapter 9.

Closing, all reported results are summarized in Chapter 10 and a brief discussion in their scientific context is provided in Chapter 11.

1.5 References

- [1] L. C. Pauling, "Chemistry and the World of Tomorrow", *Chem. Eng. News* **1984**, 62, 54-56.
- [2] United Nations, *Sustainable Development Goals*, <https://sdgs.un.org/goals>, last time visited on 26th September, 2021.
- [3] US Department of Energy, *International Energy Outlook 2019 with Projections to 2050*, **2019**, <https://www.eia.gov/outlooks/ieo/pdf/ieo2019.pdf>, last time visited on 26th September, 2021.
- [4] The Commission of the European Communities, "Commission Regulation (EC) No 244/2009", *OJ L*, **2009**, 76, 3-16.
- [5] United Nations Environment Programme, *Accelerating the global adoption of energy-efficient lighting – U4E policy guide serie 2017*, <https://www.unep.org/resources/report/accelerating-global-adoption-energy-efficient-lighting-u4e-policy-guide-series>, last time visited on 26th September, 2021.
- [6] US Department of Energy, *Energy Savings Forecast of Solid-State Lighting in General Illumination Applications 2014*, <https://www.energy.gov/sites/prod/files/2015/05/f22/energysavingsforecast14.pdf>, last time visited on 26th September, 2021.
- [7] M. Jansen, "A Concept for Synthesis Planning in Solid-State Chemistry", *Angew. Chem. Int. Ed.* **2002**, 41, 3746-3766; *Angew. Chem.* **2002**, 114, 3896–3917.
- [8] P. Pust, P. J. Schmidt, W. Schnick, "A revolution in lighting", *Nat. Mater.* **2015**, 14, 454-458.
- [9] Y. Q. Li, J. E. J. van Steen, J. W. H. van Kreveld, G. Botty, A. C. A. Delsing, F. J. DiSalvo, G. de With, H. T. Hintzen, "Luminescence properties of red-emitting $M_2Si_5N_8:Eu^{2+}$ ($M = Ca, Sr, Ba$) LED conversion phosphors", *J. Alloys Compd.* **2006**, 417, 273-279.
- [10] P. Pust, V. Weiler, C. Hecht, A. Tücks, A. S. Wochnik, A.-K. Henß, D. Wiechert, C. Scheu, P. J. Schmidt, W. Schnick, "Narrow-band red-emitting $Sr[LiAl_3N_4]:Eu^{2+}$ as a next-generation LED-phosphor material", *Nat. Mater.* **2014**, 13, 891-896.
- [11] Y. Q. Li, N. Hirosaki, R.-J. Xie, T. Takada, Y. Yamamoto, M. Mitomo, K. Shioi, "Synthesis, Crystal and Local Electronic Structures, and Photoluminescence Properties of Red-Emitting $CaAl_2SiN_{2+z}:Eu^{2+}$ with Orthorhombic Structure", *Int. J. Appl. Ceram. Technol.* **2010**, 7, 787-802.

- [12] K. Uhedaa, N. Hirosaki, Y. Yamamoto, A. Naito, T. Nakajima, H. Yamamoto, "Luminescence Properties of a Red Phosphor, $\text{CaAlSiN}_3:\text{Eu}^{2+}$, for White Light-Emitting Diodes", *Electrochem. Solid-State Lett.* **2006**, 9, H22-H25.
- [13] F. J. Pucher, A. Marchuk, P. J. Schmidt, D. Wiechert, W. Schnick, "Luminescent Nitridophosphates $\text{CaP}_2\text{N}_4:\text{Eu}^{2+}$, $\text{SrP}_2\text{N}_4:\text{Eu}^{2+}$, $\text{BaP}_2\text{N}_4:\text{Eu}^{2+}$, and $\text{BaSr}_2\text{P}_6\text{N}_{12}:\text{Eu}^{2+}$ ", *Chem. Eur. J.* **2015**, 21, 6443-6448.
- [14] A. Marchuk, W. Schnick, " $\text{Ba}_3\text{P}_5\text{N}_{10}\text{Br}:\text{Eu}^{2+}$: A Natural-White-Light Single Emitter with a Zeolite Structure Type", *Angew. Chem. Int. Ed.* **2015**, 54, 2383-2387; *Angew. Chem.* **2015**, 127, 2413-2417.
- [15] A. Marchuk, S. Wendl, N. Imamovic, F. Tambornino, D. Wiechert, P. J. Schmidt, W. Schnick, "Nontypical Luminescence Properties and Structural Relation of $\text{Ba}_3\text{P}_5\text{N}_{10}\text{X}:\text{Eu}^{2+}$ ($\text{X} = \text{Cl}, \text{I}$): Nitridophosphate Halides with Zeolite-like Structure", *Chem. Mater.* **2015**, 27, 6432-6441.
- [16] E. Riedel, C. Janiak, "Anorganische Chemie", De Gruyter, Berlin, New York, 8th Ed., **2011**.
- [17] S. G. Bratsch, "Standard Electrode Potentials and Temperature Coefficients in Water at 298.15 K", *J. Phys. Chem. Ref. Data* **1989**, 18, 1-21.
- [18] W. Schnick, "Solid State Chemistry with Nonmetal Nitrides", *Angew. Chem. Int. Ed. Engl.* **1993**, 32, 806-818; *Angew. Chem.* **1993**, 105, 846-858.
- [19] S. D. Kloß, W. Schnick, "Nitridophosphates – A Success Story of Nitride Synthesis", *Angew. Chem. Int. Ed.* **2019**, 58, 7933-7944; *Angew. Chem.* **2019**, 131, 8015-8027.
- [20] A. Stock, H. Grüneberg, "Über den Phosphorstickstoff", *Ber. Dtsch. Chem. Ges.* **1907**, 40, 2573-2578.
- [21] S. Horstmann, E. Irran, W. Schnick, "Synthesis and Crystal Structure of Phosphorus(V) Nitride $\alpha\text{-P}_3\text{N}_5$ ", *Angew. Chem. Int. Ed. Engl.* **1997**, 36, 1873-1875; *Angew. Chem.* **1997**, 109, 1938-1940.
- [22] L. Boukbir, R. Marchand, Y. Laurent, P. Bacher, G. Roult, "Preparation and time-of-flight neutron diffraction study of the cristobalite-type PON phosphorus oxynitride", *Ann. Chim. Fr.* **1989**, 14, 475-481.
- [23] J. Ronis, B. Bondars, A. Vitola, T. Millers, J. Schneider, F. Frey, "Crystal Structure of the Phosphorus Oxynitride P_4ON_6 ", *J. Solid State Chem.* **1995**, 115, 265-269.

- [24] H. P. Baldus, W. Schnick, J. Luecke, U. Wannagat, G. Bogedain, "Silicon phosphorus nitride, the first ternary compound in the silicon-phosphorus-nitrogen system", *Chem. Mater.* **1993**, 5, 845-850.
- [25] R. M. Yonco, E. Veleckis, V. A. Maroni, "Solubility of nitrogen in liquid lithium and thermal decomposition of solid Li_3N ", *J. Nucl. Mater.* **1975**, 57, 317-324.
- [26] W. Schnick, J. Lücke, "On Lithium Phosphorus Nitride. Preparation and Refinement of the Crystal Structure of $LiPN_2$ ", *Z. Anorg. Allg. Chem.* **1990**, 588, 19-25.
- [27] W. Schnick, J. Luecke, "Synthesis and crystal structure of lithium phosphorus nitride Li_7PN_4 : The first compound containing isolated PN_4 -tetrahedra", *J. Solid State Chem.* **1990**, 87, 101-106.
- [28] E.-M. Bertschler, R. Niklaus, W. Schnick, " $Li_{12}P_3N_9$ with Non-Condensed $[P_3N_9]^{12-}$ -Rings and its High-Pressure Polymorph Li_4PN_3 with Infinite Chains of PN_4 -Tetrahedra", *Chem. Eur. J.* **2017**, 23, 9592-9599.
- [29] W. Schnick, U. Berger, " $Li_{10}P_4N_{10}$ - A Lithium Phosphorus(V) Nitride with the Novel Complex Anion $P_4N_{10}^{10-}$ ", *Angew. Chem. Int. Ed. Engl.* **1991**, 30, 830-831; *Angew. Chem.* **1991**, 103, 857-858.
- [30] E.-M. Bertschler, C. Dietrich, T. Leichtweiß, J. Janek, W. Schnick, " Li^+ Ion Conductors with Adamantane-Type Nitridophosphate Anions β - $Li_{10}P_4N_{10}$ and $Li_{13}P_4N_{10}X_3$ with $X = Cl, Br$ ", *Chem. Eur. J.* **2018**, 24, 196-205.
- [31] E.-M. Bertschler, T. Bräuniger, C. Dietrich, J. Janek, W. Schnick, " $Li_{47}B_3P_{14}N_{42}$ - A Lithium Nitridoborophosphate with $[P_3N_9]^{12-}$, $[P_4N_{10}]^{10-}$, and the Unprecedented $[B_3P_3N_{13}]^{15-}$ Ion", *Angew. Chem. Int. Ed.* **2017**, 56, 4806-4809; *Angew. Chem.* **2017**, 129, 4884-4887.
- [32] W. Schnick, V. Schultz-Coulon, " Ca_2PN_3 : A New Phosphorus(V) Nitride with One-Dimensional Infinite Chains of Corner-Sharing PN_4 Tetrahedra", *Angew. Chem. Int. Ed. Engl.* **1993**, 32, 280-281; *Angew. Chem.* **1993**, 105, 308-309.
- [33] V. Schultz-Coulon, W. Schnick, " Mg_2PN_3 and Ca_2PN_3 - Phosphorus(V) Nitrides with Infinite Chains of Corner Sharing PN_4 Tetrahedra", *Z. Anorg. Allg. Chem.* **1997**, 623, 69-74.
- [34] S. Horstmann, E. Irran, W. Schnick, "Phosphorus(V) Nitride Imide HP_4N_7 : Synthesis from a Molecular Precursor and Structure Determination with Synchrotron Powder diffraction", *Angew. Chem. Int. Ed. Engl.* **1997**, 36, 1992-1994; *Angew. Chem.* **1997**, 109, 2085-2087.

- [35] W. Schnick, J. Lücke, "Preparation, Crystal Structure, and IR-spectroscopic Investigation of Phosphorus Nitride Imide, HPN_2 ", *Z. Anorg. Allg. Chem.* **1992**, 610, 121-126.
- [36] S. J. Sedlmaier, E. Mugnaioli, O. Oeckler, U. Kolb, W. Schnick, "Sr $\text{P}_3\text{N}_5\text{O}$: A Highly Condensed Layer Phosphate Structure Solved from a Nanocrystal by Automated Electron Diffraction Tomography", *Chem. Eur. J.* **2011**, 17, 11258-11265.
- [37] E. Mugnaioli, S. J. Sedlmaier, O. Oeckler, U. Kolb, W. Schnick, "Ba $_6\text{P}_{12}\text{N}_{17}\text{O}_9\text{Br}_3$ – A Column-Type Phosphate Structure Solved from Single-Nanocrystal Data Obtained by Automated Electron Diffraction Tomography", *Eur. J. Inorg. Chem.* **2012**, 2012, 121-125.
- [38] S. Correll, O. Oeckler, N. Stock, W. Schnick, "Li $_x\text{H}_{12-x-y+z}[\text{P}_{12}\text{O}_y\text{N}_{24-y}]\text{Cl}_z$ —An Oxonitridophosphate with a Zeolite-like Framework Structure Composed of 3-Rings", *Angew. Chem. Int. Ed.* **2003**, 42, 3549-3552; *Angew. Chem.* **2003**, 115, 3674-3677.
- [39] S. Correll, N. Stock, O. Oeckler, J. Senker, T. Nilges, W. Schnick, "Li $_x\text{H}_{12-x-y+z}[\text{P}_{12}\text{O}_y\text{N}_{24-y}]\text{X}_z$ (X = Cl, Br) - Oxonitridophosphate mit NPO-Zeolithstruktur", *Z. Anorg. Allg. Chem.* **2004**, 630, 2205-2217.
- [40] S. J. Sedlmaier, M. Döblinger, O. Oeckler, J. Weber, J. Schmedt auf der Günne, W. Schnick, "Unprecedented Zeolite-Like Framework Topology Constructed from Cages with 3-Rings in a Barium Oxonitridophosphate", *J. Am. Chem. Soc.* **2011**, 133, 12069-12078.
- [41] F. Golinski, H. Jacobs, "Synthesis and Crystal Structure of Rb $_8[\text{P}_4\text{N}_6(\text{NH})_4](\text{NH}_2)_2$ with the Adamantane-like Anion $[\text{P}_4\text{N}_6(\text{NH})_4]^{6-}$ ", *Z. Anorg. Allg. Chem.* **1995**, 621, 29-33.
- [42] H. Jacobs, S. Pollok, F. Golinski, "Synthesis and Crystal Structure of Na $_{10}[\text{P}_4(\text{NH})_6\text{N}_4](\text{NH}_2)_6(\text{NH}_3)_{0.5}$ with an Adamantane-like Anion $[\text{P}_4(\text{NH})_6\text{N}_4]^{4-}$ ", *Z. Anorg. Allg. Chem.* **1994**, 620, 1213-1218.
- [43] H. Jacobs, F. Golinski, "Synthesis and Crystal Structure of a Cesium-tetraimidophosphate-diamide, Cs $_5[\text{P}(\text{NH})_4](\text{NH}_2)_2 = \text{Cs}_3[\text{P}(\text{NH})_4] \cdot 2 \text{CsNH}_2$ ", *Z. Anorg. Allg. Chem.* **1994**, 620, 531-534.
- [44] H. Jacobs, R. Nymwegen, S. Doyle, T. Wroblewski, W. Kockelmann, "Crystalline Phosphorus(V) Nitride Imide, HPN_2 and DPN_2 , respectively, Structure Determination with X-Ray, Synchrotron, and Neutron Radiation", *Z. Anorg. Allg. Chem.* **1997**, 623, 1467-1474.
- [45] H. Jacobs, R. Nymwegen, "Synthesis and Crystal Structure of a Potassium Nitridophosphate, $\text{K}_3\text{P}_6\text{N}_{11}$ ", *Z. Anorg. Allg. Chem.* **1997**, 623, 429-433.

- [46] M. Mallmann, C. Maak, R. Niklaus, W. Schnick, "Ammonothermal Synthesis, Optical Properties, and DFT Calculations of Mg_2PN_3 and Zn_2PN_3 ", *Chem. Eur. J.* **2018**, 24, 13963-13970.
- [47] T. M. M. Richter, R. Niewa, "Chemistry of Ammonothermal Synthesis", *Inorganics* **2014**, 2, 29-78.
- [48] A. G. Padalko, V. A. Baklan, "Transformation in Metal Materials during Hot Isostatic Pressing", *Inorg. Mater.* **2012**, 48, 1226-1242.
- [49] K. Tsukuma, "Transparent $MgAl_2O_4$ Spinel Ceramics Produced by HIP Post-Sintering", *J. Ceram. Soc. Jpn.* **2006**, 114, 802-806.
- [50] K. Tsukuma, I. Yamashita, T. Kusunose, "Transparent 8 mol% Y_2O_3 - ZrO_2 (8Y) Ceramics", *J. Am. Ceram. Soc.* **2008**, 91, 813-818.
- [51] H. Watanabe, M. Imai, N. Kijima, "Nitridation of AEAlSi for Production of $AEAlSiN_3:Eu^{2+}$ Nitride Phosphors (AE = Ca, Sr)", *J. Am. Ceram. Soc.* **2009**, 92, 641-648.
- [52] H. Watanabe, N. Kijima, "Synthesis of $Sr_{0.99}Eu_{0.01}AlSiN_3$ from intermetallic precursor", *J. Ceram. Soc. Jpn.* **2009**, 117, 115-119.
- [53] Z. Xiao, S. Yu, Y. Li, S. Ruan, L. B. Kong, Q. Huang, Z. Huang, K. Zhou, H. Su, Z. Yao, W. Que, Y. Liu, T. Zhang, J. Wang, P. Liu, D. Shen, M. Allix, J. Zhang, D. Tang, "Materials development and potential applications of transparent ceramics: A review", *Mater. Sci. Eng. R Rep.* **2020**, 139, 100518.
- [54] K. Landskron, E. Irran, W. Schnick, "High-Temperature High-Pressure Synthesis of the Highly Condensed Nitridophosphates NaP_4N_7 , KP_4N_7 , RbP_4N_7 , and CsP_4N_7 and Their Crystal-Structure Determinations by X-ray Powder Diffraction", *Chem. Eur. J.* **1999**, 5, 2548-2553.
- [55] N. Kawai, S. Endo, "The Generation of Ultrahigh Hydrostatic Pressures by a Split Sphere Apparatus", *Rev. Sci. Instrum.* **1970**, 41, 1178-1181.
- [56] D. Walker, M. A. Carpenter, C. M. Hitch, "Some simplifications to multianvil devices for high pressure experiments", *Am. Mineral.* **1990**, 75, 1020-1028.
- [57] D. Walker, "Lubrication, gasketing, and precision in multianvil experiments", *Am. Mineral.* **1991**, 76, 1092-1100.
- [58] D. C. Rubie, "Characterising the sample environment in multianvil high-pressure experiments", *Phase Transitions* **1999**, 68, 431-451.

- [59] H. Huppertz, "Multianvil high-pressure / high-temperature synthesis in solid state chemistry", *Z. Kristallogr.* **2004**, 219, 330-338.
- [60] E.-M. Bertschler, C. Dietrich, J. Janek, W. Schnick, " $\text{Li}_{18}\text{P}_6\text{N}_{16}$ - A Lithium Nitridophosphate with Unprecedented Tricyclic $[\text{P}_6\text{N}_{16}]^{18-}$ Ions", *Chem. Eur. J.* **2017**, 23, 2185-2191.
- [61] E.-M. Bertschler, R. Niklaus, W. Schnick, "Reversible Polymerization of Adamantane-type $[\text{P}_4\text{N}_{10}]^{10-}$ Anions to Honeycomb-type $[\text{P}_2\text{N}_5]^{5-}$ Layers under High-Pressure", *Chem. Eur. J.* **2018**, 24, 736-742.
- [62] S. D. Kloß, W. Schnick, "Rare-Earth-Metal Nitridophosphates through High-Pressure Metathesis", *Angew. Chem. Int. Ed.* **2015**, 54, 11250-11253; *Angew. Chem.* **2015**, 127, 11402-11405.
- [63] S. D. Kloß, N. Weidmann, R. Niklaus, W. Schnick, "High-Pressure Synthesis of Melilite-type Rare-Earth Nitridophosphates $\text{RE}_2\text{P}_3\text{N}_7$ and a $\text{Ba}_2\text{Cu}[\text{Si}_2\text{O}_7]$ -type Polymorph", *Inorg. Chem.* **2016**, 55, 9400-9409.
- [64] S. D. Kloß, L. Neudert, M. Döblinger, M. Nentwig, O. Oeckler, W. Schnick, "Puzzling Intergrowth in Cerium Nitridophosphate Unraveled by Joint Venture of Aberration-Corrected Scanning Transmission Electron Microscopy and Synchrotron Diffraction", *J. Am. Chem. Soc.* **2017**, 139, 12724-12735.
- [65] S. D. Kloß, N. Weidmann, W. Schnick, "Antiperovskite Nitridophosphate Oxide $\text{Ho}_3[\text{PN}_4]\text{O}$ by High-Pressure Metathesis", *Eur. J. Inorg. Chem.* **2017**, 2017, 1930-1937.
- [66] S. D. Kloß, W. Schnick, " $\text{LiPr}_2\text{P}_4\text{N}_7\text{O}_3$: Structural Diversity of Oxonitridophosphates Accessed by High-Pressure Metathesis", *Inorg. Chem.* **2018**, 57, 4189-4195.
- [67] S. D. Kloß, S. Wandelt, A. Weis, W. Schnick, "Accessing Tetravalent Transition-Metal Nitridophosphates through High-Pressure Metathesis", *Angew. Chem. Int. Ed.* **2018**, 57, 3192-3195; *Angew. Chem.* **2018**, 130, 3246-3249.
- [68] S. D. Kloß, O. Janka, T. Block, R. Pöttgen, R. Glaum, W. Schnick, "Open-Shell 3d Transition Metal Nitridophosphates $\text{M}^{\text{II}}\text{P}_8\text{N}_{14}$ ($\text{M}^{\text{II}} = \text{Fe}, \text{Co}, \text{Ni}$) by High-Pressure Metathesis", *Angew. Chem. Int. Ed.* **2019**, 58, 4685-4689; *Angew. Chem.* **2019**, 131, 4733-4737.
- [69] S. Vogel, A. T. Buda, W. Schnick, "United in Nitride: The Highly Condensed Boron Phosphorus Nitride BP_3N_6 ", *Angew. Chem. Int. Ed.* **2018**, 57, 13202-13202; *Angew. Chem.* **2018**, 130, 13386-13389.

- [70] S. Vogel, A. T. Buda, W. Schnick, "Rivalry under Pressure: The Coexistence of Ambient-Pressure Motifs and Close-Packing in Silicon Phosphorus Nitride Imide $\text{SiP}_2\text{N}_4\text{NH}$ ", *Angew. Chem. Int. Ed.* **2019**, 58, 3398-3401; *Angew. Chem.* **2019**, 131, 3436-3439.
- [71] S. Vogel, *Dissertation*, Ludwig-Maximilians-Universität München (Germany) **2019**.
- [72] A. Marchuk, F. J. Pucher, F. W. Karau, W. Schnick, "A High-Pressure Polymorph of Phosphorus Nitride Imide", *Angew. Chem. Int. Ed.* **2014**, 53, 2469-2472; *Angew. Chem.* **2014**, 126, 2501-2504.
- [73] A. Marchuk, V. R. Celinski, J. Schmedt auf der Günne, W. Schnick, " $\text{MH}_4\text{P}_6\text{N}_{12}$ ($M = \text{Mg}, \text{Ca}$): New Imidonitridophosphates with an Unprecedented Layered Network Structure Type", *Chem. Eur. J.* **2015**, 21, 5836-5842.
- [74] S. Wendl, W. Schnick, " $\text{SrH}_4\text{P}_6\text{N}_{12}$ and $\text{SrP}_8\text{N}_{14}$: Insights into the Condensation Mechanism of Nitridophosphates under High Pressure", *Chem. Eur. J.* **2018**, 24, 15889-15896.
- [75] S. Vogel, W. Schnick, " $\text{SrP}_3\text{N}_5\text{NH}$: A Framework-Type Imidonitridophosphate Featuring Structure-Directing Hydrogen Bonds", *Chem. Eur. J.* **2018**, 24, 14275-14281.
- [76] F. J. Pucher, S. R. Römer, F. W. Karau, W. Schnick, "Phenakite-Type BeP_2N_4 - A Possible Precursor for a New Hard Spinel-Type Material", *Chem. Eur. J.* **2010**, 16, 7208-7214.
- [77] S. J. Sedlmaier, J. Schmedt auf der Günne, W. Schnick, " $\text{Sr}_3\text{P}_6\text{O}_6\text{N}_8$ - a highly condensed layered phosphate", *Dalton Trans.* **2009**, 4081-4084.
- [78] S. J. Sedlmaier, D. Weber, W. Schnick, "Crystal structure of barium oxonitridophosphate, $\text{Ba}_3\text{P}_6\text{O}_6\text{N}_8$ ", *Z. Kristallogr. New Cryst. Struct.* **2012**, 227, 1-2.
- [79] S. D. Kloß, *Dissertation*, Ludwig-Maximilians-Universität München (Germany) **2018**.
- [80] J. Haines, C. Chateau, J. M. Leger, A. Le Sauze, N. Diot, R. Marchand, S. Hull, "Crystal structure of moganite-type phosphorus oxynitride: relationship to other twinned-quartz-based structures", *Acta Crystallographica Section B* **1999**, 55, 677-682.
- [81] C. Chateau, J. Haines, J.-M. Léger, A. LeSauze, R. Marchand, "A moganite-type phase in the silica analog phosphorus oxynitride", *Am. Mineral.* **1999**, 207-210.
- [82] J.-M. Léger, J. Haines, L. S. de Oliveira, C. Chateau, A. Le Sauze, R. Marchand, S. Hull, "Crystal structure and high pressure behaviour of the quartz-type phase of phosphorus oxynitride PON", *J. Phys. Chem. Solids* **1999**, 60, 145-152.

- [83] D. Baumann, R. Niklaus, W. Schnick, "A High-Pressure Polymorph of Phosphorus Oxonitride with the Coesite Structure", *Angew. Chem. Int. Ed.* **2015**, 54, 4388-4391; *Angew. Chem.* **2015**, 127, 4463-4466.
- [84] D. Baumann, S. J. Sedlmaier, W. Schnick, "An Unprecedented AB_2 Tetrahedra Network Structure Type in a High-Pressure Phase of Phosphorus Oxonitride PON", *Angew. Chem. Int. Ed.* **2012**, 51, 4707-4709; *Angew. Chem.* **2012**, 124, 4785-4787.
- [85] A. Weiss, A. Weiss, "Über Siliciumchalkogenide. VI. Zur Kenntnis der faserigen Siliciumdioxid-Modifikation", *Z. Anorg. Allg. Chem.* **1954**, 276, 95-112.
- [86] A. Le Bail, "Databases of virtual inorganic crystal structures and their applications", *PCCP* **2010**, 12, 8521-8530.
- [87] M. O'Keeffe, "Uninodal 4-connected 3D nets. II. Nets with 3-rings", *Acta Crystallogr. Sect. A* **1992**, 48, 670-673.
- [88] F. Karau, W. Schnick, "A Nitridic Clathrate: $P_4N_4(NH)_4(NH_3)$ ", *Angew. Chem. Int. Ed.* **2006**, 45, 4505-4508; *Angew. Chem.* **2006**, 118, 4617-4620.
- [89] M. D. Foster, O. Delgado Friedrichs, R. G. Bell, F. A. Almeida Paz, J. Klinowski, "Chemical Evaluation of Hypothetical Uninodal Zeolites", *J. Am. Chem. Soc.* **2004**, 126, 9769-9775.
- [90] A. Marchuk, P. Schultz, C. Hoch, O. Oeckler, W. Schnick, " M_2PO_3N ($M = Ca, Sr$): ortho-Oxonitridophosphates with β - K_2SO_4 Structure Type", *Inorg. Chem.* **2016**, 55, 974-982.
- [91] F. W. Karau, W. Schnick, "High-pressure synthesis and X-ray powder structure determination of the nitridophosphate BaP_2N_4 ", *J. Solid State Chem.* **2005**, 178, 135-141.
- [92] D. Baumann, W. Schnick, "High-Pressure Polymorph of Phosphorus Nitride Imide HP_4N_7 Representing a New Framework Topology", *Inorg. Chem.* **2014**, 53, 7977-7982.
- [93] J. Lima-de-Faria, E. Hellner, F. Liebau, E. Makovicky, E. Parthe, "Nomenclature of inorganic structure types. Report of the International Union of Crystallography Commission on Crystallographic Nomenclature Subcommittee on the Nomenclature of Inorganic Structure Types", *Acta Crystallogr. Sect. A* **1990**, 46, 1-11.
- [94] U. Müller, "Anorganische Strukturchemie", Vieweg + Teubner, Wiesbaden, 6th Ed., **2008**.

- [95] K. Landskron, H. Huppertz, J. Senker, W. Schnick, "High-Pressure Synthesis of γ - P_3N_5 at 11 GPa and 1500 °C in a Multianvil Assembly: A Binary Phosphorus(V) Nitride with a Three-Dimensional Network Structure from PN_4 Tetrahedra and Tetragonal PN_5 Pyramids", *Angew. Chem. Int. Ed.* **2001**, 40, 2643-2645; *Angew. Chem.* **2001**, 113, 2713-2716.
- [96] D. Baumann, W. Schnick, "Pentacoordinate Phosphorus in a High-Pressure Polymorph of Phosphorus Nitride Imide $P_4N_6(NH)$ ", *Angew. Chem. Int. Ed. Engl.* **2014**, 53; *Angew. Chem.* **2014**, 126, 14718-14721.
- [97] R. Marchand, F. Tessier, A. Le Sauze, N. Diot, "Typical features of nitrogen in nitride-type compounds", *Int. J. Inorg. Mater.* **2001**, 3, 1143-1146.
- [98] M. Pouchard, "Framework for a molecular prison", *Nature* **2006**, 442, 878-879.
- [99] W. Schnick, J. Luecke, "Lithium ion conductivity of $LiPN_2$ and Li_7PN_4 ", *Solid State Ionics* **1990**, 38, 271-273.
- [100] S. Zhao, Z. Fu, Q. Qin, "A solid-state electrolyte lithium phosphorus oxynitride film prepared by pulsed laser deposition", *Thin Solid Films* **2002**, 415, 108-113.
- [101] M. S. Choudhary, J. K. Fink, K. Lederer, H. A. Krässig, "Investigations of the action of flame retardants in cellulose. II: Investigation of the flame-retardant action of polyphosphonitride in cellulose", *J. Appl. Polym. Sci.* **1987**, 34, 863-869.
- [102] J. A. Graves, "Getter For Incandescent Lamps and Similar Devices"; U.S. Patent 3475072, **1969**.
- [103] E. G. Zubler, "Gettering Processes for Electric Lamps and Similar Devices"; U.S. Patent 3679285, **1972**.
- [104] S. Vepřek, Z. Iqbal, J. Brunner, M. Schärli, "Preparation and properties of amorphous phosphorus nitride prepared in a low-pressure plasma", *Philos. Mag. B* **1981**, 43, 527-547.
- [105] S. Vepřek, J. Roos, "Dielectric properties of phosphorus nitride films", *J. Phys. Chem. Solids* **1976**, 37, 554.
- [106] Y. Hirota, O. Mikami, "Energy barrier height measurements of chemically vapour deposited P_3N_5 films by internal photoemission", *Thin Solid Films* **1988**, 162, 41-47.
- [107] J. L. Leclercq, J. Durand, L. Cot, R. Berjoan, C. Dupuy, "Plasma-enhanced chemical vapor deposition of phosphorus nitride thin films: Auger spectroscopy characterization", *Appl. Surf. Sci.* **1992**, 59, 289-297.

- [108] T. M. Tolhurst, C. Braun, T. D. Boyko, W. Schnick, A. Moewes, "Experiment-Driven Modeling of Crystalline Phosphorus Nitride P_3N_5 : Wide-Ranging Implications from a Unique Structure", *Chem. Eur. J.* **2016**, 22, 10475-10483.
- [109] Y. H. Jeong, G. T. Kim, S. T. Kim, K. I. Kim, W. J. Chung, "Effects of photochemical vapor deposition phosphorus-nitride interfacial layer on electrical characteristics of Au-InP Schottky diodes", *J. Appl. Phys.* **1991**, 69, 6699-6700.
- [110] Y. H. Jeong, J. H. Lee, Y. H. Bae, Y. T. Hong, "Composition of phosphorus-nitride film deposited on InP surfaces by a photochemical vapor deposition technique and electrical properties of the interface", *Appl. Phys. Lett.* **1990**, 57, 2680-2682.
- [111] J. Yoon-Ha, J. Seong-Kue, L. Bong-Hoon, T. Sugano, "Enhancement mode InP MISFET's with sulfide passivation and photo-CVD grown P_3N_5 gate insulators", *IEEE Electron Device Letters* **1995**, 16, 109-111.
- [112] E. Elzer, R. Niklaus, P. J. Strobel, V. Weiler, P. J. Schmidt, W. Schnick, " $MBe_{20}N_{14}:Eu^{2+}$ ($M = Sr, Ba$): Highly Condensed Nitridoberyllates with Exceptional Highly Energetic Eu^{2+} Luminescence", *Chem. Mater.* **2019**, 31, 3174-3182.
- [113] P. Strobel, T. de Boer, V. Weiler, P. J. Schmidt, A. Moewes, W. Schnick, "Luminescence of an Oxonitridoberyllate: A Study of Narrow-Band Cyan-Emitting $Sr[Be_6ON_4]:Eu^{2+}$ ", *Chem. Mater.* **2018**, 30, 3122-3130.
- [114] P. Strobel, C. Maak, V. Weiler, P. J. Schmidt, W. Schnick, "Ultra-Narrow-Band Blue-Emitting Oxoberyllates $AELi_2[Be_4O_6]:Eu^{2+}$ ($AE = Sr, Ba$) Paving the Way to Efficient RGB pc-LEDs", *Angew. Chem. Int. Ed.* **2018**, 57, 8739-8743; *Angew. Chem.* **2018**, 130, 8875-8879.
- [115] J. A. Kechele, O. Oeckler, F. Stadler, W. Schnick, "Structure elucidation of $BaSi_2O_2N_2$ - A host lattice for rare-earth doped luminescent materials in phosphor-converted (pc)-LEDs", *Solid State Sci.* **2009**, 11, 537-543.
- [116] M. Seibald, T. Rosenthal, O. Oeckler, F. Fahrnbauer, A. Tücks, P. J. Schmidt, W. Schnick, "Unexpected Luminescence Properties of $Sr_{0.25}Ba_{0.75}Si_2O_2N_2:Eu^{2+}$ - A Narrow Blue Emitting Oxonitridosilicate with Cation Ordering", *Chem. Eur. J.* **2012**, 18, 13446-13452.
- [117] P. Bielec, L. Eisenburger, H. L. Deubner, D. Günther, F. Kraus, O. Oeckler, W. Schnick, "Targeting Vacancies in Nitridosilicates: Aliovalent Substitution of M^{2+} ($M = Ca, Sr$) by Sc^{3+} and U^{3+} ", *Angew. Chem. Int. Ed.* **2019**, 58, 840-843; *Angew. Chem.* **2019**, 131, 850-853.

- [118] P. Bielec, O. Janka, T. Block, R. Pöttgen, W. Schnick, "*Fe₂Si₅N₈: Access to Open-Shell Transition-Metal Nitridosilicates*", *Angew. Chem. Int. Ed.* **2018**, 57, 2409-2412; *Angew. Chem.* **2018**, 130, 2433-2436.
- [119] P. Bielec, R. Nelson, R. P. Stoffel, L. Eisenburger, D. Günther, A.-K. Henß, J. P. Wright, O. Oeckler, R. Dronskowski, W. Schnick, "*Cationic Pb₂ Dumbbells Stabilized in the Highly Covalent Lead Nitridosilicate Pb₂Si₅N₈*", *Angew. Chem. Int. Ed.* 2019, 58, 1432-1436; *Angew. Chem.* **2019**, 131, 1446-1450.
- [120] P. Bielec, W. Schnick, "*Increased Synthetic Control - Gaining Access to Predicted Mg₂Si₅N₈ and β-Ca₂Si₅N₈*", *Angew. Chem. Int. Ed.* **2017**, 56, 4810-4813; *Angew. Chem.* **2017**, 129, 4888-4891.
- [121] W. Schnick, J. Lücke, "*Zn₇[P₁₂N₂₄]Cl₂ - A Sodalite with a Phosphorus Nitrogen Framework*", *Angew. Chem. Int. Ed. Engl.* **1992**, 31, 213-215; *Angew. Chem.* **1992**, 104, 208-209.
- [122] W. Schnick, J. Lücke, "*Nitrido-Sodalithe. I Synthesis, Crystal Structure, and Properties of Zn_{7-x}H_{2x}[P₁₂N₂₄]Cl, with 0 ≤ x ≤ 3*", *Z. Anorg. Allg. Chem.* **1994**, 620, 2014-2019.

2 BaP₆N₁₀NH:Eu²⁺ as a Case Study – An Imidonitridophosphate Showing Luminescence

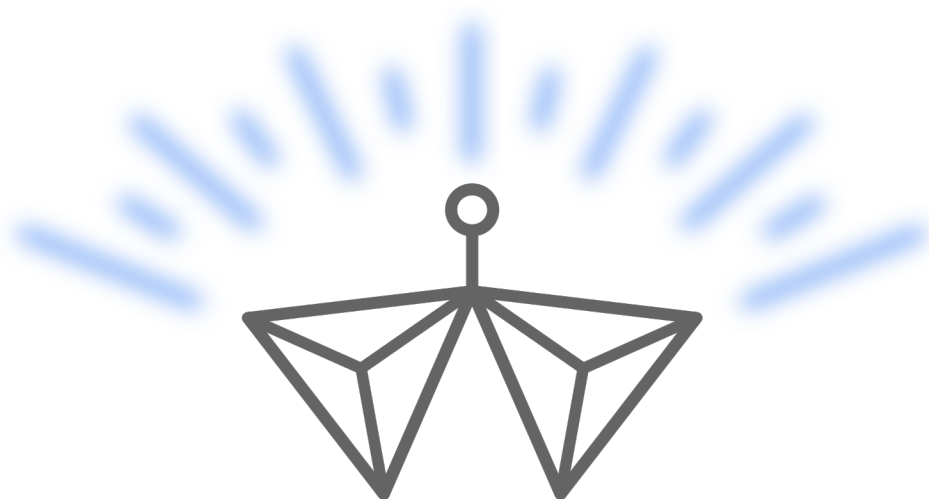
Sebastian Wendl, Lucien Eisenburger, Mirjam Zipkat, Daniel Günther, Dr. Jonathan P. Wright,

Dr. Peter J. Schmidt, Prof. Dr. Oliver Oeckler, Prof. Dr. Wolfgang Schnick

Chem. Eur. J. **2020**, 26, 5010–5016.

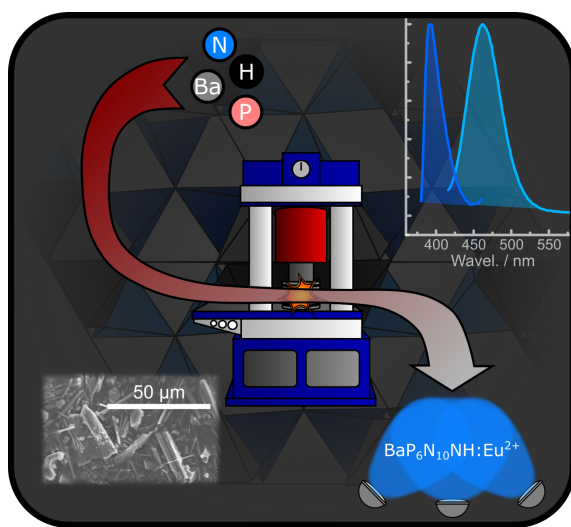
DOI: 10.1002/chem.201905082

Reprinted (adapted) with permission for non-commercial use from *Chemistry – A European Journal* (open access). Copyright 2021 John Wiley and Sons.



Illuminating Imidonitrides: Imidonitridophosphates in particular and imidonitrides in general are completely uncharted compound classes with regard to any physical and optical properties. Highly-condensed BaP₆N₁₀NH was prepared through high-pressure high-temperature synthesis starting from Ba(N₃)₂, P₃N₅, and NH₄Cl. Eu²⁺-doped samples of BaP₆N₁₀NH were used for a case study on the first luminescent imidonitridophosphates.

Abstract: Barium imidonitridophosphate $BaP_6N_{10}NH$ was synthesized at 5 GPa and 1000 °C with a high-pressure high-temperature approach using the multianvil technique. $Ba(N_3)_2$, P_3N_5 and NH_4Cl were used as starting materials, applying a combination of azide and mineralizer routes. The structure elucidation of $BaP_6N_{10}NH$ ($P6_3$, $a = 7.5633(11)$, $c = 8.512(2)$ Å, $Z = 2$) was performed by a combination of transmission electron microscopy and single-crystal diffraction with microfocused synchrotron radiation. Phase purity was verified by Rietveld refinement. 1H and ^{31}P solid-state NMR and FTIR spectroscopy are consistent with the structure model. The chemical composition was confirmed by energy-dispersive X-ray spectroscopy and CHNS analyses. Eu^{2+} -doped samples of $BaP_6N_{10}NH$ show blue emission upon excitation with UV to blue light ($\lambda_{em} = 460$ nm, $fwhm = 2423$ cm^{-1}) representing unprecedented Eu^{2+} -luminescence of an imidonitride.



2.1 Introduction

The ongoing development of advanced synthesis strategies, enabled the discovery of numerous silicate-analogous tetrahedra-based compound classes, of which nitridophosphates are a prominent example.^[1] Nitridophosphates show structural similarities with oxosilicates as the element combination P/N is isoelectronic to Si/O. Compared to oxosilicates, the synthetic access to nitridophosphates is challenging, because on the one hand high temperatures (often > 1000 °C) are needed for rearranging P–N bonds, but on the other hand P₃N₅, the most important starting material, decomposes above 850 °C. This problem can be resolved with high-pressure high-temperature syntheses according to the principle of Le Chatelier. Despite their challenging syntheses, the structural chemistry of nitridophosphates is intriguing, as they can reach even higher degrees of condensation (i.e., atomic ratio κ of tetrahedra centers and ligands) than oxosilicates ($\kappa(\text{P}_3\text{N}_5) = 0.6$, $\kappa(\text{SiO}_2) = 0.5$).^[2–8] Thus, nitridophosphates feature triply-bridging N^[3] atoms or even edge-sharing PN₄ tetrahedra.^[9] Moreover, nitridophosphates have recently been investigated as host materials for Eu²⁺-doped phosphors.^[10–12] Although the number of nitridophosphate-based phosphors is still limited, the known examples almost cover the entire visible spectrum. For example, MP₂N₄:Eu²⁺ ($M = \text{Ca}, \text{Sr}, \text{Ba}$) shows emissions from 450 to 570 nm, featuring full width at half-maximum (fwhm) values comparable to established nitride-based phosphor materials.^[10] Furthermore, Eu²⁺-doped quaternary zeolite-like nitridophosphates Ba₃P₅N₁₀X ($X = \text{Cl}, \text{Br}, \text{I}$) have been investigated concerning their luminescence properties.^[11, 12] Ba₃P₅N₁₀Br, for example, has been discussed as a natural-white-light single emitter.^[12]

In contrast, quaternary imidonitridophosphates, which have been discussed as possible intermediates on the reaction pathway to highly condensed nitridophosphates, are completely unexplored concerning their luminescence properties.^[8] These H-containing compounds can be synthesized using starting materials like amides, NH₄Cl, or the underlying ternary imide nitride HPN₂.^[13–17] For years, only the less condensed alkali metal amide/imide compounds Cs₅P(NH)₄(NH₂)₂, Rb₈[P₄N₆(NH)₄](NH₂)₂ and Na₁₀[P₄N₄(NH)₆](NH₂)₆(NH₃)_{0.5} have been known, showing discrete tetrahedra and adamantane-like [P₄N_{10–x}(NH)_x]^{(10–x)–} cages, respectively.^[13–15] The highly condensed alkaline earth metal imidonitridophosphates MH₄P₆N₁₂ ($M = \text{Mg}, \text{Ca}, \text{Sr}$) were the

first representatives showing layered network structure types.^[8, 17] In framework-type SrP₃N₅NH, internal H bonds lead to structure types that are not related to isoelectronic SrP₃N₅O compounds.^[16]

Herein, we report on the highly condensed imidonitridophosphate BaP₆N₁₀NH ($\kappa = 0.55$), initially observed as microcrystalline particles in multiphase samples. Structure elucidation by X-ray diffraction with microfocused synchrotron radiation revealed an unprecedented structure type. The results enabled the targeted synthesis of phase-pure products, leading to first studies on the luminescence properties of Eu²⁺-doped imidonitridophosphates.

2.2 Results and Discussion

Synthesis

BaP₆N₁₀NH was initially observed in a heterogeneous sample synthesized by high-pressure high-temperature reaction at 4 GPa and 1150 °C using a hydraulic press including a modified Walker-type multianvil apparatus.^[18–22] Starting from Ba(N₃)₂, P₃N₅, and NH₄Cl, a colorless microcrystalline sample was obtained. Stoichiometric reactions according to Equation (2.1) did not lead to phase-pure products.



The highest yield was obtained with a slight excess of Ba(N₃)₂ (1.2 equiv.) and a noticeable excess of NH₄Cl (4 equiv.). With NH₄Cl acting as hydrogen source and as a mineralizer, this approach is a combination of azide and mineralizer routes. EuCl₂ (1 mol%) was added as dopant. The title compound was isolated as an air- and moisture-stable colorless solid (yield per batch \approx 35 mg) and was washed with de-ionized water after synthesis. Optimized syntheses yielded rod-like crystals with an edge length up to 30 μm (Figure 2.1).

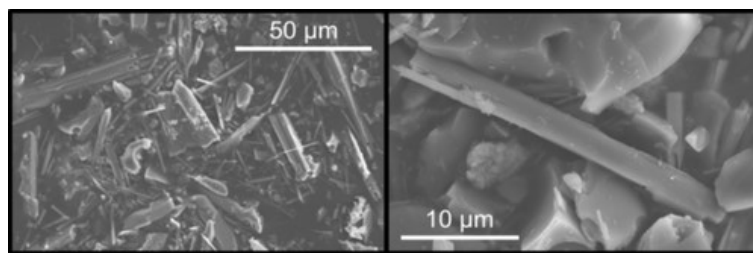


Figure 2.1. SEM images of BaP₆N₁₀NH crystals with a maximum length of about 30 μm.

Structure determination

Due to the microcrystalline and multiphase character of the original sample, neither conventional single-crystal X-ray diffraction nor structure solution from powder X-ray diffraction data were applicable. Hence, a combination of transmission electron microscopy (TEM) and microfocused synchrotron radiation was applied.^[23] Small crystallites (needles up to 8 μm in length with diameters of ca. 1–2 μm) of the target phase were identified by selected-area electron diffraction (see Supporting Information, Figure A1) and EDX analysis. The crystallites' positions were documented on finder grids and transferred to the synchrotron beamline (ID11, ESRF, Figure A2). Subsequent structure determination was based on single-crystal diffraction data collected with a microfocused synchrotron beam with a diameter of ca. 1×2 μm.

The crystal structure of the title compound was initially solved by direct methods and refined as BaP₆X₁₁ (X = O, N) in the hexagonal space group *P*6₃ (no. 173) with unit cell dimensions of $a = 7.5585(1)$ and $c = 8.5106(1)$ Å. The preliminary sum formula BaP₆X₁₁ (X = O, N) allows for two conceivable charge-balanced compositions such as BaP₆N₁₀O or BaP₆N₁₀NH. Although small maxima of residual electron densities were observed at reasonable N–H distances to N1, N2, and N5, they could not be refined, probably because H atoms are disordered on these three suitable N^[2] positions, of which each single one may only be occupied by one third of H on average. Based on the results of solid-state NMR and FTIR spectroscopy, BaP₆N₁₀NH turned out to be the correct sum formula (Figure 2.3 and Figure A3). All located atoms were refined anisotropically. The summarized crystallographic data are given in Table A1. Atom positions and anisotropic displacement parameters are listed in Tables A2 and A3 (see Supporting Information). CSD 1942108 contains the

supplementary crystallographic data for this paper. These data can be obtained free of charge from FIZ Karlsruhe via www.ccdc.cam.ac.uk/structures.

Based on the refined single-crystal structure of BaP₆N₁₀NH, Rietveld refinement of powder X-ray diffraction data confirms phase purity (Figure 2.2 and Table A4 in the Supporting Information). For the verification of the chemical composition, energy-dispersive X-ray spectroscopy (EDX) was carried out. No elements other than Ba, P, N and O were detected. The determined atomic ratio of Ba : P : N ≈ 1 : 6 : 11 corresponds to the expected sum formula (see Table A5). O was only detected in trace amounts at some points and can most likely be attributed to surface hydrolysis of the sample. CHNS analysis (Table A6) yielded a weight percentage of N that agrees well with the theoretical value, while the weight percentage of H is slightly higher than expected, again a hint at surface hydrolysis.

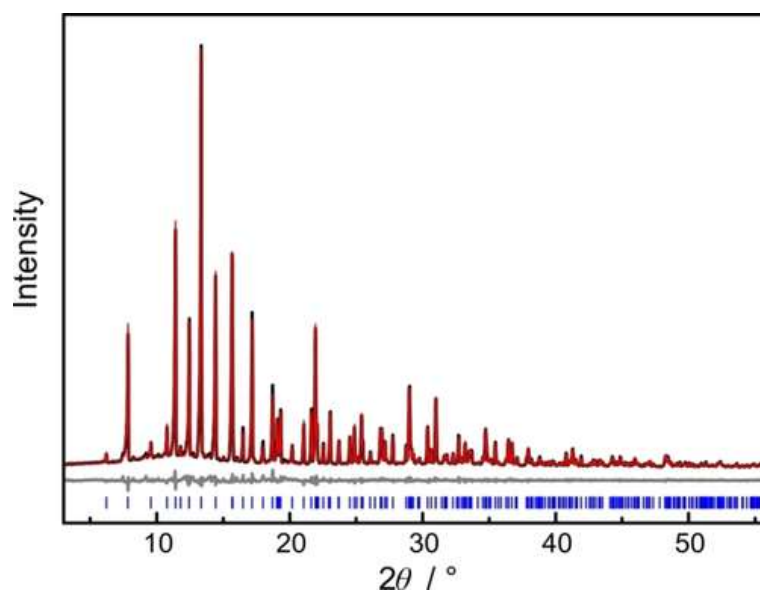


Figure 2.2. Rietveld refinement of BaP₆N₁₀NH; observed (black) and simulated (red) powder X-ray diffraction patterns and difference profile (grey). Positions of Bragg reflections of BaP₆N₁₀NH (blue) are marked with vertical blue bars.

The Fourier-transform infrared (FTIR) spectrum shows a broad vibration band with significant intensity from 2700–3400 cm⁻¹ (see Supporting Information, Figure A3). This can be attributed to N–H valence modes and is comparable to other known imidonitridophosphates.^[8, 16, 17] Further absorption bands with very strong intensities are visible in the fingerprint region (400–1500 cm⁻¹, see Figure A3). They can be assigned to symmetric and asymmetric P–N–P stretching modes.

As another verification for the presence of H atoms and the structure model in general, solid-state nuclear magnetic resonance measurements (NMR) were performed. The focus of these experiments was on H atoms in order to supplement the results of X-ray diffraction data. Therefore, ^1H , ^{31}P , and $^{31}\text{P}\{^1\text{H}\}$ magic angle spinning (MAS) experiments were carried out. At first glance, the observed ^1H MAS spectrum shows one signal at 8.7 ppm, which is rather broad in comparison to those of other imidonitridophosphates (Figure 2.3a).^[8, 16, 17] In fact, this band is composed of three signals with shifts of $\delta = 5.2$, 7.6, and 8.7 ppm, which can be assigned to the title compound (magnification in Figure 2.3a). This observation is in line with the assumption that H is statistically bound to three N atoms. The ^{31}P MAS spectrum shows two signals with chemical shifts of $\delta = -7.1$ and 1.6 ppm (Figure 2.3b, black). As these signals remain in the $^{31}\text{P}\{^1\text{H}\}$ cross-polarization spectrum, the corresponding P atoms seem to be located in a hydrogen-containing environment, and can thus be assigned to $\text{BaP}_6\text{N}_{10}\text{NH}$ (Figure 2.3b, red).

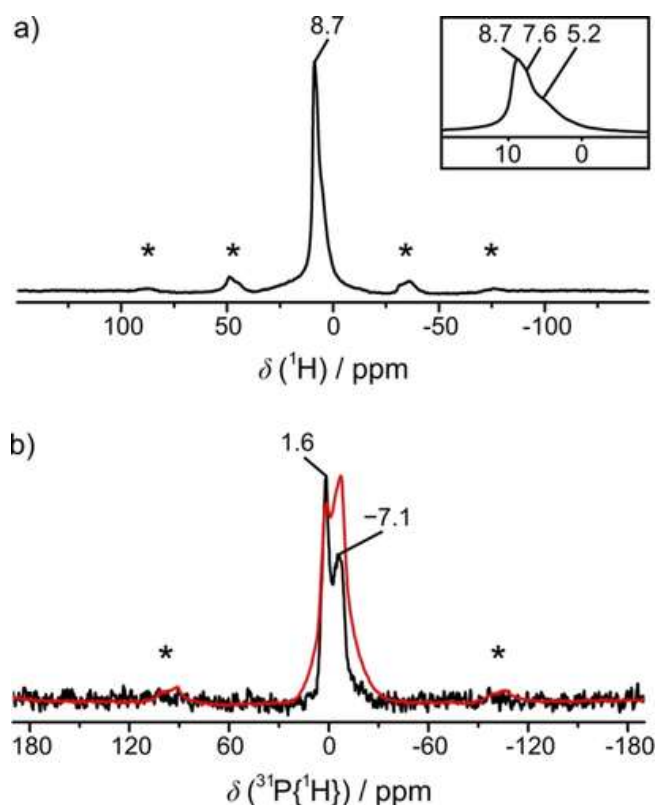


Figure 2.3. Solid-state NMR spectra of $\text{BaP}_6\text{N}_{10}\text{NH}$, measured at a sample spinning frequency of 50 kHz. a) ^1H MAS NMR spectrum: One wide band can be identified as three individual signals with shifts of 5.2, 7.6, and 8.7 ppm in the magnified area. b) ^{31}P MAS (black) and $^{31}\text{P}\{^1\text{H}\}$ (red) MAS cross polarization NMR spectra: Both show two peaks with chemical shifts of -7.1 and 1.6 ppm. Spinning side bands are marked with asterisks.

Structure description

BaP₆N₁₀NH can be classified as a highly condensed compound and shows the highest degree of condensation among quaternary imidonitridophosphates ($\kappa = n(\text{P}):n(\text{N}) = 0.55$) reaching almost the degree of condensation in HP₄N₇ ($\kappa = 0.57$).^[5-7] The structure is built up from all-side vertex-sharing PN₄ tetrahedra and can be described as a three-dimensional network of interconnected propeller-like [P₃N₁₀] subunits consisting of three PN₄ tetrahedra linked by a threefold bridging N atom like that observed in β -HP₄N₇.^[6] While these subunits are linked directly to each other as well as by additional bridging PN₄ tetrahedra in β -HP₄N₇ forming 3-, 4-, and 6-rings, the BaP₆N₁₀NH structure-type is exclusively built up from interconnected [P₃N₁₀] subunits forming 3- and 9-rings.^[6] Thereby the tetrahedra of one subunit are centered by the same P site in BaP₆N₁₀NH (Figure 2.4, P1: grey; P2: blue).

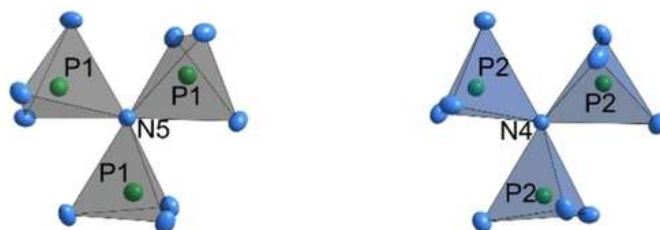


Figure 2.4. Propeller-like [P₃N₁₀] units of P1 and P2 as smallest building units of the crystal structure of BaP₆N₁₀NH.

Each [P₃N₁₀] unit is linked to six further subunits, which are centered by the other P site. This arrangement leads to a stacking of the propeller-like building blocks along [0 0 1] with an order of ABA'B'ABA'B' (Figure 2.5).

Furthermore, the combinations of the slabs A/B (dark colors) and the equivalent ones A'/B' (bright colors) can be described as layered PN₄ substructures, which are related by the 6₃ screw axis along [0 0 1] (Figures 2.6a and 2.6b).

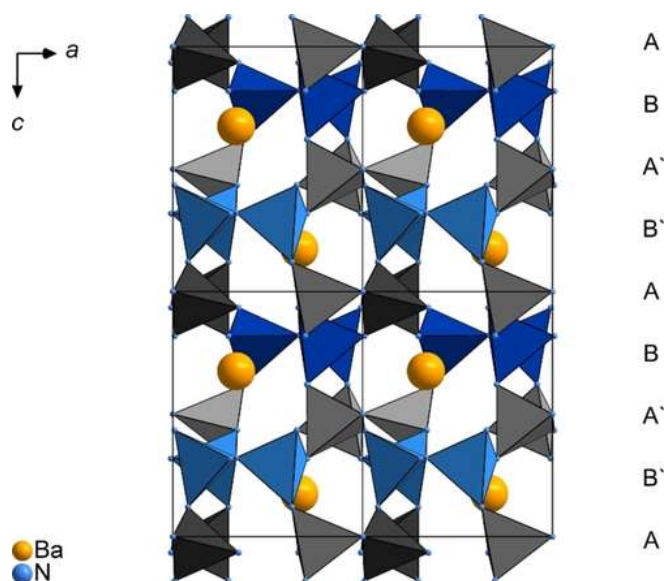


Figure 2.5. Projection of the crystal structure of $\text{BaP}_6\text{N}_{10}\text{NH}$ along $[010]$. Color coding: Ba: yellow, N: blue, P1 centered tetrahedra: grey, P2 centered tetrahedra: blue; unit cells are indicated.

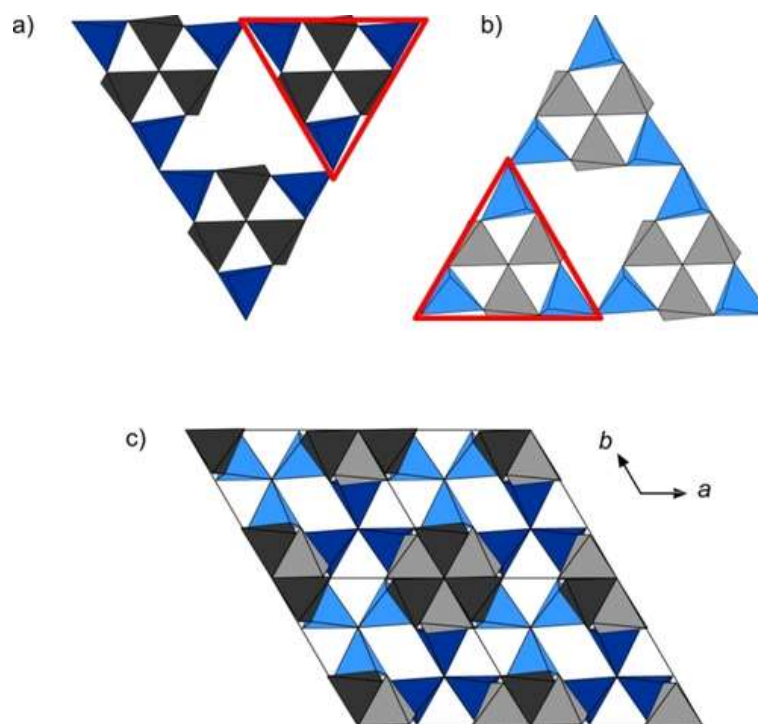


Figure 2.6. a) Triangular $[\text{P}_6\text{N}_{16}]$ units built up from layers A and B b) Triangular $[\text{P}_6\text{N}_{16}]$ units built up from layers A' and B' c) Projection of the structure of $\text{BaP}_6\text{N}_{10}\text{NH}$ along $[001]$. Color coding: P1 centered tetrahedra: grey, P2 centered tetrahedra: blue.

Within these layers, the [P₃N₁₀] subunits form larger triangular [P₆N₁₆] building blocks which are connected through common vertices (red triangles, Figures 2.6a and 2.6b). In an alternating stacking sequence of these layers, the grey tetrahedra (P1 centered) form columns whereas the blue [P₃N₁₀] units of one layer fill up the triangular channels of the other one (Figure 2.6c). In the resulting framework, P–N distances and N–P–N angles are similar to values from other alkaline earth metal nitridophosphates (P–N: 1.590(3)–1.735(1) Å, N–P–N: 102.3(1)–114.1(1)°).^[8, 10, 24] Thereby, the elongated P–N distances can be attributed to the triply bridging N^[3] atoms (P(1)–N(5), P(2)–N(4)), which is in accordance with distances observed in β-HP₄N₇.^[6] Further information about bond lengths and angles is summarized in Table A7 (see Supporting Information). The topology of the network is represented by the point symbol (3².5².6⁴.7²)(3³.4².5³.6²), which has not been observed as yet.^[25] Due to the described arrangement of PN₄ tetrahedra, the Ba atoms occupy one single crystallographic site which is coordinated by 13 N atoms in a slightly distorted sevenfold capped octahedron (Figure 2.7). Ba–N distances range from 2.884(3)–3.363(2) Å and agree with known barium nitridophosphates, as well as with the sum of the ionic radii.^[24, 26, 27]

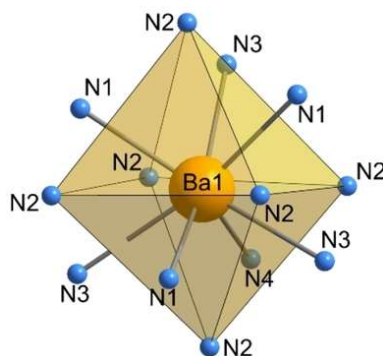


Figure 2.7. Coordination of Ba by 13 N atoms in a slightly distorted sevenfold capped octahedron in BaP₆N₁₀NH.

Temperature dependent X-ray diffraction

In order to investigate the thermal stability of BaP₆N₁₀NH, temperature dependent X-ray diffraction measurements were carried out up to 1000 °C under Ar atmosphere. BaP₆N₁₀NH is apparently stable over the entire temperature range, featuring no significant changes in the diffraction pattern (Figure A4). The evolution of the lattice parameters upon heating was determined

by Rietveld refinements of selected temperature-dependent PXRD patterns. The parameters a and c (+ 0.8%, + 0.6%) increase almost linearly, resulting in a thermal expansion of the unit cell by 2.2% in volume at 1000 °C with respect to ambient temperature (Table A8 and Figure A5).

UV/Vis reflectance spectroscopy

The optical properties of BaP₆N₁₀NH were investigated by diffuse reflectance measurements. The corresponding spectrum shows an absorption band at around 250 nm (Supporting Information, Figure A6). The Kubelka–Munk function $F(R) = (1-R)^2/2R$, with R representing the reflectance, was used for the conversion of the reflectance spectrum into a pseudo-absorption spectrum.^[28] The band gap was then determined by plotting $h\nu$ versus $(F(R)\cdot h\nu)^{1/n}$ (Tauc plot, Figure 2.8).^[29] The resulting Tauc plot shows an approximately linear region for $n = 1/2$ and suggests a direct band gap. Based on the experimental data, the optical band gap can be estimated to ≈ 5.4 eV by intersecting the aligned tangent of the linear region with the abscissa.

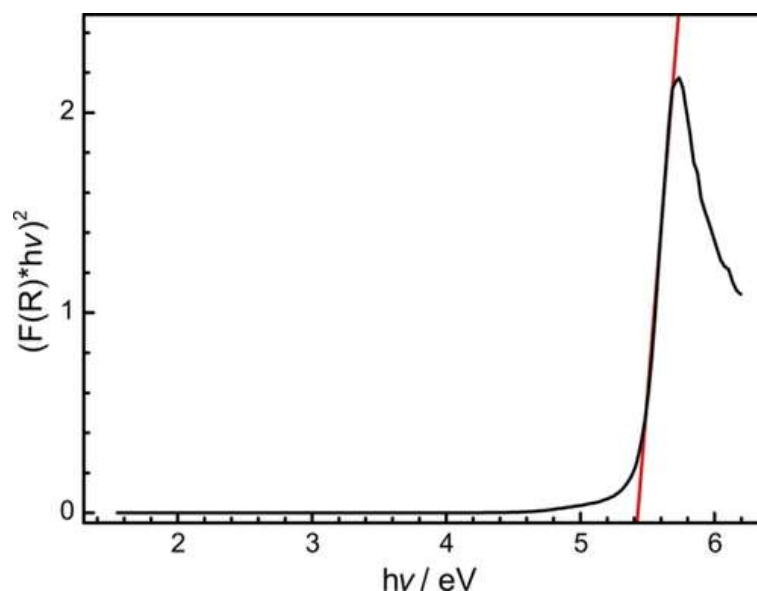


Figure 2.8. Tauc plot (black) for non-doped BaP₆N₁₀NH. Red line as a tangent at the inflection points.

Luminescence

Concluding from structural and optical properties, as well as the thermal stability, BaP₆N₁₀NH seems to be a promising candidate for a case study on the luminescence properties of imidonitridophosphates, which have not been reported so far. BaP₆N₁₀NH:Eu²⁺ can efficiently be excited by near-UV to blue light (Figure 2.9, red). Excitation at 420 nm results in blue emission ($\lambda_{\text{em}} = 460 \text{ nm}$, $\text{fwhm} = 52 \text{ nm}/2423 \text{ cm}^{-1}$) for single particles with a nominal Eu content of 1 atom% referred to Ba, making BaP₆N₁₀NH:Eu²⁺ the first luminescent imidonitride. The occurrence of the Eu²⁺-luminescence might have different reasons. Although quenching effects of oscillators like X–H ($X = \text{O}, \text{N}, \text{C}$) were discussed for aromatic organic compounds in the near-IR range, luminescence can be observed if it does not excite any overtone of the vibrational X–H modes.^[30–32] In the case of BaP₆N₁₀NH, an experimental evaluation could therefore not be performed, as the respective emission is located in the blue spectral range and corresponding wavenumbers ($\nu \approx 21.700 \text{ cm}^{-1}$) would require absorption experiments for the fifth ($n = 6$) or sixth ($n = 7$) overtone. The low intensities of high-order overtones, the low resolution of solid-state IR spectroscopy and the intrinsic broad bands for N–H valence modes preclude such investigations. Another reason for the visible emission might be given by the low concentration of potentially quenching N–H groups in BaP₆N₁₀NH. This concentration can be characterized by the ratio of H-bonding to non-H-bonding N atoms (NH/N) and amounts to 1:10 for the title compound. All other known imidonitridophosphates show significantly higher NH/N values (MH₄P₆N₁₂ \equiv MP₆N₈(NH)₄: 1/2; SrP₃N₅NH: 1/5).^[8, 16, 17] The emission spectrum of BaP₆N₁₀NH:Eu²⁺ exhibits a single emission band with a maximum at 460 nm and a full width at half maximum (fwhm) of 52 nm/2423 cm⁻¹ (see Figure 2.9). This single emission band results from the fact that Eu²⁺ is expected to occupy the single crystallographic Ba site apparent in the crystal structure. With these characteristic values, BaP₆N₁₀NH:Eu²⁺ can be compared to ternary and quaternary all-nitride Eu²⁺-doped nitridophosphates, for example, BaP₂N₄:Eu²⁺ ($\lambda_{\text{em}} = 454 \text{ nm}$, $\text{fwhm} = 2244 \text{ cm}^{-1}$) and BaSr₂P₆N₁₂:Eu²⁺ ($\lambda_{\text{em}} = 456 \text{ nm}$, $\text{fwhm} = 2240 \text{ cm}^{-1}$).^[10] The similar emission values might be explained by the similar environment of the alkaline earth metals in the mentioned compounds, as BaP₂N₄:Eu²⁺ (Ba–N: 2.78–3.48 Å) and BaSr₂P₆N₁₂:Eu²⁺ (M–N: 2.80–3.40 Å) each exhibit two crystallographic Ba/Sr sites, which are coordinated by twelve N atoms.^[10]

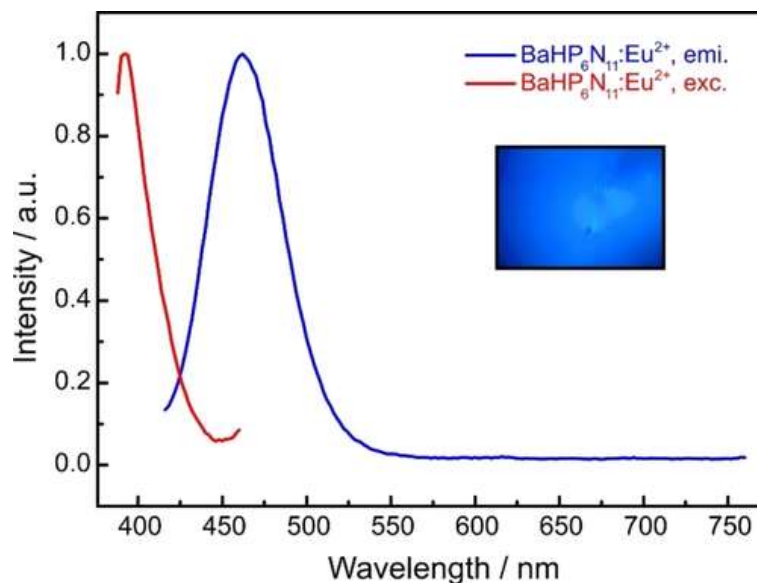


Figure 2.9. Normalized excitation (red) and emission (blue) spectra ($\lambda_{\text{exc}} = 420$ nm) of BaP₆N₁₀NH:Eu²⁺.

2.3 Conclusions

We report on synthesis and characterization of the first barium imidonitridophosphate BaP₆N₁₀NH. Among imidonitridophosphates, it exhibits a very high degree of condensation ($\kappa = 0.55$) and the smallest NH/N ratio. Its structural framework is built up from condensed [P₃N₁₀] units, forming larger triangular [P₆N₁₆] building blocks. Orientation and arrangement of the latter reveals cavities occupied by Ba atoms in a 13-fold coordination by N atoms. As previous reports claim that imidonitridophosphates might be less condensed intermediates on the way to highly condensed ternary nitridophosphates, BaP₆N₁₀NH seems to be a promising candidate for access to high degrees of condensation in nitridophosphates.^[8] Investigations on the luminescence of imidonitridophosphates show that Eu²⁺-doped samples of BaP₆N₁₀NH exhibit blue emission ($\lambda_{\text{emi}} = 460$ nm, $\text{fwhm} = 2423$ cm⁻¹) upon excitation with near UV to blue light and make the title compound the first luminescent imidonitride opening up this compound class for the research field of luminescence. Comparison of the observed values and additional thermal stability up to at least 1000 °C make BaP₆N₁₀NH, and imidonitridophosphates in general, promising candidates for new luminescent materials. Future studies may focus on more detailed investigations of the luminescence properties, for example the determination of the quantum efficiency in a Eu²⁺ concentration series.

BaP₆N₁₀NH also suggests the existence of isotopic compounds of the lighter alkaline earth metals in order to tune the emission. Additionally, more stoichiometric compositions among this compound class should be investigated due to their luminescence properties, as even these first investigations show interesting features without any optimization. This might also bring more insights concerning the assumption that the NH/N concentration may influence the luminescence properties of solid-state compounds.

2.4 Experimental Section

Synthesis of Ba(N₃)₂

Synthesis of Ba(N₃)₂ was carried out with a cation exchanger (Amberlyst 15), based on the synthesis by Suhrmann as modified by Karau.^[33, 34] Thereby, diluted HN₃ was formed in situ by passing an aqueous solution of NaN₃ (Acros Organics, 99%, extra pure) through the cation exchanger. Subsequently, the acidic solution of HN₃ was dropped carefully into a stirring suspension of BaCO₃ (Sigma Aldrich, 99.995%, trace metals basis) in H₂O. The end of the reaction is reached when the liquid phase turned completely clear. Excess BaCO₃ was filtered off and the filtrate was boiled down with a rotary evaporator (50 mbar, 40 °C). Ba(N₃)₂ was obtained as a colorless powder and recrystallized from acetone for purification. Finally, the product was dried under vacuum and its phase purity was confirmed by FTIR spectroscopy and X-ray diffraction.

Caution: Special care is necessary at handling HN₃, as even diluted solutions are potentially explosive. Additionally, poisoning threatens upon inhalation of HN₃ vapors.

Synthesis of P₃N₅

Following Stock und Grüneberg, P₄S₁₀ (ca. 8.0 g, Sigma Aldrich 99.99%) was treated in a tube furnace lined with a silica tube (Ø = 5 cm) by a constant flow of dried NH₃ (≈ 3.6 l h⁻¹, Air Liquide 5.0).^[35] Previously, a silica reaction vessel was placed in the reaction tube and the apparatus was dried under reduced pressure (< 10⁻³ mbar) for 4 h at 1000 °C. P₄S₁₀ was carefully loaded into the vessel under Ar counter-stream. At this point it is important to load a limited amount of the starting material, as otherwise there is danger to clog the silica tube by deposition of by-products. First, the

apparatus was purged with NH_3 for 4 h and then heated up to 850 °C within 3 h. The temperature was kept for 4 h and then decreased to room temperature within 3 h again. By flushing with Ar for 1 h the remaining NH_3 was removed. P_3N_5 was obtained as a pale orange product and washed with water, ethanol, and acetone. Phase purity and the absence of possible H containing species were verified by powder X-ray diffraction and FTIR spectroscopy.

High-pressure high-temperature synthesis of $\text{BaP}_6\text{N}_{10}\text{NH}$

$\text{BaP}_6\text{N}_{10}\text{NH}$ was synthesized applying a 1000 t press (Voggenreiter, Mainleus, Germany) with a modified Walker-type multianvil apparatus.^[18–22] The synthesis started from NH_4Cl , P_3N_5 , and $\text{Ba}(\text{N}_3)_2$. Phase-pure products required the surplus of NH_4Cl and $\text{Ba}(\text{N}_3)_2$. The precise amounts of the starting materials are given in the Supporting Information (Table A9). With $\text{Ba}(\text{N}_3)_2$ as an air-sensitive starting material, all manipulations were carried out in an argon-filled glovebox (Unilab, MBraun, Garching, $\text{O}_2 < 1$ ppm, $\text{H}_2\text{O} < 0.1$ ppm) under exclusion of oxygen and moisture. The mixture of the starting materials was ground thoroughly and packed into a cylindrical crucible made of hexagonal boron nitride (HeBoSint® S100, Henze, Kempten, Germany). The crucible was transferred into a Cr_2O_3 -doped (5%) MgO octahedron (edge length 18 mm, Ceramic Substrates & Components, Isle of Wight, UK), which served as pressure medium. The octahedron was drilled through centrally and filled up with a ZrO_2 sleeve (Cesima Ceramics, Wust-Fischbeck, Germany), a Mo plate, a MgO plate (Cesima Ceramics, Wust-Fischbeck, Germany) and two graphite tubes (Schunk Kohlenstofftechnik GmbH, Gießen, Germany). Thereby, the ZrO_2 sleeve serves as thermal insulator, MgO as spacer, and the combination of two thin graphite tubes with different lengths was used as electrical resistance furnaces with minimum temperature gradient. The Mo plate ensures the electrical contact of the graphite tubes to the surrounding setup. After inserting the crucible, the symmetric assembly was completed by sealing with a hexagonal boron nitride cap, a further MgO plate, and a second Mo plate, closing the circuit. The distribution of the uniaxial pressure, exerted by a 1000 t press, was handled by the usage of the mentioned Walker-type apparatus and an inserted setup of eight Co-doped (7%) WC cubes (Hawedia, Marklkofen, Germany) with truncated edges (edge length 11 mm). For electrical insulation, half of the latter were prepared with Bristol board (369 g m^{-2}) and half with a PTFE film (Vitaflon Technische Produkte GmbH, Bad Kreuznach, Germany). Pyrophyllite gaskets (Ceramic Substrates & Components, Isle of Wight, UK) were used

to avoid the outflow of the pressure medium.^[36] During synthesis BaP₆N₁₀NH was compressed to 4 GPa at room temperature and subsequently heated up to 1150 °C within 60 min. The temperature was held for further 60 min and then cooled down to room temperature within 180 min. After decompression of the setup the title compound was recovered as a colorless and crystalline solid, non-sensitive towards air and moisture.

Scanning electron microscopy (SEM) and energy-dispersive X-ray spectroscopy (EDX)

The investigations of the morphology and chemical composition of the title compound were performed on a Dualbeam Helios Nanolab G3 UC (FEI, Hillsboro) with a X-Max 80 SDD EDX detector (Oxford Instruments, Abingdon). Samples were fixed on adhesive carbon pads and additionally coated with carbon using an electron beam evaporator (BAL-TEC MED 020, Bal Tec AG), in order to provide electrical conductivity.

Transmission electron microscopy (TEM)

A small part of the sample was ground in an agate mortar, suspended in absolute ethanol and then drop-cast on a copper finder grid (S160NH2C, PLANO GmbH, Wetzlar). Crystals were selected using a FEI Tecnai G20 transmission electron microscope (TEM) with thermal emitter (LaB₆) operating at 200 keV. SAED patterns and bright-field images were recorded using a TVIPS camera. The elemental composition of individual crystallites was investigated by energy-dispersive X-ray spectroscopy (EDX, EDAX Apollo XLT detector). Bright-field images of the crystals at different magnifications aided in positioning the crystallites in the synchrotron beam.

Single-crystal X-ray diffraction

Single-crystal diffraction data were collected at ID11, ESRF, Grenoble, on a Symétrie Hexapods Nanopos device ($\lambda = 0.309 \text{ \AA}$), after recovering the preselected crystal by optical centering and fluorescence scans. The collected data were integrated with CrysAlisPro and SADABS was used for semiempirical absorption correction.^[37, 38] A correction for incomplete absorption of X-ray radiation in the phosphor of the CCD detector was applied as well.^[39] The program package SHELX-2014 was used for structure determination and least-squares refinement.^[40]

CCDC 1942108 contains the supplementary crystallographic data for this paper. These data are provided free of charge by The Cambridge Crystallographic Data Centre / FIZ Karlsruhe joint deposition service.

CHNS analysis

A Vario Micro Cube device (Elementar, Langensfeld, Germany) was used to perform elemental analysis.

FTIR spectroscopy

A sample of BaP₆N₁₀NH was ground with KBr and compressed to a disk. An IFS 66 v/S spectrometer (Bruker, Karlsruhe, Germany) was used to record the FTIR spectrum.

Powder X-ray diffraction

A Stadi P powder diffractometer (STOE, Darmstadt, Germany) was used to collect data in parafocussing Debye–Scherer geometry. The diffractometer was equipped with a Ge(111) monochromator (Mo-K_{α1} radiation) and a MYTHEN 1 K Si strip detector (Dectris, Baden, Switzerland; angular range $\Delta 2\theta = 12.5^\circ$). Samples were filled into a glass capillary with 0.3 mm diameter and a wall-thickness of 0.01 mm (Hilgenberg GmbH, Malsfeld, Germany) for executing measurements. Rietveld refinements were carried out with the TOPAS Academic 6.1 package, using the fundamental parameters approach (direct convolution of source emission profiles, axial instrument contributions, and crystallite size and microstrain effects).^[41] While the background was modeled with a shifted Chebychev function, a fourth-order spherical harmonics model was applied to describe the potential preferred orientation of the block-like crystallites.

Solid-state NMR spectroscopy

The ¹H resonance of 1% Si(CH₃)₄ in CDCl₃ was used as an external secondary reference, using the δ value for ³¹P relative to 85% H₃PO₄ as reported by the IUPAC.^[42] The solid-state MAS NMR experiments were carried out on a DSX Avance 500 spectrometer (Bruker, Karlsruhe, Germany) equipped with a commercial double-resonance MAS probe, operating at a field strength of 11.7 T

with a 2.5 mm ZrO₂ rotor at a spinning frequency of 50 kHz. Relaxation times were determined by saturation recovery measurements.

UV/Vis Spectroscopy

Diffuse reflectance UV/Vis spectroscopy measurements were performed on a Jasco V-650 UV/vis spectrophotometer with a deuterium and a halogen lamp (JASCO, Pfungstadt, Germany, Czerny-Turner monochromator with 1200 lines mm⁻¹, concave grating, photomultiplier tube detector).

Luminescence

For luminescence measurements, small particles of Eu²⁺-doped samples of BaP₆N₁₀NH were sealed in fused silica capillaries. The measurements were performed on a HORIBA Fluoromax4 spectrofluorimeter system, connected to an Olympus BX51 microscope via optical fibers. The excitation wavelength was $\lambda_{\text{exc}} = 420$ nm and the emission spectra were recorded in a range from 400 to 800 nm with a step size of 2 nm.

2.5 Acknowledgements

We thank Christian Minke for EDX and NMR measurements. Furthermore, we thank Dr. Thomas Bräuniger (both at Department of Chemistry of LMU Munich) for help with NMR experiments. Moreover, we thank Volker Weiler (Lumileds Phosphor Center Aachen) for performing luminescence measurements. We also thank the ESRF, Grenoble, for granting beamtime (project CH-5149). Dr. Christopher Benndorf, Markus Nentwig and Christina Fraunhofer are acknowledged for help during the beamtime.

2.6 References

- [1] S. D. Kloß, W. Schnick, "Nitridophosphates – A Success Story of Nitride Synthesis", *Angew. Chem. Int. Ed.* **2019**, 58, 7933-7944; *Angew. Chem.* **2019**, 131, 8015-8027.
- [2] S. Horstmann, E. Irran, W. Schnick, "Phosphor(V)-nitrid α - P_3N_5 : Synthese ausgehend von Tetraaminphosphoniumiodid und Kristallstrukturaufklärung mittels Synchrotron-Pulver-Röntgenbeugung", *Z. Anorg. Allg. Chem.* **1998**, 624, 620-628.
- [3] S. Horstmann, E. Irran, W. Schnick, "Synthesis and Crystal Structure of Phosphorus(V) Nitride α - P_3N_5 ", *Angew. Chem. Int. Ed. Engl.* **1997**, 36, 1873-1875; *Angew. Chem.* **1997**, 109, 1938-1940.
- [4] K. Landskron, H. Huppertz, J. Senker, W. Schnick, "High-Pressure Synthesis of γ - P_3N_5 at 11 GPa and 1500 °C in a Multianvil Assembly: A Binary Phosphorus(V) Nitride with a Three-Dimensional Network Structure from PN_4 Tetrahedra and Tetragonal PN_5 Pyramids", *Angew. Chem. Int. Ed.* **2001**, 40, 2643-2645; *Angew. Chem.* **2001**, 113, 2713-2716.
- [5] S. Horstmann, E. Irran, W. Schnick, "Phosphorus(V) Nitride Imide HP_4N_7 : Synthesis from a Molecular Precursor and Structure Determination with Synchrotron Powder diffraction", *Angew. Chem. Int. Ed. Engl.* **1997**, 36, 1992-1994; *Angew. Chem.* **1997**, 109, 2085-2087.
- [6] D. Baumann, W. Schnick, "High-Pressure Polymorph of Phosphorus Nitride Imide HP_4N_7 Representing a New Framework Topology", *Inorg. Chem.* **2014**, 53, 7977-7982.
- [7] D. Baumann, W. Schnick, "Pentacoordinate Phosphorus in a High-Pressure Polymorph of Phosphorus Nitride Imide $P_4N_6(NH)$ ", *Angew. Chem. Int. Ed. Engl.* **2014**, 53; *Angew. Chem.* **2014**, 126, 14718-14721.
- [8] S. Wendl, W. Schnick, " $SrH_4P_6N_{12}$ and SrP_8N_{14} : Insights into the Condensation Mechanism of Nitridophosphates under High Pressure", *Chem. Eur. J.* **2018**, 24, 15889-15896.
- [9] Superscripted numbers in square brackets following element symbols denote coordination numbers.
- [10] F. J. Pucher, A. Marchuk, P. J. Schmidt, D. Wiechert, W. Schnick, "Luminescent Nitridophosphates $CaP_2N_4:Eu^{2+}$, $SrP_2N_4:Eu^{2+}$, $BaP_2N_4:Eu^{2+}$, and $BaSr_2P_6N_{12}:Eu^{2+}$ ", *Chem. Eur. J.* **2015**, 21, 6443-6448.

- [11] A. Marchuk, S. Wendl, N. Imamovic, F. Tambornino, D. Wiechert, P. J. Schmidt, W. Schnick, "Nontypical Luminescence Properties and Structural Relation of Ba₃P₅N₁₀X:Eu²⁺ (X = Cl, I): Nitridophosphate Halides with Zeolite-like Structure", *Chem. Mater.* **2015**, 27, 6432-6441.
- [12] A. Marchuk, W. Schnick, "Ba₃P₅N₁₀Br:Eu²⁺: A Natural-White-Light Single Emitter with a Zeolite Structure Type", *Angew. Chem. Int. Ed.* **2015**, 54, 2383-2387; *Angew. Chem.* **2015**, 127, 2413-2417.
- [13] H. Jacobs, F. Golinski, "Synthesis and Crystal Structure of a Cesium-tetraimidophosphate-diamide, Cs₅[P(NH)₄](NH₂)₂ = Cs₃[P(NH)₄] · 2 CsNH₂", *Z. Anorg. Allg. Chem.* **1994**, 620, 531-534.
- [14] F. Golinski, H. Jacobs, "Synthesis and Crystal Structure of Rb₈[P₄N₆(NH)₄](NH₂)₂ with the Adamantane-like Anion [P₄N₆(NH)₄]⁶⁻", *Z. Anorg. Allg. Chem.* **1995**, 621, 29-33.
- [15] H. Jacobs, S. Pollok, F. Golinski, "Synthesis and Crystal Structure of Na₁₀[P₄(NH)₆N₄](NH₂)₆(NH₃)_{0.5} with an Adamantane-like Anion [P₄(NH)₆N₄]⁴⁻", *Z. Anorg. Allg. Chem.* **1994**, 620, 1213-1218.
- [16] S. Vogel, W. Schnick, "SrP₃N₅NH: A Framework-Type Imidonitridophosphate Featuring Structure-Directing Hydrogen Bonds", *Chem. Eur. J.* **2018**, 24, 14275-14281.
- [17] A. Marchuk, V. R. Celinski, J. Schmedt auf der Günne, W. Schnick, "MH₄P₆N₁₂ (M = Mg, Ca): New Imidonitridophosphates with an Unprecedented Layered Network Structure Type", *Chem. Eur. J.* **2015**, 21, 5836-5842.
- [18] N. Kawai, S. Endo, "The Generation of Ultrahigh Hydrostatic Pressures by a Split Sphere Apparatus", *Rev. Sci. Instrum.* **1970**, 41, 1178-1181.
- [19] D. Walker, M. A. Carpenter, C. M. Hitch, "Some simplifications to multianvil devices for high pressure experiments", *Am. Mineral.* **1990**, 75, 1020-1028.
- [20] D. Walker, "Lubrication, gasketing, and precision in multianvil experiments", *Am. Mineral.* **1991**, 76, 1092-1100.
- [21] D. C. Rubie, "Characterising the sample environment in multianvil high-pressure experiments", *Phase Transitions* **1999**, 68, 431-451.
- [22] H. Huppertz, "Multianvil high-pressure / high-temperature synthesis in solid state chemistry", *Z. Kristallogr.* **2004**, 219, 330-338.

- [23] F. Fahrnbauer, T. Rosenthal, T. Schmutzler, G. Wagner, G. B. M. Vaughan, J. P. Wright, O. Oeckler, "Discovery and Structure Determination of an Unusual Sulfide Telluride through an Effective Combination of TEM and Synchrotron Microdiffraction", *Angew. Chem. Int. Ed.* **2015**, *54*, 10020-10023; *Angew. Chem.* **2015**, *127*, 10158-10161.
- [24] F. Karau, W. Schnick, "High-Pressure Synthesis of $\text{BaSr}_2\text{P}_6\text{N}_{12}$ and $\text{BaCa}_2\text{P}_6\text{N}_{12}$ and Comparison of the Structures of BaP_2N_4 , $\text{BaCa}_2\text{P}_6\text{N}_{12}$ and $\text{BaSr}_2\text{P}_6\text{N}_{12}$ ", *Z. Anorg. Allg. Chem.* **2006**, *632*, 231-237.
- [25] V. A. Blatov, A. P. Shevchenko, D. M. Proserpio, "Applied Topological Analysis of Crystal Structures with the Program Package ToposPro", *Cryst. Growth Des.* **2014**, *14*, 3576-3586.
- [26] R. Shannon, "Revised effective ionic radii and systematic studies of interatomic distances in halides and chalcogenides", *Acta Crystallogr. Sect. A* **1976**, *32*, 751-767.
- [27] S. J. Sedlmaier, D. Weber, W. Schnick, "Crystal structure of barium oxonitridophosphate, $\text{Ba}_3\text{P}_6\text{O}_6\text{N}_8$ ", *Z. Kristallogr. New Cryst. Struct.* **2012**, *227*, 1-2.
- [28] R. López, R. Gómez, "Band-gap energy estimation from diffuse reflectance measurements on sol-gel and commercial TiO_2 : a comparative study", *J. Sol-Gel Sci. Technol.* **2012**, *61*, 1-7.
- [29] J. Tauc, R. Grigorovici, A. Vancu, "Optical Properties and Electronic Structure of Amorphous Germanium", *Phys. Status Solidi B* **1966**, *15*, 627-637.
- [30] V. L. Ermolaev, E. B. Sveshnikova, "The application of luminescence-kinetic methods in the study of the formation of lanthanide ion complexes in solution", *Russ. Chem. Rev.* **1994**, *63*, 905-922.
- [31] E. Kreidt, C. Kruck, M. Seitz, *Handbook on the Physics and Chemistry of Rare Earths*, Elsevier, Amsterdam, **2018**, pp. 35-79.
- [32] C. Doffek, N. Alzakhem, C. Bischof, J. Wahsner, T. Güden-Silber, J. Lügger, C. Platas-Iglesias, M. Seitz, "Understanding the Quenching Effects of Aromatic C-H- and C-D-Oscillators in Near-IR Lanthanoid Luminescence", *J. Am. Chem. Soc.* **2012**, *134*, 16413-16423.
- [33] F. W. Karau, *Dissertation*, Ludwig-Maximilians-Universität München (Germany) **2007**.
- [34] R. Suhrmann, K. Clusius, "Über die Reindarstellung der Alkalimetalle", *Z. Anorg. Allg. Chem.* **1926**, *152*, 52-58.
- [35] A. Stock, H. Grüneberg, "Über den Phosphorstickstoff", *Ber. Dtsch. Chem. Ges.* **1907**, *40*, 2573-2578.

- [36] H. Huppertz, *Habilitationsschrift*, Ludwig-Maximilians-Universität München (Germany) **2003**.
- [37] Agilent Technologies, *CrysAlis Pro*, Yarnton, Oxfordshire, England, **2011**.
- [38] Bruker AXS, Inc., *SADABS*, Madison, Wisconsin, USA, **2001**.
- [39] G. Wu, B. L. Rodrigues, P. Coppens, "The correction of reflection intensities for incomplete absorption of high-energy X-rays in the CCD phosphor", *J. Appl. Crystallogr.* **2002**, 35, 356-359.
- [40] G. M. Sheldrick, "SHELXT - Integrated space-group and crystal-structure determination", *Acta Crystallogr. Sect. C* **2015**, 71, 3-8.
- [41] A. A. Coelho, *TOPAS Academic*, Version 6, Coelho Software, Brisbane, Australia, **2016**.
- [42] R. K. Harris, E. D. Becker, S. M. C. d. Menezes, P. Granger, R. E. Hoffman, K. W. Zilm, "Further conventions for NMR shielding and chemical shifts (IUPAC Recommendations 2008)", *Pure Appl. Chem.* **2008**, 80, 59-84.

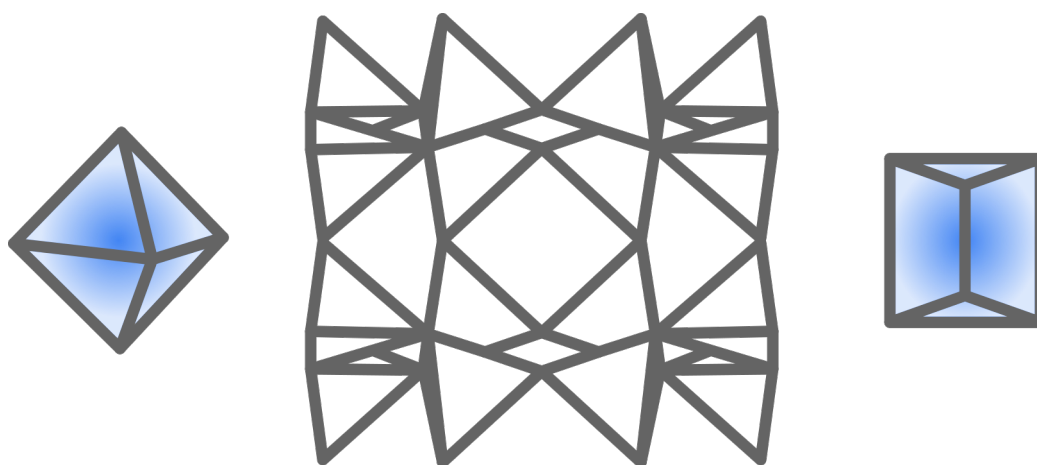
3 Nitridophosphate-Based Ultra-Narrow-Band Blue-Emitters: Luminescence Properties of $AEP_8N_{14}:Eu^{2+}$ ($AE = Ca, Sr, Ba$)

*Sebastian Wendl, Lucien Eisenburger, Dr. Philipp Strobel, Daniel Günther, Dr. Jonathan P. Wright,
Dr. Peter J. Schmidt, Prof. Dr. Oliver Oeckler, Prof. Dr. Wolfgang Schnick*

Chem. Eur. J. **2020**, *26*, 7292–7298.

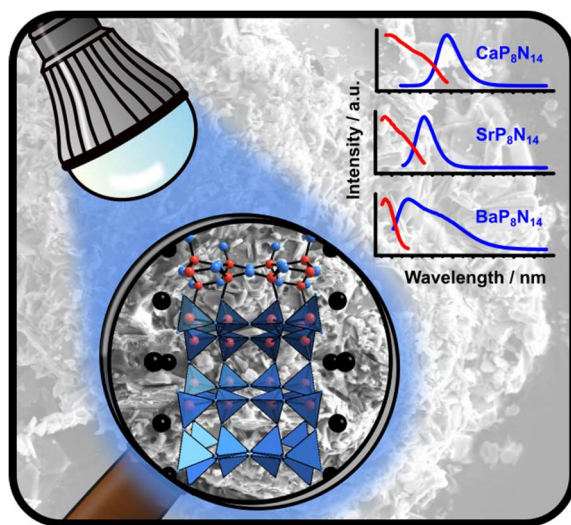
DOI: 10.1002/chem.202001129

Reprinted (adapted) with permission for non-commercial use from *Chemistry – A European Journal* (open access). Copyright 2021 John Wiley and Sons.



Ultra-narrow-band blue-emitters: Ternary alkaline earth metal nitridophosphates AEP_8N_{14} ($AE = Ca, Sr, Ba$) were prepared under HP/HT conditions starting from P_3N_5 , and the respective alkaline earth metal azides $AE(N_3)_2$. AEP_8N_{14} shows the hitherto highest degree of condensation ($\kappa \approx 0.57$) among AE/P/N compounds. Excitation with UV to blue light rendered $CaP_8N_{14}:Eu^{2+}$ and $SrP_8N_{14}:Eu^{2+}$ the first P/N-based ultra-narrow-band blue-emitters.

Abstract: The nitridophosphates AEP_8N_{14} ($AE = Ca, Sr, Ba$) were synthesized at 4–5 GPa and 1050–1150 °C applying a 1000 t press with multianvil apparatus, following the azide route. The crystal structures of CaP_8N_{14} and SrP_8N_{14} are isotopic. The space group $Cmcm$ was confirmed by powder X-ray diffraction. The structure of BaP_8N_{14} (space group $Amm2$) was elucidated by a combination of transmission electron microscopy and diffraction of microfocused synchrotron radiation. Phase purity was confirmed by Rietveld refinement. IR spectra are consistent with the structure models and the chemical compositions were confirmed by X-ray spectroscopy.



Luminescence properties of Eu^{2+} -doped samples were investigated upon excitation with UV to blue light. CaP_8N_{14} ($\lambda_{em}=470$ nm; $fwhm=1380$ cm^{-1}) and SrP_8N_{14} ($\lambda_{em}=440$ nm; $fwhm=1350$ cm^{-1}) can be classified as the first ultra-narrow-band blue-emitting Eu^{2+} -doped nitridophosphates. BaP_8N_{14} shows a notably broader blue emission ($\lambda_{em}=417/457$ nm; $fwhm=2075$ 3550 cm^{-1}).

3.1 Introduction

The importance of advanced, highly efficient phosphor materials is continuously growing, as phosphor-converted light-emitting diodes (pc-LEDs) have revolutionized the global lighting market with increased durability, colour rendering and enormous energy savings. This technique uses blue-emitting primary LEDs, mostly based on InGaN, which are coated with phosphors to achieve emission of white light by colour mixing. Demands on potential coatings are manifold and reach from chemical and thermal stability, efficient absorption of blue light (primary LED) over optical transparency and a small Stokes shift to high quantum efficiency and low thermal quenching.^[1]

The most common coating for pc-LEDs is the oxide phosphor YAG:Ce ($Y_{3-x}Gd_xAl_{5-x}Ga_yO_{12}:Ce^{3+}$).^[2,3] Eu^{2+} -doped nitrides, however, show intense broad-band emission upon excitation with UV to blue light due to the parity-allowed $4f^65d^1 \rightarrow 4f^7(^8S_{7/2})$ transition. (Oxo)nitridosilicates especially, have turned out to meet the above listed demands. $AE_2Si_2O_2N_2:Eu^{2+}$, $AE_2Si_5N_8:Eu^{2+}$, and the so far narrowest nitride-based Eu^{2+} red emitter $Sr[Mg_3SiN_4]:Eu^{2+}$ have to be mentioned in this context.^[4-8] Over the years, research on new phosphors expanded to a range of related compound classes, such as nitridoalumosilicates and nitridolithoaluminates, with $Ca[AlSiN_3]:Eu^{2+}$ and $Sr[LiAl_3N_4]:Eu^{2+}$ showing highly efficient red emission.^[9,10] Recently, beryllium-containing nitrides have been shown to feature extremely narrow-band emissions in the blue to cyan spectral region.^[11-13]

Nitridophosphates have repeatedly been discussed as phosphor materials as well, but only very few examples are known so far. The corresponding crystal structures are built up from anionic PN_4 tetrahedra networks that host the cations.^[14] Among ternary all-nitride representatives, only $AEP_2N_4:Eu^{2+}$ ($AE = Ca, Sr, Ba$) and $Sr_3P_3N_7:Eu^{2+}$ are known.^[15,16] However, these few members illustrate the versatility of nitridophosphates, as they cover a major part of the visible spectrum ($\lambda_{emi} = 450-680$ nm) and also feature high quantum efficiencies even for non-optimized powder samples.^[15-18] The great potential of nitridophosphates is underlined by zeolite-like compounds $Ba_3P_5N_{10}X:Eu^{2+}$ ($X = Cl, Br, I$), of which $Ba_3P_5N_{10}Br:Eu^{2+}$ has to be highlighted, as it has been discussed as a natural-white-light single emitter.^[17,18]

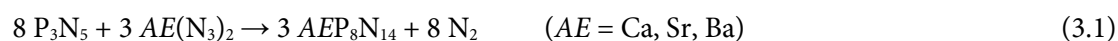
Fundamental research on nitridophosphates has established various synthetic approaches as recently reviewed in literature.^[14] Alkaline earth nitridophosphates are commonly prepared in high-pressure high-temperature reactions starting from P_3N_5 and the respective alkaline earth azide.^[17–20] High-pressure conditions prevent the thermal decomposition of P_3N_5 that otherwise starts at 850 °C and high-temperature enables the reversible cleavage and formation of P–N bonds.^[21]

In our previous work, we have reported on synthesis of highly condensed SrP_8N_{14} following the azide route.^[20] Considering its crystal structure, which features octahedrally coordinated Sr atom sites, SrP_8N_{14} and structurally related compounds appear as candidates for promising luminescence properties. In this contribution, we expand the AEP_8N_{14} system by the new compounds CaP_8N_{14} and BaP_8N_{14} , and discuss structural relations within this series of nitridophosphates. Furthermore, we present intriguing luminescence properties of all three Eu^{2+} -doped compounds that classify $AEP_8N_{14}:Eu^{2+}$ as the first P/N-based ultra-narrow-band blue-light emitters.

3.2 Results and Discussion

Synthesis

The nitridophosphates AEP_8N_{14} ($AE = Ca, Sr, Ba$) were synthesized by high-pressure high-temperature reactions at 4–5 GPa and 1050–1150 °C, using a modified Walker-type multianvil apparatus.^[22–26] The syntheses follow the azide route, starting from P_3N_5 and the respective metal azide (Equation 3.1). In order to investigate luminescence properties, Eu^{2+} -doped samples were obtained by addition of minor amounts of $EuCl_2$ (≈ 3 mole%) to the mixture of starting materials.



White (AEP_8N_{14}) and yellowish ($AEP_8N_{14}:Eu^{2+}$) products have been formed as microcrystalline powders and appeared stable against treatment with air and water (Figure 3.1).

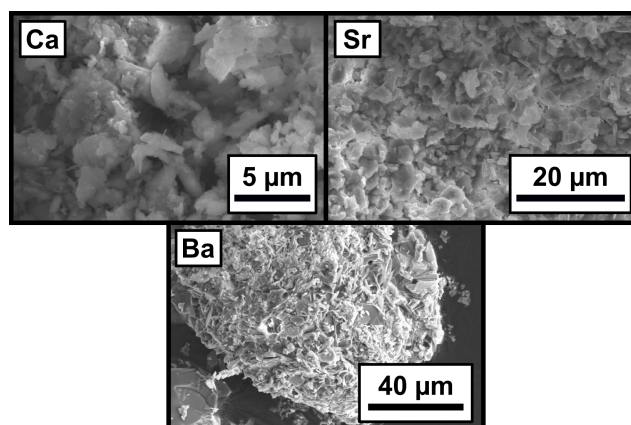


Figure 3.1. SEM images of $AEP_8N_{14}:Eu^{2+}$ ($AE=Ca, Sr, Ba$), illustrating the microcrystalline character of the samples.

Structure elucidation

Owing to the lack of suitable single crystals, the structure of CaP_8N_{14} was refined from powder X-ray diffraction data employing the Rietveld method, where the published structure model of SrP_8N_{14} served as starting model (Figure 3.2).^[20] The Rietveld method was further used to confirm phase purity of obtained SrP_8N_{14} (Figure 3.2). During refinement all atoms were refined with isotropic displacement parameters, using equal values for P and N atoms, respectively. Atomic coordinates and isotropic displacement parameters are listed in Tables B1 and B2 in Supporting Information. Detailed crystallographic information on the refinements of CaP_8N_{14} and SrP_8N_{14} is provided in Table B3. Further details on CaP_8N_{14} can be obtained from the Fachinformationszentrum Karlsruhe (FIZ) by quoting the deposition number CSD 1979592 via www.ccdc.cam.ac.uk/structures.

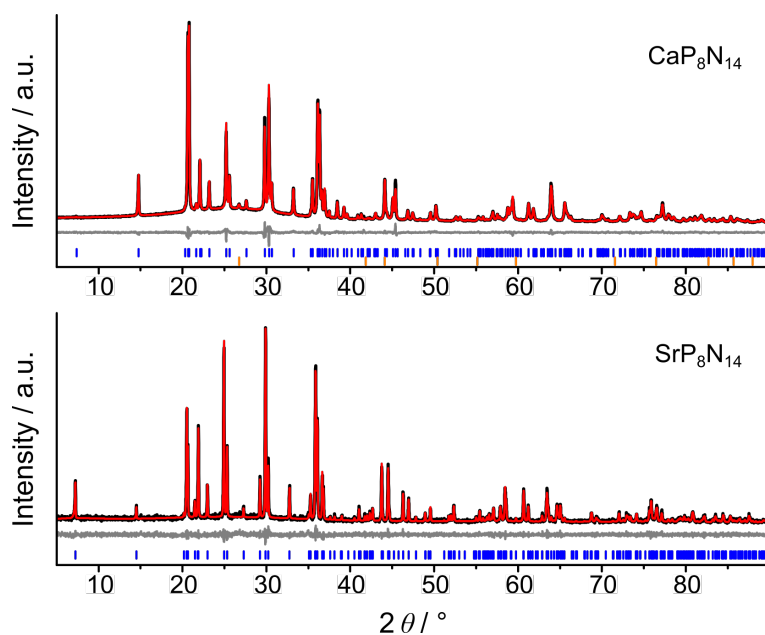


Figure 3.2. Rietveld refinements for CaP_8N_{14} and SrP_8N_{14} : observed (black, $Cu-K\alpha_1$) and calculated (red) powder X-ray diffraction patterns are displayed with corresponding difference profiles (gray). Vertical blue bars mark the Bragg reflections of the title compounds, orange bars mark the Bragg positions of h-BN (crucible material) that appeared as a minor side phase of CaP_8N_{14} .

At first glance, the PXRD pattern of BaP_8N_{14} bears similarities with those of AEP_8N_{14} ($AE = Ca, Sr$) (Figure B1). However, corresponding Rietveld refinement did not yield reasonable results. Hence, a combination of transmission electron microscopy (TEM) and diffraction of microfocused synchrotron radiation was used for structure determination as described in previous works.^[27,28] For this purpose, micron-sized crystals of BaP_8N_{14} were identified on a TEM grid by EDX analysis and selected area electron diffraction. Their precise positions were recorded (Figure B2) and single-crystal X-ray diffraction data were collected at the ESRF (beamline ID11) using a microfocused synchrotron beam (diameter $\approx 1 \times 2 \mu m$).

The crystal structure of BaP_8N_{14} was solved and refined in orthorhombic space group $Amm2$ (no. 38) with unit cell dimensions $a = 12.4862(7)$, $b = 8.6648(3)$ and $c = 5.1373(2)$ Å. All atoms were refined anisotropically. Crystallographic data are summarized in the Supporting Information (Tables B4–B6) and can be obtained from the Fachinformationszentrum Karlsruhe (FIZ) by quoting the deposition number CSD 1980141 via www.ccdc.cam.ac.uk/structures.

The refined structure model was used to verify the phase purity of BaP_8N_{14} by Rietveld refinement (Figure 3.3). More information on the Rietveld refinement for BaP_8N_{14} is provided in Table B7.

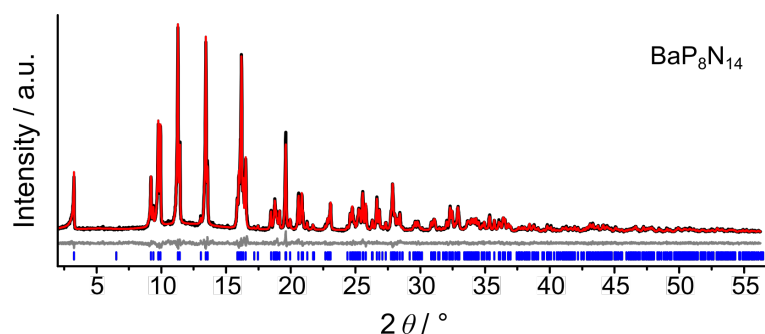


Figure 3.3. Rietveld refinement for BaP₈N₁₄:Eu²⁺; observed (black, Mo-K_α) and refined (red) diffraction pattern. The difference profile is displayed in gray. Positions of Bragg reflections of BaP₈N₁₄ are marked with vertical blue bars.

The chemical compositions of the title compounds were confirmed by energy-dispersive X-ray spectroscopy (EDX, Tables B8–B10). The spectra show trace amounts of oxygen, which may be attributed to partial surface hydrolysis during water treatment.

Fourier-transform infrared spectroscopy demonstrates the absence of N–H groups (Figures B4). The spectra feature only vibrations in the fingerprint region (400–1500 cm⁻¹) and do not indicate N–H valence modes.

Structure description

The compounds AEP₈N₁₄ (AE = Ca, Sr, Ba) can be classified as highly condensed nitridophosphates with a degree of condensation $\kappa = 8/14 \approx 0.57$, which is defined by the ratio of tetrahedra centres $n(\text{P}) = 8$ to the number of N atoms $n(\text{N}) = 14$. All title compounds feature quadruple layers that are separated by metal atoms (Figure 3.4). A more detailed description of the layered structure is provided in literature and the Supporting Information (Figure B5).^[20] The structure types of AEP₈N₁₄ (AE = Ca, Sr) and BaP₈N₁₄ differ with respect to the stacking pattern of the quadruple layers. In CaP₈N₁₄ and SrP₈N₁₄, these layers are related by rotation according to a 2₁ screw axis along [001] and by inversion symmetry. In the non-centrosymmetric structure of BaP₈N₁₄, however, they are related by a mirror plane \parallel (001) (Figure 3.4), resulting in a unit cell with half volume.

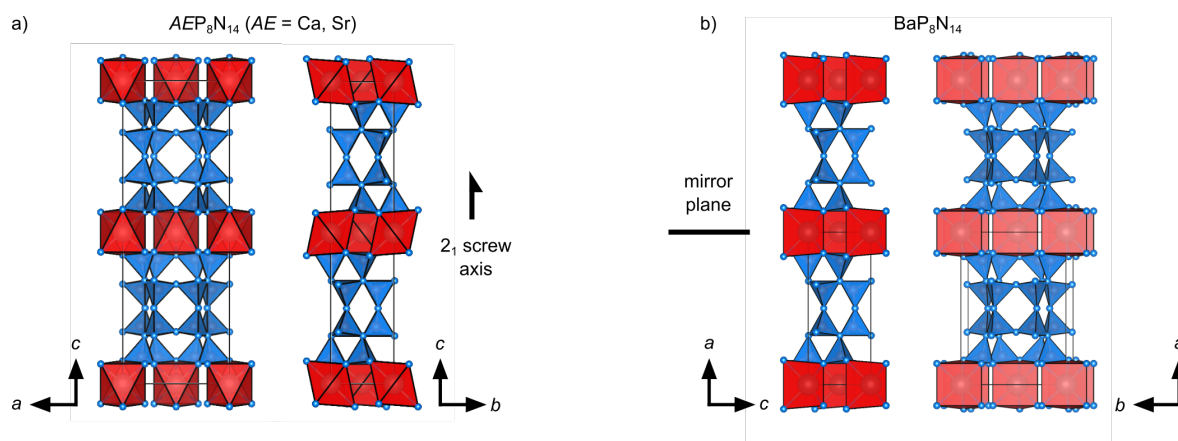


Figure 3.4. a) Projection of the crystal structure of AEP_8N_{14} ($AE = Ca, Sr$) along $[010]$ and $[100]$; b) projection of the crystal structure of BaP_8N_{14} along $[010]$ and (approximately) $[001]$. The structural relation of neighboring quadruple layers is indicated by the respective symmetry elements. PN_4 tetrahedra are displayed in blue, AEN_6 polyhedra in red. N atoms are depicted as blue spheres.

In CaP_8N_{14} and SrP_8N_{14} , the alkaline earth atom occupies one crystallographic site, that is octahedrally coordinated by N atoms with mean interatomic distances $AE-N$ of 2.55 and 2.70 Å, respectively. In contrast, Ba occupies one crystallographic site, as well, but is located in a trigonal-prismatic coordination with a mean interatomic $Ba-N$ distance of 2.83 Å. All observed $AE-N$ distances are in good agreement with values of other known nitridophosphates as well as with the sums of the ionic radii.^[15, 17, 18, 20, 29–31] This change of the coordination sphere is reminiscent of the AEP_8N_{14} ($AE = Mg, Ca, Sr$) compounds.^[20, 30] More detailed information on the coordination spheres in AEP_8N_{14} is provided in the Supporting Information (Figure B6 and Tables B11–B13).

For all title compounds, the P–N distances and N–P–N angles vary between 1.540(2)–1.737(4) Å and 103.1(2)–122.2(1)°, respectively, which is in good agreement with other nitridophosphates (Tables B11–B13).^[15, 17, 18, 20, 29–31] The P–N distances dominate the coordination environments for N atoms with shorter distances for P–N^[2] and slightly larger ones for P–N^[3].^[32]

Temperature dependent X-ray diffraction (HTXRD)

For the highly condensed nitridophosphates AEP_8N_{14} ($AE = Ca, Sr, Ba$), significant thermal stability can be expected, considering the highly covalent character of the P–N network. Therefore, temperature dependent X-ray diffraction was carried out between room temperature and 950 °C (Figures B7–B9). The compounds are stable over this temperature range and diffraction patterns show nothing but a linear increase of lattice parameters (Figures B7–B12). A quantification of the respective thermal expansion was derived by Rietveld refinements for selected temperatures. It reveals an increase in volume of 1.0% to 1.8% with respect to ambient temperature (Tables B14 and B15).

Luminescence

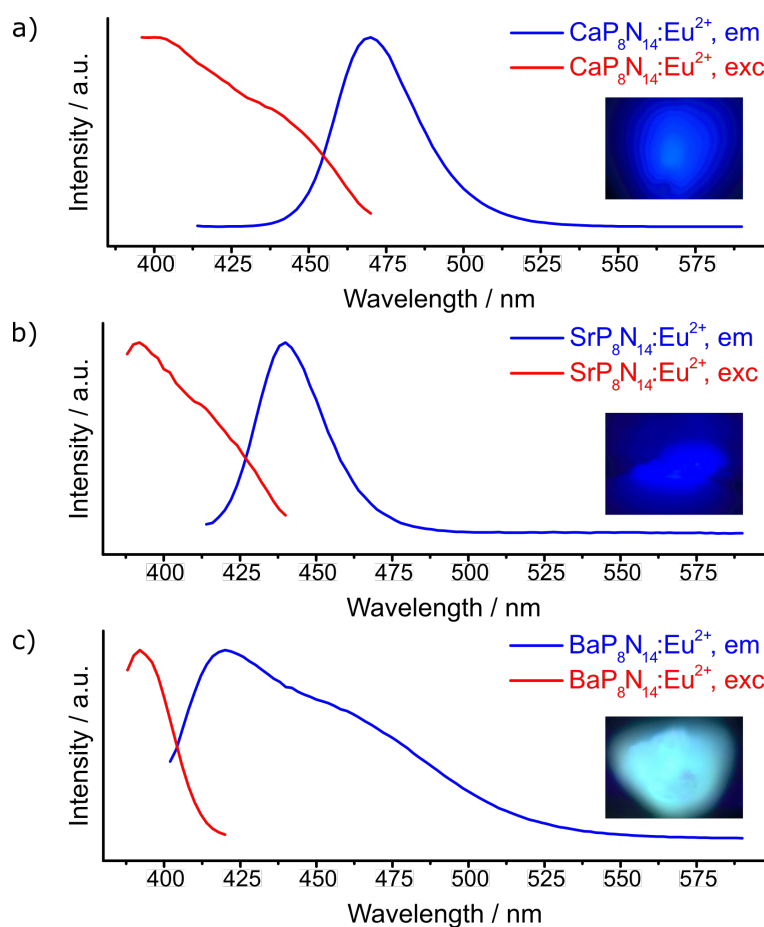


Figure 3.5. Normalized excitation (red) and emission spectra (blue) of $CaP_8N_{14}:Eu^{2+}$ (a), $SrP_8N_{14}:Eu^{2+}$ (b), and $BaP_8N_{14}:Eu^{2+}$ (c) measured at room temperature with respective micrographs of the measured crystals; $\lambda_{exc}(CaP_8N_{14}:Eu^{2+})$, $\lambda_{exc}(SrP_8N_{14}:Eu^{2+}) = 400$ nm, $\lambda_{exc}(BaP_8N_{14}:Eu^{2+}) = 390$ nm.

Considering the structural features as well as the chemical and thermal stability, AEP_8N_{14} ($AE = Ca, Sr, Ba$) appeared as promising host materials for phosphors, and thus were doped with Eu^{2+} (nominal ≈ 3 mole% referred to AE^{2+}) to investigate their luminescence properties. Upon excitation with near-UV to blue light, particles of all compounds show blue emission. Figures 3.5a and b show the excitation and emission spectra for $CaP_8N_{14}:Eu^{2+}$ and $SrP_8N_{14}:Eu^{2+}$, respectively. According to a single crystallographic site for AE^{2+} , on which Eu^{2+} is expected to be localized, both compounds show only one emission band. Corresponding emission wavelengths ($\lambda_{em}(CaP_8N_{14}:Eu^{2+}) = 470$ nm; $\lambda_{em}(SrP_8N_{14}:Eu^{2+}) = 440$ nm) are comparable with other alkaline earth nitridophosphates, for example, $BaP_2N_4:Eu^{2+}$ ($\lambda_{em} = 454$ nm), despite the different coordination spheres of the activator ions (Table 3.1). Considering the fwhm of 1380 cm^{-1} (31 nm) and 1350 cm^{-1} (26 nm), respectively, $CaP_8N_{14}:Eu^{2+}$ and $SrP_8N_{14}:Eu^{2+}$ can be classified as the first P/N-based ultra-narrow-band blue emitters and can compete with related (oxo)nitridoberyllate and -silicate phosphors.^[4, 11–13]

In contrast to $CaP_8N_{14}:Eu^{2+}$ and $SrP_8N_{14}:Eu^{2+}$, $BaP_8N_{14}:Eu^{2+}$ shows a rather broad emission band at 417 nm (fwhm = 36 nm/2075 cm^{-1}) next to a significantly wider band at ≈ 457 nm (fwhm = 74 nm/3350 cm^{-1} , Figure 3.5c). In order to elucidate the maxima and fwhm of this emission, the spectrum was deconvoluted with two pseudo-Voigt functions (Figure B13; $\lambda_{em1} = 417$ nm, $fwhm_1 = 36$ nm/2075 cm^{-1} , $\lambda_{em2} = 457$ nm, $fwhm_2 = 74$ nm/3350 cm^{-1}). The position of the first band fits well to the series of $AEP_8N_{14}:Eu^{2+}$ ($AE = Ca, Sr$) and is assigned to the one Ba site in BaP_8N_{14} . The second emission band can be explained by the comparison of the excitation spectra monitored at different wavelengths ($\lambda_{mon} = 425$ –516 nm; Figure B14). Due to the very similar spectra for different λ_{mon} , the second emission band can unambiguously be assigned to the title compound as well, indicating large Stokes shifted impurity trapped exciton emission. Similar effects have already been observed for Ba compounds in literature.^[33] The assumption that this artefact might be caused by a side phase can be excluded, as the emission band was observed in several phase-pure samples (Figure B15). The different relative intensities of the two emission bands in the different samples are most likely attributable to different excitation wavelengths (Figure B15). Characteristic parameters of the luminescent properties of $AEP_8N_{14}:Eu^{2+}$ ($AE = Ca, Sr, Ba$) are listed in Table 3.1, providing a brief comparison with other relevant blue phosphors.

Table 3.1. Comparison of the luminescence properties at room temperature of $AEP_8N_{14}:Eu^{2+}$ ($AE = Ca, Sr, Ba$) with selected blue-emitting Eu^{2+} -doped (oxo)nitride materials.

Compound	CN	λ_{em} / nm	λ_{exc} / nm	fwhm / nm	fwhm / cm^{-1}	Reference
CaP_8N_{14}	6	470	400	31	1380	This work
SrP_8N_{14}	6	450	400	26	1350	This work
BaP_8N_{14}	6	417	390	36	2075	This work
		457		~74	3550	
BaP_2N_4	12	454	400	47	2244	[15]
$BaSr_2P_6N_{12}$	12	456	400	47	2240	[15]
$BaP_6N_{10}NH$	13	460	420	52	2423	[28]
$SrSi_6N_8$	10	450	370	44	-	[37]
$SrBe_{20}N_{14}$	12	428	380	22	1180	[11]
		540		> 100	-	
$BaBe_{20}N_{14}$	12	426	380	25	1310	[11]
		530		> 110	-	
$SrBe_6ON_4$	10	495	-	35	1400	[12]
$SrLi_2Be_4O_6$	8	456	400	25	1200	[13]
$BaLi_2Be_4O_6$	8	454	400	25	1200	[13]
$Sr_{0.25}Ba_{0.75}Si_2O_2N_2$	8	472	400	36	-	[4]
$BaSi_2O_2N_2$	8	492	450	37	-	[5]

3.3 Conclusions

In this contribution, we report on syntheses of the highly condensed nitridophosphates AEP_8N_{14} ($AE = Ca, Sr, Ba$) and illustrate their structural relation. Although all three compounds feature quadruple layers separated by metal atoms, only SrP_8N_{14} and CaP_8N_{14} proved isotypic. The structure of BaP_8N_{14} as refined from diffraction data using microfocused synchrotron radiation differs in the orientation of these layers. Here, the layer stacking leads to a trigonal-prismatic environment of Ba^{2+} , while Ca^{2+} and Sr^{2+} are coordinated in octahedral fashion. Corresponding luminescence investigations on Eu^{2+} -doped samples show blue emission upon excitation with UV to blue light. The extremely narrow emission bands of $CaP_8N_{14}:Eu^{2+}$ and $SrP_8N_{14}:Eu^{2+}$ render these compounds competitive phosphors in comparison with other established classes of compounds. Especially, the Ca compound with its small Stokes shift shows very attractive luminescence properties for an

application in solid-state lighting, because the lowest lying absorption band matches very well in spectral position with blue emitting InGaN LEDs. Hence, the spectral emission intensity distribution can lower the spectral gap between blue pump LED and green phosphor emission, which is typically being observed in state-of-the-art white pc-LEDs. Filling this „cyan gap“ of a white spectrum will significantly enhance colour rendition of a light source.^[34, 35] Moreover, pronounced thermal stability and absence of toxic elements further highlight the great potential of the $AEP_8N_{14}:Eu^{2+}$ compounds. Future studies may thus focus on an alternative synthetic access in order to provide the preconditions for industrial application. Ammonothermal synthesis appears promising, as such syntheses of partially crystalline SrP_8N_{14} have already been reported.^[36] Moreover, such methods could provide sufficient sample quantities for a more precise characterization of the luminescence performance, meaning for example, temperature-dependent emission spectra.

3.4 Experimental Section

Synthesis of P_3N_5

P_3N_5 was synthesized by ammonolysis starting from P_4S_{10} (ca. 7.0 g, Sigma Aldrich 99.99%) in a tube furnace lined with a silica tube. The apparatus, including the silica reaction boat, was heated for 4 h at 1000 °C under vacuum ($\leq 10^{-3}$ mbar) for drying. Subsequently, the starting material was loaded into the reaction boat under Ar flow. Only a limited amount of P_4S_{10} can be used, as otherwise the reaction tube may be clogged by by-products. After saturating the atmosphere in the silica tube for 4 h with a constant flow of dried NH_3 (≈ 3.6 L h^{-1} , Air Liquide 5.0), P_4S_{10} was heated to 850 °C (rate: 5 °C min^{-1}) and held at this temperature for 4 h. Finally, the furnace was allowed to cool down to room temperature (rate: 5 °C min^{-1}) and the apparatus was flushed with Ar for 1 h in order to remove remaining NH_3 . The recovered product showed orange coloured grains, which were purified by washing with water, ethanol, and acetone. Further information on the synthesis are given in literature.^[38–40] P_3N_5 was identified by powder X-ray diffraction and FTIR spectroscopy.

Synthesis of $AE(N_3)_2$ ($AE = Ca, Sr, Ba$)

Alkaline earth azides $AE(N_3)_2$ ($AE = Ca, Sr, Ba$) were synthesized by reactions of the respective alkaline earth carbonates ($CaCO_3$: Alfa Aesar, 99.5%; $SrCO_3$: Sigma Aldrich, 99.995%; $BaCO_3$: Grüssing, 99.8%) with HN_3 prepared by means with a cation exchanger (Amberlyst 15) according to the procedure described by Suhrmann and modified by Karau.^[38, 41] A diluted solution of HN_3 is formed in situ by passing an aqueous solution of NaN_3 (Acros Organics, 99%, extra pure) through the cation exchanger. HN_3 then drops into a stirred aqueous suspension of the carbonate until the eluate shows a neutral pH value and the solution turns clear. Residues of the carbonate were filtered off and the solvent was removed with a rotary evaporator (50 mbar, 40 °C). The products were obtained as colourless fine powders, which were recrystallized from acetone and dried under vacuum. $AE(N_3)_2$ ($AE = Ca, Sr, Ba$) were investigated for purity by powder X-ray diffraction and FTIR spectroscopy. **Caution:** Since HN_3 is potentially explosive and highly poisonous in its gaseous form, special care is necessary.

Synthesis of AEP_8N_{14} ($AE = Ca, Sr, Ba$)

The nitridophosphates AEP_8N_{14} ($AE = Ca, Sr, Ba$) were obtained by high-pressure high-temperature synthesis using a 1000 t press with a modified Walker-type multianvil apparatus.^[22–26] All products were synthesized from stoichiometric amounts of P_3N_5 and the respective alkaline earth azide (see Supporting Information, Table B16). Owing to the high air-sensitivity of the azides, the starting materials were handled in an Ar-filled glovebox (Unilab, MBraun, Garching, $O_2 < 1$ ppm, $H_2O < 0.1$ ppm) and ground thoroughly in an agate mortar. The mixture was transferred into a cylindrical crucible made from hexagonal boron nitride (HeBoSint® S100, Henze, Kempten, Germany) and sealed with a boron nitride cap. The crucible was then placed in a specially prepared octahedron (MgO, doped with Cr_2O_3 (5%), edge length 18 mm, Ceramic Substrates & Components, Isle of Wight, UK), which was drilled through and loaded with different components. First, a ZrO_2 sleeve (Cesima Ceramics, Wust-Fischbeck, Germany) was fixed in the borehole and closed on one side by a Mo plate. Then, a long graphite tube (Schunk Kohlenstofftechnik GmbH, Gießen, Germany), a MgO spacer (Cesima Ceramics, Wust-Fischbeck, Germany) and a short graphite tube were put into the octahedron. While ZrO_2 served as thermal insulator, the two graphite tubes were used as electrical resistance furnace, whereby the combination of two single tubes is necessary to

decrease the temperature gradient. After inserting the crucible with the sample, the assembly was completed by adding a second MgO spacer and a further Mo plate to ensure a symmetric setup. In order to generate approximately hydrostatic conditions, the uniaxial force of the hydraulic press was converted by a Walker-type module with inserted steel wedges, forming a cubic cavity. This cavity was filled by eight Co-doped (7%) WC cubes (Hawedia, Marklkofen, Germany). To enclose the sample octahedron, the edges of the WC cubes were truncated (11 mm edge length). Furthermore, four of the cubes were equipped with a PTFE film (Vitaflon Technische Produkte GmbH, Bad Kreuznach, Germany) for electrical insulation. The remaining cubes were prepared with pyrophyllite gaskets (Cermaic Substrates & Components, Isle of Wight, UK) to prevent the outflow of the MgO octahedron. Bristol board (369 gm^{-2}) was used to fix the gaskets. Further information on the experimental high-pressure setup is given in the literature.^[42] Different pressure and temperature settings were used (CaP_8N_{14} : 5 GPa, $\approx 1075 \text{ }^\circ\text{C}$; SrP_8N_{14} : 5 GPa, $\approx 1075 \text{ }^\circ\text{C}$; BaP_8N_{14} : 4 GPa, $\approx 1150 \text{ }^\circ\text{C}$). Detailed programs are given in Table S17.

Scanning electron microscopy (SEM) and energy-dispersive X-ray diffraction (EDX)

The morphology of the samples was investigated with a Dualbeam Helios Nanolab G3 UC (FEI, Hillsboro). An X-Max 80 SDD EDX detector (Oxford Instruments, Abingdon) was used for chemical analyses. An adhesive carbon film was used to fix the samples on a holder. To ensure electrical conductivity, the samples were coated with carbon with an electron beam evaporator (BAL-TEC MED 020, Bal Tec AG). Data were analyzed with the Aztec software.^[43]

Transmission electron microscopy (TEM)

The sample was ground in an agate mortar, suspended in ethanol and drop-cast on a copper grid with holey carbon film (S160NH2C, Plano GmbH, Wetzlar, Germany). The grid was mounted on a double-tilt holder and isolated crystallites of BaP_8N_{14} were identified by EDX and electron diffraction using a FEI Tecnai G20 transmission electron microscope (TEM) with a thermal emitter (LaB_6) operated at 200 keV. Selected area electron diffraction patterns and bright-field images were recorded using a TVIPS camera (TemCam F216, Tietz) with a resolution of 2048×2048 pixels.

Single-crystal X-ray diffraction

The TEM grid was mounted on a Symétrie Hexapods Nanopos device. A BaP₈N₁₄ crystal of about 2×3×0.5 μm in size was recovered at beamline ID11 ($\lambda=0.309$ Å, ESRF, Grenoble) by a telescope with large magnification, using the copper crossbars of the grid as landmarks. The crystallite was centred using Ba X-ray fluorescence scans. The single-crystal data set was then collected using a microfocused synchrotron beam of 1×2 μm. CrysAlisPro and SADABS were used for the integration and the semiempirical absorption correction of the data.^[44,45] The incomplete absorption of X-ray radiation in the CCD phosphor was corrected.^[46] The crystal structure was solved by direct methods and refined by least-squares methods with SHELX-2014.^[47]

CCDC 1979592 (Ca) and 1980141 (Ba) contain the supplementary crystallographic data for this paper. These data are provided free of charge by The Cambridge Crystallographic Data Centre through the CCDC/FIZ Karlsruhe joint deposition service.

FTIR spectroscopy

FTIR spectra of the title compounds were collected on a Spectrum BX II spectrometer (PerkinElmer, Waltham, MA, USA) between 600 and 4000 cm⁻¹ with DuraSampler attenuated total reflectance unit (ATR).

Powder X-ray diffraction

Powder X-ray diffraction data were collected with a Stoe Stadi P diffractometer with Cu-K_{α1} ($\lambda = 1.5406$ Å) or Mo-K_{α1} ($\lambda = 0.71073$ Å) radiation. The diffractometers were equipped with Ge(111) monochromators and Mythen 1K Si strip detectors (Dectris, Baden, Switzerland). The ground samples were transferred into glass capillaries with 0.3 mm diameter (Hilgenberg GmbH, Malsfeld, Germany). The TOPAS Academic 6.1 package was used for Rietveld refinements using the fundamental parameters approach and a shifted Chebyshev function for handling the background.^[48] Temperature dependent powder X-ray diffraction data were collected on a Stoe Stadi P diffractometer (Mo-K_α radiation; Ge(111) monochromator) with a resistance graphite furnace (Stoe) and IP-PSD detector. Samples were loaded into fused silica capillaries (0.5 mm diameter) and heated

from room temperature to 950 °C with steps of 25 °C and a heating rate of 10 °C min⁻¹. At each step data were collected with constant temperature.

Luminescence

Luminescence spectra of Eu²⁺-doped samples (≈ 3 mole%) were examined on a HORIBA Fluoromax4 spectrofluorimeter system with Olympus BX51 microscope. Emission spectra were collected at room temperature with $\lambda_{exc} = 400$ nm for $AE = Ca, Sr$, and $\lambda_{exc} = 390$ nm for Ba , respectively, in a range from 400 to 800 nm (step width: 2 nm). Excitation spectra were recorded with monitoring wavelength λ_{mon} from 425 to 516 nm.

3.5 Acknowledgements

We thank Lisa Gamperl (Department of Chemistry at LMU) for EDX measurements. Furthermore, we thank Volker Weiler (Lumileds Phosphor Center Aachen) for luminescence measurements. We also thank the ESRF, Grenoble, for granting beam time (project CH-5149) and the Deutsche Forschungsgemeinschaft (DFG) for financial support (projects OE 530/6-1 and SCHN 377/18-1). Dr. Christopher Benndorf, Markus Nentwig and Christina Fraunhofer are acknowledged for support during the beamtime.

3.6 References

- [1] P. Pust, P. J. Schmidt, W. Schnick, "A revolution in lighting", *Nat. Mater.* **2015**, *14*, 454-458.
- [2] A. A. Setlur, "Phosphors for LED-based Solid-State Lighting", *Electrochem. Soc. Interface* **2009**, *18*, 32-36.
- [3] T. N. Moriguchi, Y.; Sakano, K.; Shimizu, Y.; *Light emitting device having a nitride compound semiconductor and a phosphor containing a garnet fluorescent material*, **1999**, US Patent 5998925 A.
- [4] M. Seibald, T. Rosenthal, O. Oeckler, F. Fahrnbauer, A. Tücks, P. J. Schmidt, W. Schnick, "Unexpected Luminescence Properties of $Sr_{0.25}Ba_{0.75}Si_2O_2N_2:Eu^{2+}$ - A Narrow Blue Emitting Oxonitridosilicate with Cation Ordering", *Chem. Eur. J.* **2012**, *18*, 13446-13452.
- [5] J. A. Kechele, O. Oeckler, F. Stadler, W. Schnick, "Structure elucidation of $BaSi_2O_2N_2$ - A host lattice for rare-earth doped luminescent materials in phosphor-converted (pc)-LEDs", *Solid State Sci.* **2009**, *11*, 537-543.
- [6] H. A. Höpfe, H. Lutz, P. Morys, W. Schnick, A. Seilmeier, "Luminescence in Eu^{2+} -doped $Ba_2Si_5N_8$: fluorescence, thermoluminescence, and upconversion", *J. Phys. Chem. Solids* **2000**, *61*, 2001-2006.
- [7] Y. Q. Li, J. E. J. van Steen, J. W. H. van Krevel, G. Botty, A. C. A. Delsing, F. J. DiSalvo, G. de With, H. T. Hintzen, "Luminescence properties of red-emitting $M_2Si_5N_8:Eu^{2+}$ ($M = Ca, Sr, Ba$) LED conversion phosphors", *J. Alloys Compd.* **2006**, *417*, 273-279.
- [8] S. Schmiechen, H. Schneider, P. Wagatha, C. Hecht, P. J. Schmidt, W. Schnick, "Toward New Phosphors for Application in Illumination-Grade White pc-LEDs: The Nitridomagnesosilicates $Ca[Mg_3SiN_4]:Ce^{3+}$, $Sr[Mg_3SiN_4]:Eu^{2+}$, and $Eu[Mg_3SiN_4]$ ", *Chem. Mater.* **2014**, *26*, 2712-2719.
- [9] K. Uhedaa, N. Hirosakib, Y. Yamamotoa, A. Naitoa, T. Nakajimaa, H. Yamamotoa, "Luminescence Properties of a Red Phosphor, $CaAlSiN_3:Eu^{2+}$, for White Light-Emitting Diodes", *Electrochem. Solid-State Lett.* **2006**, *9*, H22-H25.
- [10] P. Pust, V. Weiler, C. Hecht, A. Tücks, A. S. Wochnik, A.-K. Henß, D. Wiechert, C. Scheu, P. J. Schmidt, W. Schnick, "Narrow-band red-emitting $Sr[LiAl_3N_4]:Eu^{2+}$ as a next-generation LED-phosphor material", *Nat. Mater.* **2014**, *13*, 891-896.

- [11] E. Elzer, R. Niklaus, P. J. Strobel, V. Weiler, P. J. Schmidt, W. Schnick, "*MBe₂₀N₁₄:Eu²⁺* ($M = \text{Sr}, \text{Ba}$): Highly Condensed Nitridoberyllates with Exceptional Highly Energetic Eu^{2+} Luminescence", *Chem. Mater.* **2019**, *31*, 3174-3182.
- [12] P. Strobel, T. de Boer, V. Weiler, P. J. Schmidt, A. Moewes, W. Schnick, "*Luminescence of an Oxonitridoberyllate: A Study of Narrow-Band Cyan-Emitting Sr[Be₆ON₄]:Eu²⁺*", *Chem. Mater.* **2018**, *30*, 3122-3130.
- [13] P. Strobel, C. Maak, V. Weiler, P. J. Schmidt, W. Schnick, "*Ultra-Narrow-Band Blue-Emitting Oxoberyllates AELi₂[Be₄O₆]:Eu²⁺* ($AE = \text{Sr}, \text{Ba}$) Paving the Way to Efficient RGB pc-LEDs", *Angew. Chem. Int. Ed.* **2018**, *57*, 8739-8743; *Angew. Chem.* **2018**, *130*, 8875-8879.
- [14] S. D. Kloß, W. Schnick, "*Nitridophosphates – A Success Story of Nitride Synthesis*", *Angew. Chem. Int. Ed.* **2019**, *58*, 7933-7944; *Angew. Chem.* **2019**, *131*, 8015-8027.
- [15] F. J. Pucher, A. Marchuk, P. J. Schmidt, D. Wiechert, W. Schnick, "*Luminescent Nitridophosphates CaP₂N₄:Eu²⁺*, *SrP₂N₄:Eu²⁺*, *BaP₂N₄:Eu²⁺*, and *BaSr₂P₆N₁₂:Eu²⁺*", *Chem. Eur. J.* **2015**, *21*, 6443-6448.
- [16] M. Mallmann, S. Wendl, P. Strobel, P. J. Schmidt, W. Schnick, "*Sr₃P₃N₇: Complementary Approach by Ammonothermal and High-Pressure Syntheses*", *Chem. Eur. J.* **2020**, *26*, 6257-6263.
- [17] A. Marchuk, W. Schnick, "*Ba₃P₅N₁₀Br:Eu²⁺: A Natural-White-Light Single Emitter with a Zeolite Structure Type*", *Angew. Chem. Int. Ed.* **2015**, *54*, 2383-2387; *Angew. Chem.* **2015**, *127*, 2413-2417.
- [18] A. Marchuk, S. Wendl, N. Imamovic, F. Tambornino, D. Wiechert, P. J. Schmidt, W. Schnick, "*Nontypical Luminescence Properties and Structural Relation of Ba₃P₅N₁₀X:Eu²⁺* ($X = \text{Cl}, \text{I}$): Nitridophosphate Halides with Zeolite-like Structure", *Chem. Mater.* **2015**, *27*, 6432-6441.
- [19] F. Karau, W. Schnick, "*Hochdrucksynthese von BaSr₂P₆N₁₂ und BaCa₂P₆N₁₂ und Strukturvergleich der Reihe BaP₂N₄, BaCa₂P₆N₁₂ und BaSr₂P₆N₁₂*", *Z. Anorg. Allg. Chem.* **2006**, *632*, 231-237.
- [20] S. Wendl, W. Schnick, "*SrH₄P₆N₁₂ and SrP₈N₁₄: Insights into the Condensation Mechanism of Nitridophosphates under High Pressure*", *Chem. Eur. J.* **2018**, *24*, 15889-15896.
- [21] W. Schnick, "*Solid State Chemistry with Nonmetal Nitrides*", *Angew. Chem. Int. Ed. Engl.* **1993**, *32*, 806-818; *Angew. Chem.* **1993**, *105*, 846-858.

- [22] H. Huppertz, "Multianvil high-pressure / high-temperature synthesis in solid state chemistry", *Z. Kristallogr.* **2004**, 219, 330-338.
- [23] N. Kawai, S. Endo, "The Generation of Ultrahigh Hydrostatic Pressures by a Split Sphere Apparatus", *Rev. Sci. Instrum.* **1970**, 41, 1178-1181.
- [24] D. C. Rubie, "Characterising the sample environment in multianvil high-pressure experiments", *Phase Transitions* **1999**, 68, 431-451.
- [25] D. Walker, "Lubrication, gasketing, and precision in multianvil experiments", *Am. Mineral.* **1991**, 76, 1092-1100.
- [26] D. Walker, M. A. Carpenter, C. M. Hitch, "Some simplifications to multianvil devices for high pressure experiments", *Am. Mineral.* **1990**, 75, 1020-1028.
- [27] F. Fahrnbauer, T. Rosenthal, T. Schmutzler, G. Wagner, G. B. M. Vaughan, J. P. Wright, O. Oeckler, "Discovery and Structure Determination of an Unusual Sulfide Telluride through an Effective Combination of TEM and Synchrotron Microdiffraction", *Angew. Chem. Int. Ed.* **2015**, 54, 10020-10023; *Angew. Chem.* **2015**, 127, 10158-10161.
- [28] S. Wendl, L. Eisenburger, M. Zipkat, D. Günther, J. P. Wright, P. J. Schmidt, O. Oeckler, W. Schnick, "*BaP₆N₁₀NH:Eu²⁺* as a Case Study - An Imidonitridophosphate Showing Luminescence", *Chem. Eur. J.* **2020**, 26, 5010-5016.
- [29] W. H. Baur, "Effective Ionic Radii in Nitrides", *Crystallogr. Rev.* **1987**, 1, 59-83.
- [30] A. Marchuk, V. R. Celinski, J. Schmedt auf der Günne, W. Schnick, "*MH₄P₆N₁₂* (M = Mg, Ca): New Imidonitridophosphates with an Unprecedented Layered Network Structure Type", *Chem. Eur. J.* **2015**, 21, 5836-5842.
- [31] R. Shannon, "Revised effective ionic radii and systematic studies of interatomic distances in halides and chalcogenides", *Acta Crystallogr. Sect. A* **1976**, 32, 751-767.
- [32] Superscripted numbers in square brackets following element symbols denote coordination numbers.
- [33] P. Dorenbos, "Anomalous luminescence of *Eu²⁺* and *Yb²⁺* in inorganic compounds", *J. Phys.: Condens. Matter* **2003**, 15, 2645-2665.
- [34] J. J. Joos, J. Botterman, P. F. Smet, "Evaluating the use of blue phosphors in white LEDs: the case of *Sr_{0.25}Ba_{0.75}Si₂O₂N₂:Eu²⁺*", *J. Solid State Lighting* **2014**, 1, 6.

- [35] A. Piquette, W. Bergbauer, B. Galler, K. C. Mishra, "On Choosing Phosphors for Near-UV and Blue LEDs for White Light", *ECS J. Solid State Sci. Technol.* **2016**, 5, R3146-R3159.
- [36] M. Mallmann, S. Wendl, W. Schnick, "Crystalline Nitridophosphates by Ammonothermal Synthesis", *Chem. Eur. J.* **2020**, 26, 2067-2072.
- [37] K. Shioi, N. Hirosaki, R.-J. Xie, T. Takeda, Y. Q. Li, "Luminescence Properties of $SrSi_6N_8$ ", *J. Mater. Sci* **2008**, 43, 5659-5661.
- [38] F. W. Karau, *Dissertation*, Ludwig-Maximilians-Universität München (Germany) **2007**.
- [39] J. Lücke, *Dissertation*, Rheinische Friedrich-Wilhelms-Universität Bonn (Germany) **1994**.
- [40] A. Stock, H. Grüneberg, "Über den Phosphorstickstoff", *Ber. Dtsch. Chem. Ges.* **1907**, 40, 2573-2578.
- [41] R. Suhrmann, K. Clusius, "Über die Reindarstellung der Alkalimetalle", *Z. Anorg. Allg. Chem.* **1926**, 152, 52-58.
- [42] H. Huppertz, *Habilitationsschrift*, Ludwig-Maximilians-Universität München (Germany) **2003**.
- [43] Oxford Instruments, *AZtecEnergy Vers. 3.1*, Abingdon, United Kingdom, **2016**.
- [44] Agilent Technologies, *CrysAlis Pro*, Yarnton, Oxfordshire, England, **2011**.
- [45] Bruker AXS, Inc., *SADABS*, Madison, Wisconsin, USA, **2001**.
- [46] G. Wu, B. L. Rodrigues, P. Coppens, "The correction of reflection intensities for incomplete absorption of high-energy X-rays in the CCD phosphor", *J. Appl. Crystallogr.* **2002**, 35, 356-359.
- [47] G. M. Sheldrick, "Crystal structure refinement with SHELXL", *Acta Crystallogr. Sect. C* **2015**, 71, 3-8.
- [48] A. A. Coelho, *TOPAS Academic*, Version 6, Coelho Software, Brisbane, Australia, **2016**.

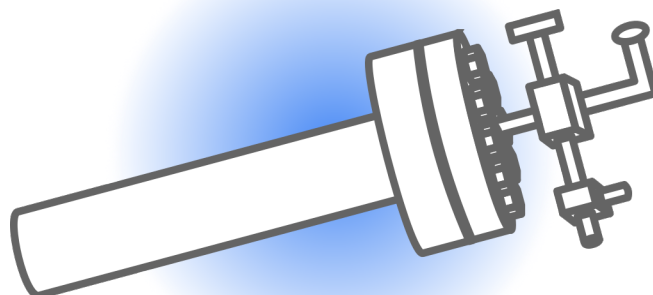
4 Crystalline Nitridophosphates by Ammonothermal Synthesis

Dr. Mathias Mallmann, Sebastian Wendl, Prof. Dr. Wolfgang Schnick

Chem. Eur. J. **2020**, 26, 2067–2072.

DOI: 10.1002/chem.201905227

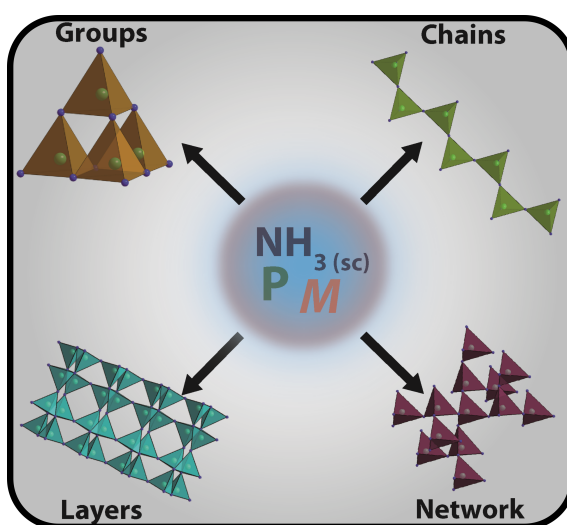
Reprinted (adapted) with permission for non-commercial use from *Chemistry – A European Journal* (open access). Copyright 2021 John Wiley and Sons.



Ammonothermal Synthesis: *P/N-based model compounds with different degrees of condensation, namely α -Li₁₀P₄N₁₀, β -Li₁₀P₄N₁₀, Li₁₈P₆N₁₆, Ca₂PN₃, SrP₈N₁₄, and LiPN₂, were synthesized applying the ammonothermal technique. The applicability of the presented approach on group-, chain-, layer-, and network-type structures demonstrates its great potential.*

Abstract: Nitridophosphates are a well-studied class of compounds with high structural diversity. However, their synthesis is quite challenging, particularly due to the limited thermal stability of starting materials like P_3N_5 . Typically, it requires even high-pressure techniques (e.g. multianvil) in most cases. Herein, we establish the ammonothermal method as a versatile synthetic tool to access nitridophosphates with different degrees of condensation. α - $Li_{10}P_4N_{10}$, β - $Li_{10}P_4N_{10}$,

$Li_{18}P_6N_{16}$, Ca_2PN_3 , SrP_8N_{14} , and $LiPN_2$ were synthesized in supercritical NH_3 at temperatures and pressures up to 1070 K and 200 MPa employing ammonobasic conditions. The products were analyzed by powder X-ray diffraction, energy dispersive X-ray spectroscopy, and FTIR spectroscopy. Moreover, we established red phosphorus as a starting material for nitridophosphate synthesis instead of commonly used and not readily available precursors, such as P_3N_5 . This opens a promising preparative access to the emerging compound class of nitridophosphates.



4.1 Introduction

By analogy with well-known hydrothermal syntheses, the ammonothermal method was developed by Jacobs and co-workers and was established as an innovative synthetic approach for amides, imides and nitrides.^[1-5] The ammonothermal technique gained fundamental interest in materials science as it facilitates the growth of high-quality GaN single crystals up to 50 mm in diameter with growth rates of several hundred μm per day.^[6-9]

Recent explorative syntheses under ammonothermal conditions made crystalline wurtzite-type Grimm–Sommerfeld analogous nitrides available, such as InN, *II-IV-N*₂ compounds (*II* = Mg, Mn, Zn; *IV* = Si, Ge) and CaGaSiN₃, as well as oxide nitride perovskites such as *LnTaON*₂ (*Ln* = La, Ce, Pr, Nd, Sm, Gd).^[10-15] Applying the ammonothermal technique, even the challenging preparation of a few nitridophosphates has been accomplished successfully as reported for K₃P₆N₁₁ and the double nitrides Mg₂PN₃ and Zn₂PN₃.^[16-18] Furthermore, various phosphorus-containing imidonitrides were synthesized in supercritical ammonia and thus, the ammonothermal method appears as a promising general synthetic approach for nitridophosphate synthesis.^[19-22]

Nitridophosphates are built up from PN₄ tetrahedra and their tetrahedra-based networks can be characterized by the degree of condensation $\kappa = n(T)/n(X)$, which represents the atomic ratio of tetrahedral centers (*T* = P) and coordinating atoms (*X* = N). Accordingly, compounds that are built up from non-condensed PN₄ tetrahedra (e.g. Li₇PN₄)^[23] possess a degree of condensation of $\kappa = 1/4$, whereas highly condensed frameworks feature $\kappa \geq 1/2$ (e.g. LiPN₂).^[24] For $1/4 < \kappa < 1/2$, partially condensed PN₄ tetrahedra may form complex anions, such as adamantane-like groups (α -Li₁₀P₄N₁₀, β -Li₁₀P₄N₁₀),^[25, 26] chain structures (e.g. Ca₂PN₃),^[27] or layers (e.g. Ho₂P₃N₇).^[28] The degree of condensation may further be correlated with materials properties, such as chemical inertness and rigidity of the network as well as physical properties like ion conductivity.^[18] Nitridophosphate synthesis, however, is a challenging issue, as these compounds are prone to thermal decomposition starting at 1020 K and the elimination of N₂ at elevated temperatures [Eq. 4.1]:



Consequently, the number of nitridophosphates synthesized at ambient pressure so far is limited (e.g. Ca_2PN_3 , $\alpha\text{-Li}_{10}\text{P}_4\text{N}_{10}$, $\beta\text{-Li}_{10}\text{P}_4\text{N}_{10}$, LiPN_2 or Mg_2PN_3).^[24–27, 29] Following Le Chatelier's principle, thermal decomposition, however, can be suppressed by applying pressure. In this context, especially the multianvil technique ($p \leq 25$ GPa) turned out to be a powerful synthetic tool.^[18] This high-pressure high-temperature method revealed numerous nitridophosphates with different types of anionic tetrahedra-based networks (e.g. $\text{SrP}_8\text{N}_{14}$, $\text{Li}_{18}\text{P}_6\text{N}_{16}$ or LiNdP_4N_8).^[30–32] Nevertheless, utilizing high-pressure techniques implicates small sample volumes, which limits detailed characterization of materials properties as well as practical applications. Furthermore, precursors like P_3N_5 are typically used,^[18] requiring a multistep synthesis procedure. Thus, the ammonothermal method is a promising and innovative alternative, as it enables the preparation of large-volume samples, while suppressing thermal decomposition by medium pressures ($p \leq 300$ MPa). However, there has been no systematic investigation on the ammonothermal synthesis of nitridophosphates that covers their broad structural diversity.

In this contribution, we exemplarily present the ammonothermal synthesis ($T \leq 1070$ K, $p \leq 200$ MPa) of six nitridophosphates that feature non-condensed PN_4 tetrahedra groups, infinite PN_4 tetrahedra chains, layered substructures, and highly condensed frameworks, namely $\alpha\text{-Li}_{10}\text{P}_4\text{N}_{10}$, $\beta\text{-Li}_{10}\text{P}_4\text{N}_{10}$, $\text{Li}_{18}\text{P}_6\text{N}_{16}$, Ca_2PN_3 , $\text{SrP}_8\text{N}_{14}$, and LiPN_2 . This is a major extension of the structural diversity of ammonothermally accessible ternary and multinary compounds, which have hitherto been limited mainly to wurtzite-type derivatives and oxide nitride perovskites. In addition, red phosphorus (P_{red}), which was up to now only used for the synthesis of HPN_2 in ammonia,^[33] is employed as a starting material for nitridophosphates. This makes highly reactive and chlorine-containing precursors (e.g. PCl_5 , $(\text{PNCl}_2)_3$) dispensable, which can produce toxic and corrosive byproducts, emphasizing the innovative character of the ammonothermal approach.

4.2 Results and Discussion

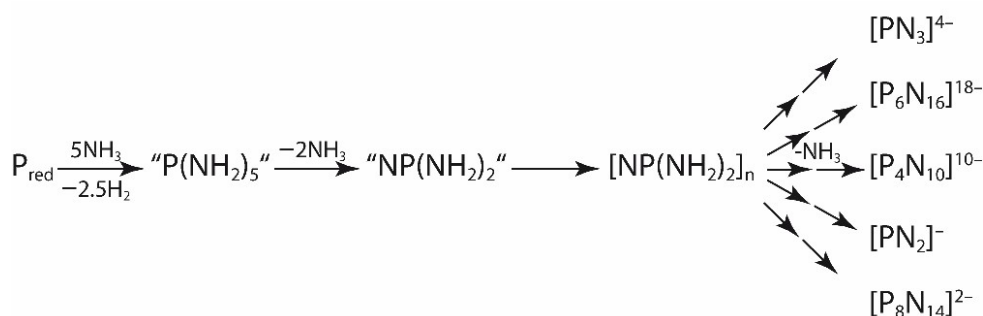
Ammonothermal synthesis

Nitridophosphates α -Li₁₀P₄N₁₀, β -Li₁₀P₄N₁₀, Li₁₈P₆N₁₆, Ca₂PN₃, SrP₈N₁₄, and LiPN₂ were synthesized ammonothermally using custom-built high-pressure, high-temperature autoclaves. P₃N₅ or P_{red} were used as phosphorus source during syntheses. The other starting materials as well as the corresponding reaction conditions (maximum reaction temperature T_{\max} , maximum pressure p_{\max} , reaction time at maximum temperature t) are summarized in Table 4.1. Ammonobasic mineralizers, such as alkali metals, alkali metal nitrides, alkali metal azides or alkaline earth metal azides, which react in situ to the corresponding metal amides, were added to increase the solubility of the starting materials by forming soluble intermediate species. Since such intermediates are preferentially formed at lower temperatures, an additional temperature step at 670 K (holding time: 16 h) was conducted for all reactions before heating to T_{\max} .^[5] The addition of these mineralizers can also dissolve compounds such as P_{red}, which are actually insoluble in NH₃ even at temperatures above the critical point.^[34] Therefore, in the case of the synthesized lithium nitridophosphates (α -Li₁₀P₄N₁₀, β -Li₁₀P₄N₁₀, Li₁₈P₆N₁₆ and LiPN₂), Li₃N or Li was added, respectively, in excess to increase the solubility of P_{red}. While NaN₃ was added for the synthesis of Ca₂PN₃, to increase both, the solubility of Ca and P_{red}, no additional mineralizer was added for the synthesis of SrP₈N₁₄. Instead, Sr(N₃)₂ acts as an ammonobasic mineralizer itself by forming Sr(NH₂)₂, as the heavier alkaline earth metals have been discussed as ammonobasic mineralizers as well.^[35] Possible intermediates are mixed-metal amides, such as NaCa(NH₂)₃, and reactive P/N compounds, for example, hexaaminocyclotriphosphazene (PN(NH₂)₂)₃, the corresponding ammoniate (PN(NH₂)₂)₃·0.5 NH₃ or imidonitrides in analogy to Na₁₀[P₄(NH)₆N₄](NH₂)₆(NH₃)_{0.5}, which have already been synthesized using the ammonothermal method.^[20, 36–38] A possible condensation mechanism of phosphorus containing intermediates is illustrated in Scheme 4.1. When starting from P_{red}, the element has to be oxidized in a first step to an oxidation state of +V forming an intermediate species like hypothetical „P(NH₂)₅“, in which two possible mechanisms are conceivable. On the one hand, N₂, which originates from the decomposition of NH₃, could act as oxidizing agent, on the other hand, NH₃ could directly react with P_{red} under elimination of H₂. „P(NH₂)₅“ could immediately form „NP(NH₂)₂“ by elimination of ammonia,

which can react to reactive P/N compounds such as $(\text{PN}(\text{NH}_2)_2)_3$.^[37] However, for a precise statement on possible reaction mechanisms or phosphorus containing intermediates, in situ measurements like Raman or NMR spectroscopy could be helpful.

Table 4.1. Starting materials, mineralizers and reaction conditions of the ammonothermal synthesis of α - $\text{Li}_{10}\text{P}_4\text{N}_{10}$, β - $\text{Li}_{10}\text{P}_4\text{N}_{10}$, $\text{Li}_{18}\text{P}_6\text{N}_{16}$, Ca_2PN_3 , $\text{SrP}_8\text{N}_{14}$, and LiPN_2 .

Compd.	Starting material	Mineralizer	T_{max} [K]	p_{max} [MPa]	t [h]
α - $\text{Li}_{10}\text{P}_4\text{N}_{10}$	$\text{Li}_3\text{N} + \text{P}_{\text{red}}$	Li_3N	920	100	72
β - $\text{Li}_{10}\text{P}_4\text{N}_{10}$	$\text{Li}_3\text{N} + \text{P}_{\text{red}}$	Li_3N	1070	135	72
$\text{Li}_{18}\text{P}_6\text{N}_{16}$	$\text{Li}_3\text{N} + \text{P}_3\text{N}_5$	Li_3N	970	165	50
Ca_2PN_3	$\text{CaH}_2 + \text{P}_{\text{red}}$	NaN_3	870	200	96
$\text{SrP}_8\text{N}_{14}$	$\text{Sr}(\text{N}_3)_2 + \text{P}_3\text{N}_5$	$\text{Sr}(\text{N}_3)_2$	1070	170	96
LiPN_2	$\text{Li} + \text{P}_{\text{red}}$	Li	1070	135	96



Scheme 4.1. Simplified condensation sequence of nitridophosphates during ammonothermal synthesis, starting from P_{red} .

Subsequent heating from 670 K to the maximum temperature T_{max} (see Table 4.1) leads to decomposition of the discussed intermediates and formation of the corresponding nitridophosphates under elimination of NH_3 (see Scheme 4.1). After reaction, residual mineralizers and intermediate species were removed by washing of the products with dry ethanol (α - $\text{Li}_{10}\text{P}_4\text{N}_{10}$, β - $\text{Li}_{10}\text{P}_4\text{N}_{10}$, $\text{Li}_{18}\text{P}_6\text{N}_{16}$, and Ca_2PN_3) or 1 m HCl ($\text{SrP}_8\text{N}_{14}$ and LiPN_2). SEM images of octahedrally shaped β - $\text{Li}_{10}\text{P}_4\text{N}_{10}$ and needle-shaped $\text{SrP}_8\text{N}_{14}$ crystallites are illustrated in Figure 4.1, while the other compounds were obtained as microcrystalline powders.

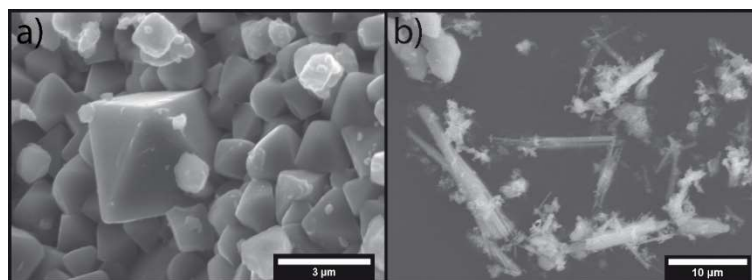


Figure 4.1. SEM images of octahedrally shaped crystals of β - $\text{Li}_{10}\text{P}_4\text{N}_{10}$ (a) and crystalline needles of $\text{SrP}_8\text{N}_{14}$ (b).

As mentioned above, both P_3N_5 and P_{red} were used as starting materials. While α - $\text{Li}_{10}\text{P}_4\text{N}_{10}$, β - $\text{Li}_{10}\text{P}_4\text{N}_{10}$, Ca_2PN_3 , and LiPN_2 were synthesized starting from P_{red} , $\text{Li}_{18}\text{P}_6\text{N}_{16}$ and $\text{SrP}_8\text{N}_{14}$ could only be obtained starting from P_3N_5 . A possible explanation could be the higher reactivity of P_3N_5 compared to P_{red} , which is needed for the synthesis of $\text{Li}_{18}\text{P}_6\text{N}_{16}$ and $\text{SrP}_8\text{N}_{14}$.^[24–27, 30, 31] Probably, higher synthesis temperatures and pressures would lead to successful synthesis of these two compounds starting from P_{red} as well.

The introduction of P_{red} as a starting material for nitridophosphate synthesis as well as the use of simple starting materials like pure elements, lower reaction temperatures, pressures and larger sample volumes compared to other synthesis methods, indicates the high potential of the ammonothermal approach as an alternative synthetic tool for a systematic access to nitridophosphates.

Crystallographic investigation

The purified products were analyzed by PXRD. Rietveld refinements of α - $\text{Li}_{10}\text{P}_4\text{N}_{10}$, β - $\text{Li}_{10}\text{P}_4\text{N}_{10}$, $\text{Li}_{18}\text{P}_6\text{N}_{16}$, Ca_2PN_3 , and LiPN_2 were conducted starting from atomic coordinates and Wyckoff positions known from the literature.^[24–27, 31] An exemplary Rietveld plot of Ca_2PN_3 is illustrated in Figure 4.2. The Rietveld plots of α - $\text{Li}_{10}\text{P}_4\text{N}_{10}$, β - $\text{Li}_{10}\text{P}_4\text{N}_{10}$, $\text{Li}_{18}\text{P}_6\text{N}_{16}$, and LiPN_2 can be found in the Supporting Information (Figures C.1 and C.6, Supporting Information). The crystallographic data as well as atomic coordinates are summarized in Tables C.1–C.4, C.6–C.7 and C.10–C.11 in the Supporting Information. In the case of $\text{Li}_{18}\text{P}_6\text{N}_{16}$ additional reflections could be observed, which can

be attributed to α - $\text{Li}_{10}\text{P}_4\text{N}_{10}$ and LiPN_2 . Due to the fact that $\text{Li}_{18}\text{P}_6\text{N}_{16}$ is so far only reported using high-pressure conditions (1270 K, 5.5 GPa), a possible explanation for these side phases could be that higher reaction pressures would be necessary to achieve phase purity.^[31] In analogy, higher pressures as well as temperatures would be necessary for the synthesis of $\text{SrP}_8\text{N}_{14}$, as the synthesis at 1070 K and 170 MPa resulted in broad reflections in the measured PXRD pattern (see Figure C.5 in the Supporting Information), suggesting a nanocrystalline sample morphology. However, further increases of temperature or pressure are challenging and not possible with the current high-pressure equipment. Therefore, the measured PXRD was only compared with a simulated pattern from literature data (see Figure C.5, Supporting Information)^[30] and may most likely be characterized as $\text{SrP}_8\text{N}_{14}$.

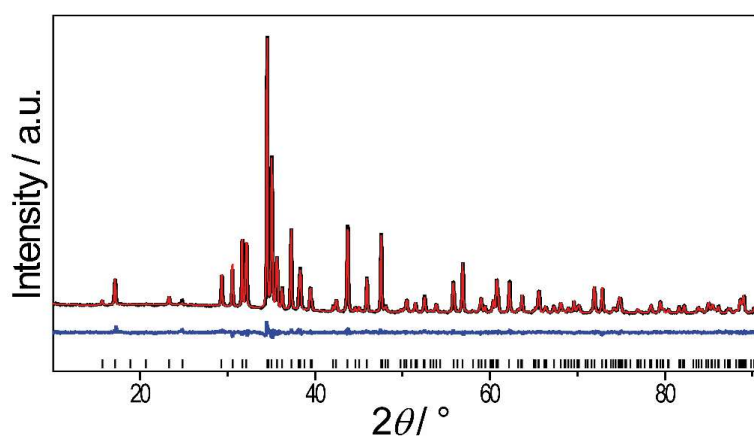


Figure 4.2. Rietveld refinement of PXRD pattern ($\lambda = 1.5406 \text{ \AA}$) of Ca_2PN_3 with experimental data (black line), calculated data (red line), difference profile (blue line) and reflection positions (black bars). Start values for Rietveld refinement were taken from literature.^[27] Unknown reflections between 6 and 10° only occur after washing treatment and were, therefore, not taken into account during the refinement.

EDX measurements of all compounds are summarized in Tables C.5, C.8, C.9, and C.12 in the Supporting Information. Deviations from the theoretical values can be explained by surface hydrolysis during sample preparation, washing treatment or by crystalline and amorphous side phases. The absence of any NH_x functionality in the Li containing nitridophosphates was confirmed by FTIR spectroscopy (Figures C.2–C.4 and C.7 in the Supporting Information).

Crystal structures

α -Li₁₀P₄N₁₀, β -Li₁₀P₄N₁₀, and Li₁₈P₆N₁₆ are built up from corner sharing PN₄ tetrahedra. While α -Li₁₀P₄N₁₀ and β -Li₁₀P₄N₁₀ contain adamantane-like T2 supertetrahedra ([P₄N₁₀]¹⁰⁻) with a degree of condensation of $\kappa = 2/5$, Li₁₈P₆N₁₆ is built up from [P₆N₁₆]¹⁸⁻ anions corresponding to a degree of condensation of $\kappa = 3/8$ (see Figure 4.3). These [P₆N₁₆]¹⁸⁻ units consist of four PN₄ tetrahedra forming a *vierer*-ring, which is connected to two further PN₄ tetrahedra forming two *dreier*-rings.^[39, 40] In contrast to these non-condensed tetrahedra groups, the anionic P/N-structure of Ca₂PN₃ is composed of *zweier* single chains running along [100] made up of corner sharing PN₄ tetrahedra (see Figure 4.3).^[39, 40] The chains exhibit a stretching factor of $f_s = 1.0$ and a degree of condensation of $\kappa = 1/3$. The crystal structure of SrP₈N₁₄ is composed of PN₄ tetrahedra forming a layered structure (see Figure 4.3) and can be described as a highly condensed nitridophosphate with a degree of condensation of $\kappa = 4/7$. This is the highest degree of condensation observed in nitridophosphates so far. LiPN₂ is composed of all-side vertex-sharing PN₄ tetrahedra, which are connected via common corners forming a 3D anionic network with a degree of condensation of $\kappa = 1/2$ (see Figure 4.3) isoelectronic and homeotypic to β -cristobalite (SiO₂). Detailed crystal structure descriptions of all six compounds are given in the literature.^[24–27, 30, 31] As shown in Figure 4.3, the above described nitridophosphates can be divided into different groups regarding their anionic P/N-substructures (non-condensed tetrahedra groups, tetrahedra chains, tetrahedra layers, and tetrahedra networks). This is a major extension of the structural diversity of ammonothermally accessible ternary and multinary nitrides, which have hitherto been limited mainly to wurtzite-type derivatives and oxide nitride perovskites. Furthermore, the degree of condensation of ammonothermally accessible nitridophosphates is widely extended and ranges now from $\kappa = 1/3$ to $4/7$ (see Figure 4.4), covering almost the entirely accessible range. These results show the great potential of the ammonothermal method and can pave the way for synthesis of hitherto unknown nitridophosphates using the ammonothermal approach.

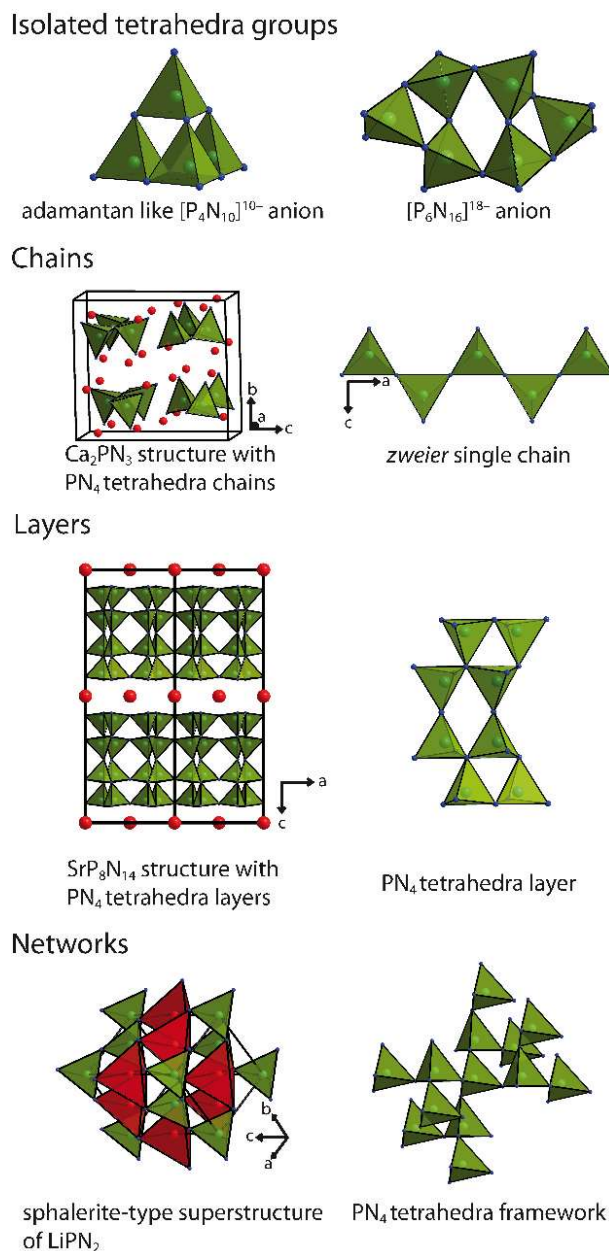


Figure 4.3. Crystal structures and/or constituting PN_4 tetrahedra units (green) occurring in α - $Li_4P_4N_{10}$, β - $Li_{10}P_4N_{10}$, $Li_{18}P_6N_{16}$, Ca_2PN_3 , SrP_8N_{14} , and $LiPN_2$. Ca^{2+} and Sr^{2+} cations as well as LiN_4 tetrahedra are depicted in red.

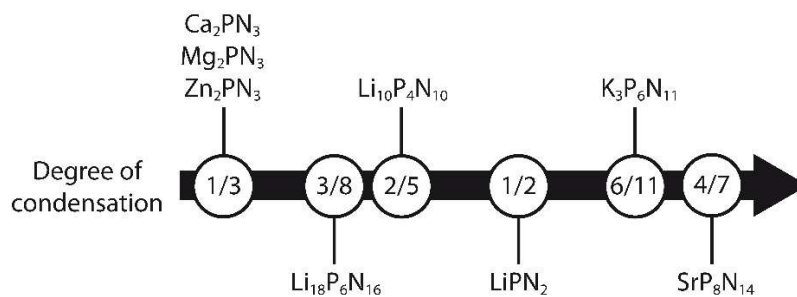


Figure 4.4. Ammonothermally synthesized nitridophosphates, arranged in order of their degree of condensation.

4.3 Conclusions

Recently, we reported on the synthesis and crystal growth of wurtzite-type Mg_2PN_3 and Zn_2PN_3 under ammonothermal conditions, raising the question of a systematic access to nitridophosphates using supercritical NH_3 .^[17] In this contribution we report on the ammonothermal syntheses of $\alpha\text{-Li}_{10}\text{P}_4\text{N}_{10}$, $\beta\text{-Li}_{10}\text{P}_4\text{N}_{10}$, $\text{Li}_{18}\text{P}_6\text{N}_{16}$, Ca_2PN_3 , $\text{SrP}_8\text{N}_{14}$, and LiPN_2 . Those compounds feature a degree of condensation in the range $1/3 \leq \kappa \leq 4/7$ (Figure 4.4), corresponding to different types of anionic tetrahedra-based substructures, such as non-condensed tetrahedra groups, chains, layers and 3D-networks. In contrast to established high-pressure techniques, the ammonothermal method requires only moderate pressures and temperatures, exemplifying the high potential of this preparative approach. Furthermore, readily available red phosphorus was introduced as a starting material in nitridophosphate syntheses, avoiding the usage of halide or sulfur-containing precursors (e.g. $(\text{PNCl}_2)_3$, P_4S_{10}). Using simple starting materials and yielding large sample volumes, the ammonothermal method enables more detailed characterization of material properties of nitridophosphates. Supporting fundamental research on the reaction mechanisms, intermediate species and dissolution/crystallization processes, however, might be necessary. Therefore, in situ measurements such as X-ray, NMR, or Raman techniques may provide important insights into these processes.^[41, 42]

4.4 Experimental Section

General

Loading of the autoclaves with solid starting materials (see below) were conducted under exclusion of oxygen and moisture in an argon-filled glovebox (Unilab, MBraun, Garching, $\text{O}_2 < 1$ ppm, $\text{H}_2\text{O} < 1$ ppm). The condensation of ammonia into the autoclaves was performed using a vacuum line (≤ 0.1 Pa) with argon and ammonia (both: Air Liquide, 99.999%) supply. The gases were further purified by gas cartridges (Micro torr FT400-902 (for Ar) and MC400-702FV (for NH_3), SAES Pure Gas Inc., San Luis Obispo, CA, USA), providing a purity level of < 1 ppbV H_2O , O_2 and

CO₂. The amount of condensed ammonia was detected using a mass flow meter (d-6320-DR, Bronkhorst, Ruurlo, Netherlands).

Synthesis of P₃N₅

P₃N₅ was synthesized by reaction of P₄S₁₀ (Sigma Aldrich, 99%) in a continuous flow of NH₃ (Air Liquid, 99.999%).^[43] After saturation with NH₃ (4 h), the silica tube was heated with a rate of 5 K min⁻¹ to 1125 K and held for 4 h. After cooling to room temperature (5 K min⁻¹), the orange product was washed with ethanol, water and acetone and dried under vacuum. Powder X-ray diffraction was used to confirm phase purity.

Synthesis of Sr(N₃)₂

Based on the work of Suhrmann and Karau,^[44, 45] Sr(N₃)₂ was synthesized by reaction of in situ formed diluted HN₃ (by passing aqueous NaN₃ (Acros Organics, 99%) through a cation exchanger (Amberlyst 15)) with SrCO₃ (Sigma Aldrich, 99.995%). The HN₃-solution was dropped slowly into an aqueous suspension of SrCO₃ and stirred until the liquid phase turned completely clear. Residual SrCO₃ was removed by filtration and the clear filtrate was evaporated under reduced pressure (50 mbar, 40 °C). After evaporation, the product was recrystallized from acetone and dried *in vacuo*. PXRD and FTIR measurements were used to confirm phase purity.

Caution! Since HN₃ solutions are potentially explosive and the vapor is highly poisonous, special care issues are necessary.

Ammonothermal synthesis of α- and β-Li₁₀P₄N₁₀

For ammonothermal synthesis of α- and β-Li₁₀P₄N₁₀, Li₃N (3 mmol, 104.5 mg, Sigma–Aldrich, 99.99%) and red P (3 mmol, 92.9 mg, Merck, 99%) were ground and transferred to Ta-liners, for protection of the samples against autoclave impurities. The liners were then placed in high-temperature autoclaves (Haynes[®] 282[®], max. 1100 K, 170 MPa, 10 mL) and sealed with a lid via flange joints using a sealing gasket (silver coated Inconel[®] 718 ring, GFD seals). The autoclave body and the upper part, consisting of a hand valve (SITEC) with integrated bursting disc (SITEC) and pressure transmitter (HBM P2VA1/5000 bar), are connected by an Inconel[®] 718 high-pressure tube.^[12] The

closed autoclave was evacuated and cooled to 198 K using an ethanol/liquid nitrogen mixture. Afterwards, NH_3 (≈ 4 mL) was directly condensed into the autoclaves via a pressure regulating valve. For both reactions, the autoclaves were primarily heated to 670 K within 2 h, kept at this temperature for 16 h and subsequently heated to 920 K ($\alpha\text{-Li}_{10}\text{P}_4\text{N}_{10}$) or 1070 K ($\beta\text{-Li}_{10}\text{P}_4\text{N}_{10}$) within 3 h and held at this temperature for 72 h, reaching maximum pressures of 100 ($\alpha\text{-Li}_{10}\text{P}_4\text{N}_{10}$) and 135 MPa ($\beta\text{-Li}_{10}\text{P}_4\text{N}_{10}$), respectively. After cooling and removal of NH_3 , the colorless products were separated under argon, washed with EtOH and dried *in vacuo*.

Ammonothermal synthesis of $\text{Li}_{18}\text{P}_6\text{N}_{16}$

$\text{Li}_{18}\text{P}_6\text{N}_{16}$ was synthesized ammonothermally starting from Li_3N (3.75 mmol, 130.6 mg, Sigma–Aldrich, 99.99%), P_3N_5 (1.5 mmol, 244.4 mg) and NH_3 (≈ 5 mL) in a Ta-liner. Following the autoclave preparation (as described for $\text{Li}_{10}\text{P}_4\text{N}_{10}$), the vessel was heated to 670 K within 2 h, kept at this temperature for 16 h, heated to 970 K within 3 h and held at this temperature for 50 h reaching a maximum pressure of 165 MPa. After cooling and removing of NH_3 , the colorless product was separated under argon, washed with EtOH and dried *in vacuo*.

Ammonothermal synthesis of Ca_2PN_3

Ca_2PN_3 was synthesized under ammonothermal conditions using an Inconel® 718 autoclave (max. 870 K, 300 MPa, 10 mL). The setup and preparation of the autoclave is analogous to the autoclaves described above. CaH_2 (3 mmol, 126.3 mg, Sigma–Aldrich, 99.99%), red P (1.5 mmol, 46.5 mg, Merck, 99%), NaN_3 (7.5 mmol, 487.5 mg, Sigma–Aldrich, 99.5%) as mineralizer and NH_3 (≈ 6.5 mL) were used as starting materials in a Ta-liner. After autoclave preparation (as described above), the reaction mixture was heated to 670 K within 2 h, held for 16 h, heated to 870 K within 2 h and kept at this temperature for 96 h, resulting in a maximum pressure of 200 MPa. The beige product was separated after cooling and ammonia removed under argon, washed with EtOH and dried *in vacuo*.

Ammonothermal synthesis of SrP₈N₁₄

Sr(N₃)₂ (0.375 mmol, 64.4 mg), P₃N₅ (1 mmol, 163 mg) were ground, transferred to a Ta-liner, which was placed in a Haynes° 282° autoclave. After preparation of the autoclave as described above, NH₃ (≈ 5 mL) was condensed into the autoclave. Subsequently, the autoclave was heated to 670 K within 2 h, held at this temperature for 16 h, heated to 1070 K within 3 h, and kept at this temperature for 96 h, reaching a maximum pressure of 170 MPa. After cooling and removal of NH₃, the colorless product was isolated in air, washed with 1 M HCl and dried at 370 K.

Ammonothermal synthesis of LiPN₂

For the synthesis of LiPN₂ in supercritical ammonia, Li (10 mmol, 69.4 mg, Alfa Aesar, 99%) and red P (7.5 mmol, 232.3 mg, Merck, 99%) were transferred in a Ta-liner and placed in a Haynes° 282° autoclave. After preparation of the autoclave as described above, approximately 4 mL NH₃ were added. The reaction mixture was heated to 670 K within 2 h, held for 16 h, heated to 1070 K within 3 h and kept at this temperature for 96 h, resulting in maximum pressures of 135 MPa. After cooling and elimination of NH₃, the isolated colorless product was washed with 1 M HCl and dried at 370 K.

Powder X-ray diffraction

The purified products were filled and sealed in glass capillaries (0.3–0.5 mm diameter, 0.01 mm wall thickness, Hilgenberg GmbH). A Stoe STADI P diffractometer with Cu-K_{α1} radiation (λ = 1.5406 Å), Ge(111) monochromator and Mythen 1K detector in Debye–Scherrer geometry was used for data collection. TOPAS was used for Rietveld refinement.^[46]

Scanning electron microscopy

A Dualbeam Helios Nanolab G3 UC (FEI) scanning electron microscope, equipped with an EDX detector (X-Max 80 SDD, Oxford instruments) was used for EDX measurements. For this purpose, the samples were placed on adhesive carbon pads and coated with a conductive carbon film using a high-vacuum sputter coater (BAL-TEC MED 020, Bal Tec A).

FTIR spectroscopy

A FTIR-IFS 66 v/S spectrometer (Bruker) was used for recording of IR spectra of air-sensitive samples. The samples were mixed with KBr (Acros Organics, 99%) under argon and pressed into a pellet. The spectra were measured in the range of 400–4000 cm^{-1} and evaluated by OPUS.^[47]

A FTIR spectrum of LiPN_2 was recorded on a Perkin–Elmer BX II FTIR spectrometer equipped with a DuraSampler Diamond ATR (attenuated total reflection) unit under exposure to air.

4.5 Acknowledgements

The authors gratefully acknowledge financial support by the Deutsche Forschungsgemeinschaft (DFG) within the research group “Chemistry and Technology of the Ammonothermal Synthesis of Nitrides” (FOR 1600), project SCHN377/16-2 and the project SCHN377/18-1 “Neue Wege zu nitridischen Phosphat-Netzwerken”. Furthermore, we want to thank the group of Prof. Dr. E. Schlücker for fabrication of the autoclaves (FAU Erlangen-Nürnberg), Marion Sokoll for IR measurements and Christian Minke for EDX measurements (both at Department of Chemistry, LMU Munich).

4.6 References

- [1] H. Jacobs, R. Juza, "Darstellung und Eigenschaften von Magnesiumamid und -imid", *Z. Anorg. Allg. Chem.* **1969**, 370, 254-261.
- [2] R. Juza, H. Jacobs, "Ammonothermal Synthesis of Magnesium and Beryllium Amides", *Angew. Chem. Int. Ed. Engl.* **1966**, 5, 247; *Angew. Chem.* **1966**, 78, 208.
- [3] H. Jacobs, E. von Pinkowski, "Synthese ternärer nitride von alkalimetallen: Verbindungen mit tantal, $MTaN_2$ mit $M = Na, K, Rb$ und Cs ", *J. Less Common Met.* **1989**, 146, 147-160.
- [4] J. Häusler, W. Schnick, "Ammonothermal Synthesis of Nitrides: Recent Developments and Future Perspectives", *Chem. Eur. J.* **2018**, 24, 11864-11879.
- [5] T. Richter, R. Niewa, "Chemistry of Ammonothermal Synthesis", *Inorganics* **2014**, 2, 29-78.
- [6] R. Dwiliński, R. Doradziński, J. Garczyński, L. Sierzputowski, R. Kucharski, M. Zajac, M. Rudziński, R. Kudrawiec, W. Strupiński, J. Misiewicz, "Ammonothermal GaN substrates: Growth accomplishments and applications", *Phys. Status Solidi A* **2011**, 208, 1489-1493.
- [7] S. Pimputkar, S. Kawabata, J. S. Speck, S. Nakamura, "Improved growth rates and purity of basic ammonothermal GaN", *J. Cryst. Growth* **2014**, 403, 7-17.
- [8] W. Jiang, D. Ehrentraut, J. Cook, D. S. Kamber, R. T. Pakalapati, M. P. D'Evelyn, "Transparent, conductive bulk GaN by high temperature ammonothermal growth", *Phys. Status Solidi B* **2015**, 252, 1069-1074.
- [9] J. B. Shim, G. H. Kim, Y. K. Lee, "Basic ammonothermal growth of bulk GaN single crystal using sodium mineralizers", *J. Cryst. Growth* **2017**, 478, 85-88.
- [10] J. Hertrampf, P. Becker, M. Widenmeyer, A. Weidenkaff, E. Schlücker, R. Niewa, "Ammonothermal Crystal Growth of Indium Nitride", *Cryst. Growth Des.* **2018**, 18, 2365-2369.
- [11] J. Häusler, R. Niklaus, J. Minár, W. Schnick, "Ammonothermal Synthesis and Optical Properties of Ternary Nitride Semiconductors $Mg-IV-N_2$, $Mn-IV-N_2$ and $Li-IV_2-N_3$ ($IV=Si, Ge$)", *Chem. Eur. J.* **2018**, 24, 1686-1693.
- [12] J. Häusler, S. Schimmel, P. Wellmann, W. Schnick, "Ammonothermal Synthesis of Earth-Abundant Nitride Semiconductors $ZnSiN_2$ and $ZnGeN_2$ and Dissolution Monitoring by In Situ X-ray Imaging", *Chem. Eur. J.* **2017**, 23, 12275-12282.

- [13] J. Häusler, L. Neudert, M. Mallmann, R. Niklaus, A.-C. L. Kimmel, N. S. A. Alt, E. Schlücker, O. Oeckler, W. Schnick, "Ammonothermal Synthesis of Novel Nitrides: Case Study on CaGaSiN_3 ", *Chem. Eur. J.* **2017**, *23*, 2583-2590.
- [14] M. Mallmann, R. Niklaus, T. Rackl, M. Benz, T. G. Chau, D. Johrendt, J. Minár, W. Schnick, "Solid Solutions of Grimm-Sommerfeld Analogous Nitride Semiconductors II-IV-N₂ (II = Mg, Mn, Zn; IV = Si, Ge): Ammonothermal Synthesis and DFT Calculations", *Chem. Eur. J.* **2019**, *25*, 15887-15895.
- [15] N. Cordes, W. Schnick, "Ammonothermal Synthesis of Crystalline Oxonitride Perovskites LnTaON_2 (Ln=La, Ce, Pr, Nd, Sm, Gd)", *Chem. Eur. J.* **2017**, *23*, 11410-11415.
- [16] H. Jacobs, R. Nymwegen, "Synthesis and Crystal Structure of a Potassium Nitridophosphate, $\text{K}_3\text{P}_6\text{N}_{11}$ ", *Z. Anorg. Allg. Chem.* **1997**, *623*, 429-433.
- [17] M. Mallmann, C. Maak, R. Niklaus, W. Schnick, "Ammonothermal Synthesis, Optical Properties, and DFT Calculations of Mg_2PN_3 and Zn_2PN_3 ", *Chem. Eur. J.* **2018**, *24*, 13963-13970.
- [18] S. D. Kloß, W. Schnick, "Nitridophosphates – A Success Story of Nitride Synthesis", *Angew. Chem. Int. Ed.* **2019**, *58*, 7933-7944; *Angew. Chem.* **2019**, *131*, 8015-8027.
- [19] H. Jacobs, R. Nymwegen, S. Doyle, T. Wroblewski, W. Kockelmann, "Crystalline Phosphorus(V) Nitride Imide, HPN_2 and DPN_2 , respectively, – Structure Determination with X-Ray, Synchrotron, and Neutron Radiation", *Z. Anorg. Allg. Chem.* **1997**, *623*, 1467-1474.
- [20] H. Jacobs, S. Pollok, F. Golinski, "Synthesis and Crystal Structure of $\text{Na}_{10}[\text{P}_4(\text{NH})_6\text{N}_4](\text{NH}_2)_6(\text{NH}_3)_{0.5}$ with an Adamantane-like Anion $[\text{P}_4(\text{NH})_6\text{N}_4]^{4-}$ ", *Z. Anorg. Allg. Chem.* **1994**, *620*, 1213-1218.
- [21] H. Jacobs, F. Golinski, "Synthesis and Crystal Structure of a Cesium-tetraimidophosphate-diamid, $\text{Cs}_5[\text{P}(\text{NH})_4](\text{NH}_2)_2 = \text{Cs}_3[\text{P}(\text{NH})_4] \cdot 2 \text{CsNH}_2$ ", *Z. Anorg. Allg. Chem.* **1994**, *620*, 531-534.
- [22] F. Golinski, H. Jacobs, "Synthesis and Crystal Structure of $\text{Rb}_8[\text{P}_4\text{N}_6(\text{NH})_4](\text{NH}_2)_2$, with the Adamantane-like Anion $[\text{P}_4\text{N}_6(\text{NH})_4]^{6-}$ ", *Z. Anorg. Allg. Chem.* **1995**, *621*, 29-33.
- [23] W. Schnick, J. Luecke, "Synthesis and Crystal Structure of Lithium Phosphorus Nitride Li_7PN_4 : The First Compound Containing Isolated PN_4 -Tetrahedra", *J. Solid State Chem.* **1990**, *87*, 101-106.

- [24] W. Schnick, J. Lücke, "On Lithium Phosphorus Nitride. Preparation and Refinement of the Crystal Structure of LiPN_2 ", *Z. Anorg. Allg. Chem.* **1990**, 588, 19-25.
- [25] W. Schnick, U. Berger, " $\text{Li}_{10}\text{P}_4\text{N}_{10}$ - A Lithium Phosphorus(V) Nitride with the Novel Complex Anion $\text{P}_4\text{N}_{10}^{10-}$ ", *Angew. Chem. Int. Ed. Engl.* **1992**, 31, 213-214; *Angew. Chem.* **1991**, 103, 857-858.
- [26] E. M. Bertschler, C. Dietrich, T. Leichtweiß, J. Janek, W. Schnick, " Li^+ Ion Conductors with Adamantane-Type Nitridophosphate Anions $\beta\text{-Li}_{10}\text{P}_4\text{N}_{10}$ and $\text{Li}_{13}\text{P}_4\text{N}_{10}\text{X}_3$ with $\text{X}=\text{Cl}, \text{Br}$ ", *Chem. Eur. J.* **2018**, 24, 196-205.
- [27] W. Schnick, V. Schultz-Coulon, " Ca_2PN_3 - A Novel Phosphorus(V) Nitride with One-Dimensional Infinite Chains of Corner-Sharing PN_4 Tetrahedra", *Angew. Chem. Int. Ed. Engl.* **1993**, 32, 280-281; *Angew. Chem.* **1993**, 105, 308-309.
- [28] S. D. Kloß, N. Weidmann, R. Niklaus, W. Schnick, "High-Pressure Synthesis of Melilite-type Rare-Earth Nitridophosphates $\text{RE}_2\text{P}_3\text{N}_7$ and a $\text{Ba}_2\text{Cu}[\text{Si}_2\text{O}_7]$ -type Polymorph", *Inorg. Chem.* **2016**, 55, 9400-9409.
- [29] V. Schultz-Coulon, W. Schnick, " Mg_2PN_3 and Ca_2PN_3 - Phosphorus(V) Nitrides with Infinite Chains of Corner Sharing PN_4 Tetrahedra", *Z. Anorg. Allg. Chem.* **1997**, 623, 69-74.
- [30] S. Wendl, W. Schnick, " $\text{SrH}_4\text{P}_6\text{N}_{12}$ and $\text{SrP}_8\text{N}_{14}$: Insights into the Condensation Mechanism of Nitridophosphates under High Pressure", *Chem. Eur. J.* **2018**, 24, 15889-15896.
- [31] E.-M. Bertschler, C. Dietrich, J. Janek, W. Schnick, " $\text{Li}_{18}\text{P}_6\text{N}_{16}$ - A Lithium Nitridophosphate with Unprecedented Tricyclic $[\text{P}_6\text{N}_{16}]^{18-}$ Ions", *Chem. Eur. J.* **2017**, 23, 2185-2191.
- [32] S. D. Kloß, W. Schnick, "Rare-Earth-Metal Nitridophosphates through High-Pressure Metathesis", *Angew. Chem. Int. Ed.* **2015**, 54, 11250-11253; *Angew. Chem.* **2015**, 127, 11402-11405.
- [33] J. M. Sullivan, "Ammoniated phosphonitrilic amides, imides, and nitrides. I. The equilibrium $4\text{NH}_3(\text{g}) + 2\text{P}(\text{r}) = 2\text{PN}_2\text{H}(\text{s}) + 5\text{H}_2(\text{g})$ ", *Inorg. Chem.* **1976**, 15, 1055-1059.
- [34] F. Friedrichs, "Critical Phenomena in Binary Systems", *J. Am. Chem. Soc.* **1913**, 35, 1866-1883.
- [35] J. Hertrampf, N. S. A. Alt, E. Schlücker, R. Niewa, "Three Solid Modifications of $\text{Ba}[\text{Ga}(\text{NH}_2)_4]_2$: A Soluble Intermediate in Ammonothermal GaN Crystal Growth", *Eur. J. Inorg. Chem.* **2017**, 902-909.

- [36] H. Jacobs, U. Fink, "Über natrium- und kaliumamidometallate des calciums, strontiums und europiums", *J. Less Common Met.* **1979**, 63, 273-286.
- [37] F. Golinski, H. Jacobs, "Crystal Structure of Hexamine Cyclotriphosphazene, $P_3N_3(NH_2)_6$ ", *Z. Anorg. Allg. Chem.* **1994**, 620, 965-968.
- [38] H. Jacobs, R. Kirchgässner, "Hexaminecyclotriphosphazenehemiammoniat, $P_3N_3(NH_2)_6 \cdot 0.5 NH_3$, a Product of High Pressure Ammonolysis of White Phosphorus ", *Z. Anorg. Allg. Chem.* **1990**, 581, 125-134.
- [39] The terms *dreier* rings, *vierer* rings and *zweier* single chain were coined by Liebau and are derived from the German words "dreier, vierer and zweier"; a *dreier* ring comprises three tetrahedra centers, a *vierer* ring four tetrahedra centers, a *zweier* chain can be described as two polyhedra within one repeating unit of the linear part of the chain.
- [40] F. Liebau, "Structural Chemistry of Silicates", Springer, Berlin, **1985**.
- [41] S. Schimmel, M. Lindner, T. G. Steigerwald, B. Hertweck, T. M. M. Richter, U. Künecke, N. S. A. Alt, R. Niewa, E. Schlücker, P. J. Wellmann, "Determination of GaN solubility in supercritical ammonia with NH_4F and NH_4Cl mineralizer by in situ x-ray imaging of crystal dissolution", *J. Cryst. Growth* **2015**, 418, 64-69.
- [42] T. G. Steigerwald, J. Balouschek, B. Hertweck, A.-C. L. Kimmel, N. S. A. Alt, E. Schlücker, "In situ investigation of decomposing ammonia and ammonobasic solutions under supercritical conditions via UV/vis and Raman Spectroscopy", *J. Supercrit. Fluids* **2018**, 134, 96-105.
- [43] A. Stock, B. Hoffmann, "Die Einwirkung von Ammoniak auf Phosphorpentasulfid und der Phosphorstickstoff, P_3N_5 ", *Ber. Dtsch. Chem. Ges.* **1903**, 36, 314-319.
- [44] R. Suhrmann, K. Clusius, "Über die Reindarstellung der Alkalimetalle", *Z. Anorg. Allg. Chem.* **1926**, 152, 52-58.
- [45] F. W. Karau, *Dissertation*, Ludwig-Maximilians-Universität München (Germany) **2007**.
- [46] A. Coelho, *TOPAS Academic, Version 6*, Coelho Software, Brisbane (Australia), **2016**.
- [47] *OPUS/IR*, Bruker Analytik GmbH, Karlsruhe, **2000**.

5 Ammonothermal Synthesis of $\text{Ba}_2\text{PO}_3\text{N}$ – An Oxonitridophosphate with Non-Condensed PO_3N Tetrahedra

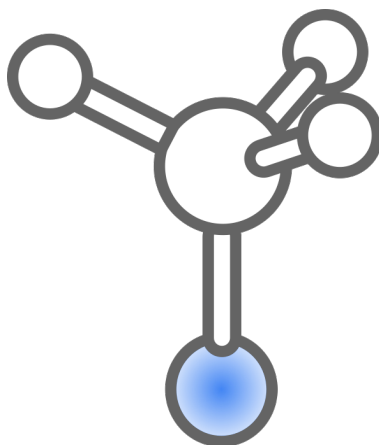
Sebastian Wendl, Dr. Mathias Mallmann, Dr. Philipp Strobel, Dr. Peter J. Schmidt,

Prof. Dr. Wolfgang Schnick

Eur. J. Inorg. Chem. **2020**, 841–846.

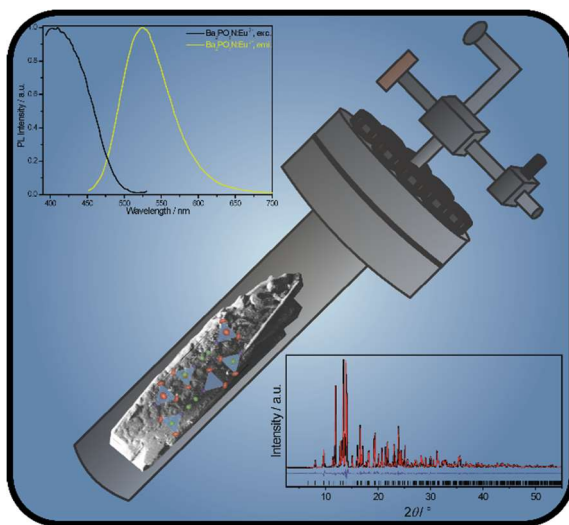
DOI: 10.1002/ejic.202000041

Reprinted (adapted) with permission for non-commercial use from *European Journal of Inorganic Chemistry* (open access). Copyright 2021 John Wiley and Sons.



Ortho-oxonitridophosphate: $\text{Ba}_2\text{PO}_3\text{N}$ was synthesized in a high-temperature autoclave starting from red phosphorus P_{red} , BaO , NaN_3 and KOH . $\text{Ba}_2\text{PO}_3\text{N}$ extends the range for accessible degrees of condensation of (oxo-)nitridophosphates to $\kappa = 1/4$ and represents the first nitridophosphate with non-condensed tetrahedra synthesized by ammonothermal technique.

Abstract: The ortho-oxonitridophosphate Ba_2PO_3N was synthesized under ammonobasic conditions ($T = 1070\text{ K}$, $p = 120\text{ MPa}$) in custom-built high-temperature autoclaves, starting from red phosphorus, BaO , NaN_3 and KOH . Thus, single crystals of up to several hundred μm were obtained, which were used for singlecrystal X-ray diffraction. Ba_2PO_3N [$Pnma$ (no. 62), $a = 7.596(2)$, $b = 5.796(1)$, $c = 10.212(3)\text{ \AA}$, $Z = 4$] crystallizes in the $\beta\text{-K}_2\text{SO}_4$ structure type with non-condensed $[PO_3N]^{4-}$ ions and isotypic to its lighter homologues EA_2PO_3N ($EA = Ca, Sr$). Powder X-ray diffraction, energy dispersive X-ray and Fourier Transformed Infrared spectroscopy corroborate the crystal structure. The optical band gap was determined by means of diffuse reflectance UV/Vis spectroscopy to be 4.3 eV . Eu^{2+} doped samples show green luminescence ($\lambda_{em} = 534\text{ nm}$, $fwhm = 85\text{ nm}/2961\text{ cm}^{-1}$) when irradiated with UV light ($\lambda_{exc} = 420\text{ nm}$). However, $Ba_2PO_3N:Eu^{2+}$ shows strong thermal quenching, even at room temperature.



5.1 Introduction

During the 1960s, Jacobs and co-workers developed the ammonothermal method, in which supercritical ammonia is used as solvent and nitrogen source for the synthesis of various imides, amides and nitrides.^[1-6] Thereby, supercritical ammonia facilitates the crystallization process, as it increases the solubility of the inorganic starting materials, which are quite insoluble in liquid ammonia.^[7,8] With the first synthesis of GaN in supercritical ammonia in 1995, the ammonothermal approach was established as important method for synthesis and crystal growth of high-quality GaN crystals.^[9-11] Subsequently, the ammonothermal approach turned out as a promising route for explorative synthesis of different (oxide) nitrides such as wurtzite-type Grimm–Sommerfeld analogous nitrides [e.g. InN, II-IV-N₂ (II = Mg, Mn, Zn; IV = Si, Ge), CaGaSiN₃ or Ca_{1-x}Li_xAl_{1-x}Ge_{1+x}N₃ ($x \approx 0.2$)] and oxide nitride perovskites [e.g. EAMO₂N (EA = Sr, Ba; M = Nb, Ta)] as well.^[12-18] Most recently, the syntheses of numerous nitridophosphates with different degrees of condensations κ (i.e. atomic ratio of tetrahedra centers to ligand) could be realized. Here, a great structural diversity ranging from non-condensed tetrahedra groups up to network structure types, exhibiting values for κ from 1/3 to 4/7, was observed.^[19-21] Compared to other synthetic methods towards nitridophosphates, such as condensation reactions, synthesis in pressure ampoules or high-pressure synthesis using the multianvil technique, the ammonothermal method exhibits significant advantages.^[22] This includes the prevention of thermal decomposition of the target compounds, the use of simple starting materials including red phosphorus (P_{red}) as well as large sample volumes for a detailed characterization of their materials properties.^[21]

However, there is no ammonothermally synthesized *ortho*-(oxo)nitridophosphate showing non-condensed [PO_{4-x}N_x]^{(3+x)-} tetrahedra, up to now. Such structural features were only observed in Li₇PN₄, Li₁₄[PON₃]₂O, EA₂PO₃N (EA = Ca, Sr) and Ho₃[PN₄]O, which were synthesized in ampoules or via high-pressure synthesis, respectively.^[23-26] Especially, the EA₂PO₃N compounds are of special interest, as they crystallize isotypically to β -K₂SO₄. Accompanied with a plethora of compounds crystallizing in this structure type, a great diversity of materials properties is observed. Especially, the potential as host lattices for luminescent materials is impressive, covering the whole visible spectrum from red (LaEASiO₃N:Eu²⁺ with EA = Sr, Ba) over green (Ca₂PO₃N:Eu²⁺) to blue (KSrPO₄:Eu²⁺) emission.^[25, 27, 28]

In this contribution, we present the ammonothermal synthesis of the *ortho*-oxonitridophosphate Ba_2PO_3N containing discrete $[PO_3N]^{4-}$ ions, extending the degree of condensation range of ammonothermally accessible nitridophosphates to $1/4 \leq \kappa \leq 4/7$. The structure was elucidated using single-crystal X-ray diffraction on ammonothermally grown crystallites with sizes up to several hundreds of μm . Bulk samples were used for further analysis as well as for examination of luminescence properties of Eu^{2+} doped Ba_2PO_3N . Together with earlier reported investigations on the ammonothermal approach, this work demonstrates once again the high potential of this method regarding synthesis and crystal growth of (oxide) nitride materials.

5.2 Results and Discussion

Synthesis

The oxonitridophosphate Ba_2PO_3N was synthesized ammonothermally using custom-built high-temperature autoclaves made of the nickel-based super-alloy Haynes® 282®. Stoichiometric amounts of P_{red} and BaO were used as starting materials. KOH and NaN_3 were added as additional oxygen and nitrogen sources as well as ammonobasic mineralizers. They form in situ $NaNH_2$ and KNH_2 , which increase the solubility of the other starting materials by the formation of soluble intermediate species, such as mixed amides [e.g. $KBa(NH_2)_3$] and phosphorus containing compounds like hexaaminocyclotriphosphazene $[PN(NH_2)_2]_3$, the corresponding ammoniate $[PN(NH_2)_2]_3 \cdot 0.5 NH_3$ or the imidonitride $Na_{10}[P_4(NH)_6N_4](NH_2)_6(NH_3)_{0.5}$.^[3, 7, 21, 29–31] When using NaOH instead of KOH, Ba_2PO_3N appears only as side-phase without any single crystals of significant size. The remaining PXRD reflections could not be assigned to any known compound. A possible explanation could be the non-existence of a Na analog to $KBa(NH_2)_3$, resulting in a lower solubility.

Based on the observation that such intermediates are preferably formed at low temperatures, the reaction mixture was heated in a first step to a temperature of 670 K. After 16 h the autoclave was subsequently heated to 1070 K, reaching a pressure of 120 MPa, in order to transform the intermediate species into the oxonitridophosphate Ba_2PO_3N . Upon adding $Eu(NH_2)_2$ to the starting materials, the product exhibits green luminescence (see Luminescence section). To prevent the

product from autoclave impurities, the reaction mixture was filled into a Ta-liner. In addition, the liner wall acted as a substrate for single-crystal growth of the product. Thereby, single crystals with sizes up to $\approx 600 \mu\text{m}$ were accessible. Figure 5.1 illustrates ammonothermally grown crystals of $\text{Ba}_2\text{PO}_3\text{N}:\text{Eu}^{2+}$. The size of the crystals, which are up to several hundred μm , as well as the fact that the crystals grew on the wall at the upper part of the liner, which is supposed to be the colder zone, suggest a solution based transport and growth mechanism via intermediate species.

The obtained white ($\text{Ba}_2\text{PO}_3\text{N}$) and yellow ($\text{Ba}_2\text{PO}_3\text{N}:\text{Eu}^{2+}$) products are slightly sensitive towards moisture and were therefore washed with dry ethanol to eliminate hygroscopic residual mineralizer and intermediate species.

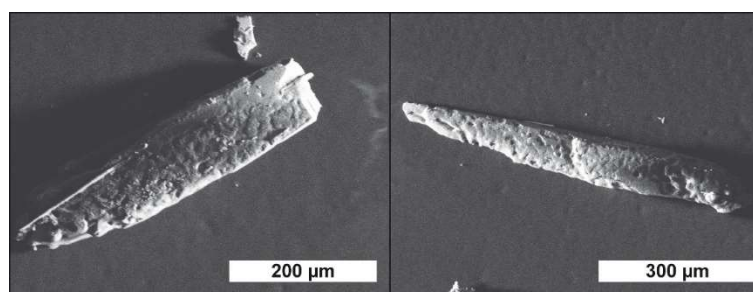


Figure 5.1. SEM images of $\text{Ba}_2\text{PO}_3\text{N}:\text{Eu}^{2+}$ crystals.

Crystal Structure

The crystal structure of $\text{Ba}_2\text{PO}_3\text{N}$ was solved and refined from single-crystal X-ray diffraction data in the orthorhombic space group $Pnma$ (no. 62) with lattice parameters $a = 7.596(2)$, $b = 5.796(1)$ and $c = 10.212(3) \text{ \AA}$. The crystallographic data are summarized in Table 5.1. Wyckoff positions and atomic coordinates, anisotropic displacement parameters, as well as interatomic distances and angles are given in Tables D.1–D.3 (Supporting Information). $\text{Ba}_2\text{PO}_3\text{N}$ crystallizes in the $\beta\text{-K}_2\text{SO}_4$ structure type and is isotopic to its lighter homologues $\text{Ca}_2\text{PO}_3\text{N}$ and $\text{Sr}_2\text{PO}_3\text{N}$.^[25] As expected, the lattice parameters of the three $\text{EA}_2\text{PO}_3\text{N}$ compounds increase linearly with increasing size of the alkaline earth ions (see Figure D.1, Supporting Information). The crystal structure is built up from non-condensed $[\text{PO}_3\text{N}]^{4-}$ tetrahedra (see Figure 5.2) and therefore exhibits a degree of condensation of $\kappa = n(\text{P})/n(\text{O},\text{N}) = 1/4$, which expands the range of ammonothermally accessible degrees of condensation for (oxo)nitridophosphates to $1/4 \leq \kappa \leq 4/7$. The assignment of O and N atoms was

carried out in accordance with the structure model of EA₂PO₃N (EA = Ca, Sr).^[25] Lattice energy calculations (MAPLE),^[32–35] bond-valance sums (BVS)^[36, 37] as well as charge distribution (CHARDI)^[38] calculations support the ordering and show only slight deviations from expected values (see Tables D.4–D.6, Supporting Information). The P–O [1.573(2)–1.602(2) Å] and P–N distances [1.578(2) Å] are in good agreement with bond lengths of other alkaline earth oxonitridophosphates known from literature (e.g. Ca₂PO₃N, Sr₂PO₃N, SrP₃N₅O, Sr₃P₆O₆N₈, Ba₃P₆O₆N₈).^[25, 39–41] The corresponding O/N–P–O/N angles vary between 107.81(9) and 112.6(2)° and deviate only slightly from the regular tetrahedron angle and are also in good agreement with values known from literature. The crystal structure contains two crystallographically different Ba positions.

Table 5.1. Crystallographic data of Ba₂PO₃N obtained from single-crystal X-ray diffraction.

Formula	Ba ₂ PO ₃ N
Crystal system	orthorhombic
Space group	<i>Pnma</i> (no. 62)
<i>a</i> / Å	7.596(2)
<i>b</i> / Å	5.796(1)
<i>c</i> / Å	10.212(3)
Cell volume / Å ³	449.6(2)
Formula units/cell	4
Density / g·cm ⁻³	5.4325
Crystal size / mm ³	0.01×0.03×0.04
μ / mm ⁻¹	17.640
<i>T</i> / K	296(2)
Diffractometer	Bruker D8 Quest
Radiation / Å	Mo-K α (0.71073)
<i>F</i> (000)	632
2 θ range / °	3.343 - 35.687
Total no. of reflections	15148
No. of independent reflections	1121
Observed reflections ($F^2 > 2\sigma(F^2)$)	1029
R_{int} ; R_σ	0.0432; 0.0182
Structure solution	SHELXT
Structure refinement	SHELXL
Refined parameters	40
Goodness of fit (χ^2)	1.197
$R1$ (all data); $R1$ ($F^2 > 2\sigma(F^2)$)	0.0210; 0.0177
$wR2$ (all data); $wR2$ ($F^2 > 2\sigma(F^2)$)	0.0344; 0.0335
$\Delta\rho_{max}$; $\Delta\rho_{min}$ [e·Å ⁻³]	1.050, -1.327

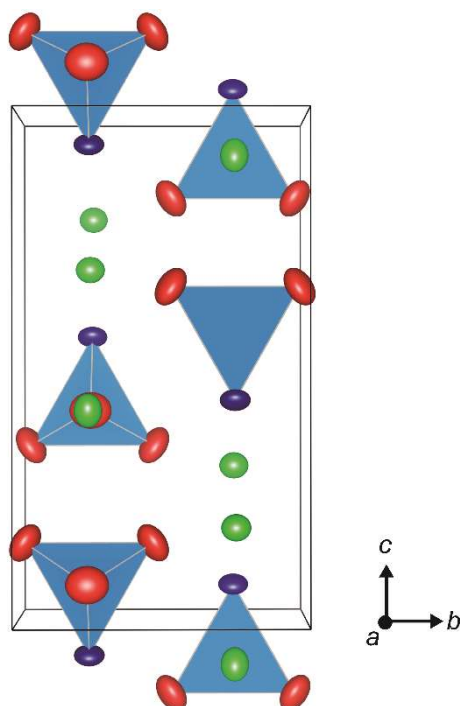


Figure 5.2. Crystal structure of $\text{Ba}_2\text{PO}_3\text{N}$ along [001] with Ba atoms in green, O atoms in red, N atoms in blue and PO_3N tetrahedra in blue (displacement parameters with 90% probability, drawings generated with VESTA).^[42]

While Ba1 is coordinated by three N and seven O atoms, Ba2 is only surrounded by two N and seven O atoms (see Figure 5.3). The Ba–O [2.764(2)–3.131(2) Å] and Ba–N distances [2.731(3)–3.043(3) Å] are in the same range as already reported for other barium (oxo)nitridophosphates (e.g. $\text{Ba}_3\text{P}_6\text{O}_6\text{N}_8$, BaP_2N_4 , $\text{Ba}_3\text{P}_5\text{N}_{10}\text{X}$).^[41, 43, 44] Based on the obtained structure model from single-crystal X-ray diffraction, a Rietveld refinement of powder X-ray diffraction data was conducted in order to check phase purity. Thereby, a small amount of an unknown side phase, which is marked with asterisks in Figure 5.4, was observed. The washed product shows no evidence of residual mineralizers such as NaNH_2 or KNH_2 . Table D.7 and D.8 in the Supporting Information summarize the crystallographic data.

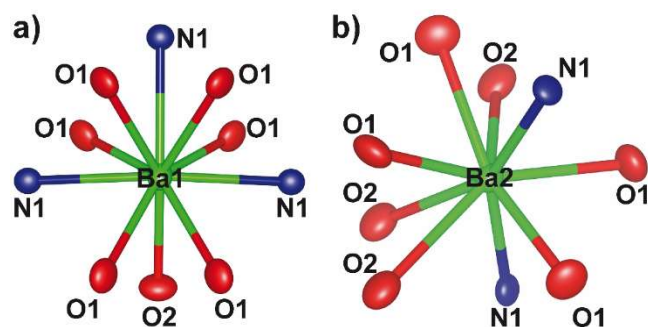


Figure 5.3. Coordination of Ba1 (a) and Ba2 (b) atoms in Ba_2PO_3N . Ba atoms are illustrated in green, O atoms in red and N atoms in blue (displacement parameters with 90% probability, drawings generated with VESTA).^[42]

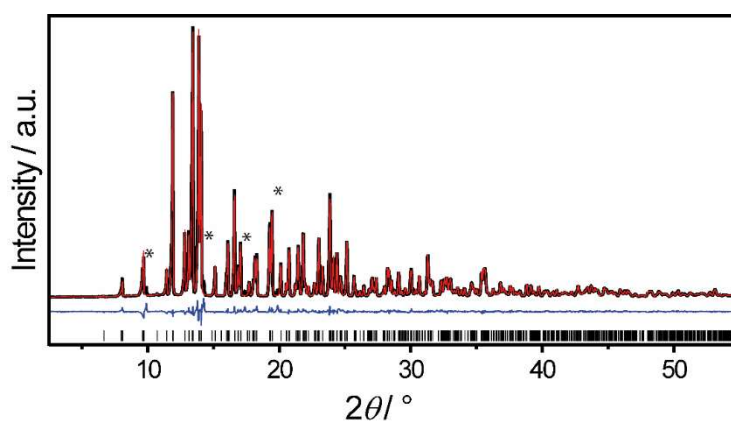


Figure 5.4. Rietveld refinement of PXRD data of Ba_2PO_3N with experimental data (black line), calculated diffraction pattern (red line), difference profile (blue line) and reflection positions of Ba_2PO_3N (black bars). Reflections of unknown side phases are marked with asterisks. Energy Dispersive X-ray Spectroscopy (EDX)

Energy Dispersive X-ray Spectroscopy (EDX)

EDX measurements on Eu^{2+} doped Ba_2PO_3N samples (nominal concentration of ≈ 1 mol% regarding to Ba) were carried out for chemical analysis and no elements other than the expected (Ba, P, O, and N) and trace amounts of Eu were detected. The obtained atomic ratio of Ba/P/O/N $\approx 2.1:1.0:2.5:0.9$ is in good agreement with the sum formula of the title compound (Table D.9, Supporting Information).

Fourier-Transform Infrared Spectroscopy (FTIR)

The exclusion of any NH_x functionality in $\text{Ba}_2\text{PO}_3\text{N}$ was performed by FTIR spectroscopy. As no significant absorption bands appear in the region around 3000 cm^{-1} (Figure D.2, Supporting Information), the absence of N–H groups in the crystal structure can be confirmed.^[45] However, the broad and weak band between 2400 and 3400 cm^{-1} can be explained by partial surface hydrolysis of the sample, owed to the measuring method. The strong absorption bands in the region between 600 and 1400 cm^{-1} can be attributed to symmetric and asymmetric stretching modes of the P–N-framework and are similar to the absorption bands of $\text{Ca}_2\text{PO}_3\text{N}$ and $\text{Sr}_2\text{PO}_3\text{N}$, indicating the structural similarity of these three compounds.^[25]

UV/Vis Spectroscopy

In order to investigate the optical properties of $\text{Ba}_2\text{PO}_3\text{N}$, diffuse reflectance spectroscopy was conducted. The spectrum shows an absorption band around 250 nm (Figure D.3, Supporting Information), which is in agreement with the white color of the sample. The Kubelka–Munk function $F(R) = (1-R)^2/2R$, where R represents the reflectance, was used to calculate a pseudo-absorption spectrum.^[46] The band gap was determined subsequently by drawing a tangent at the inflection point of the Tauc plot (see Figure 5.5), where $[F(R)\cdot h\nu]^{1/n}$ is plotted vs. $h\nu$, with $n = 1/2$ assuming a direct transition.^[47] The determined band gap is approximately 4.3 eV .

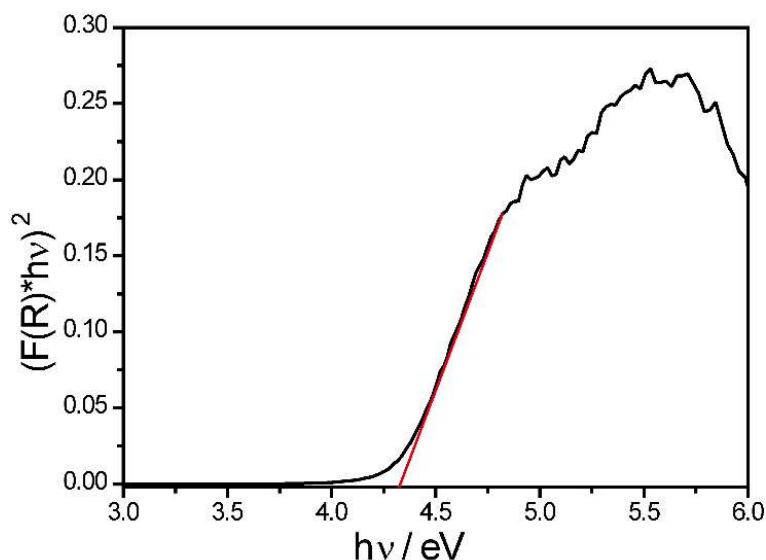


Figure 5.5. Tauc plot of Ba_2PO_3N (black line) with a tangent at the inflection point (red line).

Luminescence

$Ba_2PO_3N:Eu^{2+}$ shows strong green emission upon irradiation with UV light (see Figure D.4 in the Supporting Information). The excitation spectrum (see Figure 5.6) of a $Ba_2PO_3N:Eu^{2+}$ (≈ 1 at.% Eu^{2+}) single crystal shows a maximum at 410 nm. Upon excitation ($\lambda_{exc} = 420$ nm), the title compound shows broad emission at $\lambda_{em} = 534$ nm with a full width at half-maximum (fwhm) of 85 nm/ 2961 cm^{-1} . The broad emission arises most likely from the two emission bands, due to two different Ba positions, which can be substituted by Eu^{2+} . The luminescence behavior is similar to that of isotypic $Ca_2PO_3N:Eu^{2+}$ and the oxosilicates $M_2SiO_4:Eu^{2+}$ ($M = Ca, Sr, Ba$) crystallizing in the β - K_2SO_4 structure type as well.^[25, 48] Furthermore, the emission wavelength of $Ba_2PO_3N:Eu^{2+}$ is similar to that of $SrP_2N_4:Eu^{2+}$ ($\lambda_{em} = 529$ nm), however, the emission is broader (fwhm = 2432 cm^{-1}).^[43]

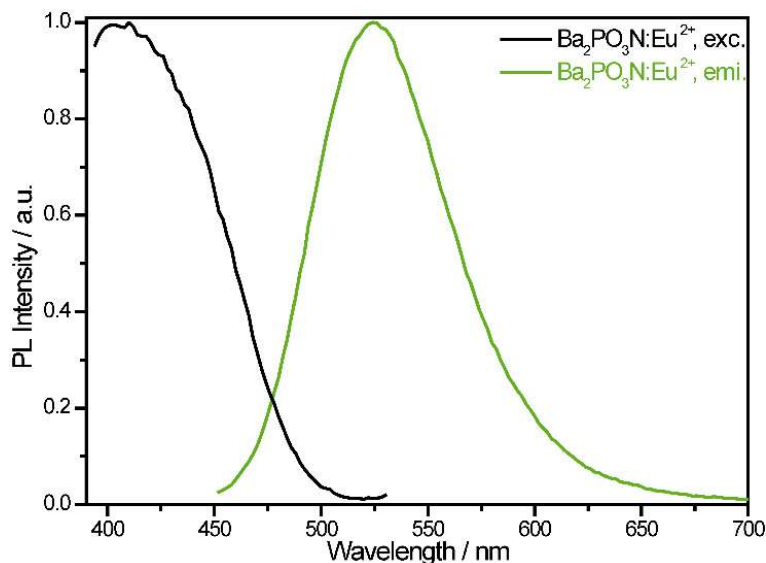


Figure 5.6. Excitation (black line) and emission (green line) spectra of $\text{Ba}_2\text{PO}_3\text{N}:\text{Eu}^{2+}$.

Low temperature measurements ($\lambda_{\text{exc}} = 390 \text{ nm}$) between 6 and 300 K were conducted on thick-bed powder samples in order to investigate thermal quenching of $\text{Ba}_2\text{PO}_3\text{N}:\text{Eu}^{2+}$. For this purpose, the luminescence intensities were measured and integrated at different temperatures (Figure D.5 in the Supporting Information). Figure 5.7 illustrates the thermal quenching of $\text{Ba}_2\text{PO}_3\text{N}:\text{Eu}^{2+}$, by decreasing the initial intensity (6 K) down to $\approx 40\%$ at room temperature. For this reason, no further measurements such as internal quantum efficiency or high-temperature measurements were conducted. The stronger thermal quenching of the title compound compared to the isotypic orthosilicates $(\text{Ba},\text{Sr})_2\text{SiO}_4:\text{Eu}^{2+}$ ($\lambda_{\text{em}} \approx 525 \text{ nm}$, $\text{fwhm} \approx 2420 \text{ cm}^{-1}$)^[48] that found practical application in solid-state lighting can be explained by the smaller optical band gap of the title compound (Ba_2SiO_4 ; $E_g = 6.81 \text{ eV}$) that results in more pronounced non-radiative de-excitation of the activator ion via a photoionization process.^[49] Additionally, the low temperature measurements reveal a second emission band, which is in accordance with the former mentioned presence of two substantially different Ba^{2+} sites. The observation of this second band, which is not obvious in the emission spectrum of the single crystal, might be traced back to the different excitation wavelengths or different activation energies of the two different excited Eu states towards photoionization.

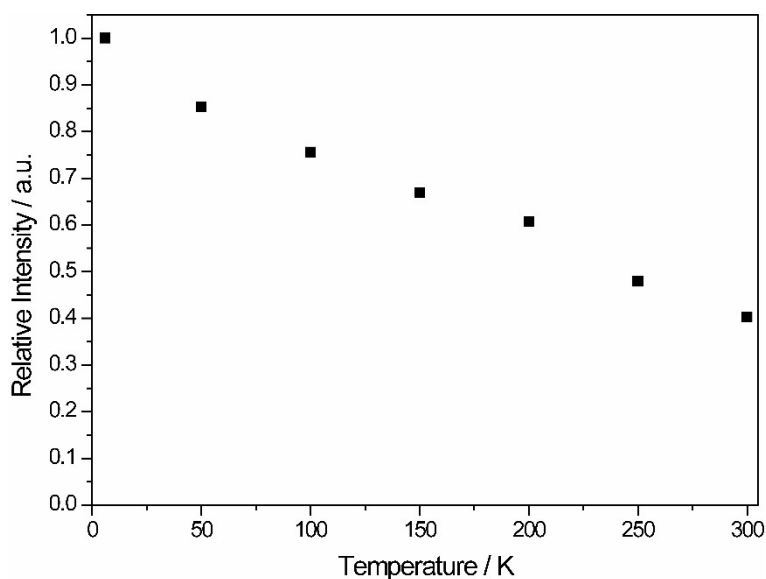


Figure 5.7. Thermal quenching data for $Ba_2PO_3N:Eu^{2+}$ at low temperatures (6–300 K).

5.3 Conclusions

The *ortho*-oxonitridophosphate Ba_2PO_3N was synthesized in supercritical ammonia starting from BaO, red phosphorus, KOH and NaN_3 at a temperature of 1070 K and a maximum pressure of 120 MPa using custom-built high-temperature autoclaves. KOH and NaN_3 act as ammonobasic mineralizers to increase the solubility of the other starting materials. In doing so, crystallites with sizes up to $\approx 600 \mu m$ grew on the wall at the upper part of the liner, which suggest a solution-based crystallization process via soluble intermediate species. The crystal structure was solved and refined from single-crystal X-ray diffraction. Ba_2PO_3N crystallizes in the β - K_2SO_4 structure type and is the first representative of an ammonothermally synthesized oxonitridophosphate with non-condensed PO_3N tetrahedra, expanding the degree of condensation range of ammonothermally accessible nitridophosphates to $1/4 \leq \kappa \leq 4/7$. The band gap was determined with diffuse reflectance spectroscopy to be 4.3 eV. Eu^{2+} doped samples show luminescence in the green region of the visible spectrum ($\lambda_{em} = 534 \text{ nm}$, $fwhm = 85 \text{ nm}/2961 \text{ cm}^{-1}$) when excited with UV light ($\lambda_{exc} = 420 \text{ nm}$). Low temperature measurements indicated strong thermal quenching even at room temperature, as only 40% intensity remains compared to the intensity at 6 K. For future investigations, it would be interesting, if the ammonothermal method is applicable for synthesis of further *ortho*-

(oxo)nitridophosphates and if the findings on ammonothermal (oxo)nitridophosphates in general could be transferred to other oxide or nitride systems such as (oxo)nitridosilicates.

5.4 Experimental Section

Due to moisture-sensitivity of the product, all manipulations were conducted under exclusion of oxygen and moisture in argon filled gloveboxes (Unilab, MBraun, Garching, $O_2 < 1$ ppm, $H_2O < 1$ ppm). The filling of the autoclaves with ammonia was performed on a vacuum line (≤ 0.1 Pa) with argon and ammonia (both: Air Liquide, 99.999%) supply. Washing treatments of the products were carried out in flame-dried Schlenk-type glassware connected to a vacuum line (≤ 0.1 Pa). All gases were further purified using gas purification cartridges [Micro Torr FT400–902 (for Ar) and MC400–702FV (for NH_3), SAES Pure Gas Inc., San Luis Obispo, CA, USA], providing a purity level of < 1 ppbV H_2O , O_2 and CO_2 (manufacturer's data).

Synthesis of $Eu(NH_2)_2$

$Eu(NH_2)_2$ was synthesized starting from Eu metal (99.99%, smart elements) in supercritical ammonia according to the synthesis described in literature.^[50]

Ammonothermal Synthesis

Ba_2PO_3N was synthesized ammonothermally starting from 0.75 mmol red P (23.2 mg, Merck, 99%), 1.5 mmol BaO (230 mg, Alfa Aesar, 99.5%), 0.75 mmol KOH (42.1 mg, Merck, 90%) and 0.75 mmol NaN_3 (48.8 mg, Sigma-Aldrich, 99.5%). In order to obtain Eu^{2+} doped samples, 0.015 mmol $Eu(NH_2)_2$ (3 mg) were added to the reaction mixture. All starting materials were ground in an agate mortar and transferred into a tantalum liner to protect the sample from autoclave impurities. After placing the liner in a Haynes® 282® autoclave (nickel based super-alloy, max. 1100 K, 170 MPa, 10 mL), the later was sealed via flange joints using a silver coated Inconel® 718 ring (GFD seals). The autoclave body is connected to a hand valve (SITEC) by an Inconel® 718 high-pressure tube. The hand valve contains a pressure transmitter (HBM P2VA1/5000 bar) and a bursting disk

(SITEC). The assembled autoclave was evacuated, cooled to 198 K using an ethanol/liquid nitrogen mixture and filled with NH_3 (≈ 3.0 mL). The amount of NH_3 was determined using a mass flow meter (D-6320-DR, Bronkhorst, Ruurlo, Netherlands). After filling, the autoclave was heated within 2 h to 670 K and held at this temperature for 16 h, then heated to 1070 K within 3 h and held for 72 h reaching a maximum pressure of 120 MPa. Subsequently, the autoclave was cooled down and residual NH_3 was removed. The white (Ba_2PO_3N) and yellow ($Ba_2PO_3N:Eu^{2+}$) products were removed and washed with dry ethanol and dried under vacuum. Irregularly shaped single crystals of the product with sizes up to several hundred of μm grew on the wall of the liner.

Single-Crystal X-ray Diffraction

For single-crystal XRD measurements, $Ba_2PO_3N:Eu^{2+}$ single crystals were placed and sealed in glass capillaries (Hilgenberg GmbH) under argon atmosphere. A Bruker D8 Quest diffractometer with $Mo-K_{\alpha}$ radiation ($\lambda = 0.71073$ Å) was used for data collection. The software package APEX3 was used for indexing and integration.^[51, 52] Furthermore, APEX3 was used for semiempirical absorption corrections (SADABS) and space group determination.^[52–54] The crystal structure was solved using the SHELXT algorithm and refined by full-matrix least-squares methods using WinGX with implemented SHELXL.^[55, 56]

CSD 1975933 (for Ba_2PO_3N) contains the supplementary crystallographic data for this paper. These data can be obtained free of charge from FIZ Karlsruhe.

Powder X-ray Diffraction

The ground product was placed and sealed in a glass capillary ($d = 0.3$ mm, Hilgenberg GmbH) in argon atmosphere for PXRD measurement. The measurement was conducted using a Stoe STADI P diffractometer with $Mo-K_{\alpha 1}$ ($\lambda = 0.71073$ Å) radiation, Ge(111) monochromator and Mythen 1K detector in modified Debye–Scherrer geometry. The program TOPAS was used for Rietveld refinement of the measured data.^[57]

Scanning Electron Microscopy

Single-crystal images as well as EDX measurements were conducted on a scanning electron microscope [Dualbeam Helios Nanolab G3 UC (FEI), equipped with an EDX detector (X-Max 80 SDD, Oxford instruments)]. For this purpose, the samples were placed on adhesive carbon pads. Coating of the samples with a conductive carbon film was performed with a high-vacuum sputter coater (BAL-TEC MED 020, Bal Tec A).

Fourier Transform Infrared Spectroscopy

A Perkin Elmer BX II FTIR spectrometer equipped with a DuraSampler Diamond ATR (attenuated total reflection) unit under exposure to air was used for collection of a FTIR spectrum of $\text{Ba}_2\text{PO}_3\text{N}$.

UV/Vis Spectroscopy

UV/Vis measurements were conducted using a Jasco V-650 UV/Vis spectrophotometer equipped with Czerny-Turner mount, photomultiplier tube detector and deuterium (190–350 nm)/halogen (330–900 nm) lamps as light sources to estimate the optical band gap of $\text{Ba}_2\text{PO}_3\text{N}$. For this purpose, a diffuse reflectance measurement of the sample at room temperature was performed.

Luminescence Measurements

Single crystals sealed in silica glass capillaries were used for investigation of the luminescence properties of $\text{Ba}_2\text{PO}_3\text{N}:\text{Eu}^{2+}$. A HORIBA Fluoromax4 spectrofluorimeter system, attached via optical fibers to an Olympus BX51 microscope was used for data collection ($\lambda_{\text{exc}} = 420 \text{ nm}$).

Low-temperature measurements were conducted in the range from 300 to 6 K performed on a thick-bed powder layer using a fiber-coupled spectroscopy system containing a thermally stabilized LED light source and a fiber-optic spectrometer from Ocean Optics (HR2000+ES) in an evacuated cooling chamber ($\lambda_{\text{exc}} = 390 \text{ nm}$). The samples was cooled via a liquid-He compressor system from Advance Research System Inc. (ARS4HW).

5.5 Acknowledgements

The authors want to thank Lisa Gamperl for EDX measurements and Arthur Haffner for single-crystal X-ray measurements (all at Department of Chemistry, LMU Munich) as well as the group of Prof. Dr. E. Schlücker (especially Anna Kimmel and Dr. Thomas Steigerwald) for fabrication of the autoclaves (FAU Erlangen-Nürnberg). Financial support by the Deutsche Forschungsgemeinschaft (DFG) within the research group “Chemistry and Technology of the Ammonothermal Synthesis of Nitrides” (FOR 1600), project SCHN377/16-2, is gratefully acknowledged.

5.6 References

- [1] R. Juza, H. Jacobs, "Ammonothermal Synthesis of Magnesium and Beryllium Amides", *Angew. Chem. Int. Ed. Engl.* **1966**, 5, 247; *Angew. Chem.* **1966**, 78, 208.
- [2] H. Jacobs, U. Fink, "Über natrium- und kaliumamidometallate des calciums, strontiums und europiums", *J. Less Common Met.* **1979**, 63, 273-286.
- [3] H. Jacobs, J. Kockelkorn, J. Birkenbeul, "Struktur und eigenschaften der ternären metallamide $\text{NaCa}(\text{NH}_2)_3$, $\text{KBa}(\text{NH}_2)_3$, $\text{RbBa}(\text{NH}_2)_3$, $\text{RbEu}(\text{NH}_2)_3$ und $\text{RbSr}(\text{NH}_2)_3$ ", *J. Less Common Met.* **1982**, 87, 215-224.
- [4] D. Peters, H. Jacobs, "Ammonothermalsynthese von kristallinem siliciumnitridimid, $\text{Si}_2\text{N}_2\text{NH}$ ", *J. Less Common Met.* **1989**, 146, 241-249.
- [5] T. Brokamp, H. Jacobs, "Darstellung und Struktur einiger Gemischtvalenter ternärer Tantalnitride mit Lithium und Magnesium", *J. Alloys Compd.* **1992**, 183, 325-344.
- [6] H. Jacobs, E. von Pinkowski, "Synthese ternärer nitride von alkalimetallen: Verbindungen mit tantal, MTaN_2 mit $M = \text{Na}, \text{K}, \text{Rb}$ und Cs ", *J. Less Common Met.* **1989**, 146, 147-160.
- [7] T. Richter, R. Niewa, "Chemistry of Ammonothermal Synthesis", *Inorganics* **2014**, 2, 29-78.
- [8] J. Häusler, W. Schnick, "Ammonothermal Synthesis of Nitrides: Recent Developments and Future Perspectives", *Chem. Eur. J.* **2018**, 24, 11864-11879.
- [9] R. Dwilinski, A. Wysmolek, J. Baranowski, M. Kaminska, R. Doradziński, H. Jacobs, "GaN synthesis by ammonothermal method", *Acta Phys. Pol., A* **1995**, 88, 833-836.
- [10] R. Dwiliński, R. Doradziński, J. Garczyński, L. Sierzputowski, R. Kucharski, M. Zając, M. Rudziński, R. Kudrawiec, W. Strupiński, J. Misiewicz, "Ammonothermal GaN substrates: Growth accomplishments and applications", *Phys. Status Solidi A* **2011**, 208, 1489-1493.
- [11] S. Pimputkar, S. Kawabata, J. S. Speck, S. Nakamura, "Improved growth rates and purity of basic ammonothermal GaN", *J. Cryst. Growth* **2014**, 403, 7-17.
- [12] J. Hertrampf, P. Becker, M. Widenmeyer, A. Weidenkaff, E. Schlücker, R. Niewa, "Ammonothermal Crystal Growth of Indium Nitride", *Cryst. Growth Des.* **2018**, 18, 2365-2369.

- [13] J. Häusler, S. Schimmel, P. Wellmann, W. Schnick, "Ammonothermal Synthesis of Earth-Abundant Nitride Semiconductors $ZnSiN_2$ and $ZnGeN_2$ and Dissolution Monitoring by In Situ X-ray Imaging", *Chem. Eur. J.* **2017**, 23, 12275-12282.
- [14] J. Häusler, R. Niklaus, J. Minár, W. Schnick, "Ammonothermal Synthesis and Optical Properties of Ternary Nitride Semiconductors $Mg-IV-N_2$, $Mn-IV-N_2$ and $Li-IV_2-N_3$ ($IV=Si, Ge$)", *Chem. Eur. J.* **2018**, 24, 1686-1693.
- [15] M. Mallmann, R. Niklaus, T. Rackl, M. Benz, T. G. Chau, D. Johrendt, J. Minár, W. Schnick, "Solid Solutions of Grimm-Sommerfeld Analogous Nitride Semiconductors $II-IV-N_2$ ($II = Mg, Mn, Zn; IV = Si, Ge$): Ammonothermal Synthesis and DFT Calculations", *Chem. Eur. J.* **2019**, 25, 15887-15895.
- [16] J. Häusler, L. Neudert, M. Mallmann, R. Niklaus, A.-C. L. Kimmel, N. S. A. Alt, E. Schlücker, O. Oeckler, W. Schnick, "Ammonothermal Synthesis of Novel Nitrides: Case Study on $CaGaSiN_3$ ", *Chem. Eur. J.* **2017**, 23, 2583-2590.
- [17] J. Häusler, L. Eisenburger, O. Oeckler, W. Schnick, "Ammonothermal Synthesis and Crystal Structure of the Nitridoalumogermanate $Ca_{1-x}Li_xAl_{1-x}Ge_{1+x}N_3$ ($x \approx 0.2$)", *Eur. J. Inorg. Chem.* **2018**, 759-764.
- [18] N. Cordes, T. Bräuniger, W. Schnick, "Ammonothermal Synthesis of $EAMO_2N$ ($EA = Sr, Ba; M = Nb, Ta$) Perovskites and ^{14}N Solid-State NMR Spectroscopic Investigations of $AM(O,N)_3$ ($A = Ca, Sr, Ba, La$)", *Eur. J. Inorg. Chem.* **2018**, 5019-5026.
- [19] H. Jacobs, R. Nymwegen, "Synthesis and Crystal Structure of a Potassium Nitridophosphate, $K_3P_6N_{11}$ ", *Z. Anorg. Allg. Chem.* **1997**, 623, 429-433.
- [20] M. Mallmann, C. Maak, R. Niklaus, W. Schnick, "Ammonothermal Synthesis, Optical Properties, and DFT Calculations of Mg_2PN_3 and Zn_2PN_3 ", *Chem. Eur. J.* **2018**, 24, 13963-13970.
- [21] M. Mallmann, S. Wendl, W. Schnick, "Crystalline Nitridophosphates by Ammonothermal Synthesis", *Chem. Eur. J.* **2020**, 26, 2067-2072.
- [22] S. D. Kloß, W. Schnick, "Nitridophosphates – A Success Story of Nitride Synthesis", *Angew. Chem. Int. Ed.* **2019**, 58, 7933-7944; *Angew. Chem.* **2019**, 131, 8015-8027.
- [23] W. Schnick, J. Luecke, "Synthesis and Crystal Structure of Lithium Phosphorus Nitride Li_7PN_4 : The First Compound Containing Isolated PN_4 -Tetrahedra", *J. Solid State Chem.* **1990**, 87, 101-106.

- [24] D. Baumann, W. Schnick, " $\text{Li}_{14}(\text{PON}_3)_2\text{O}$ – A Non-Condensed Oxonitridophosphate Oxide", *Eur. J. Inorg. Chem.* **2015**, 617-621.
- [25] A. Marchuk, P. Schultz, C. Hoch, O. Oeckler, W. Schnick, " $\text{M}_2\text{PO}_3\text{N}$ ($\text{M} = \text{Ca}, \text{Sr}$): ortho-Oxonitridophosphates with $\beta\text{-K}_2\text{SO}_4$ Structure Type", *Inorg. Chem.* **2016**, 55, 974-982.
- [26] S. D. Kloß, N. Weidmann, W. Schnick, "Antiperovskite Nitridophosphate Oxide $\text{Ho}_3[\text{PN}_4]\text{O}$ by High-Pressure Metathesis", *Eur. J. Inorg. Chem.* **2017**, 1930-1937.
- [27] A. P. Black, K. A. Denault, J. Oró-Solé, A. R. Goñi, A. Fuertes, "Red luminescence and ferromagnetism in europium oxynitridosilicates with a $\beta\text{-K}_2\text{SO}_4$ structure", *Chem. Commun.* **2015**, 51, 2166-2169.
- [28] Y.-S. Tang, S.-F. Hu, C. C. Lin, N. C. Bagkar, R.-S. Liu, "Thermally stable luminescence of $\text{KSrPO}_4\text{:Eu}^{2+}$ phosphor for white light UV light-emitting diodes", *Appl. Phys. Lett.* **2007**, 90, 151108.
- [29] F. Golinski, H. Jacobs, "Crystal Structure of Hexamine Cyclotriphosphazene, $\text{P}_3\text{N}_3(\text{NH}_2)_6$ ", *Z. Anorg. Allg. Chem.* **1994**, 620, 965-968.
- [30] H. Jacobs, R. Kirchgässner, "Hexaminecyclotriphosphazenehemiammoniat, $\text{P}_3\text{N}_3(\text{NH}_2)_6 \cdot 0,5 \text{NH}_3$, a Product of High Pressure Ammonolysis of White Phosphorus", *Z. Anorg. Allg. Chem.* **1990**, 581, 125-134.
- [31] H. Jacobs, S. Pollok, F. Golinski, "Synthesis and Crystal Structure of $\text{Na}_{10}[\text{P}_4(\text{NH})_6\text{N}_4](\text{NH}_2)_6(\text{NH}_3)_{0,5}$ with an Adamantane-like Anion $[\text{P}_4(\text{NH})_6\text{N}_4]^{4-}$ ", *Z. Anorg. Allg. Chem.* **1994**, 620, 1213-1218.
- [32] R. Hoppe, "Madelung Constants", *Angew. Chem. Int. Ed. Engl.* **1966**, 5, 95-106; *Angew. Chem.* **1966**, 78, 52-63.
- [33] R. Hoppe, "The Coordination Number – an "Inorganic Chameleon"", *Angew. Chem. Int. Ed. Engl.* **1970**, 9, 25-34; *Angew. Chem.* **1970**, 82, 7-16.
- [34] R. Hübenthal, *Maple, Program for the Calculation of MAPLE values, version 4*; University of Gießen, Germany, 1993.
- [35] W. H. Baur, "Effective Ionic Radii in Nitrides", *Crystallogr. Rev.* **1987**, 1, 59-83.
- [36] I. D. Brown, D. Altermatt, "Bond-valence parameters obtained from a systematic analysis of the Inorganic Crystal Structure Database", *Acta Crystallogr. Sect. B* **1985**, 41, 244-247.

- [37] N. E. Brese, M. O'Keeffe, "Bond-valence parameters for solids", *Acta Crystallogr. Sect. B* **1991**, 47, 192-197.
- [38] R. Hoppe, S. Voigt, H. Glaum, J. Kissel, H. P. Müller, K. Bernet, "A new route to charge distributions in ionic solids", *J. Less Common Met.* **1989**, 156, 105-122.
- [39] S. J. Sedlmaier, E. Mugnaioli, O. Oeckler, U. Kolb, W. Schnick, "SrP₃N₅O: A Highly Condensed Layer Phosphate Structure Solved from a Nanocrystal by Automated Electron Diffraction Tomography", *Chem. Eur. J.* **2011**, 17, 11258-11265.
- [40] S. J. Sedlmaier, J. Schmedt auf der Günne, W. Schnick, "Sr₃P₆O₆N₈—a highly condensed layered phosphate", *Dalton Trans.* **2009**, 4081-4084.
- [41] S. J. Sedlmaier, D. Weber, W. Schnick, "Crystal structure of barium oxonitridophosphate, Ba₃P₆O₆N₈", *Z. Kristallogr. - New Cryst. Struct.* **2012**, 227, 1-2.
- [42] K. Momma, F. Izumi, "VESTA 3 for three-dimensional visualization of crystal, volumetric and morphology data", *J. Appl. Crystallogr.* **2011**, 44, 1272-1276.
- [43] F. J. Pucher, A. Marchuk, P. J. Schmidt, D. Wiechert, W. Schnick, "Luminescent Nitridophosphates CaP₂N₄:Eu²⁺, SrP₂N₄:Eu²⁺, BaP₂N₄:Eu²⁺, and BaSr₂P₆N₁₂:Eu²⁺", *Chem. Eur. J.* **2015**, 21, 6443-6448.
- [44] A. Marchuk, S. Wendl, N. Imamovic, F. Tambornino, D. Wiechert, P. J. Schmidt, W. Schnick, "Nontypical Luminescence Properties and Structural Relation of Ba₃P₅N₁₀X:Eu²⁺ (X = Cl, I): Nitridophosphate Halides with Zeolite-like Structure", *Chem. Mater.* **2015**, 27, 6432-6441.
- [45] S. Wendl, W. Schnick, "SrH₄P₆N₁₂ and SrP₈N₁₄: Insights into the Condensation Mechanism of Nitridophosphates under High Pressure", *Chem. Eur. J.* **2018**, 24, 15889-15896.
- [46] R. López, R. Gómez, "Band-gap energy estimation from diffuse reflectance measurements on sol-gel and commercial TiO₂: a comparative study", *J. Sol-Gel Sci. Technol.* **2012**, 61, 1-7.
- [47] J. Tauc, R. Grigorovici, A. Vancu, "Optical Properties and Electronic Structure of Amorphous Germanium", *Phys. Status Solidi B* **1966**, 15, 627-637.
- [48] T. L. Barry, "Fluorescence of Eu²⁺-Activated Phases in Binary Alkaline Earth Orthosilicate Systems", *J. Electrochem. Soc.* **1968**, 115, 1181-1184.
- [49] P. Dorenbos, "Thermal quenching of Eu²⁺ 5d–4f luminescence in inorganic compounds", *J. Phys.: Condens. Matter* **2005**, 17, 8103-8111.

- [50] M. Mallmann, J. Häusler, N. Cordes, W. Schnick, "Ammonothermal Synthesis of Alkali-Alkaline Earth Metal and Alkali-Rare Earth Metal Carbodiimides: $K_{5-x}M_x(CN_2)_{2+x}(HCN_2)_{1-x}$ ($M = Sr, Eu$) and $Na_{4.32}Sr_{0.68}(CN_2)_{2.68}(HCN_2)_{0.32}$ ", *Z. Anorg. Allg. Chem.* **2017**, 643, 1956-1961.
- [51] SAINT, Data Integration Software, Madison, Wisconsin, USA, **1997**.
- [52] APEX 3, Vers. 2016.2015-2010, Bruker-AXS, Karlsruhe, **2016**.
- [53] G. M. Sheldrick, SADABS, *Multi-Scan Absorption Correction*, v.2, Bruker-AXS, Madison, WI, USA, **2012**.
- [54] XPREP *Reciprocal Space Exploration*, Vers. 6.12, Bruker-AXS, Karlsruhe, **2001**.
- [55] G. M. Sheldrick, "SHELXT - Integrated space-group and crystal-structure determination", *Acta Crystallogr. Sect. A* **2015**, 71, 3-8.
- [56] G. M. Sheldrick, "Crystal structure refinement with SHELXL", *Acta Crystallogr. Sect. C* **2015**, 71, 3-8.
- [57] A. Coelho, TOPAS Academic, Version 6, Coelho Software, Brisbane (Australia), **2016**.

6 Sr₃P₃N₇: Complementary Approach of Ammonothermal and High-Pressure Methods

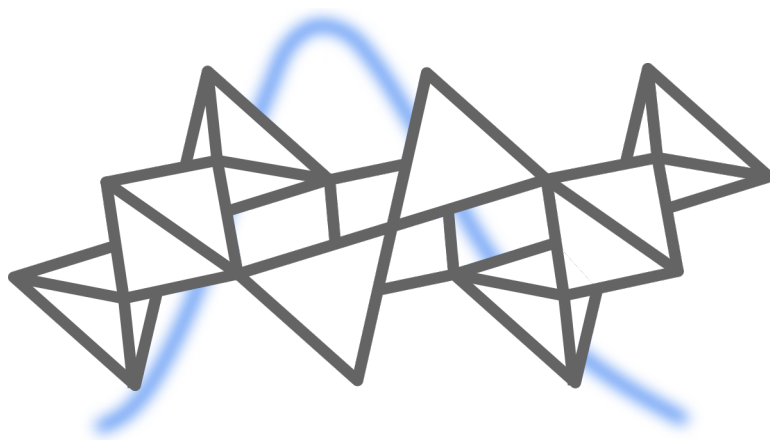
Dr. Mathias Mallmann, Sebastian Wendl, Dr. Philipp Strobel, Dr. Peter J. Schmidt,

Prof. Dr. Wolfgang Schnick

Chem. Eur. J. **2020**, 26, 6257–6263.

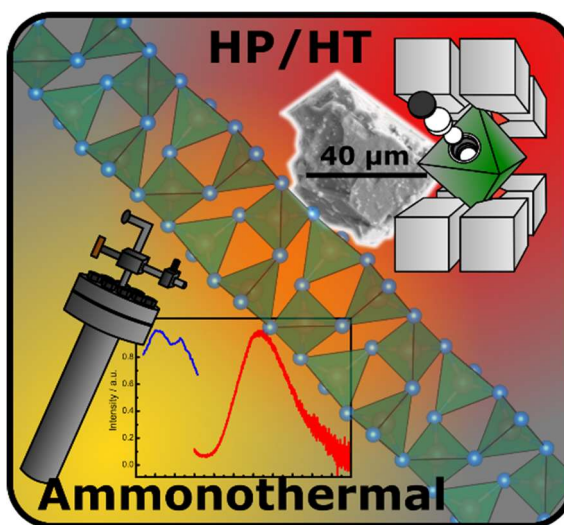
DOI: 10.1002/chem.202000297.

Reprinted (adapted) with permission for non-commercial use from *Chemistry – A European Journal* (open access). Copyright 2021 John Wiley and Sons.



Collaborating methods: Sr₃P₃N₇ was prepared by ammonothermal and multianvil syntheses. The combination of medium- and high-pressure methods with their respective benefits enabled fast structure elucidation, as well as, phase pure synthesis and studies on luminescence properties of Eu²⁺-doped samples. Sr₃P₃N₇ exhibits infinite dreier double chains and extends the class of ternary alkaline earth nitridophosphates by the degree of condensation of $\kappa = 3/7$.

Abstract: Nitridophosphates exhibit an intriguing structural diversity with different structural motifs, e.g. chains, layers or frameworks. In this contribution we present the novel nitridophosphate $Sr_3P_3N_7$ with unprecedented dreier double chains. Crystalline powders were synthesized using the ammonothermal method, while single crystals were obtained by high-pressure multianvil technique. The crystal structure of $Sr_3P_3N_7$ was solved and refined from single-crystal X-ray diffraction and confirmed by powder X-ray methods. $Sr_3P_3N_7$ crystallizes in monoclinic space group $P2_1/c$. Energy dispersive X-ray and Fourier transformed infrared spectroscopy were conducted to confirm the chemical composition as well as the absence of NH_x functionality. The optical band gap was estimated to be 4.4 eV using diffuse reflectance UV/Vis spectroscopy. Upon doping with Eu^{2+} , $Sr_3P_3N_7$ shows a broad deep-red to infrared emission ($\lambda_{em} = 681$ nm, $fwhm \approx 3402$ cm^{-1}) with an internal quantum efficiency of 42%.



6.1 Introduction

Due to the fact that the element combination P/N is isoelectronic to Si/O, nitridophosphates exhibit structural analogies to silicates and are built up from condensed or non-condensed PN_4 tetrahedra. In recent years, numerous nitridophosphates have been synthesized with a high structural diversity with different degrees of condensation κ (ratio of tetrahedra centers to ligands) ranging from 1/4 to 4/7.^[1] Thereby, different structural motifs like non-condensed tetrahedra, chains, layers or frameworks can occur.^[2-5] Particularly due to their structural diversity, these compounds exhibit diverse, interesting physical properties, for example luminescence upon doping with Eu^{2+} . So far, P/N-network and -layer compounds such as MP_2N_4 ($M = \text{Ca}, \text{Sr}, \text{Ba}$), $\text{Ba}_3\text{P}_5\text{N}_{10}\text{X}$ ($X = \text{Cl}, \text{Br}, \text{I}$) or $\text{BaP}_6\text{N}_{10}\text{NH}$ were used as host lattices, almost covering emission in the entire visible spectrum.^[6-9] Especially, $\text{Ba}_3\text{P}_5\text{N}_{10}\text{Br}$, crystallizing in a zeolite-like structure, exhibits intriguing luminescence properties and is discussed as natural-white-light single emitter, demonstrating nicely the potential of nitridophosphate materials.^[7]

But in contrast to silicates, only a few nitridophosphates could be synthesized under ambient pressure conditions (e.g. Ca_2PN_3 , $\text{Li}_{10}\text{P}_4\text{N}_{10}$).^[3, 10, 11] This is due to the fact that the appropriate temperature range for crystallization of nitridophosphates is significantly beyond the decomposition temperature of the most important starting material P_3N_5 , which can be circumvented by applying high-pressure methods.

Among these, the multianvil approach is the most frequently employed method, following Le Chatelier's principle in order to compensate thermal decomposition. Over the years, different synthesis strategies using the multianvil approach were developed, including the azide route, high-pressure metathesis or the synthesis with ammonium chloride as mineralizer.^[5, 6, 12] The most valuable advantage of this technique is, that the enormous pressure allows for sufficient temperatures for the reconstructive cleavage of P–N bonds. Furthermore, in many cases these high temperatures enable the formation of single crystals, facilitating structure elucidation significantly. However, a drawback of such high-pressure methods is the low sample volume, especially in the context of materials characterization and application.

Therefore, a promising alternative for nitridophosphate synthesis is the ammonothermal approach as a medium pressure method. Herein, the reduced pressure, compared to the multianvil technique, is compensated by the usage of a highly reactive supercritical ammonia atmosphere. In 1997 Jacobs and coworkers used this approach to synthesize $K_3P_6N_{11}$.^[13] In the meantime, the ammonothermal method enabled synthesis of nitridophosphates with isolated tetrahedra units, chains, layers and frameworks.^[14, 15] Even nitridophosphates like SrP_8N_{14} or $Li_{18}P_6N_{16}$, which were so far only accessible by the high-pressure multianvil approach, could be synthesized under ammonothermal conditions in high yield, simplifying the investigation of their physical properties significantly. Although, the ammonothermal method was already used for synthesis of numerous nitride materials,^[16-22] the crystal growth of ternary or quaternary nitrides during ammonothermal synthesis, except for a few examples like Mg_2PN_3 or $MTaN_2$ ($M = Na, K, Rb, Cs$), is still challenging.^[15, 23]

In this contribution, we present a combination of medium- and high-pressure methods with their respective advantages for the investigation of unknown nitridophosphates. Herein, we report on $Sr_3P_3N_7$ as a case study for a complementary approach of ammonothermal and multianvil syntheses. $Sr_3P_3N_7$ extends the class of ternary alkaline earth nitridophosphates by the degree of condensation of $\kappa = 3/7$. Structure elucidation was based on single-crystal X-ray diffraction data, enabled by high-pressure synthesis, while ammonothermal methods facilitated bulk synthesis targeting for further analysis as well as studies on the luminescence properties of $Sr_3P_3N_7:Eu^{2+}$.

6.2 Results and Discussion

Synthesis

The title compound initially has been observed in heterogeneous products obtained by ammonothermal as well as high-pressure methods, targeting new nitridophosphates with low degree of condensation. While high-pressure high-temperature synthesis leads to suitable single crystals for structure elucidation, ammonothermal synthesis provided the highest yield of bulk samples, expressing the complementary approach. The synthesis of single crystals was started from

stoichiometric amounts of $\text{Sr}(\text{N}_3)_2$ and P_3N_5 according to Equation 6.1 together with small amounts of EuCl_2 . The starting mixture was treated by high-pressure high-temperature reaction at 5 GPa and 1270 K. These reaction conditions were achieved by using a hydraulic 1000 t press and a modified Walker-type multianvil apparatus.^[24, 25]



Analogously, translucent orange $\text{Sr}_3\text{P}_3\text{N}_7:\text{Eu}^{2+}$ crystals of up to 40 μm in length were isolated (see Scanning electron microscopy section). After optimizing the synthesis based on the results of single-crystal X-ray diffraction and energy dispersive X-ray spectroscopy, bulk samples of $\text{Sr}_3\text{P}_3\text{N}_7$ were prepared under ammonothermal conditions in custom-built high-temperature autoclaves using SrH_2 , P_3N_5 and the ammonobasic mineralizer NaN_3 . NaN_3 decomposes at elevated temperatures and forms in situ NaNH_2 , which increases the solubility of the other starting materials by formation of intermediate species (e.g. $\text{Na}_2\text{Sr}_3(\text{NH}_2)_8$, $\text{Na}_{10}[\text{P}_4(\text{NH})_6]\text{N}_4(\text{NH}_2)_6(\text{NH}_3)_{0.5}$ or $\text{P}_3\text{N}_3(\text{NH}_2)_6$) which have already been observed under ammonothermal conditions at temperatures around 670 K.^[26–28] Subsequent heating to 1070 K, reaching a maximum pressure of 140 MPa in the autoclave, resulted in synthesis of $\text{Sr}_3\text{P}_3\text{N}_7$ as a crystalline white powder, which hydrolyzes slowly on exposure to moist air. The product was therefore washed with dry ethanol to remove residual mineralizer and intermediate species. Analogous syntheses with red phosphorus instead of P_3N_5 also resulted in the desired product. Doping with Eu^{2+} (nominal concentration of 2 mol% regarding to Sr) in the form of $\text{Eu}(\text{NH}_2)_2$ resulted in deep red luminescence of $\text{Sr}_3\text{P}_3\text{N}_7:\text{Eu}^{2+}$ when irradiated with UV light (see Luminescence section).

Crystal structure

The crystal structure of $\text{Sr}_3\text{P}_3\text{N}_7$ was solved and refined from single-crystal X-ray diffraction data in monoclinic space group $P2/c$ (no. 13). Details on the structure determination are summarized in Table 6.1. Atomic coordinates and anisotropic displacement parameters are given in Table E1 and E2 in the Supporting Information. Selected interatomic distances and bond angles are summarized

in the Supporting Information (Table E3). With $\kappa = n(P)/n(N) = 3/7$, $Sr_3P_3N_7$ has a hitherto unknown degree of condensation of an alkaline earth nitridophosphate and is composed of infinite PN_4 -tetrahedra *dreier* double chains. A degree of condensation of $\kappa = 3/7$ is already known for rare earth nitridophosphates ($RE_2P_3N_7$ with $RE = La, Ce, Pr, Nd, Sm, Eu, Ho, Yb$), however, there is no structural correlation between these compounds.^[29] Apart from Ca_2PN_3 , $Sr_3P_3N_7$ is the only known alkaline earth nitridophosphate with a chain structure, while Mg_2PN_3 crystallizes strictly speaking in a wurtzite-type superstructure and can be interpreted as a double nitride.^[3, 30] The chains in $Sr_3P_3N_7$ show a periodicity of $P = 3$ and a stretching factor of $f_s = 0.90$ (see Figure 6.1) and are built up from *dreier*-rings according to Liebau.^[31, 32] Two of these *dreier*-rings, which are structurally related to each other by a rotating mirror axis ($2/m$), are connected via two common corners forming an additional *vierer*-ring. The resulting $[P_6N_{16}]$ -units were already found in $Li_{18}P_6N_{16}$ as non-condensed $[P_6N_{16}]^{18-}$ anion.^[14, 33] In the title compound these subunits are connected via two common corners on each side, forming infinite chains. The P–N distances vary from 1.575 to 1.683 Å. As expected, the shortest distances belong to the terminal P(2)–N(2) atoms. The corresponding N–P–N bond angles are between 103.3(5) and 115.0(4)°. Angles as well as distances are in good agreement with values observed in other nitridophosphates described in literature.^[3, 4, 13, 29]

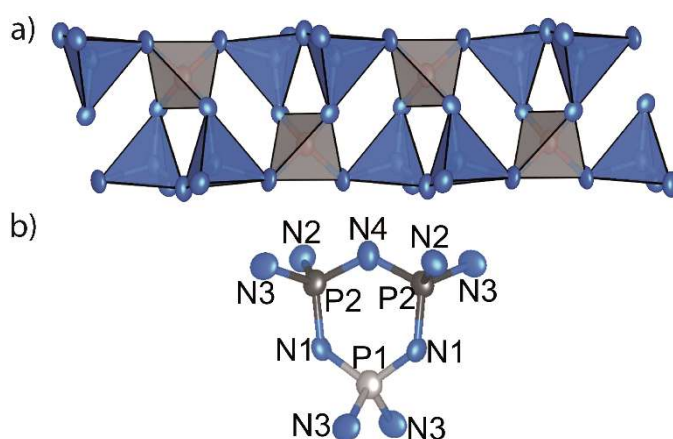


Figure 6.1. Infinite dreier double chain (a) and dreier-ring subunit (b). Thermal ellipsoids are depicted at 90% probability.

Table 6.1. Crystallographic data of Sr₃P₃N₇ (synthesized by the multianvil approach) obtained from single-crystal X-ray diffraction.

Formula	Sr ₃ P ₃ N ₇
Crystal system	monoclinic
Space group	<i>P</i> 2/ <i>c</i> (no. 13)
<i>a</i> / Å	6.882(8)
<i>b</i> / Å	7.416(9)
<i>c</i> / Å	7.036(8)
β / °	104.96(3)
Cell volume / Å ³	346.9(7)
Formula units/cell	2
Density / g·cm ⁻³	4.345
Crystal size / mm	0.02x0.02x0.03
μ / mm ⁻¹	23.617
<i>T</i> / K	298(2)
Diffractometer	Bruker D8 Quest
Radiation / Å	Mo-K α (0.71073)
<i>F</i> (000)	416
θ range / °	2.7 - 30.5
Total no. of reflections	3621
No. of independent reflections	1064
Observed reflections ($F^2 > 2\sigma(F^2)$)	728
R_{int} ; R_{σ}	0.0858; 0.0970
Structure solution	SHELXT
Structure refinement	SHELXL
Refined parameters	61
Goodness of fit (χ^2)	1.044
R_1 (all data); R_1 ($F^2 > 2\sigma(F^2)$)	0.100; 0.059
wR_2 (all data); wR_2 ($F^2 > 2\sigma(F^2)$)	0.131; 0.117
$\Delta\rho_{\text{max}}$; $\Delta\rho_{\text{min}}$ [e·Å ⁻³]	1.892, -1.790

The infinite chains are oriented along [001] and are stacked congruently in *a* and *b* (see Figure 6.2). The crystal structure contains two crystallographically different Sr sites. The Sr1 site is located between two chains stacked along [100] and is coordinated by 10 N atoms with distances between 2.740(9) and 3.068(10) Å. In contrast, the second Sr site (Sr2) is located between two chains stacked along [010] and is coordinated by 9 N atoms with distances ranging from 2.504(10) to 3.283(10) Å. The coordination polyhedra of both sites are illustrated in Figure E1 in the Supporting

Information. All Sr–N distances are in good agreement with values from other Sr (oxo)nitridophosphates known from literature (e.g. SrP_2N_4 , SrP_3N_5O , $Sr_3P_6O_6N_8$).^[34–36]

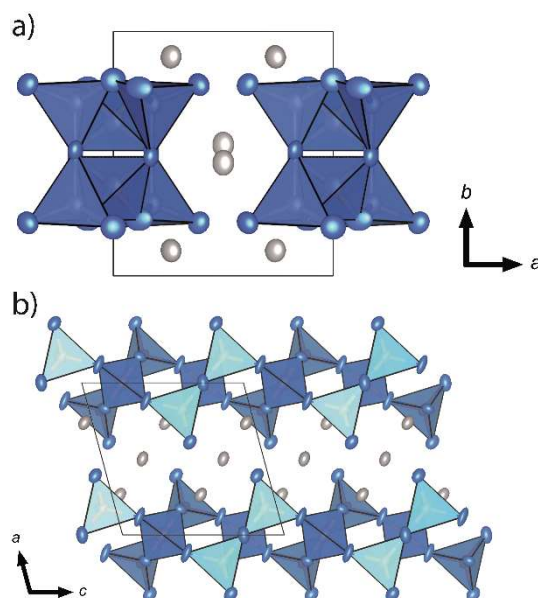


Figure 6.2. Crystal structure of $Sr_3P_3N_7$ viewed along [001] (a) and [010] (b). PN_4 tetrahedra and N atoms are depicted in blue, Sr atoms in gray. Thermal ellipsoids are depicted at 90% probability.

To confirm the structure model obtained from single-crystal X-ray data, a PXRD measurement and subsequent Rietveld refinement were conducted (Figure 6.3). The refined crystallographic data as well as Wyckoff positions are summarized in Table E4 and E5 in the Supporting Information. As described above (Synthesis section), residual mineralizer ($NaNH_2$) can be removed by washing with dry ethanol. However, the sample partially decomposes during the washing process, resulting in the formation of an amorphous side-phase. Due to this fact, the unwashed sample was used for Rietveld refinement. A comparison of washed and unwashed samples is illustrated in Figure E2 in the Supporting Information.

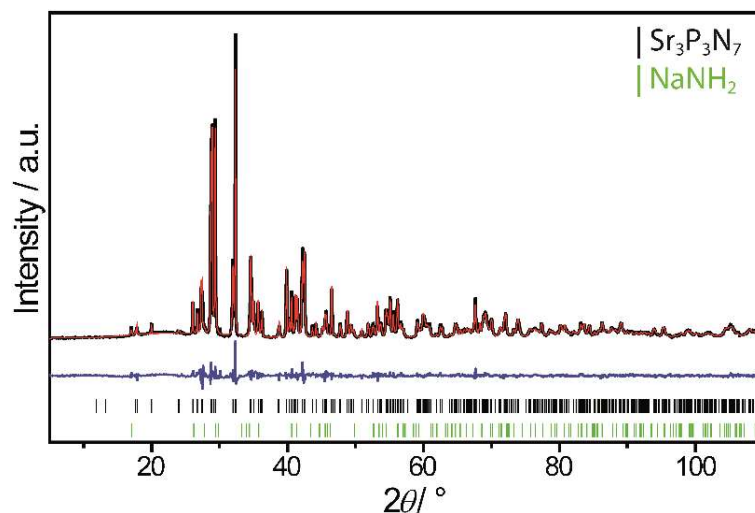


Figure 6.3. Rietveld refinement of PXRD measurements of ammonothermally synthesized $\text{Sr}_3\text{P}_3\text{N}_7$ with experimental data (black line), calculated data (red line), difference profile (blue line) and reflection positions ($\text{Sr}_3\text{P}_3\text{N}_7$: black bars, NaNH_2 : green bars).

Scanning electron microscopy

Energy dispersive X-ray (EDX) spectroscopy was used for determination of the chemical composition. The determined atomic ratios are in good agreement with the expected chemical formulas (see Table E5 in the Supporting Information). Traces of europium can be attributed to doping of the sample and oxygen impurities to surface hydrolysis of the products. Furthermore, a scanning electron micrograph of the product was collected and is illustrated in Figure 6.4.

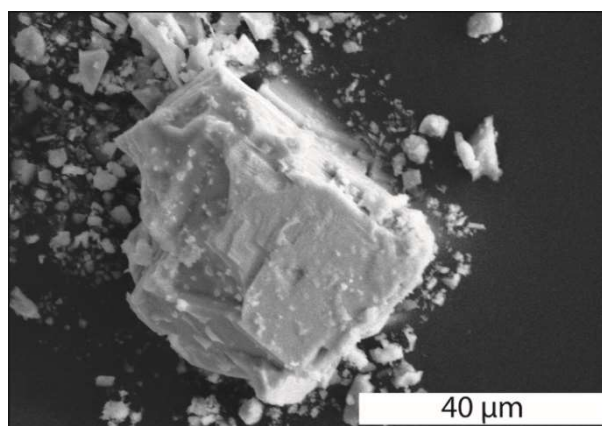


Figure 6.4. SEM image of a $\text{Sr}_3\text{P}_3\text{N}_7$ single crystal obtained from high-pressure synthesis.

Fourier Transformed Infrared spectroscopy

A FTIR spectrum was recorded in order to prove the absence of any NH_x functionality in $\text{Sr}_3\text{P}_3\text{N}_7$. The spectrum (see Figure E3 in the Supporting Information) shows no significant absorption bands around 3000 cm^{-1} , indicating the absence of N–H groups in accordance to the crystal structure obtained from single-crystal X-ray diffraction, since the presence of imide or amide groups would lead to strong absorption bands.^[4] Weak signals could be attributed to partial surface hydrolysis of the products. The absorption bands between 500 and 1300 cm^{-1} can be attributed to symmetric and asymmetric stretching modes of the P–N-framework and are characteristic for nitridophosphates.

UV/Vis spectroscopy

Diffuse reflectance UV/Vis spectroscopy was conducted to estimate the optical band gap of the undoped sample. Therefore, the Kubelka-Munk function $F(R) = (1-R)^2/2R$ was used to convert the measured diffuse reflectance spectrum to a pseudoabsorption spectrum.^[37] A Tauc plot (see Figure 6.5) was then used to estimate the optical band gap by plotting $(F(R)\cdot h\nu)^{1/n}$ versus $h\nu$ (with $n = 1/2$, assuming direct transition) and drawing of a tangent at the inflection point.^[38] The diffuse reflectance spectrum shows an absorption band around 250 nm (see Figure E4 in the Supporting Information). The determined band gap is approximately 4.4 eV .

A diffuse reflectance spectrum of the Eu^{2+} doped sample is illustrated in Figure E5 in the Supporting Information. It shows an additional broad absorption band between 400 and 550 nm , which can be attributed to dopant absorption and is in good agreement with the corresponding excitation spectrum (see Luminescence section).

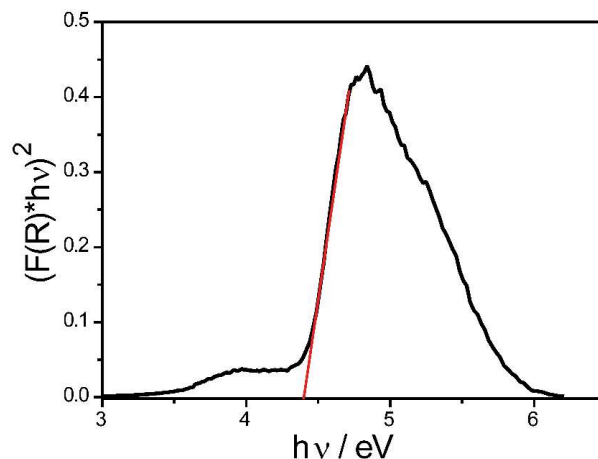


Figure 6.5. Tauc plot (black line) of ammonothermally synthesized $\text{Sr}_3\text{P}_3\text{N}_7$. Red line as a tangent at the inflection point.

Luminescence

Luminescence properties of $\text{Sr}_3\text{P}_3\text{N}_7:\text{Eu}^{2+}$ were measured from crystalline powder samples. $\text{Sr}_3\text{P}_3\text{N}_7:\text{Eu}^{2+}$ shows deep-red luminescence when irradiated with UV to blue light (see Figure E6 in the Supporting Information). The emission spectrum ($\lambda_{\text{exc}} = 450 \text{ nm}$) and the excitation spectrum are illustrated in Figure 6.6. The excitation spectrum has two maxima at around 405 and 465 nm, while the emission spectrum (2 mol% Eu regarding to Sr) shows one broad band in the deep red to infrared region ($\lambda_{\text{em}} = 681 \text{ nm}$) with a full width at half maximum (fwhm) of $162 \text{ nm}/3402 \text{ cm}^{-1}$.

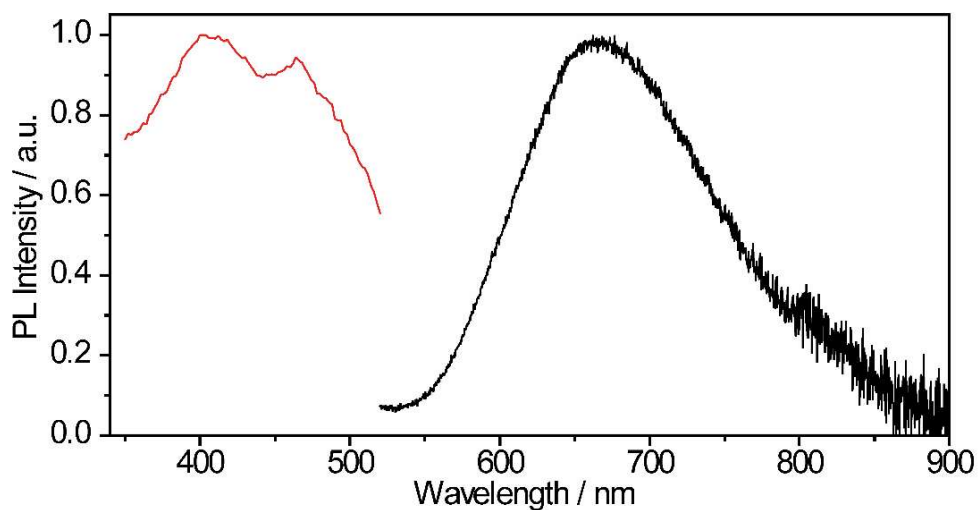


Figure 6.6. Excitation (red line) and emission (black line) spectra of ammonothermally synthesized $\text{Sr}_3\text{P}_3\text{N}_7:\text{Eu}^{2+}$.

The broad emission band probably results from the different coordination of the cations (see Crystal structure section). In order to capture the complete emission spectrum, a second spectrometer was used for the measurement ($\lambda_{\text{exc}} = 410 \text{ nm}$) of the emission in the IR region beyond 800 nm. This leads to the higher background level above 800 nm. The internal quantum efficiency (IQE) was determined with an excitation wavelength of 438 nm to be 42% in the range up to 800 nm. These luminescent properties make Sr₃P₃N₇:Eu²⁺ interesting, as such materials may be applied in horticultural lighting, as they can convert green light into the red to IR spectral range with increased photosynthesis quantum efficiency. A further possible application field is, for example, hyper- or multispectral imaging, with diverse applications in e.g. agriculture, automated driving or molecular biology.^[39, 40]

6.3 Conclusions

In this contribution we present a complementary approach of ammonothermal and multianvil techniques as a powerful combination for a simplified and much faster access to a detailed structural and physical analysis of nitridophosphates. Exploitation of the advantages of each method leads to the discovery of the new nitridophosphate Sr₃P₃N₇. Thereby, the best crystallization conditions were realized via a high-pressure approach using the azide route, allowing higher temperatures during syntheses compared to the ammonothermal approach. The structure model was solved and refined from single-crystal X-ray diffraction data. Sr₃P₃N₇ is composed of unprecedented *dreier* double chains made up of PN₄ tetrahedra with a degree of condensation $\kappa = 3/7$, which is hitherto unknown for alkaline earth nitridophosphates. Due to larger sample volumes, studies on the physical properties of the title compound were carried out with bulk samples obtained from ammonothermal synthesis. The band gap (4.4 eV) was determined using diffuse reflectance spectroscopy. Upon doping with Eu²⁺, Sr₃P₃N₇ exhibits a broad emission band in the deep-red to infrared region ($\lambda_{\text{em}} = 681 \text{ nm}$, $\text{fwhm} \approx 3402 \text{ cm}^{-1}$) with an internal quantum efficiency of 42%, making it practically interesting for commercial applications (e.g. horticultural lighting). For this purpose, stoichiometry and doping concentration optimization as major parts of an industrial process development will further improve the luminescence efficiency.

6.4 Experimental Section

All manipulations were conducted in argon-filled gloveboxes (Unilab, MBraun, Garching, $O_2 < 1$ ppm, $H_2O < 1$ ppm) under exclusion from oxygen and moisture because of the air-sensitivity of starting materials and products. A vacuum line (≤ 0.1 Pa) with argon and ammonia (both: Air Liquide, 99.999%) supply was used for filling of the autoclaves with NH_3 . The gases were further purified by gas cartridges (Micro Torr FT400-902 (for Ar) and MC400-702FV (for NH_3), SAES Pure Gas Inc., San Luis Obispo, CA, USA), providing a purity level of < 1 ppbV H_2O , O_2 and CO_2 .

Synthesis of $Eu(NH_2)_2$

$Eu(NH_2)_2$ was synthesized ammonothermally starting from Eu metal (99.99%, smart elements). The experiment was carried out analogously to the synthesis described in literature.^[41]

Synthesis of P_3N_5

P_3N_5 was synthesized following Stock et al.^[42] by ammonolysis of P_4S_{10} (Sigma Aldrich, 99%) at 1125 K for 4 h (heating rate: 5 K/min). Before reaction, the silica tube was saturated with NH_3 for 4 h. After cooling down to room temperature (5 K/min), the received product was washed in multiple steps with ethanol, water and acetone and dried under vacuum. Powder X-ray diffraction was conducted to confirm phase purity.

Synthesis of $Sr(N_3)_2$

$Sr(N_3)_2$ was synthesized starting from $SrCO_3$ (Sigma Aldrich, 99.995%) and *in situ* formed HN_3 (using aqueous NaN_3 (Acros Organics, 99%) and a cation exchanger (Amberlyst 15)) following the syntheses of Suhrmann and Karau.^[43, 44] HN_3 was slowly added to an aqueous suspension of $SrCO_3$ until the liquid turned clear. After filtration, the solution was evaporated under reduced pressure (50 mbar, 40 °C), recrystallized from acetone and dried under vacuum. FTIR and PXRD measurements were conducted to confirm phase purity.

Caution! Since HN₃ solutions are potentially explosive and the vapor is highly poisonous, special care issues are necessary.

Ammonothermal synthesis

Sr₃P₃N₇ was synthesized under ammonothermal conditions starting from 0.5 mmol P₃N₅ (81.5 mg), 1.5 mmol SrH₂ (134.4 mg, Materion, 99.5%) and 5 mmol NaN₃ (325.0 mg, Sigma-Aldrich, 99.5%) as ammonobasic mineralizer. For the synthesis of Eu²⁺-doped product 0.03 mmol Eu(NH₂)₂ (5.5 mg) was added to the reaction mixture. The starting materials were ground using an agate mortar and transferred into a Ta-liner, which protects the reaction mixture against autoclave impurities. The liner was placed in a high-temperature autoclave constructed of a nickel based super-alloy (Haynes® 282®, max. 1100 K, 170 MPa, 10 mL). The autoclave is sealed with a lid via flange joints using a silver coated Inconel® 718 ring (GFD seals). An Inconel® 718 high-pressure tube connects the lid with a hand valve (SITEC), which is equipped with a pressure transmitter (HBM P2VA1/5000 bar) and a bursting disc (SITEC). After evacuation, the sealed autoclave was cooled to 198 K using an ethanol/liquid nitrogen mixture and filled with NH₃ (≈ 3.7 mL). A mass flow meter (D-6320-DR, Bronkhorst, Ruurlo, Netherlands) was used for detection of the amount of inserted ammonia. The filled autoclave was heated in two steps (heated to 670 K within 2 h, held at this temperature for 16 h, heated to 1070 K within 3 h and held at this temperature for 96 h) to 1070 K reaching a maximum pressure of 140 MPa. After cooling to room temperature and removal of NH₃, the reaction products were separated under argon, washed with ethanol and dried under vacuum. While the undoped product exhibit a white color, the Eu²⁺-doped sample is orange.

High-pressure synthesis

Single crystals of Sr₃P₃N₇:Eu²⁺ were synthesized starting from stoichiometric amounts of Sr(N₃)₂ and P₃N₅ as well as small amounts of EuCl₂ (Strem Chemicals, 99.9%) as dopant using a modified Walker-type multianvil press.^[24, 25] The reactants were mixed and grounded in an agate mortar and packed in a capsule of hexagonal boron nitride (Henze, Kempten). After sealing with a BN-cap the sample was placed in the middle of a MgO octahedron (doped with 5% Cr₂O₃, edge length 18 mm, Ceramic Substrates & Components Ltd, Isle of Wight) using two MgO spacers (Cesima Ceramics, Wust-Fischbach). To ensure heating of the sample, the octahedron was further equipped with two

graphite furnaces (Schunk Kohlenstofftechnik GmbH, Zolling), a ZrO₂ tube (Cesima Ceramics, Wust-Fischbach) for thermal insulation and two Mo plates for electrical contact between the graphite furnaces and the anvils of the multianvil press. The assembled octahedron was placed between eight WC cubes (doped with 7% Co, Hawedia, Marklkofen, Germany) with truncated edges (edge length 11 mm), which were separated with pyrophyllite gaskets (Ceramic Substrates & Components, Isle of Wight, UK). Further details on the experimental setup and the multianvil apparatus are given in literature.^[25] The sample was slowly compressed to 5 GPa and subsequently heated to 1270 K within 30 min. After 30 min at 1270 K the sample was allowed to cool down to room temperature within 30 minutes and slowly decompressed. The crystalline orange product was isolated and stored under argon.

Single-crystal X-ray diffraction

Single crystals of Sr₃P₃N₇:Eu²⁺ were placed and sealed in glass capillaries (Hilgenberg GmbH) in argon atmosphere for single-crystal XRD measurements. The data were collected using a Bruker D8 Quest diffractometer with Mo-K_α radiation ($\lambda = 0.71073 \text{ \AA}$). The measured data were indexed and integrated with the software package APEX3.^[45,46] APEX3 was also used for semi-empirical absorption corrections (SADABS) and the determination of the space group.^[46–48] The crystal structure was solved using the SHELXT algorithm and refined by full-matrix least-squares methods using WinGX with implemented SHELXL.^[49–51]

CSD 1975990 (for Sr₃P₃N₇) contains the supplementary crystallographic data for this paper. These data can be obtained free of charge from FIZ Karlsruhe.

Powder X-ray diffraction

For powder XRD measurements, the grounded product was filled and sealed in a glass capillary ($d = 0.3 \text{ mm}$, Hilgenberg GmbH). A Stoe STADI P diffractometer with Cu-K_{α1} ($\lambda = 1.5406 \text{ \AA}$) radiation, Ge(111) monochromator and Mythen 1K detector in modified Debye-Scherrer geometry was used for the measurements. TOPAS was used for Rietveld refinement of the data.^[52]

Scanning electron microscopy

A scanning electron microscope (Dualbeam Helios Nanolab G3 UC (FEI), equipped with an EDX detector (X-Max 80 SDD, Oxford instruments)) was used for imaging of the crystals and for EDX measurements. Thereto, the crystallites were placed on adhesive carbon pads. A high-vacuum sputter coater (BAL-TEC MED 020, Bal Tec A) was used for coating of the samples with a conductive carbon film.

Fourier Transformed Infrared (FTIR) spectroscopy

An IR spectrum (range between 400 and 4000 cm⁻¹) were collected using a FTIR-IFS 66 v/S spectrometer (Bruker). The samples were mixed with KBr (Acros Organics, 99%) and pressed into pellets under argon. OPUS was used for evaluation of the measurements.^[53]

UV/Vis spectroscopy

The optical band gaps were estimated using UV-Vis spectroscopy. For this purpose, diffuse reflectance measurements of the samples at room temperature were performed using a Jasco V-650 UV/VIS spectrophotometer equipped with Czerny-Turner mount, photomultiplier tube detector and deuterium (190–350 nm) / halogen (330–900 nm) lamps as light sources.

Luminescence

A microcrystalline powder of Sr₃P₃N₇:Eu²⁺ was used to determine luminescence properties. The measurement was conducted on a PTFE sample holder using an in-house built system based on a 5.3" integration sphere and a spectrofluorimeter equipped with a 150 W Xe lamp, two 500 mm Czerny–Turner monochromators, 1800 1/mm lattices, and 250/500 nm lamps, with a spectral range from 230 to 820 nm ($\lambda_{\text{exc}} = 450$ nm). Additional data from a spectrometer sensitive in the 600–1100 nm wavelength range (Avantes) ($\lambda_{\text{exc}} = 410$ nm) were used to obtain the complete emission band by merging data of both measurements. A comparison of integrated emission intensities and absorption at excitation wavelength ($\lambda_{\text{exc}} = 438$ nm) of the sample with reference materials (BaSO₄, Merck for white standard DIN 5033 commercial (Sr,Ca)AlSiN₃:Eu²⁺, Mitsubishi Chemical, and Y₃Al₅O₁₂:Ce³⁺, Philips) were conducted to determine the internal quantum efficiency (IQE).

6.5 Acknowledgements

We acknowledge the Deutsche Forschungsgemeinschaft (DFG) for financial support within the research group “Chemistry and Technology of the Ammonothermal Synthesis of Nitrides” (FOR 1600), project SCHN377/16-2. We also want to thank Arthur Haffner for single-crystal measurements, Marion Sokoll for FTIR measurements and Lisa Gamperl for EDX measurements (all at Department of Chemistry, LMU Munich) as well as the group of Prof. Dr. E. Schlücker for fabrication of the autoclaves (FAU Erlangen-Nürnberg).

6.6 References

- [1] S. D. Kloß, W. Schnick, "Nitridophosphates – A Success Story of Nitride Synthesis", *Angew. Chem. Int. Ed.* **2019**, 58, 7933-7944; *Angew. Chem.* **2019**, 131, 8015-8027.
- [2] W. Schnick, J. Luecke, "Synthesis and Crystal Structure of Lithium Phosphorus Nitride Li₇PN₄: The First Compound Containing Isolated PN₄-Tetrahedra", *J. Solid State Chem.* **1990**, 87, 101-106.
- [3] W. Schnick, V. Schultz-Coulon, "Ca₂PN₃ - A Novel Phosphorus(V) Nitride with One-Dimensional Infinite Chains of Corner-Sharing PN₄ Tetrahedra", *Angew. Chem. Int. Ed. Engl.* **1993**, 32, 280-281; *Angew. Chem.* **1993**, 105, 308-309.
- [4] S. Wendl, W. Schnick, "SrH₄P₆N₁₂ and SrP₈N₁₄: Insights into the Condensation Mechanism of Nitridophosphates under High Pressure", *Chem. Eur. J.* **2018**, 24, 15889-15896.
- [5] S. D. Kloß, W. Schnick, "Rare-Earth-Metal Nitridophosphates through High-Pressure Metathesis", *Angew. Chem. Int. Ed.* **2015**, 54, 11250-11253; *Angew. Chem.* **2015**, 127, 11402-11405.
- [6] F. J. Pucher, A. Marchuk, P. J. Schmidt, D. Wiechert, W. Schnick, "Luminescent Nitridophosphates CaP₂N₄:Eu²⁺, SrP₂N₄:Eu²⁺, BaP₂N₄:Eu²⁺, and BaSr₂P₆N₁₂:Eu²⁺", *Chem. Eur. J.* **2015**, 21, 6443-6448.
- [7] A. Marchuk, W. Schnick, "Ba₃P₅N₁₀Br:Eu²⁺: A Natural-White-Light Single Emitter with a Zeolite Structure Type", *Angew. Chem. Int. Ed.* **2015**, 54, 2383-2387; *Angew. Chem.* **2015**, 127, 2413-2417.
- [8] A. Marchuk, S. Wendl, N. Imamovic, F. Tambornino, D. Wiechert, P. J. Schmidt, W. Schnick, "Nontypical Luminescence Properties and Structural Relation of Ba₃P₅N₁₀X:Eu²⁺ (X = Cl, I): Nitridophosphate Halides with Zeolite-like Structure", *Chem. Mater.* **2015**, 27, 6432-6441.
- [9] S. Wendl, L. Eisenburger, M. Zipkat, D. Günther, J. P. Wright, P. J. Schmidt, O. Oeckler, W. Schnick, "BaP₆N₁₀NH:Eu²⁺ as a Case Study – An Imidonitridophosphate Showing Luminescence", *Chem. Eur. J.* **2020**, 26, 5010–5016.
- [10] E. M. Bertschler, C. Dietrich, T. Leichtweiß, J. Janek, W. Schnick, "Li⁺ Ion Conductors with Adamantane-Type Nitridophosphate Anions β-Li₁₀P₄N₁₀ and Li₁₃P₄N₁₀X₃ with X=Cl, Br", *Chem. Eur. J.* **2018**, 24, 196-205.

- [11] W. Schnick, U. Berger, "*Li₁₀P₄N₁₀ - A Lithium Phosphorus(V) Nitride with the Novel Complex Anion P₄N₁₀¹⁰⁻*", *Angew. Chem. Int. Ed. Engl.* **1992**, 31, 213-214; *Angew. Chem.* **1991**, 103, 857-858.
- [12] A. Marchuk, F. J. Pucher, F. W. Karau, W. Schnick, "*A High-Pressure Polymorph of Phosphorus Nitride Imide*", *Angew. Chem. Int. Ed.* **2014**, 53, 2469-2472; *Angew. Chem.* **2014**, 126, 2501-2504.
- [13] H. Jacobs, R. Nymwegen, "*Synthesis and Crystal Structure of a Potassium Nitridophosphate, K₃P₆N₁₁*", *Z. Anorg. Allg. Chem.* **1997**, 623, 429-433.
- [14] M. Mallmann, S. Wendl, W. Schnick, "*Crystalline Nitridophosphates by Ammonothermal Synthesis*", *Chem. Eur. J.* **2020**, 26, 2067-2072.
- [15] M. Mallmann, C. Maak, R. Niklaus, W. Schnick, "*Ammonothermal Synthesis, Optical Properties, and DFT Calculations of Mg₂PN₃ and Zn₂PN₃*", *Chem. Eur. J.* **2018**, 24, 13963-13970.
- [16] R. Dwilinski, A. Wysmolek, J. Baranowski, M. Kaminska, R. Doradziński, H. Jacobs, "*GaN synthesis by ammonothermal method*", *Acta Phys. Pol., A* **1995**, 88, 833-836.
- [17] J. Hertrampf, P. Becker, M. Widenmeyer, A. Weidenkaff, E. Schlücker, R. Niewa, "*Ammonothermal Crystal Growth of Indium Nitride*", *Cryst. Growth Des.* **2018**, 18, 2365-2369.
- [18] J. Li, T. Watanabe, H. Wada, T. Setoyama, M. Yoshimura, "*Low-Temperature Crystallization of Eu-Doped Red-Emitting CaAlSiN₃ from Alloy-Derived Ammonometallates*", *Chem. Mater.* **2007**, 19, 3592-3594.
- [19] T. Watanabe, K. Nonaka, J. Li, K. Kishida, M. Yoshimura, "*Low temperature ammonothermal synthesis of europium-doped SrAlSiN₃ for a nitride red phosphor*", *J. Ceram. Soc. Jpn.* **2012**, 120, 500-502.
- [20] J. Häusler, L. Neudert, M. Mallmann, R. Niklaus, A.-C. L. Kimmel, N. S. A. Alt, E. Schlücker, O. Oeckler, W. Schnick, "*Ammonothermal Synthesis of Novel Nitrides: Case Study on CaGaSiN₃*", *Chem. Eur. J.* **2017**, 23, 2583-2590.
- [21] J. Häusler, S. Schimmel, P. Wellmann, W. Schnick, "*Ammonothermal Synthesis of Earth-Abundant Nitride Semiconductors ZnSiN₂ and ZnGeN₂ and Dissolution Monitoring by In Situ X-ray Imaging*", *Chem. Eur. J.* **2017**, 23, 12275-12282.
- [22] M. Mallmann, R. Niklaus, T. Rackl, M. Benz, T. G. Chau, D. Johrendt, J. Minár, W. Schnick, "*Solid Solutions of Grimm-Sommerfeld Analogous Nitride Semiconductors II-IV-N₂ (II = Mg,*

- Mn, Zn; IV = Si, Ge): Ammonothermal Synthesis and DFT Calculations*", *Chem. Eur. J.* **2019**, *25*, 15887-15895.
- [23] N. Cordes, R. Niklaus, W. Schnick, "Ammonothermal Crystal Growth of ATaN₂ with A = Na, K, Rb, and Cs and Their Optical and Electronic Properties", *Cryst. Growth Des.* **2019**, *19*, 3484-3490.
- [24] D. Walker, "Lubrication, gasketing, and precision in multianvil experiments", *Am. Mineral.* **1991**, *76*, 1092-1100.
- [25] H. Huppertz, "Multianvil high-pressure / high-temperature synthesis in solid state chemistry", *Z. Kristallogr.* **2004**, *219*, 330-338.
- [26] H. Jacobs, U. Fink, "Über natrium- und kaliumamidometallate des calciums, strontiums und europiums", *J. Less Common Met.* **1979**, *63*, 273-286.
- [27] H. Jacobs, S. Pollok, F. Golinski, "Synthesis and Crystal Structure of Na₁₀[P₄(NH)₆N₄](NH₂)₆(NH₃)_{0.5} with an Adamantane-like Anion [P₄(NH)₆N₄]⁴⁻", *Z. Anorg. Allg. Chem.* **1994**, *620*, 1213-1218.
- [28] F. Golinski, H. Jacobs, "Crystal Structure of Hexamine Cyclotriphosphazene, P₃N₃(NH₂)₆", *Z. Anorg. Allg. Chem.* **1994**, *620*, 965-968.
- [29] S. D. Kloß, N. Weidmann, R. Niklaus, W. Schnick, "High-Pressure Synthesis of Melilite-type Rare-Earth Nitridophosphates RE₂P₃N₇ and a Ba₂Cu[Si₂O₇]-type Polymorph", *Inorg. Chem.* **2016**, *55*, 9400-9409.
- [30] V. Schultz-Coulon, W. Schnick, "Mg₂PN₃ and Ca₂PN₃ – Phosphorus(V) Nitrides with Infinite Chains of Corner Sharing PN₄ Tetrahedra", *Z. Anorg. Allg. Chem.* **1997**, *623*, 69-74.
- [31] F. Liebau, "Structural Chemistry of Silicates", Springer, Berlin, **1985**.
- [32] The terms *dreier* rings, *vierer* rings and *zweier* single chain were coined by Liebau and are derived from the German words "dreier, vierer and zweier"; a *dreier* ring comprises three tetrahedra centers, a *vierer* ring four tetrahedra centers, a *zweier* chain can be described as two polyhedra within one repeating unit of the linear part of the chain.
- [33] E.-M. Bertschler, C. Dietrich, J. Janek, W. Schnick, "Li₁₈P₆N₁₆ – A Lithium Nitridophosphate with Unprecedented Tricyclic [P₆N₁₆]¹⁸⁻ Ions", *Chem. Eur. J.* **2017**, *23*, 2185-2191.

- [34] F. W. Karau, L. Seyfarth, O. Oeckler, J. Senker, K. Landskron, W. Schnick, "The Stuffed Framework Structure of SrP_2N_4 : Challenges to Synthesis and Crystal Structure Determination", *Chem. Eur. J.* **2007**, *13*, 6841-6852.
- [35] S. J. Sedlmaier, E. Mugnaioli, O. Oeckler, U. Kolb, W. Schnick, "SrP₃N₅O: A Highly Condensed Layer Phosphate Structure Solved from a Nanocrystal by Automated Electron Diffraction Tomography", *Chem. Eur. J.* **2011**, *17*, 11258-11265.
- [36] S. J. Sedlmaier, J. Schmedt auf der Günne, W. Schnick, "Sr₃P₆O₆N₈—a highly condensed layered phosphate", *Dalton Trans.* **2009**, 4081-4084.
- [37] R. López, R. Gómez, "Band-gap energy estimation from diffuse reflectance measurements on sol-gel and commercial TiO₂: a comparative study", *J. Sol-Gel Sci. Technol.* **2012**, *61*, 1-7.
- [38] J. Tauc, R. Grigorovici, A. Vancu, "Optical Properties and Electronic Structure of Amorphous Germanium", *Phys. Status Solidi B* **1966**, *15*, 627-637.
- [39] L. M. Dale, A. Thewis, C. Boudry, I. Rotar, P. Dardenne, V. Baeten, J. A. F. Pierna, "Hyperspectral Imaging Applications in Agriculture and Agro-Food Product Quality and Safety Control: A Review", *Appl. Spectrosc. Rev.* **2013**, *48*, 142-159.
- [40] A. A. Gowen, Y. Feng, E. Gaston, V. Valdramidis, "Recent applications of hyperspectral imaging in microbiology", *Talanta* **2015**, *137*, 43-54.
- [41] M. Mallmann, J. Häusler, N. Cordes, W. Schnick, "Ammonothermal Synthesis of Alkali-Alkaline Earth Metal and Alkali-Rare Earth Metal Carbodiimides: $K_{5-x}M_x(CN_2)_{2+x}(HCN_2)_{1-x}$ ($M = Sr, Eu$) and $Na_{4.32}Sr_{0.68}(CN_2)_{2.68}(HCN_2)_{0.32}$ ", *Z. Anorg. Allg. Chem.* **2017**, *643*, 1956-1961.
- [42] A. Stock, B. Hoffmann, "Die Einwirkung von Ammoniak auf Phosphorpentasulfid und der Phosphorstickstoff, P₃N₅", *Ber. Dtsch. Chem. Ges.* **1903**, *36*, 314-319.
- [43] R. Suhrmann, K. Clusius, "Über die Reindarstellung der Alkalimetalle", *Z. Anorg. Allg. Chem.* **1926**, *152*, 52-58.
- [44] F. W. Karau, *Dissertation*, Ludwig-Maximilians-Universität München (Germany) **2007**.
- [45] SAINT, Data Integration Software, Madison, Wisconsin, USA, **1997**.
- [46] APEX 3, Vers. 2016.2015-2010, Bruker-AXS, Karlsruhe, **2016**.
- [47] G. M. Sheldrick, SADABS, *Multi-Scan Absorption Correction*, v.2, Bruker-AXS, Madison, WI, USA, **2012**.
- [48] XPREP Reciprocal Space Exploration, Vers. 6.12, Bruker-AXS, Karlsruhe, **2001**.

- [49] G. M. Sheldrick, "*SHELXT - Integrated space-group and crystal-structure determination*", *Acta Crystallogr. Sect. A* **2015**, *71*, 3-8.
- [50] G. M. Sheldrick, *SHELXL-97: A program for crystal structure refinement*, University of Göttingen, Germany, **1997**.
- [51] G. M. Sheldrick, "*Crystal structure refinement with SHELXL*", *Acta Crystallogr. Sect. C* **2015**, *71*, 3-8.
- [52] A. Coelho, *TOPAS Academic, Version 6*, Coelho Software, Brisbane (Australia), **2016**.
- [53] *OPUS/IR*, Bruker Analytik GmbH, Karlsruhe, **2000**.

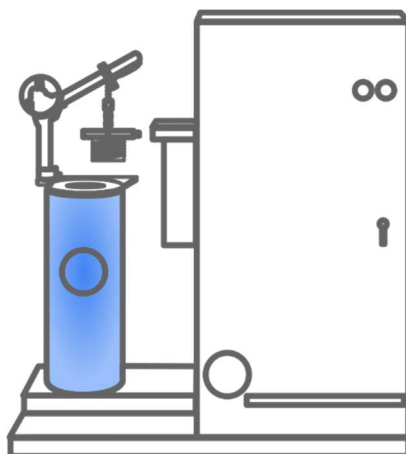
7 HIP to be Square: Simplifying Nitridophosphate Synthesis in a Hot Isostatic Press

Sebastian Wendl, Sara Mardazad, Dr. Philipp Strobel, Dr. Peter J. Schmidt, Prof. Dr. Wolfgang Schnick

Angew. Chem. Int. Ed. **2020**, *59*, 18240–18243; *Angew. Chem.* **2020**, *132*, 18397–18400.

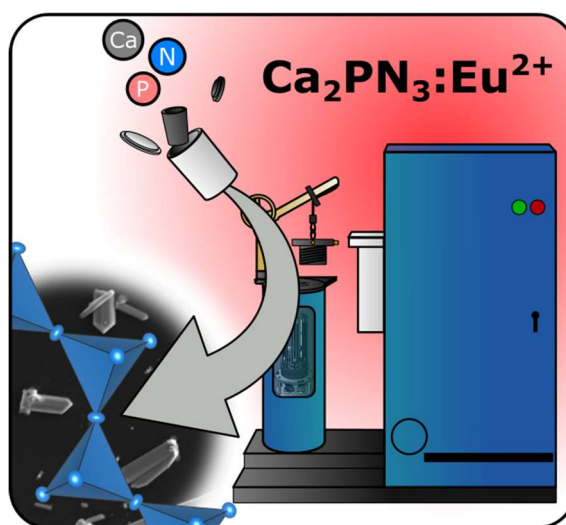
DOI: 10.1002/anie.202008570; 10.1002/ange.202008570.

Reprinted (adapted) with permission for non-commercial use from *Angewandte Chemie* (open access). Copyright 2021 John Wiley and Sons.



Hot Isostatic Press: Ca_2PN_3 was prepared as model compound for nitridophosphate synthesis in a hot isostatic press. After following literature known protocols, the use of red phosphorus was adapted from ammonothermal syntheses. The presented far-reaching proof-of-principle demonstrates the general applicability of HIP methods for nitridophosphate synthesis.

Abstract: (Oxo)Nitridophosphates have recently been identified as a promising compound class for application in the field of solid-state lighting. Especially, the latest medium-pressure syntheses under ammonothermal conditions draw attention of the semiconductor and lighting industry on nitridophosphates. In this contribution, we introduce hot isostatic presses as a new type of medium-pressure synthetic tool, further simplifying nitridophosphate synthesis. In



a second step, phosphorus nitride was replaced as starting material by red phosphorus, enabling the synthesis of Ca_2PN_3 as model compound, starting only from readily available compounds. Moreover, first luminescence investigations on Eu^{2+} -doped samples reveal $\text{Ca}_2\text{PN}_3:\text{Eu}^{2+}$ as a promising broadband red-emitter ($\lambda_{em} = 650 \text{ nm}$; $fwhm = 1972 \text{ cm}^{-1}$). Besides simple handling, the presented synthetic method offers access to large sample volumes, and the underlying reaction conditions facilitate single-crystal growth, required for excellent optical properties.

7.1 Introduction with Results and Discussions

By now, (oxo/imido)nitridophosphates have evolved to one of the best known nitride-based compound classes.^[1] The preparation of nitridophosphates, however, has ever been a challenging issue. Initially, using ambient and medium-pressure methods (i.e. (pressure-)ampoules and autoclaves), research on nitridophosphates was significantly accelerated within the last decade by employing high-pressure high-temperature (HP/HT) methods (e.g., multianvil technique).^[1-12]

The reason for application of high pressure is that the specially prepared and most commonly used starting material P_3N_5 is thermally not very stable. Therefore, reactions under ambient and medium pressure have to be carried out under gentle conditions, meaning low temperatures ($T > 850$ °C; decomposition temperature of P_3N_5) and extraordinary long-term reactions (up to several weeks). According to Le Chatelier's principle, reactions can be performed much faster under HP/HT conditions, because high pressures prevent thermal decomposition of phosphorus nitride and high-temperature conditions enable reversible cleavage and re-formation of covalent P–N bonds.^[13] As reviewed, different synthetic strategies within the high-pressure high-temperature approach could be established, as there are nitride/azide routes, metathesis reactions, Li_3N (self-)flux approaches, and the use of mineralizers.^[1, 14-18] Consequently, the number of nitridophosphates has steadily been increased, and they have been shown to feature an immense structural diversity.^[1] Furthermore, investigations on their materials properties revealed intriguing optical and physical properties, such as luminescence or ion conductivity, illustrating the great potential of nitridophosphates for practical applications.^[16, 19] Therefore, nitridophosphate research diverged into two different fields, recently. On the one hand, fundamental research focuses on chemical and structural aspects using more sophisticated conditions.^[18, 20, 21] Here, one may consider the synthesis of BP_3N_6 that starts from refractory h-BN and uses in situ generated HCl as mineralizer, as well as the observation of six-fold N-coordinated phosphorus under extreme pressure ($p > 40$ GPa).^[18, 20, 21] On the other hand, the second branch of nitridophosphate research concerns the examination of their optical and physical properties, with a special focus on luminescent materials, for example, $AEP_8N_{14}:Eu^{2+}$ ($AE = Ca, Sr$) has recently been proven as promising host material for Eu^{2+} doping.^[19] To enable applications on an industrial scale, however, innovative synthetic routes are required, as sufficient sample quantities cannot be provided by established high-pressure techniques. Therefore,

an advanced ammonothermal approach using improved autoclave materials was reconsidered, enabling the access to various nitridophosphates in a medium-pressure range and at higher temperatures.^[22–25] However, this method is only restrictedly applicable for industrial use due to scaling issues as it requires operations in supercritical ammonia. Thus, the sought-after large-scale access to nitridophosphates remains a stated goal, until now.

In this contribution, we report on the explorative nitridophosphate synthesis in a hot isostatic press (HIP) that is typically used for sintering and annealing processes in ceramics production and powder metallurgy, but is also an established large-scale technique for nitridosilicate synthesis.^[26–31] The HIP approach enables fast chemical reactions under elevated nitrogen pressure, which yield large-volume and crystalline sample quantities, representing a milestone in nitridophosphate synthesis. In order to demonstrate the benefits of HIP syntheses, Ca_2PN_3 serves as model compound in this contribution. Ca_2PN_3 is a lowly condensed ($\kappa = n(\text{P})/n(\text{N}) = 1/3$) nitridophosphate, which was initially obtained as microcrystalline powder by reaction of Ca_3N_2 and P_3N_5 in N_2 filled ampoules at 800 °C over a period of 14 d [Eq. (7.1)].^[6,7]



Employing hot isostatic conditions (150 MPa N_2 , 1200 °C), this synthesis was initially performed in 10 h (Figures A1 and A2 in the Supporting Information). Subsequently, an alternative protocol starting from $\text{Ca}(\text{N}_3)_2$ was established [Eq. (7.2)].



As a third approach, P_3N_5 was replaced by red phosphorus P_{red} as an alternative starting material for further simplification, as shown for ammonothermal synthesis of Ca_2PN_3 .^[22] Until now, P_{red} could only be used for synthesis of nitridophosphates in combination with (supercritical) ammonia, forming intermediates like “ $\text{P}(\text{NH}_2)_5$ ” and “ $\text{NP}(\text{NH}_2)_2$ ”.^[22–24,32] Applying the HIP approach the use of ammonia can be circumvented. Here, P_{red} initially transforms most likely into gaseous/molecular and

highly reactive phosphorus P_4 (or P_2) under the given conditions [Eq. (7.3)], followed by oxidation into the P^V state. Depending on the starting materials, either azide ions or nitrogen itself serve as redox partner [Eqs (7.4) and (7.5)]. Ca_2PN_3 can thus be synthesized in N_2 atmosphere using only commercially available starting materials, which serves as a far-reaching proof-of-principle for nitridophosphate synthesis in general.



All products of the syntheses above arise as colorless to light beige sinter cakes and are highly sensitive towards air and moisture. For the first time, rod-shaped single crystals ($> 100 \mu\text{m}$) of the title compound were obtained (Figure 7.1).

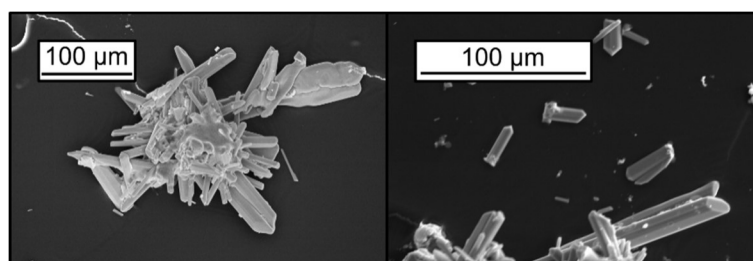


Figure 7.1. SEM images of Ca_2PN_3 . Rod-shaped single-crystals $> 100 \mu\text{m}$ are observed.

Therefore, Ca_2PN_3 was for the first time investigated by means of single-crystal X-ray diffraction. Its crystal structure was refined in space group $Cmce$ with cell dimension of $a = 5.1987(4)$, $b = 10.3145(10)$ and $c = 11.2834(14) \text{ \AA}$, which is in good agreement with previous refinements on the basis of powder X-ray diffraction data (Table F1).^[6, 7, 33] A projection of the crystal structure is displayed in Figure 2, and Figure 3 shows the coordination polyhedral of the two crystallographic Ca sites. A more detailed description of the crystal structure is provided in the literature.^[6, 7]

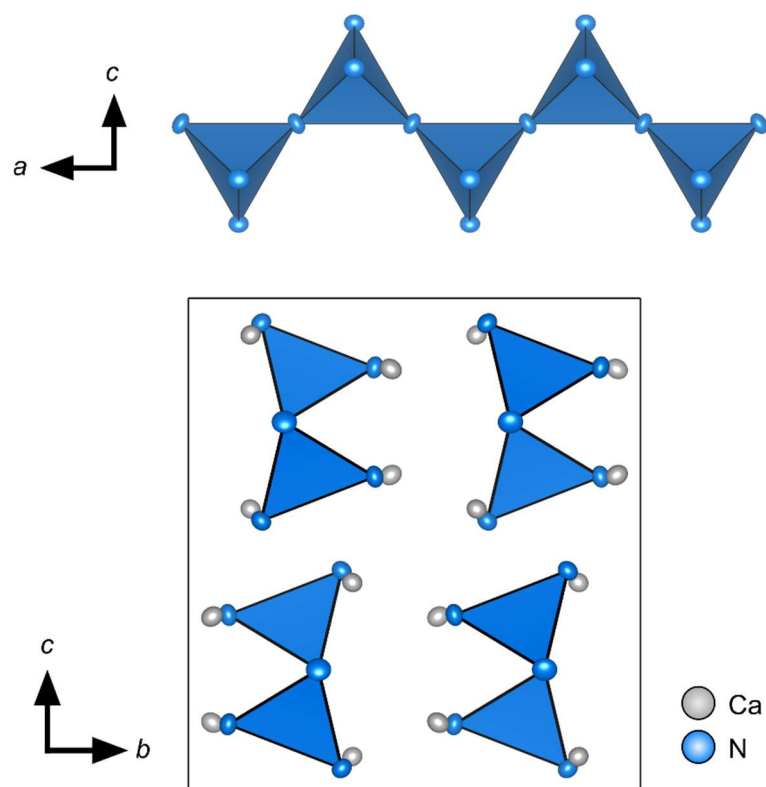


Figure 7.2. Top: *Zweier* single chains in Ca_2PN_3 ; bottom: projection of the crystal structure of Ca_2PN_3 along [100]; Ca: gray, N: blue, PN_4 tetrahedra: blue; atoms are displayed with 95% probability.

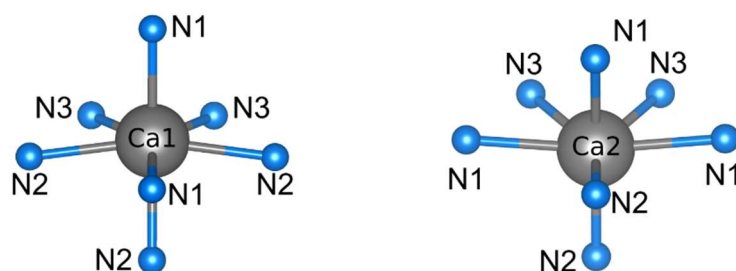


Figure 7.3. Coordination polyhedra of the two crystallographic Ca^{2+} sites in Ca_2PN_3 , as obtained from single-crystal XRD refinement.

The as-refined crystallographic data and a brief comparison to the data provided in literature are given in the Supporting Information (Tables F1– F4).^[6, 7]

Phase purity of the Ca_2PN_3 samples was confirmed by Rietveld refinement of powder X-ray diffraction data. Although no additional reflections are observed using the obtained structure model

from single-crystal X-ray diffraction, significant deviations in intensities arose during Rietveld refinement (Figures F3 and Table F5). This observation is discussed in more detail in the Supporting Information (Figures F4–F6).

The chemical composition was verified by energy dispersive X-ray (EDX) spectroscopy. The averaged stoichiometry $\text{Ca}_{1.9(2)}\text{P}_{1.0(1)}\text{N}_{3.4(3)}$ is in good agreement with the expected sum formula, while trace amounts of oxygen are assigned to surface hydrolysis. Additional traces of chlorine originate from EuCl_2 as dopant. The points of measurement and determined values for all elements are documented in the Supporting Information (Figure F7 and Table F6).

In order to investigate luminescence properties of Ca_2PN_3 , Eu^{2+} -doped (≈ 3 mol% Eu^{2+} with respect to Ca^{2+}) samples were synthesized using EuCl_2 as an additional starting material. The as-obtained samples show deep-red emission ($\lambda_{\text{em}} = 650$ nm) upon excitation with blue light ($\lambda_{\text{exc}} = 440$ nm, Figure 4). Considering the full width at half maximum (fwhm) of 84 nm/1972 cm^{-1} $\text{Ca}_2\text{PN}_3:\text{Eu}^{2+}$ represents the nitridophosphate phosphor with the most narrow red emission band reported so far. Moreover, $\text{Ca}_2\text{PN}_3:\text{Eu}^{2+}$ shows remarkable internal quantum efficiency (IQE) of $\approx 32\%$ for as-synthesized samples. Besides a concentration series for Eu^{2+} -doping in order to increase quantum efficiency, the thermal quenching behaviour could be investigated for potential application.

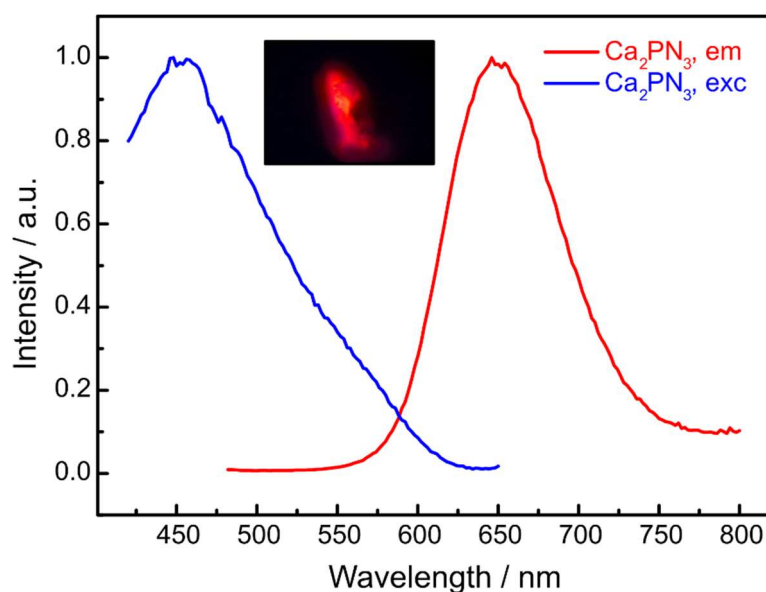


Figure 7.4. Normalized excitation (blue) and emission spectra (red) of $\text{Ca}_2\text{PN}_3:\text{Eu}^{2+}$. The small picture section shows a particle of $\text{Ca}_2\text{PN}_3:\text{Eu}^{2+}$ under illumination with UV to blue light.

Such narrow-band red-emitters are still subject of today's research as they are essential to compensate the low sensitivity of the human eye in the near infrared region.^[34,35] Avoiding any infrared spillover facilitates high luminous efficacy and allows for a high color rendering index (CRI) and low correlated color temperature (CCT).^[34,35] In general, the hitherto obtained results make $\text{Ca}_2\text{PN}_3:\text{Eu}^{2+}$ look competitive in terms of luminescence properties with established red-emitting phosphors from related compound classes, such as CaAlSiN_3 (CASN, $\lambda_{\text{em}} = 650 \text{ nm}$, $\text{fwhm} = 90 \text{ nm}/2166 \text{ cm}^{-1}$) or $\text{Sr}_2\text{Si}_5\text{N}_8$ (Sr-258, $\lambda_{\text{em}} = 630 \text{ nm}$, $\text{fwhm} = 85 \text{ nm}/2150 \text{ cm}^{-1}$), emphasizing the great potential of nitridophosphates. A brief comparison of relevant red-emitting phosphors and their characteristic emission values is provided in Table 7.1.

Table 7.1. Comparison of emission properties of $\text{Ca}_2\text{PN}_3:\text{Eu}^{2+}$ with relevant red-emitting Eu^{2+} -doped phosphors.

Compound	$\lambda_{\text{exc}} / \text{nm}$	$\lambda_{\text{em}} / \text{nm}$	fwhm / nm	$\text{fwhm} / \text{cm}^{-1}$	Reference
Ca_2PN_3	440	650	84	1972	This work
$\text{Sr}_3\text{P}_3\text{N}_7$	450	681	162	3402	23
$\text{Sr}_2\text{Si}_5\text{N}_8$	450	630	85	2150	36
CaSiN_2	450	630	110	2790	37
CaAlSiN_3	450	650	90	2166	38, 39
$\text{SrAlSi}_4\text{N}_7$	450	632	-	2955	40
$\text{Sr}[\text{Mg}_3\text{SiN}_4]$	450	615	43	1170	41
$\text{Ba}[\text{Mg}_3\text{SiN}_4]$	450	670	78	1970	42
$\text{Sr}[\text{LiAl}_3\text{N}_4]$	440	650	50	1180	43
$\text{Sr}[\text{Li}_2\text{Al}_2\text{O}_2\text{N}_2]$	460	614	48	1286	44

Recapitulating, we present a novel synthetic route to nitridophosphates that uses only readily available precursors and gentle reaction conditions, thus providing industrial scalability of luminescent nitridophosphates for the first time. Especially, the recently introduced PN-based phosphors (e.g.: $\text{AEP}_8\text{N}_{14}:\text{Eu}^{2+}$ or $\text{Ba}_3\text{P}_5\text{N}_{10}\text{Br}:\text{Eu}^{2+}$) underpin the quest for such an innovative access, as hitherto established methods are sophisticated (supercritical ammonia, specially prepared starting materials), require long reaction times (ampoules, e.g., Ca_2PN_3 : 14 d), or provide only insufficient sample quantities (HP/HT). By introducing nitridophosphate synthesis in a hot isostatic press, all above mentioned circumstances can be evaded. Besides easy handling, large-volume samples (> 400 mg) can be produced at gentle conditions starting from P_{red} and other commercially available

precursors. Thus, the overall duration of nitridophosphate synthesis is speeded up (Ca_2PN_3 : 10 h) by hot isostatic pressing. This synthetic tool may considerably accelerate fundamental research on nitridophosphates in particular and on nitridometallates in general. For instance, next to the radically reduced reaction times, fast screenings are enabled, which will facilitate a more thorough characterization of physical properties. Combined with the impressive single-crystal growth, hot isostatic pressing may also simplify structure elucidation of unknown nitride compounds. Accompanied with the possibility of ammonia-free synthesis on a large scale, our work has brought nitridophosphates a step closer to industrial application. In this context, $\text{Ca}_2\text{PN}_3:\text{Eu}^{2+}$ is a promising phosphor and offers numerous possibilities for further investigations of optical properties. Especially, the synthesis of solid solutions $\text{Sr}_x\text{Ca}_{2-x}\text{PN}_3:\text{Eu}^{2+}$ should be in focus, as substitution of Ca^{2+} by larger Sr^{2+} ions may lead to a blue shift of the emission band ending up in the favored emission region between 610 and 620 nm with an even smaller fwhm, avoiding IR spillover. Closing, the synthetic limits of this medium-pressure method should be investigated by the preparation of highly-condensed nitridophosphates.

7.2 Acknowledgements

We thank Dr. Constantin Hoch and Arthur Haffner (both Department of Chemistry at LMU) for single-crystal measurements, Volker Weiler (Lumileds Phosphor Center Aachen) for luminescence measurements, and Lisa Gamperl for EDX and SEM investigations. Eugenia Elzer, Lisa Gamperl, and Tobias Gifftaler (all Department of Chemistry at LMU) are gratefully acknowledged for their help with experiments. Inspiring contributions from Dr. Peter Wagatha and discussions with Dr. Sebastian Vogel (both Department of Chemistry at LMU) are gratefully appreciated. Open access funding enabled and organized by Projekt DEAL.

7.3 References

- [1] S. D. Kloß, W. Schnick, "Nitridophosphates – A Success Story of Nitride Synthesis", *Angew. Chem. Int. Ed.* **2019**, 58, 7933-7944; *Angew. Chem.* **2019**, 131, 8015-8027.
- [2] W. Schnick, J. Lücke, "On Lithium Phosphorus Nitride. Preparation and Refinement of the Crystal Structure of LiPN_2 ", *Z. Anorg. Allg. Chem.* **1990**, 588, 19-25.
- [3] W. Schnick, U. Berger, " $\text{Li}_{10}\text{P}_4\text{N}_{10}$ - A Lithium Phosphorus(V) Nitride with the Novel Complex Anion $\text{P}_4\text{N}_{10}^{10-}$ ", *Angew. Chem. Int. Ed. Engl.* **1991**, 30, 830-831; *Angew. Chem.* **1991**, 103, 857-858.
- [4] W. Schnick, J. Lücke, "Preparation, Crystal Structure, and IR-spectroscopic Investigation of Phosphorus Nitride Imide, HPN_2 ", *Z. Anorg. Allg. Chem.* **1992**, 610, 121-126.
- [5] W. Schnick, J. Lücke, " $\text{Zn}_7[\text{P}_{12}\text{N}_{24}]\text{Cl}_2$ - A Sodalite with a Phosphorus Nitrogen Framework", *Angew. Chem. Int. Ed. Engl.* **1992**, 31, 213-215; *Angew. Chem.* **1992**, 104, 208-209.
- [6] W. Schnick, V. Schultz-Coulon, " Ca_2PN_3 : A New Phosphorus(V) Nitride with One-Dimensional Infinite Chains of Corner-Sharing PN_4 Tetrahedra", *Angew. Chem. Int. Ed. Engl.* **1993**, 32, 280-281; *Angew. Chem.* **1993**, 105, 308-309.
- [7] V. Schultz-Coulon, W. Schnick, " Mg_2PN_3 and Ca_2PN_3 – Phosphorus(V) Nitrides with Infinite Chains of Corner Sharing PN_4 Tetrahedra", *Z. Anorg. Allg. Chem.* **1997**, 623, 69-74.
- [8] H. Jacobs, F. Golinski, "Synthesis and Crystal Structure of a Cesium-tetraimidophosphate-diamide, $\text{Cs}_5[\text{P}(\text{NH})_4](\text{NH}_2)_2 = \text{Cs}_3[\text{P}(\text{NH})_4] \cdot 2 \text{CsNH}_2$ ", *Z. Anorg. Allg. Chem.* **1994**, 620, 531-534.
- [9] F. Golinski, H. Jacobs, "Synthesis and Crystal Structure of $\text{Rb}_8[\text{P}_4\text{N}_6(\text{NH})_4](\text{NH}_2)_2$ with the Adamantane-like Anion $[\text{P}_4\text{N}_6(\text{NH})_4]^{6-}$ ", *Z. Anorg. Allg. Chem.* **1995**, 621, 29-33.
- [10] H. Jacobs, R. Nymwegen, "Synthesis and Crystal Structure of a Potassium Nitridophosphate, $\text{K}_3\text{P}_6\text{N}_{11}$ ", *Z. Anorg. Allg. Chem.* **1997**, 623, 429-433.
- [11] H. Jacobs, R. Nymwegen, S. Doyle, T. Wroblewski, W. Kockelmann, "Crystalline Phosphorus(V) Nitride Imide, HPN_2 and DPN_2 , respectively, Structure Determination with X-Ray, Synchrotron, and Neutron Radiation", *Z. Anorg. Allg. Chem.* **1997**, 623, 1467-1474.

- [12] H. Jacobs, S. Pollok, F. Golinski, "Synthesis and Crystal Structure of $\text{Na}_{10}[\text{P}_4(\text{NH})_6\text{N}_4](\text{NH}_2)_6(\text{NH}_3)_{0.5}$ with an Adamantane-like Anion $[\text{P}_4(\text{NH})_6\text{N}_4]^{4-}$ ", *Z. Anorg. Allg. Chem.* **1994**, 620, 1213-1218.
- [13] W. Schnick, "Solid State Chemistry with Nonmetal Nitrides", *Angew. Chem. Int. Ed. Engl.* **1993**, 32, 806-818; *Angew. Chem.* **1993**, 105, 846-858.
- [14] F. J. Pucher, S. R. Römer, F. W. Karau, W. Schnick, "Phenakite-Type BeP_2N_4 - A Possible Precursor for a New Hard Spinel-Type Material", *Chem. Eur. J.* **2010**, 16, 7208-7214.
- [15] F. W. Karau, W. Schnick, "High-pressure synthesis and X-ray powder structure determination of the nitridophosphate BaP_2N_4 ", *J. Solid State Chem.* **2005**, 178, 135-141.
- [16] E.-M. Bertschler, C. Dietrich, J. Janek, W. Schnick, " $\text{Li}_{18}\text{P}_6\text{N}_{16}$ - A Lithium Nitridophosphate with Unprecedented Tricyclic $[\text{P}_6\text{N}_{16}]^{18-}$ Ions", *Chem. Eur. J.* **2017**, 23, 2185-2191.
- [17] S. D. Kloß, W. Schnick, "Rare-Earth-Metal Nitridophosphates through High-Pressure Metathesis", *Angew. Chem. Int. Ed.* **2015**, 54, 11250-11253; *Angew. Chem.* **2015**, 127, 11402-11405.
- [18] S. Vogel, A. T. Buda, W. Schnick, "United in Nitride: The Highly Condensed Boron Phosphorus Nitride BP_3N_6 ", *Angew. Chem. Int. Ed.* **2018**, 57, 13202-13202; *Angew. Chem.* **2018**, 130, 13386-13389.
- [19] S. Wendl, L. Eisenburger, P. Strobel, D. Günther, J. P. Wright, P. J. Schmidt, O. Oeckler, W. Schnick, "Nitridophosphate-Based Ultra-Narrow-Band Blue-Emitters: Luminescence Properties of $\text{AEP}_8\text{N}_{14}:\text{Eu}^{2+}$ ($\text{AE} = \text{Ca}, \text{Sr}, \text{Ba}$)", *Chem. Eur. J.* **2020**, 26, 7292-7298.
- [20] S. Vogel, M. Bykov, E. Bykova, S. Wendl, S. D. Kloß, A. Pakhomova, S. Chariton, E. Koemets, N. Dubrovinskaia, L. Dubrovinsky, W. Schnick, "Boron Phosphorus Nitride at Extremes: PN_6 Octahedra in the High-Pressure Polymorph $\beta\text{-BP}_3\text{N}_6$ ", *Angew. Chem. Int. Ed.* **2019**, 58, 9060-9063; *Angew. Chem.* **2019**, 131, 9158-9161.
- [21] S. Vogel, M. Bykov, E. Bykova, S. Wendl, S. D. Kloß, A. Pakhomova, N. Dubrovinskaia, L. Dubrovinsky, W. Schnick, "Nitride Spinel: An Ultraincompressible High-Pressure Form of BeP_2N_4 ", *Angew. Chem. Int. Ed.* **2020**, 59, 2730-2734; *Angew. Chem.* **2020**, 132, 2752-2756.
- [22] M. Mallmann, S. Wendl, W. Schnick, "Crystalline Nitridophosphates by Ammonothermal Synthesis", *Chem. Eur. J.* **2020**, 26, 2067-2072.

- [23] M. Mallmann, S. Wendl, P. Strobel, P. J. Schmidt, W. Schnick, "Sr₃P₃N₇: Complementary Approach by Ammonothermal and High-Pressure Syntheses", *Chem. Eur. J.* **2020**, 26, 6257-6263.
- [24] S. Wendl, M. Mallmann, P. Strobel, P. J. Schmidt, W. Schnick, "Ammonothermal Synthesis of Ba₂PO₃N – An Oxonitridophosphate with Non-Condensed PO₃N Tetrahedra", *Eur. J. Inorg. Chem.* **2020**, 2020, 841-846.
- [25] M. Mallmann, C. Maak, R. Niklaus, W. Schnick, "Ammonothermal Synthesis, Optical Properties, and DFT Calculations of Mg₂PN₃ and Zn₂PN₃", *Chem. Eur. J.* **2018**, 24, 13963-13970.
- [26] Z. Xiao, S. Yu, Y. Li, S. Ruan, L. B. Kong, Q. Huang, Z. Huang, K. Zhou, H. Su, Z. Yao, W. Que, Y. Liu, T. Zhang, J. Wang, P. Liu, D. Shen, M. Allix, J. Zhang, D. Tang, "Materials development and potential applications of transparent ceramics: A review", *Mater. Sci. Eng. R Rep.* **2020**, 139, 100518.
- [27] K. Tsukuma, "Transparent MgAl₂O₄ Spinel Ceramics Produced by HIP Post-Sintering", *J. Ceram. Soc. Jpn.* **2006**, 114, 802-806.
- [28] K. Tsukuma, I. Yamashita, T. Kusunose, "Transparent 8 mol% Y₂O₃-ZrO₂ (8Y) Ceramics", *J. Am. Ceram. Soc.* **2008**, 91, 813-818.
- [29] A. G. Padalko, V. A. Baklan, "Transformation in metal materials during hot isostatic pressing", *Inorg. Mater.* **2012**, 48, 1226-1242.
- [30] H. Watanabe, M. Imai, N. Kijima, "Nitridation of AEAlSi for Production of AEAlSiN₃:Eu²⁺ Nitride Phosphors (AE = Ca, Sr)", *J. Am. Ceram. Soc.* **2009**, 92, 641-648.
- [31] H. Watanabe, N. Kijima, "Synthesis of Sr_{0.99}Eu_{0.01}AlSiN₃ from intermetallic precursor", *J. Ceram. Soc. Jpn.* **2009**, 117, 115-119.
- [32] J. M. Sullivan, "Ammoniated phosphonitrilic amides, imides, and nitrides. I. The equilibrium 4 NH₃(g) + 2 P(r) = 2 PN₂H(s) + 5 H₂(g)", *Inorg. Chem.* **1976**, 15, 1055-1059.
- [33] Crystal data of Ca₂PN₃ from single-crystal XRD refinement: $M = 153.15 \text{ gmol}^{-1}$, orthorhombic, *Cmce* (no. 64), $a = 5.1987(4)$, $b = 10.3145(10)$ and $c = 11.283(1) \text{ \AA}$, $V = 605.04(11) \text{ \AA}^3$, $Z = 8$, $\rho = 3.363 \text{ gcm}^{-3}$, $\mu = 4.031 \text{ mm}^{-1}$, Mo-K α ($\lambda = 0.71073 \text{ \AA}$, Bruker D8 Quest), $T = 293 \text{ K}$, 11096 observed reflections, 755 independent reflections, 36 parameters, $R_{\text{int}} = 0.055$, $R_{\sigma} = 0.024$, $R_1 = 0.017$, $wR_2 = 0.043$, $GoF = 1.085$, residual electron density 0.358, -0.603 e\AA^{-3} . Deposition number 2008630 contains the supplementary crystallographic data for this paper. These data

are provided free of charge by the joint Cambridge Crystallographic Data Centre and Fachinformationszentrum Karlsruhe Access Structures service www.ccdc.cam.ac.uk/structures.

- [34] C. C. Lin, A. Meijerink, R.-S. Liu, "Critical Red Components for Next-Generation White LEDs", *J. Phys. Chem. Lett.* **2016**, 7, 495-503.
- [35] P. Pust, P. J. Schmidt, W. Schnick, "A revolution in lighting", *Nat. Mater.* **2015**, 14, 454-458.
- [36] Y. Q. Li, J. E. J. van Steen, J. W. H. van Krevel, G. Botty, A. C. A. Delsing, F. J. DiSalvo, G. de With, H. T. Hintzen, "Luminescence properties of red-emitting $M_2Si_5N_8:Eu^{2+}$ ($M = Ca, Sr, Ba$) LED conversion phosphors", *J. Alloys Compd.* **2006**, 417, 273-279.
- [37] Y. Q. Li, N. Hirosaki, R.-J. Xie, T. Takada, Y. Yamamoto, M. Mitomo, K. Shioi, "Synthesis, Crystal and Local Electronic Structures, and Photoluminescence Properties of Red-Emitting $CaAl_2SiN_{2+z}:Eu^{2+}$ with Orthorhombic Structure", *Int. J. Appl. Ceram. Technol.* **2010**, 7, 787-802.
- [38] K. Uhedaa, N. Hirosaki, Y. Yamamoto, A. Naito, T. Nakajima, H. Yamamoto, "Luminescence Properties of a Red Phosphor, $CaAlSiN_3:Eu^{2+}$, for White Light-Emitting Diodes", *Electrochem. Solid-State Lett.* **2006**, 9, H22-H25.
- [39] H. S. Kim, K.-i. Machida, T. Horikawa, H. Hanzawa, "Luminescence properties of $CaAlSiN_3:Eu^{2+}$ phosphor prepared by direct-nitriding method using fine metal hydride powders", *J. Alloys Compd.* **2015**, 633, 97-103.
- [40] C. Hecht, F. Stadler, P. J. Schmidt, J. S. auf der Günne, V. Baumann, W. Schnick, "SrAlSi₄N₇:Eu²⁺ – A Nitridoalumosilicate Phosphor for Warm White Light (pc)LEDs with Edge-Sharing Tetrahedra", *Chem. Mater.* **2009**, 21, 1595-1601.
- [41] S. Schmiechen, H. Schneider, P. Wagatha, C. Hecht, P. J. Schmidt, W. Schnick, "Toward New Phosphors for Application in Illumination-Grade White pc-LEDs: The Nitridomagnesosilicates $Ca[Mg_3SiN_4]:Ce^{3+}$, $Sr[Mg_3SiN_4]:Eu^{2+}$, and $Eu[Mg_3SiN_4]$ ", *Chem. Mater.* **2014**, 26, 2712-2719.
- [42] S. Schmiechen, P. Strobel, C. Hecht, T. Reith, M. Siegert, P. J. Schmidt, P. Huppertz, D. Wiechert, W. Schnick, "Nitridomagnesosilicate $Ba[Mg_3SiN_4]:Eu^{2+}$ and Structure–Property Relations of Similar Narrow-Band Red Nitride Phosphors", *Chem. Mater.* **2015**, 27, 1780-1785.
- [43] P. Pust, V. Weiler, C. Hecht, A. Tücks, A. S. Wochnik, A.-K. Henß, D. Wiechert, C. Scheu, P. J. Schmidt, W. Schnick, "Narrow-band red-emitting $Sr[LiAl_3N_4]:Eu^{2+}$ as a next-generation LED-phosphor material", *Nat. Mater.* **2014**, 13, 891-896.

- [44] G. J. Hoerder, M. Seibald, D. Baumann, T. Schröder, S. Peschke, P. C. Schmid, T. Tyborski, P. Pust, I. Stoll, M. Bergler, C. Patzig, S. Reißaus, M. Krause, L. Berthold, T. Höche, D. Johrendt, H. Huppertz, "*Sr[Li₂Al₂O₂N₂]:Eu²⁺—A high performance red phosphor to brighten the future*", *Nat. Comm.* **2019**, *10*, 1824.

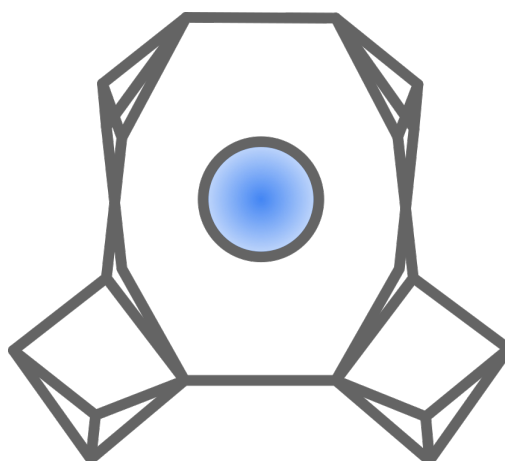
8 Synthesis of Nitride Zeolites in a Hot Isostatic Press

Sebastian Wendl, Mirjam Zipkat, Dr. Philipp Strobel, Dr. Peter J. Schmidt, Prof. Dr. Wolfgang Schnick

Angew. Chem. Int. Ed. **2021**, *60*, 4470–4473; *Angew. Chem.* **2021**, *133*, 4520–4523.

DOI: 10.1002/anie.202012722; 10.1002/ange.202012722.

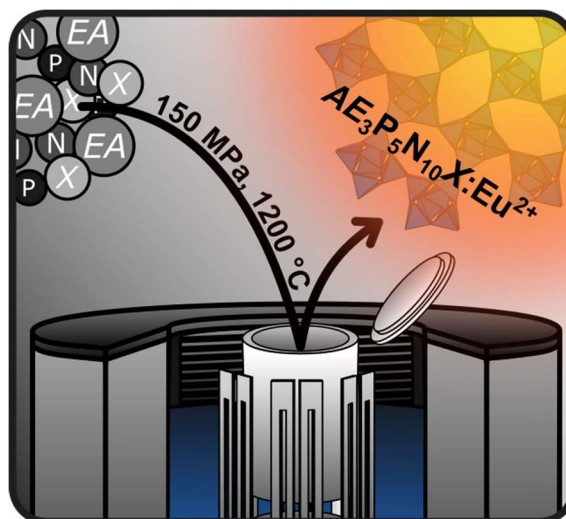
Reprinted (adapted) with permission for non-commercial use from *Angewandte Chemie* (open access). Copyright 2021 John Wiley and Sons.



Nitride Zeolites: $AE_3P_5N_{10}X$ ($AE = Sr, Ba, X = Cl, Br$) were synthesized in a hot isostatic press starting from the respective alkaline earth metal azides and halides, as well as, P_3N_5 or P_{red} . Therefore, the broad applicability of HIPs for nitridophosphate synthesis is demonstrated by extending the accessible degree to $\kappa = 0.5$. The preparation of the introduced strontium compounds suggests the existence of phases being exclusively accessible under medium-pressure conditions.

Abstract: The recently introduced nitridophosphate synthesis in a hot isostatic press (HIP) enabled simple access to large-scale product quantities starting from exclusively commercially available starting materials. Herein, we show that this method is suitable for the synthesis of highly condensed functional nitridophosphates, as well. Hence, the syntheses of the nitridophosphate zeolites $Ba_3P_5N_{10}X$ ($X = Cl, Br$) are presented as proof of concept for this innovative access.

Furthermore, samples of unprecedented $Sr_3P_5N_{10}X$ ($X = Cl, Br$) were prepared and characterized to demonstrate the advantages of this synthetic approach over commonly used methods. Luminescence investigations on Eu^{2+} -doped samples of $AE_3P_5N_{10}X$ ($AE = Sr, Ba; X = Cl, Br$) were carried out and characteristics of observed emission bands are discussed.



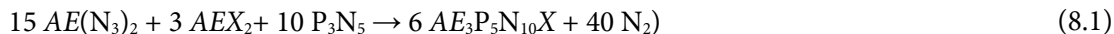
8.1 Introduction with Results and Discussions

The versatile compound class of nitridophosphates has been researched in detail for more than 30 years.^[1] The structural diversity of nitridophosphates can be derived from their close relationship to oxosilicates, as the element combination Si/O is isoelectronic with P/N, and similar with oxosilicates which are built up from SiO₄ tetrahedra, the PN₄ tetrahedron is the fundamental building unit in nitridophosphates. However, nitridophosphates can even feature edge-sharing tetrahedra due to the higher covalence (and lower polarity) of P–N bonds compared to Si–O in oxosilicates.^[1,2] Additionally, the higher valence of nitrogen allows for higher degrees of condensation (i.e. atomic ratio κ of tetrahedra centers to tetrahedra vertices).^[1,3] But despite numerous investigations, nitridophosphate synthesis has ever been challenging, as the most common starting material phosphorus(V) nitride (P₃N₅) is prone to thermal decomposition above 850 °C.^[4] Therefore, high-pressure high-temperature methods (e.g. multianvil technique) have been employed for their synthesis, since elevated nitrogen pressure suppresses the thermally induced elimination of N₂ from P₃N₅.^[1] This high-pressure strategy led to a large number of nitridophosphates with various incorporated electropositive elements.^[5–9] However, sample quantities have intrinsically been limited by high-pressure techniques. Investigations on the associated optical and physical properties of nitridophosphates, such as ion conductivity or luminescence, have however quickly revealed the potential of this functional materials class.^[5,10–12] In particular, the intriguing luminescence properties of nitridophosphates like Ba₃P₅N₁₀X:Eu²⁺ (X = Cl, Br, I) and AEP₈N₁₄:Eu²⁺ (AE = Ca, Sr, Ba) clearly underline the quest for a synthetic approach that can be transformed to a large batch scale.^[3,11,13] Here, ambient and medium-pressure methods that have been used for the early syntheses of phosphorus nitrides and nitridophosphates come to mind.^[14–23] However, only a limited number of such nitride compounds could be synthesized applying these techniques, as gentle conditions or tailored starting materials had to be used. This limitation has changed only recently, as improved high-temperature ammonothermal techniques and the use of red phosphorus as starting material enabled synthesis of diverse nitridophosphates.^[24–27] However, ammonothermal syntheses of nitridophosphates may not be performed industrially due to its demanding handling and the stated goal for a large-scale access remained. Recently, we have reported on the successful synthesis of Ca₂PN₃ in a hot isostatic press (HIP) under nitrogen pressure, which thus appears as a promising

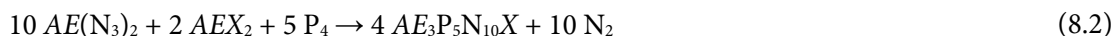
innovative approach for nitridophosphate synthesis.^[28] HIPs do not only provide large sample quantities, but also shorten reaction times and facilitate crystal growth under comparatively gentle reaction conditions. Moreover, we have demonstrated that red phosphorus can serve as a starting material in HIPs as well, simplifying nitridophosphate syntheses even more.^[28]

Within the scope of this work, this approach is further developed to grant access to highly condensed nitridophosphates with a degree of condensation $\kappa = 1/2$. For this purpose, $Ba_3P_5N_{10}X$ ($X = Cl, Br$) were chosen as model compounds, because of their above-mentioned luminescence properties.^[11, 13] Furthermore, hitherto unknown compounds $Sr_3P_5N_{10}X$ ($X = Cl, Br$) were synthesized and investigated with regard to luminescence properties.

All alkaline earth nitridophosphate zeolites $AE_3P_5N_{10}X$ ($AE = Ba, Sr; X = Cl, Br$) were synthesized under nitrogen atmosphere in a HIP applying hot isostatic conditions (150 MPa N_2 , 1000 °C, Figures G1 and G2). In an initial attempt, the title compounds were synthesized from specially prepared P_3N_5 and the respective alkaline earth azides and halides following Equation 8.1 (Table G1).



Subsequently, all variants of $AE_3P_5N_{10}X$ ($AE = Ba, Sr; X = Cl, Br$) were prepared using commercial red phosphorus (P_{red}), replacing P_3N_5 as phosphorus source [Eq. 8.2, Table G1]. The reaction equation is balanced with P_4 , since P_{red} is considered to transform into molecular/gaseous phosphorus at reaction conditions of 150 MPa and 1000 °C.^[28]



Subsequent oxidation into P^V is coupled to the disproportionation of azide ions into network-forming nitride anions and elemental nitrogen. Thereby, it is conceivable that activated P_4 is gradually oxidized and present as P^{III} in form of molecular “PN” after initial reaction with N_2 . In a second oxidization step, halide-containing intermediates, such as $(P^VNCl_2)_3$, might be formed. $(PNCl_2)_3$ in turn serves as starting material for laboratory synthesis of P_3N_5 and may facilitate the *in*

situ formation of the latter, leading to the desired zeolites $AE_3P_5N_{10}X$. An experimental evidence for this hypothesis by *in situ* measurements is still pending.

To investigate luminescence properties of $AE_3P_5N_{10}X$, Eu^{2+} -doped samples were prepared by adding 3 mol% $EuCl_2$ (with regard to alkaline earth ions) to the mixture of starting materials.

The undoped samples are yielded as colorless cube-like crystals, while sinter cakes of Eu^{2+} -doped products exhibit yellow (Ba compounds) to orange body colors (Sr compounds). All products have been washed with de-ionized water and are not sensitive towards air or moisture. SEM imaging of the products reveals the microcrystalline character of Ba compounds (edge length up to $\approx 3 \mu\text{m}$, Figure 8.1). Sr compounds form slightly larger crystals with edge lengths up to 15–20 μm (Figure 8.1). Phase purity of $Ba_3P_5N_{10}X$ ($X = \text{Cl}, \text{Br}$) was confirmed by Rietveld refinements, using literature known structures as starting models.^[11, 13] Detailed information on the refinements is provided in the Supporting Information (Figures G3 and G4, Table G2).

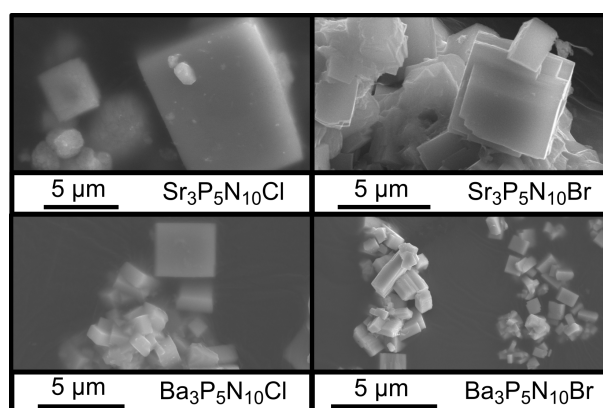


Figure 8.1. SEM images of obtained $AE_3P_5N_{10}X$ samples ($AE = \text{Sr}, \text{Ba}; X = \text{Cl}, \text{Br}$) containing single crystals.

The structures of $Sr_3P_5N_{10}X$ ($X = \text{Cl}, \text{Br}$) were elucidated from a single-crystal XRD measurement of $Sr_3P_5N_{10}Cl$. $Sr_3P_5N_{10}Br$ was refined using the Rietveld method and using the structure of $Sr_3P_5N_{10}Cl$ as starting model (Figure G5, Table G7). Both compounds crystallize homeotypically to the Ba compounds in the JOZ zeolite structure type ($Pnma$; $Z = 8$; $Sr_3P_5N_{10}Cl$: $a = 12.240(3)$; $b = 12.953(3)$; $c = 13.427(3)$ Å; $Sr_3P_5N_{10}Br$: $a = 12.297(1)$; $b = 12.990(1)$; $c = 13.458(1)$ Å.^[29–31] The crystal structure of $Sr_3P_5N_{10}X$ is shown exemplarily for $X = \text{Cl}$ in Figure 8.2. The as-refined crystallographic data is summarized in the Supporting Information (Tables S3–S5) and a more detailed description of the

crystal structure is provided in literature.^[11, 13] Phase purity of $\text{Sr}_3\text{P}_5\text{N}_{10}\text{Cl}$ has been confirmed by Rietveld refinement (Figure G6, Table G7). In contrast to the Ba compounds, $\text{Sr}_3\text{P}_5\text{N}_{10}\text{X}$ ($\text{X} = \text{Cl}, \text{Br}$) show split positions of the Sr5 site. Although the split position is not present in the Ba compounds the corresponding Ba5 site in $\text{Ba}_3\text{P}_5\text{N}_{10}\text{X}$, however, shows the most elongated ellipsoids and Ba–X distances (Figure G7).^[11, 13] This observation can be explained by the significantly smaller space filling of Sr^{2+} compared to Ba^{2+} and the associated increasing displacement of ions.^[32, 33] Moreover, owing to the larger radius of Br^- , the distance between the split position is reduced in $\text{Sr}_3\text{P}_5\text{N}_{10}\text{Br}$ (Figure G8).

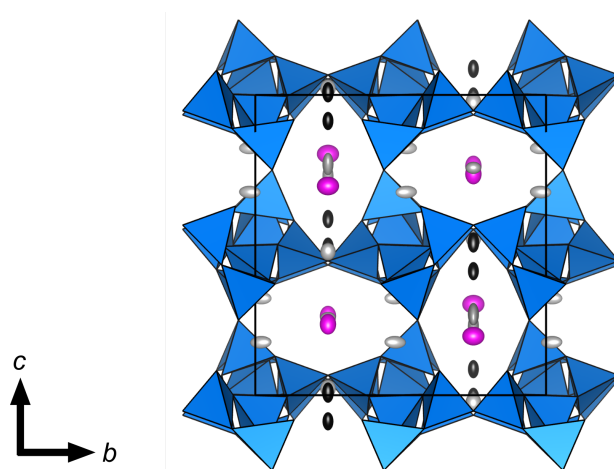


Figure 8.2. Projection of the crystal structure of $\text{Sr}_3\text{P}_5\text{N}_{10}\text{Cl}$ along [100]: PN_4 tetrahedra blue, Cl atoms pink, Sr1–Sr4 atoms gray, split position of Sr5 black. All atoms are displayed with 95% probability.^[29]

These observations may explain the reason for $\text{Sr}_3\text{P}_5\text{N}_{10}\text{X}$ ($\text{X} = \text{Cl}, \text{Br}$) being exclusively accessible at medium-pressure conditions, as the pressure has to be well balanced. Although increased pressure is necessary to prevent thermal decomposition, it must not be chosen too high for $\text{Sr}_3\text{P}_5\text{N}_{10}\text{X}$ syntheses to prevent collapsing of the large cages, considering the reduced space filling of the Sr^{2+} ions. In line with this hypothesis, the Ba compounds are rather difficult to access at ambient pressure, as well, and phase pure samples have only been obtained at 1–5 GPa, thus far.^[11, 13]

The interatomic P–N distances and N–P–N angles of $\text{Sr}_3\text{P}_5\text{N}_{10}\text{X}$ ($\text{X} = \text{Cl}, \text{Br}$) are in very good agreement with values reported for other nitridophosphates (Table G9).^[3, 11, 13] In line with previous refinements, the observed AE–N/X distances differ significantly depending on the coordination number of the alkaline earth metal ion (Figure G8). A detailed list of the interatomic AE–N/X

distances is provided in literature for $\text{Ba}_3\text{P}_5\text{N}_{10}\text{X}$ and in the Supporting Information for $\text{Sr}_3\text{P}_5\text{N}_{10}\text{X}$ (Table G8).^[11, 13]

The chemical compositions of the title compounds were confirmed by energy dispersive X-ray spectroscopy (EDX), with details provided in the Supporting Information (Tables G10).

Eu^{2+} -doped samples of $\text{Ba}_3\text{P}_5\text{N}_{10}\text{X}$ ($X = \text{Cl}, \text{Br}$) have already been discussed as promising phosphor materials, but any industrial application had been ruled out, owing to limited sample volumes.^[11, 13] With the innovative approach that is presented herein, large-volume samples become accessible. Additionally, hitherto unknown $\text{Sr}_3\text{P}_5\text{N}_{10}\text{X}:\text{Eu}^{2+}$ ($X = \text{Cl}, \text{Br}$) is introduced as new luminescent material.

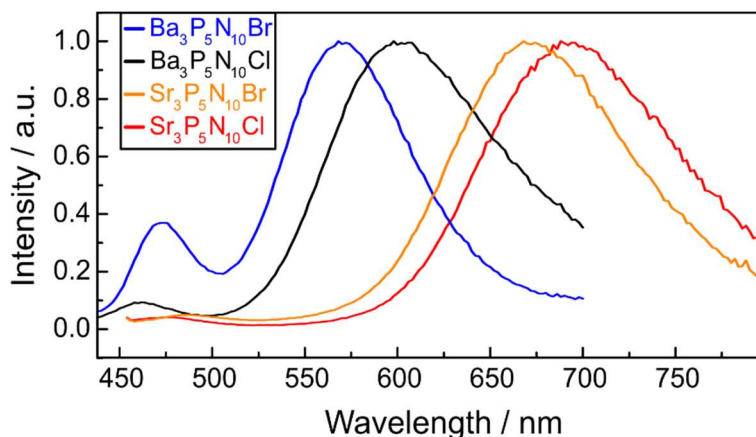


Figure 8.3. Measured emission spectra of $\text{AE}_3\text{P}_5\text{N}_{10}\text{X}:\text{Eu}^{2+}$ ($\text{AE} = \text{Sr}, \text{Ba}; X = \text{Cl}, \text{Br}$) at room temperature with a nominal doping level of 3 mol% Eu^{2+} referred to AE^{2+} .

Excitation with UV to blue light ($\lambda_{\text{exc}} = 420 \text{ nm}$) induces natural-white ($\text{Ba}_3\text{P}_5\text{N}_{10}\text{Br}:\text{Eu}^{2+}$), orange ($\text{Ba}_3\text{P}_5\text{N}_{10}\text{Cl}:\text{Eu}^{2+}$), and deep-red emission ($\text{Sr}_3\text{P}_5\text{N}_{10}\text{X}:\text{Eu}^{2+}$), which features two emission maxima for each compound (Figures 8.3 and G9–G13). The two emission maxima likely correspond to the different Eu^{2+} coordination spheres that are provided by the host lattice. The sites $\text{AE}1$, $\text{AE}4$, and $\text{AE}5$ are coordinated by eight N and two X ions ($\text{CN} = 10$) and thus, feature rather elongated $\text{AE}-\text{X}$ and $\text{AE}-\text{N}$ distances, causing a weak crystal field (Figure G8, Table G8). Therefore, the higher energetic emission bands can be assigned to Eu^{2+} ions occupying these sites according to the parity-allowed transition $4f^7 \rightarrow 4f^65d^1$. Consequently, the second emission band is assigned to Eu^{2+} ions located on AE sites with lower coordination number ($\text{AE}2$, $\text{AE}3$: $\text{CN} = 8$, six N and two X ions), which feature

shorter $AE-X$ and $AE-N$ distances and thus a strong crystal field (Figure G8, Table G8). A detailed illustration of the emission and excitation spectra for each element combination $AE-X$ is provided in the Supporting Information (Figures G10– G13).

When comparing the emission spectra, two trends are particularly striking. First, emission bands of $AE_3P_5N_{10}Cl$ and $AE_3P_5N_{10}Br$ are shifted comparing $AE = Ba$ and $AE = Sr$. This effect is attributable to the different AE radii and the associated $AE-N/X$ and $Eu^{2+}-N/X$ distances, leading to an increased crystal field splitting for Eu^{2+} on the Sr site and a red-shift in emission. The second trend describes the influence of the halide ions on the position of the emission maxima. While the higher energetic bands are shifted red with increasing size of X , lower energetic bands are shifted blue. A detailed discussion of these observations is provided in the Supporting Information.

Furthermore, measurements of the internal quantum efficiency have been carried out for non-optimized powder samples of the title compounds. The IQE of $Sr_3P_5N_{10}X:Eu^{2+}$ was determined to 29 % ($X = Cl$) and 32 % ($X = Br$). Measurements on $Ba_3P_5N_{10}X:Eu^{2+}$ yield quantum efficiency of 12% each, which shows potential for improvement of the investigated samples, as values of > 60% have been reported for $Ba_3P_5N_{10}X:Eu^{2+}$ ($X = Cl, Br$; 2 mol% Eu^{2+} referred to Ba^{2+}), previously.^[11, 13] The luminescence characteristics of the title compounds are summarized in Table G11.

Recapping, we have extended the possibilities of nitridophosphate syntheses by hot isostatic pressing. Prior to this work, this approach has been limited to preparation of lowly condensed $Ca_2PN_3:Eu^{2+}$. In this work, we have succeeded in synthesizing highly condensed nitridophosphates $AE_3P_5N_{10}X$ ($AE = Sr, Ba$; $X = Cl, Br$), increasing the maximum degree of condensation reachable for nitridophosphates by HIP synthesis to 1/2. It is particularly noteworthy that the used conditions allow for the synthesis of $Sr_3P_5N_{10}X$, which was not accessible by conventional methods, so far. Presumably, in this case only medium-pressure methods, such as hot isostatic pressing, enable pressure balancing in a way that the synthesis is possible at all. The pressure should be high enough to prevent thermal decomposition, but not too high, otherwise large cages collapse due to lower space filling of Sr^{2+} .

The presented results suggest that the pressure range generally applied under HP/HT conditions may exceed the actually required synthesis pressure for nitridophosphates by far. Since the minimum pressure to suppress thermal decomposition is not known, numerous published and some novel

nitridophosphates are already accessible under medium-pressure conditions. Consequently, future investigations may focus on synthesis of $\text{Ca}_3\text{P}_5\text{N}_{10}\text{X}$, other P/N based zeolites (e.g. *NPO* or *NPT*), and even higher condensed nitridophosphates (e.g. *AEP*₈*N*₁₄). In particular, the successful activation of red phosphorus as starting material could contribute to a considerable acceleration of these investigations. It should also be examined whether other starting materials, such as nitrides, can be replaced by precursors, like metals or alloys. The fact that N_2 can serve as necessary redox partner has already been shown in the synthesis of Ca_2PN_3 .^[28] These significant simplifications in synthesis, the wide range of achievable degrees of condensation and the large sample volumes may allow that nitridophosphates could find their way into industrial application as phosphor materials.

8.2 Acknowledgements

The authors thank Dr. Peter Mayer (Department of Chemistry at LMU) for the collection of single-crystal data, Volker Weiler (Lumileds Phosphor Center Aachen) for luminescence measurements, Lisa Gamperl for EDX and SEM measurements and Tobias Gifftaler (all Department of Chemistry) for support in practical work. Open access funding enabled and organized by Projekt DEAL.

8.3 References

- [1] S. D. Kloß, W. Schnick, "Nitridophosphates – A Success Story of Nitride Synthesis", *Angew. Chem. Int. Ed.* **2019**, 58, 7933-7944; *Angew. Chem.* **2019**, 131, 8015-8027.
- [2] S. Horstmann, E. Irran, W. Schnick, "Phosphorus(V) Nitride Imide HP_4N_7 : Synthesis from a Molecular Precursor and Structure Determination with Synchrotron Powder diffraction", *Angew. Chem. Int. Ed. Engl.* **1997**, 36, 1992-1994; *Angew. Chem.* **1997**, 109, 2085-2087.
- [3] S. Wendl, L. Eisenburger, P. Strobel, D. Günther, J. P. Wright, P. J. Schmidt, O. Oeckler, W. Schnick, "Nitridophosphate-Based Ultra-Narrow-Band Blue-Emitters: Luminescence Properties of $AEP_8N_{14}:Eu^{2+}$ ($AE = Ca, Sr, Ba$)", *Chem. Eur. J.* **2020**, 26, 7292-7298.
- [4] W. Schnick, "Solid State Chemistry with Nonmetal Nitrides", *Angew. Chem. Int. Ed. Engl.* **1993**, 32, 806-818; *Angew. Chem.* **1993**, 105, 846-858.
- [5] E.-M. Bertschler, C. Dietrich, J. Janek, W. Schnick, " $Li_{18}P_6N_{16}$ - A Lithium Nitridophosphate with Unprecedented Tricyclic $[P_6N_{16}]^{18-}$ Ions", *Chem. Eur. J.* **2017**, 23, 2185-2191.
- [6] F. W. Karau, W. Schnick, "High-pressure synthesis and X-ray powder structure determination of the nitridophosphate BaP_2N_4 ", *J. Solid State Chem.* **2005**, 178, 135-141.
- [7] S. D. Kloß, W. Schnick, "Rare-Earth-Metal Nitridophosphates through High-Pressure Metathesis", *Angew. Chem. Int. Ed.* **2015**, 54, 11250-11253; *Angew. Chem.* **2015**, 127, 11402-11405.
- [8] F. J. Pucher, S. R. Römer, F. W. Karau, W. Schnick, "Phenakite-Type BeP_2N_4 - A Possible Precursor for a New Hard Spinel-Type Material", *Chem. Eur. J.* **2010**, 16, 7208-7214.
- [9] S. Vogel, A. T. Buda, W. Schnick, "United in Nitride: The Highly Condensed Boron Phosphorus Nitride BP_3N_6 ", *Angew. Chem. Int. Ed.* **2018**, 57, 13202-13202; *Angew. Chem.* **2018**, 130, 13386-13389.
- [10] E.-M. Bertschler, C. Dietrich, T. Leichtweiß, J. Janek, W. Schnick, " Li^+ Ion Conductors with Adamantane-Type Nitridophosphate Anions β - $Li_{10}P_4N_{10}$ and $Li_{13}P_4N_{10}X_3$ with $X = Cl, Br$ ", *Chem. Eur. J.* **2018**, 24, 196-205.
- [11] A. Marchuk, S. Wendl, N. Imamovic, F. Tambornino, D. Wiechert, P. J. Schmidt, W. Schnick, "Nontypical Luminescence Properties and Structural Relation of $Ba_3P_3N_{10}X:Eu^{2+}$ ($X = Cl, I$): Nitridophosphate Halides with Zeolite-like Structure", *Chem. Mater.* **2015**, 27, 6432-6441.

- [12] F. J. Pucher, A. Marchuk, P. J. Schmidt, D. Wiechert, W. Schnick, "Luminescent Nitridophosphates $\text{CaP}_2\text{N}_4:\text{Eu}^{2+}$, $\text{SrP}_2\text{N}_4:\text{Eu}^{2+}$, $\text{BaP}_2\text{N}_4:\text{Eu}^{2+}$, and $\text{BaSr}_2\text{P}_6\text{N}_{12}:\text{Eu}^{2+}$ ", *Chem. Eur. J.* **2015**, *21*, 6443-6448.
- [13] A. Marchuk, W. Schnick, " $\text{Ba}_3\text{P}_5\text{N}_{10}\text{Br}:\text{Eu}^{2+}$: A Natural-White-Light Single Emitter with a Zeolite Structure Type", *Angew. Chem. Int. Ed.* **2015**, *54*, 2383-2387; *Angew. Chem.* **2015**, *127*, 2413-2417.
- [14] F. Golinski, H. Jacobs, "Synthesis and Crystal Structure of $\text{Rb}_8[\text{P}_4\text{N}_6(\text{NH})_4](\text{NH}_2)_2$ with the Adamantane-like Anion $[\text{P}_4\text{N}_6(\text{NH})_4]^{6-}$ ", *Z. Anorg. Allg. Chem.* **1995**, *621*, 29-33.
- [15] H. Jacobs, F. Golinski, "Synthesis and Crystal Structure of a Cesium-tetraimidophosphate-diamide, $\text{Cs}_5[\text{P}(\text{NH})_4](\text{NH}_2)_2 = \text{Cs}_3[\text{P}(\text{NH})_4] \cdot 2 \text{CsNH}_2$ ", *Z. Anorg. Allg. Chem.* **1994**, *620*, 531-534.
- [16] H. Jacobs, R. Nymwegen, "Synthesis and Crystal Structure of a Potassium Nitridophosphate, $\text{K}_3\text{P}_6\text{N}_{11}$ ", *Z. Anorg. Allg. Chem.* **1997**, *623*, 429-433.
- [17] H. Jacobs, R. Nymwegen, S. Doyle, T. Wroblewski, W. Kockelmann, "Crystalline Phosphorus(V) Nitride Imide, HPN_2 and DPN_2 , respectively, Structure Determination with X-Ray, Synchrotron, and Neutron Radiation", *Z. Anorg. Allg. Chem.* **1997**, *623*, 1467-1474.
- [18] H. Jacobs, S. Pollok, F. Golinski, "Synthesis and Crystal Structure of $\text{Na}_{10}[\text{P}_4(\text{NH})_6\text{N}_4](\text{NH}_2)_6(\text{NH}_3)_{0.5}$ with an Adamantane-like Anion $[\text{P}_4(\text{NH})_6\text{N}_4]^{4-}$ ", *Z. Anorg. Allg. Chem.* **1994**, *620*, 1213-1218.
- [19] W. Schnick, U. Berger, " $\text{Li}_{10}\text{P}_4\text{N}_{10}$ - A Lithium Phosphorus(V) Nitride with the Novel Complex Anion $\text{P}_4\text{N}_{10}^{10-}$ ", *Angew. Chem. Int. Ed. Engl.* **1991**, *30*, 830-831; *Angew. Chem.* **1991**, *103*, 857-858.
- [20] W. Schnick, J. Lücke, "On Lithium Phosphorus Nitride. Preparation and Refinement of the Crystal Structure of LiPN_2 ", *Z. Anorg. Allg. Chem.* **1990**, *588*, 19-25.
- [21] W. Schnick, J. Lücke, "Preparation, Crystal Structure, and IR-spectroscopic Investigation of Phosphorus Nitride Imide, HPN_2 ", *Z. Anorg. Allg. Chem.* **1992**, *610*, 121-126.
- [22] W. Schnick, J. Lücke, " $\text{Zn}_7[\text{P}_{12}\text{N}_{24}]\text{Cl}_2$ - A Sodalite with a Phosphorus Nitrogen Framework", *Angew. Chem. Int. Ed. Engl.* **1992**, *31*, 213-215; *Angew. Chem.* **1992**, *104*, 208-209.

- [23] W. Schnick, V. Schultz-Coulon, "*Ca₂PN₃: A New Phosphorus(V) Nitride with One-Dimensional Infinite Chains of Corner-Sharing PN₄ Tetrahedra*", *Angew. Chem. Int. Ed. Engl.* **1993**, 32, 280-281; *Angew. Chem.* **1993**, 105, 308-309.
- [24] M. Mallmann, C. Maak, R. Niklaus, W. Schnick, "*Ammonothermal Synthesis, Optical Properties, and DFT Calculations of Mg₂PN₃ and Zn₂PN₃*", *Chem. Eur. J.* **2018**, 24, 13963-13970.
- [25] M. Mallmann, S. Wendl, W. Schnick, "*Crystalline Nitridophosphates by Ammonothermal Synthesis*", *Chem. Eur. J.* **2020**, 26, 2067-2072.
- [26] M. Mallmann, S. Wendl, P. Strobel, P. J. Schmidt, W. Schnick, "*Sr₃P₃N₇: Complementary Approach by Ammonothermal and High-Pressure Syntheses*", *Chem. Eur. J.* **2020**, 26, 6257-6263.
- [27] S. Wendl, M. Mallmann, P. Strobel, P. J. Schmidt, W. Schnick, "*Ammonothermal Synthesis of Ba₂PO₃N – An Oxonitridophosphate with Non-Condensed PO₃N Tetrahedra*", *Eur. J. Inorg. Chem.* **2020**, 2020, 841-846.
- [28] S. Wendl, S. Mardazad, P. Strobel, P. J. Schmidt, W. Schnick, "*HIP to be Square: Simplifying Nitridophosphate Synthesis in a Hot Isostatic Press*", *Angew. Chem. Int. Ed.* **2020**, 59, 18240-18243; *Angew. Chem.* **2020**, 132, 18397-18400.
- [29] Crystal data of Sr₃P₅N₁₀X (orthorhombic, *Pnma* (no. 62)); X = Cl: *M* = 593.26 gmol⁻¹, *a* = 12.241(2), *b* = 12.953(3) and *c* = 13.427(3) Å, *V* = 2128.9(8) Å³, *Z* = 8, ρ = 3.702 gcm⁻³, μ = 15.980 mm⁻¹, Mo-K α (λ = 0.71073 Å, Bruker D8 Venture), *T* = 293 K, 33698 observed reflections, 3522 independent reflections, 116 parameters, *R*_{int} = 0.036, *R* _{σ} = 0.072, *R*₁ = 0.034, *wR*₂ = 0.069, *GoF* = 1.065, residual electron density 3.360, -1.277 eÅ⁻³; X = Br: *M* = 637.70 gmol⁻¹, orthorhombic, *Pnma* (no. 62), *a* = 12.2970(2), *b* = 12.9896(2) and *c* = 13.4585(2) Å, *V* = 2149.76(5) Å³, *Z* = 8, ρ = 3.942 gcm⁻³, μ = 30.520 mm⁻¹, Cu-K α 1 (λ = 1.5406 Å, Stoe StadiP), *T* = 293 K, 993 observed reflections, 101 parameters, *R*_p = 0.035, *R*_{wp} = 0.046, *R*_{exp} = 0.020, *R*_{Bragg} = 0.022, *GoF* = 2.257. Deposition numbers 2011982 (Cl) and 2012398 (Br) contain the supplementary crystallographic data for this paper. These data are provided free of charge by the joint Cambridge Crystallographic Data Centre and Fachinformationszentrum Karlsruhe Access Structures service www.ccdc.cam.ac.uk/structures.

- [30] C. Baerlocher, L. B. McCusker, *Database of Zeolites Structures*: <http://www.iza-structure.org/databases/>, accessed June 2020.
- [31] J. A. Armstrong, M. T. Weller, "Beryllsilicate Frameworks and Zeolites", *J. Am. Chem. Soc.* **2010**, *132*, 15679-15686.
- [32] W. H. Baur, "Effective Ionic Radii in Nitrides", *Crystallogr. Rev.* **1987**, *1*, 59-83.
- [33] R. Shannon, "Revised effective ionic radii and systematic studies of interatomic distances in halides and chalcogenides", *Acta Crystallogr. Sect. A* **1976**, *32*, 751-767.

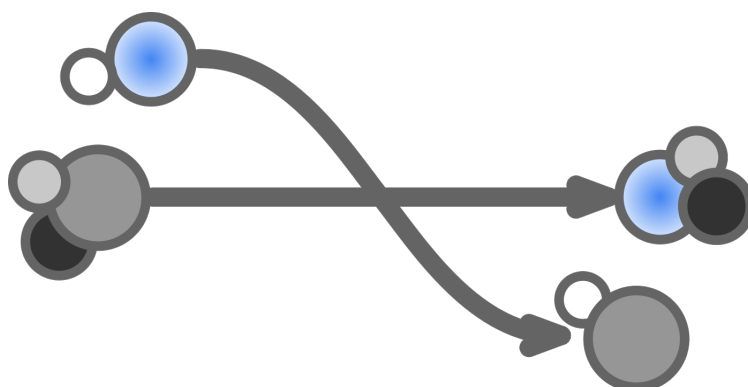
9 Post-Synthetic Modification: Systematic Study on a Simple Access to Nitridophosphates

Sebastian Wendl, Lisa Seidl, Patrick Schüler, Prof. Dr. Wolfgang Schnick

Angew. Chem. Int. Ed. **2020**, *59*, 23579–23582; *Angew. Chem.* **2020**, *132*, 23785–23788.

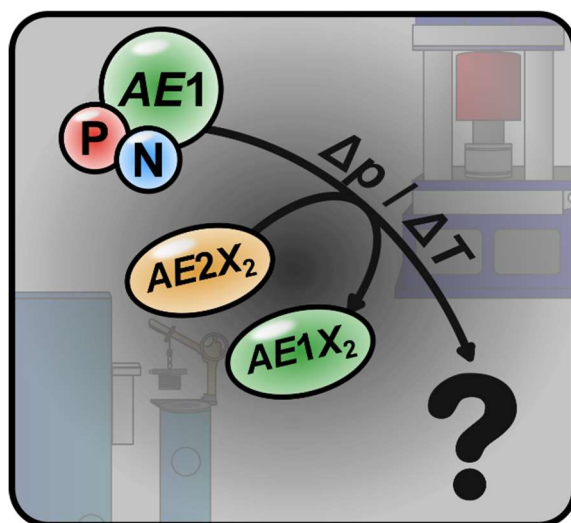
DOI: 10.1002/anie.202011835; 10.1002/ange.202011835.

Reprinted (adapted) with permission for non-commercial use from *Angewandte Chemie* (open access). Copyright 2021 John Wiley and Sons.



Reactions with Halides: *First systematic studies on a top-down strategy for nitridophosphate synthesis are presented. Therefore, pre-synthesized compounds were reacted with halides of lighter homologues under medium- or high-pressure conditions. A multifaceted reaction behavior was observed investigating chain-, layer-, and framework-type nitridophosphates.*

Abstract: Nitridophosphates are a well-studied class of nitrides with diverse materials properties, such as luminescence or ion conductivity. Despite the growing interest in this compound class, their synthesis mostly works through direct combination of starting materials. Herein, we present a systematic study on a promising method for post-synthetic modification by treating pre-synthesized nitridophosphates with halides under elevated pressures and temperatures. Herein, we



focus on the applicability of this approach to P/N compounds with different degrees of condensation. Accordingly, BaP_2N_4 , $\text{Ba}_3\text{P}_5\text{N}_{10}\text{Br}$, $\text{SrH}_4\text{P}_6\text{N}_{12}$, $\text{CaP}_8\text{N}_{14}$, and Ca_2PN_3 are investigated as model compounds for framework-, layer-, and chain-type nitridophosphates. The formation of structurally related, as well as, completely unrelated compounds, compared to the starting materials, shows the great potential of the approach, which increases the synthetic possibilities for nitridophosphates significantly.

9.1 Introduction with Results and Discussions

Over the last years, the research on (oxo/imido)nitridophosphates gained attention due to their structural, optical, and physical properties and the development of new technologies and synthesis strategies.^[1,2] Nitridophosphates per se can be compared with the oxosilicate class of compounds, as they form tetrahedra-based structures as well. Already initially used ambient and medium-pressure (MP) methods ((pressure-)ampoules, autoclaves) have enabled the preparation of various (oxo/imido)nitridophosphates, phosphorus nitrides, and related compounds.^[1,3-10] The variety of nitridophosphates, which are accessible under MP conditions, has recently been increased by hot isostatic pressing and systematic investigations using high-temperature ammonothermal methods.^[2,11-14] Despite these advances in MP synthesis, high-pressure high-temperature (HP/HT) conditions are still most commonly used for nitridophosphate synthesis.^[1] As recently reviewed, several synthetic routes have been established within this technique, realizing a great diversity of incorporated electropositive elements in anionic P/N tetrahedra substructures.^[1,15-19]

Nevertheless, the above mentioned methods and routes are mostly limited to reactions that reassemble starting materials on a fundamental (i.e. atomic) level by bond cleavage and reformation of anionic network structures with embedded counter ions. Even though these approaches have made nitridophosphates one of the most diverse nitride classes, only a restricted synthesis planning and control is possible. While the degree of condensation (i.e. atomic ratio of P/N) of the desired products might be influenced by varying the composition of starting materials, precise structural details can hardly be predicted or even targeted. In order to increase the influence on structural motifs of products, the development of innovative synthesis strategies is essential. Therefore, especially post-synthetic modification appears as a powerful tool, as already pre-arranged nitridophosphates are typically employed. Such topotactic ion-exchange reactions on nitridophosphates have so far only been reported for the synthesis of sodalite-like $\text{Zn}_7[\text{P}_{12}\text{N}_{24}]\text{Cl}_2$ by deprotonating $\text{Zn}_5\text{H}_4[\text{P}_{12}\text{N}_{24}]\text{Cl}_2$ with ZnCl_2 .^[6,20] Moreover, post-synthetic modification by ion exchange has generally been investigated very sparsely on nitride substance classes, although the huge potential of this approach has been demonstrated for related nitridosilicates.^[21-24]

In this contribution we present the first systematic study on the post-synthetic modification of nitridophosphates by ion exchange reactions. But, as preliminary tests have shown, that an analogous approach as used for (nitrido-)silicates cannot be easily transferred to nitridophosphates (Figure H1–H3), we combine ion exchange reactions/salt metathesis with HP/HT and MP methods within this work. In particular, we investigate the reaction of pre-synthesized alkaline earth nitridophosphates, which represent framework- (BaP_2N_4 and $\text{Ba}_3\text{P}_5\text{N}_{10}\text{Br}$), layer- ($\text{SrH}_4\text{P}_6\text{N}_{12}$ and $\text{CaP}_8\text{N}_{14}$), and chain-type (Ca_2PN_3) structures, with halides of the lighter alkaline earth homologues.^[10, 16, 25–28] During these reactions the more negative formation enthalpies of stable byproducts should generate the necessary driving force (e.g. $\Delta H^0(\text{CaCl}_2) < \Delta H^0(\text{MgCl}_2)$).^[29] Moreover, in accordance to Coulomb's law, smaller cations show stronger interactions with anionic nitridophosphate structures, powering the exchange reactions, as well. In order to ensure complete substitution of the initial cations, a 1.5 equivalent excess of the halide was used. Surplus and in situ formed halides were removed after reaction by washing with de-ionized water, given that products are not sensitive to hydrolysis.

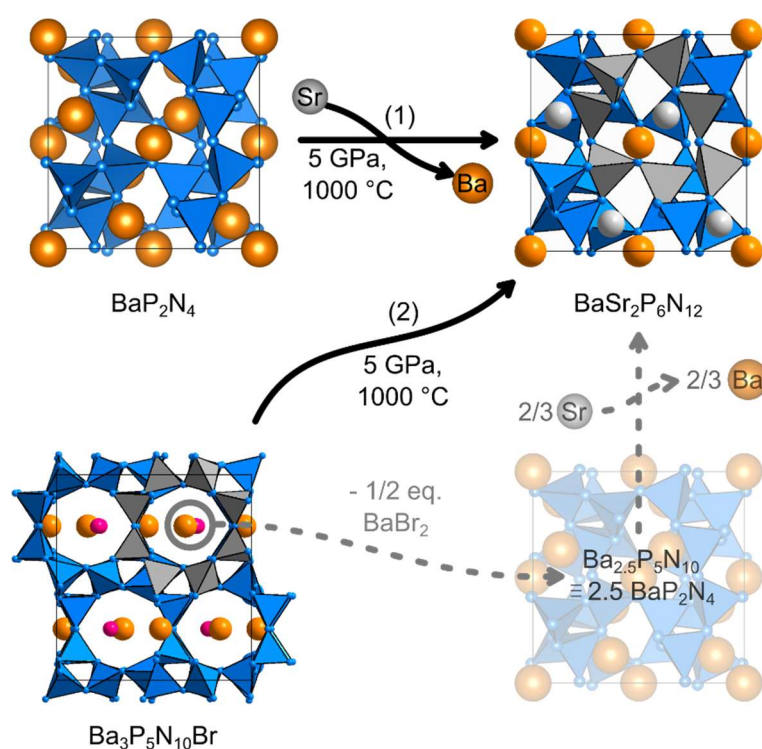


Figure 9.1. Behavior of BaP_2N_4 and $\text{Ba}_3\text{P}_5\text{N}_{10}\text{Br}$ reacting with SrCl_2 (route 1) and SrBr_2 (route 2), respectively. $\text{BaSr}_2\text{P}_6\text{N}_{12}$ is yielded as product for both reactions. Therefore, BaP_2N_4 may be considered as an intermediate during reaction of $\text{Ba}_3\text{P}_5\text{N}_{10}\text{Br}$. Selected *achter* and *siebener* rings in gray, in order to illustrate the structural collapse.^[31] Ba in orange, Br in magenta, Sr in gray, PN_4 tetrahedra in blue/gray.

Structure analyses were performed by Rietveld refinements and chemical compositions of the reaction products were investigated by energy dispersive X-ray spectroscopy (EDX, Table H3). Detailed information on the analyses is provided in the Supporting Information.

First experiments were carried out on BaP_2N_4 , as it can be classified as a highly condensed framework like the $\text{AE}_2\text{Si}_5\text{N}_8$ structure, for which the ion exchange reaction has been established.^[21-24] Using the multianvil technique (5 GPa, 1000 °C) and aiming for BaP_2N_4 -type β - SrP_2N_4 , a partial replacement of 2/3 of the Ba atoms could be achieved by reaction with SrCl_2 , yielding homeotypic, literature-known $\text{BaSr}_2\text{P}_6\text{N}_{12}$ [Eq. 9.1, Figures 9.1 and H5, Table H4].^[30]



Changing the excess of halides (up to 3 equivalents) or reaction times (10 to 180 min) did not lead to any other observations.

Further the introduced synthesis strategy was conducted on the zeolite-like framework-type nitridophosphate $\text{Ba}_3\text{P}_5\text{N}_{10}\text{Br}$, which was reacted with SrBr_2 , targeting $\text{Sr}_3\text{P}_5\text{N}_{10}\text{Br}$ [Eq. 9.2].



Desired $\text{Sr}_3\text{P}_5\text{N}_{10}\text{Br}$ was not formed during reaction, but $\text{BaSr}_2\text{P}_6\text{N}_{12}$ was yielded as a reaction product (Figures 9.1 and H6, Table H5). Thus, the partial substitution of Ba with Sr leads to a structural collapse of the zeolite-like framework yielding a denser packed structure with smaller tetrahedra rings (*achter* rings in $\text{Ba}_3\text{P}_5\text{N}_{10}\text{Br}$, *siebener* rings in $\text{BaSr}_2\text{P}_6\text{N}_{12}$) and cages. Consequently, the mechanism of this reaction cannot be interpreted as a formal ion exchange. Rather, metathesis reactions can be assumed under the applied conditions, underlining the great potential of this method, as the introduction of smaller cations into rigid networks requires the reconstructive rearrangement of P–N bonds and may therefore lead to new structures, as well.

Since both, BaP_2N_4 and $\text{Ba}_3\text{P}_5\text{N}_{10}\text{Br}$ transform into $\text{BaSr}_2\text{P}_6\text{N}_{12}$ upon the reaction with $\text{SrCl}_2/\text{SrBr}_2$, one may consider the formation of BaP_2N_4 as an intermediate step during the ion exchange reaction of $\text{Ba}_3\text{P}_5\text{N}_{10}\text{Br}$ [Eq. 9.3 and 9.4].



The potential of post-synthetic modification is further emphasized by its applicability to layered nitridophosphates. For this purpose, $\text{SrH}_4\text{P}_6\text{N}_{12}$ was reacted with CaCl_2 under HP/HT conditions [5 GPa, 1000 °C, Eq. 9.5].



The obtained $\text{CaH}_4\text{P}_6\text{N}_{12}$ shows slight structural changes compared to used $\text{SrH}_4\text{P}_6\text{N}_{12}$ (Figures 9.2 and H7, Table H6). First, the exchange of Sr with Ca induces a change of the *AE* coordination sphere (SrN_6 prism in $\text{SrH}_4\text{P}_6\text{N}_{12}$, CaN_6 octahedra in $\text{CaH}_4\text{P}_6\text{N}_{12}$). Second, an additional rearrangement of the PN_4 tetrahedra within the layers is observed. Despite these changes, layered nitridophosphates seem basically appropriate for a post-synthetic incorporation of smaller ions, which could to a certain extent be expected given numerous ion exchange experiments on related phyllosilicates and other lamellar clay minerals.^[32–34] This might be due to a great tolerance to the ionic radii of counter ions. While the covalent P–N bonds in the tetrahedra layers are rigid, the more ionic *AE*-N contacts are less directional and therefore more flexible. Thus, smaller ionic radii may be countered by decreasing the distances between layers, or a rotation/horizontal shift of the layers, as observed for $\text{CaH}_4\text{P}_6\text{N}_{12}$. Similar translation effects have already been described for silicates, as well.^[35] Corresponding investigations on 2D structure types had not been performed on any related nitride compound classes, as yet.

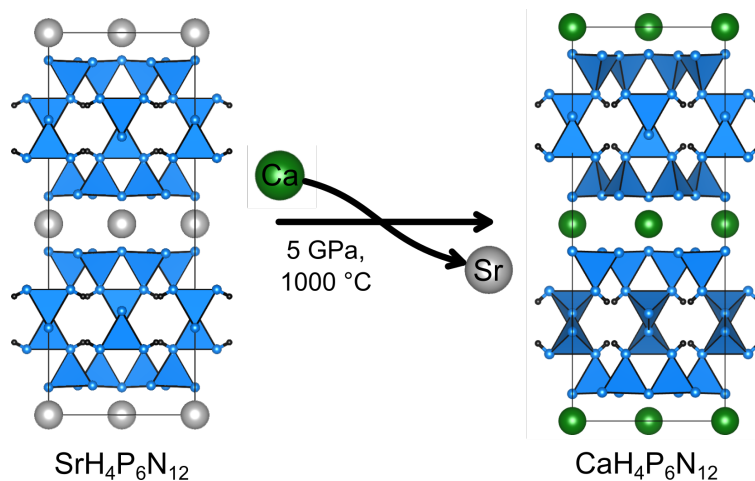


Figure 9.2. Illustration of the reaction of $\text{SrH}_4\text{P}_6\text{N}_{12}$ with CaCl_2 , yielding $\text{CaH}_4\text{P}_6\text{N}_{12}$. Sr in gray, Ca in green, H in black, PN_4 tetrahedra in blue.

A second layered nitridophosphate, namely $\text{CaP}_8\text{N}_{14}$, which is structurally related to $\text{CaH}_4\text{P}_6\text{N}_{12}$, was reacted with MgCl_2 at HP/HT conditions of 5 GPa, 1000 °C resulting in $\text{MgP}_8\text{N}_{14}$ [Eq. 9.6, Figure 9.3].

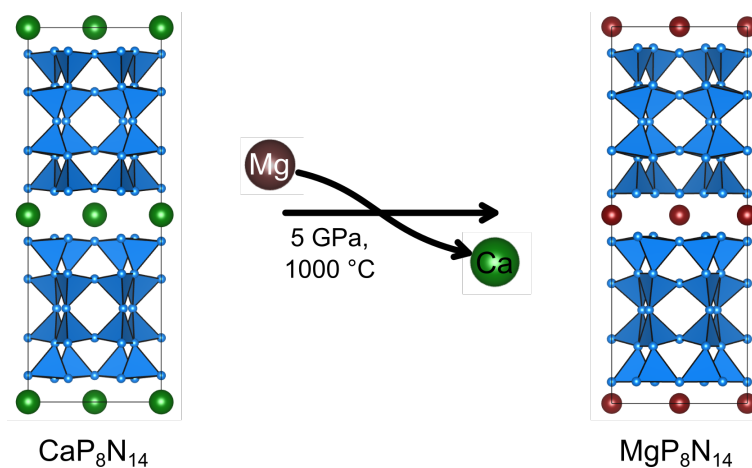


Figure 9.3. Observed reaction for $\text{CaP}_8\text{N}_{14}$ with MgCl_2 . Ca in green, Mg in brown, PN_4 tetrahedra in blue.

The obtained $\text{MgP}_8\text{N}_{14}$ has previously not been accessible by conventional synthesis and its structure was now elucidated from powder diffraction data, with a detailed discussion provided in the Supporting Information (Figures H8 and H9, Table H7).^[36]

The closely similar structures of $\text{AEP}_8\text{N}_{14}$ ($\text{AE} = \text{Mg}, \text{Ca}$) indicate a topotactic reaction, which might be realized through the highly-condensed quadruple layers of $\text{CaP}_8\text{N}_{14}$ with ($\kappa = 0.57$). Thus, the PN_4 tetrahedra layers are assumed to be rather rigid, while Ca^{2+} ions in between remain mobile and easily accessible.

However, even for this reaction not all aspects suggest an ion-exchange mechanism, according to the common principle. For instance, when comparing the powder X-ray diffraction data of the starting material and the product, it is noticeable that an amorphous portion of the product decreases significantly (Figure H10). Such recrystallization effects indicate increased crystal growth during reaction, which might require reconstructive cleavage and reformation of P–N bonds, as well.

The results described so far suggest that lower dimensional networks are suitable for post-synthetic modification. Therefore, lowly condensed Ca_2PN_3 was examined as a model compound for nitridophosphates with one-dimensional chain structures (Figures 9.4). In a hot isostatic press, Ca_2PN_3 was reacted at 150 MPa and 1000 °C with MgCl_2 , following Equation 9.7, resulting in the formation of Mg_2PN_3 and CaCl_2 with MgO as a minor side phase (Figure H11, Table H8).

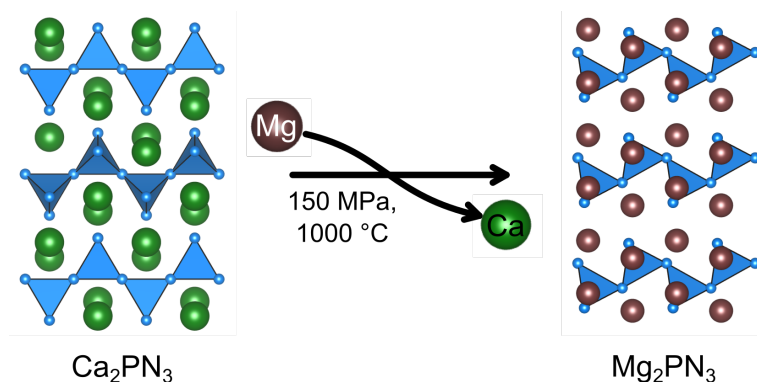


Figure 9.4. Schematic reaction for Ca_2PN_3 with MgCl_2 . Ca in green, Mg in brown, PN_4 tetrahedra in blue.

In contrast to $\text{CaP}_8\text{N}_{14}$, the exchange of Ca by Mg causes structural changes for AE_2PN_3 ($\text{AE} = \text{Mg}, \text{Ca}$). While the *zweier* single chains are stretched for Ca, they are distorted for Mg_2PN_3 in order to counter the smaller ionic radius. This leads to a change from pentagonal bipyramidal (Ca^{2+}) to tetrahedral coordination (Mg^{2+}) of the *AE* ion.

Inspired by the ion exchange on nitridosilicates we have tried to transfer the applied principle to nitridophosphates using MP and HP/HT techniques. Thereby, we found a versatile reaction behavior for nitridophosphates. Apart from homeotypic compounds ($\text{BaSr}_2\text{P}_6\text{N}_{12}$, $\text{MgP}_8\text{N}_{14}$), related structures ($\text{CaH}_4\text{P}_6\text{N}_{12}$, Mg_2PN_3) and even completely different structure types ($\text{BaSr}_2\text{P}_6\text{N}_{12}$ starting from $\text{Ba}_3\text{P}_5\text{N}_{10}\text{Br}$) can be obtained by the reaction of pre-synthesized nitridophosphates with halides.

Considering possible driving forces of the presented approach, the targeted formation of the more stable halides and Coulomb's law certainly have a major influence. Similar explanations are given for metathesis reactions or a corresponding ion exchange in nitridosilicates.^[21–24, 37] Furthermore, a possible reduction in volume can be considered as driving force, as MP and HP/HT conditions were applied. However, more precise conclusions about this assumption cannot be drawn, since structural information on all starting materials and products under the experimental reaction conditions would be necessary.

In summary, the reaction behavior of pre-synthesized nitridophosphates, that represent framework-, layer-, and chain-type structures and cover the degree of condensation from $\kappa = 1/3$ to $4/7$, was investigated in presence of alkaline earth halides by means of ion exchange under elevated pressures. Within the presented substantial overview a diverse reaction behavior of the starting materials was observed, demonstrating the enormous potential and the broad applicability of this alternative approach. Even if only the three-dimensional structure of $\text{Ba}_3\text{P}_5\text{N}_{10}\text{Br}$ has completely collapsed, some of the lower dimensional nitridophosphates show structural changes, as well. Thus, both the simple synthesis of unprecedented isotopic compounds, as well as the synthesis of completely new structure types may be enabled in the future. Therefore, our work can be seen as a far-reaching proof-of-principle that pre-synthesized nitridophosphates can be reacted with halides. However, no trends regarding reaction mechanisms or the accessibility of different structure types can be deduced in the context of this work. At this point, in situ investigations at elevated pressures are essential for a better understanding of these reactions and should be subject to future

investigations, as well as the investigation of the reaction behavior of further nitridophosphates towards halides.

Furthermore, the experiments will be expanded to other metal halides, in order to increase the variety of cations (transition, rare-earth, noble metals) in nitridophosphates. Consequently, this post-synthetic strategy could therefore present a breakthrough in the search for a universal access to nitridophosphates with embedded cations of various types.

9.2 Acknowledgements

We gratefully thank the Deutsche Forschungsgemeinschaft (DFG, project SCHN 377/18-1) as well as the Fonds der Chemischen Industrie (FCI) for financial support. Furthermore, we thank Christian Minke and Lisa Gamperl (both at Department of Chemistry of LMU Munich) for carrying out EDX measurements. Open access funding enabled and organized by Projekt DEAL.

9.3 References

- [1] S. D. Kloß, W. Schnick, "Nitridophosphates – A Success Story of Nitride Synthesis", *Angew. Chem. Int. Ed.* **2019**, 58, 7933-7944; *Angew. Chem.* **2019**, 131, 8015-8027.
- [2] M. Mallmann, S. Wendl, W. Schnick, "Crystalline Nitridophosphates by Ammonothermal Synthesis", *Chem. Eur. J.* **2020**, 26, 2067-2072.
- [3] W. Schnick, J. Lücke, "On Lithium Phosphorus Nitride. Preparation and Refinement of the Crystal Structure of LiPN_2 ", *Z. Anorg. Allg. Chem.* **1990**, 588, 19-25.
- [4] W. Schnick, U. Berger, " $\text{Li}_{10}\text{P}_4\text{N}_{10}$ - A Lithium Phosphorus(V) Nitride with the Novel Complex Anion $\text{P}_4\text{N}_{10}^{10-}$ ", *Angew. Chem. Int. Ed. Engl.* **1991**, 30, 830-831; *Angew. Chem.* **1991**, 103, 857-858.
- [5] W. Schnick, J. Lücke, "Preparation, Crystal Structure, and IR-spectroscopic Investigation of Phosphorus Nitride Imide, HPN_2 ", *Z. Anorg. Allg. Chem.* **1992**, 610, 121-126.
- [6] W. Schnick, J. Lücke, " $\text{Zn}_7[\text{P}_{12}\text{N}_{24}]\text{Cl}_2$ - A Sodalite with a Phosphorus Nitrogen Framework", *Angew. Chem. Int. Ed. Engl.* **1992**, 31, 213-215; *Angew. Chem.* **1992**, 104, 208-209.
- [7] H. Jacobs, R. Nymwegen, "Synthesis and Crystal Structure of a Potassium Nitridophosphate, $\text{K}_3\text{P}_6\text{N}_{11}$ ", *Z. Anorg. Allg. Chem.* **1997**, 623, 429-433.
- [8] H. Jacobs, S. Pollok, F. Golinski, "Synthesis and Crystal Structure of $\text{Na}_{10}[\text{P}_4(\text{NH})_6\text{N}_4](\text{NH}_2)_6(\text{NH}_3)_{0.5}$ with an Adamantane-like Anion $[\text{P}_4(\text{NH})_6\text{N}_4]^{4-}$ ", *Z. Anorg. Allg. Chem.* **1994**, 620, 1213-1218.
- [9] F. Golinski, H. Jacobs, "Synthesis and Crystal Structure of $\text{Rb}_8[\text{P}_4\text{N}_6(\text{NH})_4](\text{NH}_2)_2$ with the Adamantane-like Anion $[\text{P}_4\text{N}_6(\text{NH})_4]^{6-}$ ", *Z. Anorg. Allg. Chem.* **1995**, 621, 29-33.
- [10] V. Schultz-Coulon, W. Schnick, " Mg_2PN_3 and Ca_2PN_3 – Phosphorus(V) Nitrides with Infinite Chains of Corner Sharing PN_4 Tetrahedra", *Z. Anorg. Allg. Chem.* **1997**, 623, 69-74.
- [11] M. Mallmann, C. Maak, R. Niklaus, W. Schnick, "Ammonothermal Synthesis, Optical Properties, and DFT Calculations of Mg_2PN_3 and Zn_2PN_3 ", *Chem. Eur. J.* **2018**, 24, 13963-13970.
- [12] M. Mallmann, S. Wendl, P. Strobel, P. J. Schmidt, W. Schnick, " $\text{Sr}_3\text{P}_3\text{N}_7$: Complementary Approach by Ammonothermal and High-Pressure Syntheses", *Chem. Eur. J.* **2020**, 26, 6257-6263.
- [13] S. Wendl, M. Mallmann, P. Strobel, P. J. Schmidt, W. Schnick, "Ammonothermal Synthesis of $\text{Ba}_2\text{PO}_3\text{N}$ – An Oxonitridophosphate with Non-Condensed PO_3N Tetrahedra", *Eur. J. Inorg. Chem.* **2020**, 2020, 841-846.

- [14] S. Wendl, S. Mardazad, P. Strobel, P. J. Schmidt, W. Schnick, "HIP to be Square: Simplifying Nitridophosphate Synthesis in a Hot Isostatic Press", *Angew. Chem. Int. Ed.* **2020**, *59*, 18240-18243; *Angew. Chem.* **2020**, *132*, 18397-18400.
- [15] E.-M. Bertschler, R. Niklaus, W. Schnick, " $Li_{12}P_3N_9$ with Non-Condensed $[P_3N_9]^{12-}$ -Rings and its High-Pressure Polymorph Li_4PN_3 with Infinite Chains of PN_4^- Tetrahedra", *Chem. Eur. J.* **2017**, *23*, 9592-9599.
- [16] F. W. Karau, W. Schnick, "High-pressure synthesis and X-ray powder structure determination of the nitridophosphate BaP_2N_4 ", *J. Solid State Chem.* **2005**, *178*, 135-141.
- [17] S. D. Kloß, O. Janka, T. Block, R. Pöttgen, R. Glaum, W. Schnick, "Open-Shell 3d Transition Metal Nitridophosphates $M^II P_8 N_{14}$ ($M^II = Fe, Co, Ni$) by High-Pressure Metathesis", *Angew. Chem. Int. Ed.* **2019**, *58*, 4685-4689; *Angew. Chem.* **2019**, *131*, 4733-4737.
- [18] S. Vogel, A. T. Buda, W. Schnick, "United in Nitride: The Highly Condensed Boron Phosphorus Nitride BP_3N_6 ", *Angew. Chem. Int. Ed.* **2018**, *57*, 13202-13202; *Angew. Chem.* **2018**, *130*, 13386-13389.
- [19] S. D. Kloß, W. Schnick, "Rare-Earth-Metal Nitridophosphates through High-Pressure Metathesis", *Angew. Chem. Int. Ed.* **2015**, *54*, 11250-11253; *Angew. Chem.* **2015**, *127*, 11402-11405.
- [20] W. Schnick, J. Lücke, "Nitrido-Sodalithe. I Synthesis, Crystal Structure, and Properties of $Zn_{7-x}H_{2x}[P_{12}N_{24}]Cl$, with $0 \leq x \leq 3$ ", *Z. Anorg. Allg. Chem.* **1994**, *620*, 2014-2019.
- [21] P. Bielec, W. Schnick, "Increased Synthetic Control - Gaining Access to Predicted $Mg_2Si_5N_8$ and β - $Ca_2Si_5N_8$ ", *Angew. Chem. Int. Ed.* **2017**, *56*, 4810-4813; *Angew. Chem.* **2017**, *129*, 4888-4891.
- [22] P. Bielec, O. Janka, T. Block, R. Pöttgen, W. Schnick, " $Fe_2Si_5N_8$: Access to Open-Shell Transition-Metal Nitridosilicates", *Angew. Chem. Int. Ed.* **2018**, *57*, 2409-2412; *Angew. Chem.* **2018**, *130*, 2433-2436.
- [23] P. Bielec, L. Eisenburger, H. L. Deubner, D. Günther, F. Kraus, O. Oeckler, W. Schnick, "Targeting Vacancies in Nitridosilicates: Aliovalent Substitution of M^{2+} ($M = Ca, Sr$) by Sc^{3+} and U^{3+} ", *Angew. Chem. Int. Ed.* **2019**, *58*, 840-843; *Angew. Chem.* **2019**, *131*, 850-853.
- [24] P. Bielec, R. Nelson, R. P. Stoffel, L. Eisenburger, D. Günther, A.-K. Henß, J. P. Wright, O. Oeckler, R. Dronskowski, W. Schnick, "Cationic Pb_2 Dumbbells Stabilized in the Highly Covalent Lead Nitridosilicate $Pb_2Si_5N_8$ ", *Angew. Chem. Int. Ed.* **2019**, *58*, 1432-1436; *Angew. Chem.* **2019**, *131*, 1446-1450.
- [25] W. Schnick, V. Schultz-Coulon, " Ca_2PN_3 : A New Phosphorus(V) Nitride with One-Dimensional Infinite Chains of Corner-Sharing PN_4 Tetrahedra", *Angew. Chem. Int. Ed. Engl.* **1993**, *32*, 280-281; *Angew. Chem.* **1993**, *105*, 308-309.

- [26] A. Marchuk, W. Schnick, "*Ba₃P₃N₁₀Br:Eu²⁺: A Natural-White-Light Single Emitter with a Zeolite Structure Type*", *Angew. Chem. Int. Ed.* **2015**, *54*, 2383-2387; *Angew. Chem.* **2015**, *127*, 2413-2417.
- [27] S. Wendl, L. Eisenburger, P. Strobel, D. Günther, J. P. Wright, P. J. Schmidt, O. Oeckler, W. Schnick, "*Nitridophosphate-Based Ultra-Narrow-Band Blue-Emitters: Luminescence Properties of AEP₈N₁₄:Eu²⁺ (AE = Ca, Sr, Ba)*", *Chem. Eur. J.* **2020**, *26*, 7292-7298.
- [28] S. Wendl, W. Schnick, "*SrH₄P₆N₁₂ and SrP₈N₁₄: Insights into the Condensation Mechanism of Nitridophosphates under High Pressure*", *Chem. Eur. J.* **2018**, *24*, 15889-15896.
- [29] A. F. Holleman, N. Wiberg, E. Wiberg, "*Anorganische Chemie I. Band: Grundlagen und Hauptgruppenelemente*", De Gruyter, Berlin, Boston **2017**.
- [30] F. Karau, W. Schnick, "*High-Pressure Synthesis of BaSr₂P₆N₁₂ and BaCa₂P₆N₁₂ and Comparison of the Structures of BaP₂N₄, BaCa₂P₆N₁₂ and BaSr₂P₆N₁₂*", *Z. Anorg. Allg. Chem.* **2006**, *632*, 231-237.
- [31] F. Liebau, "*Structural Chemistry of Silicates*", Springer, Berlin **1985**.
- [32] A. Weiss, "*Über das Kationenaustauschvermögen der Tonminerale. II. Der Kationenaustausch bei den Mineralen der Glimmer-, Vermikulit- und Montmorillonitgruppe*", *Z. Anorg. Allg. Chem.* **1958**, *297*, 257-286.
- [33] A. Weiss, "*Über das Kationenaustauschvermögen der Tonminerale. III. Der Kationenaustausch bei Kaolinit*", *Z. Anorg. Allg. Chem.* **1959**, *299*, 92-120.
- [34] G. Lagaly, K. Beneke, "*Intercalation and exchange reactions of clay minerals and non-clay layer compounds*", *Colloid. Polym. Sci.* **1991**, *269*, 1198-1211.
- [35] M. M. Herling, J. Breu, "*The Largely Unknown Class of Microporous Hybrid Materials: Clays Pillared by Molecules*", *Z. Anorg. Allg. Chem.* **2014**, *640*, 547-560.
- [36] Crystal data of MgP₈N₁₄ from powder X-ray diffraction and Rietveld refinement: $M = 468.19 \text{ gmol}^{-1}$, orthorhombic, $Cmc2_1$ (no. 36), $a = 8.3646(1)$, $b = 5.0215(1)$ and $c = 23.1963(3) \text{ \AA}$, $V = 974.3(1) \text{ \AA}^3$, $Z = 4$, $\rho = 3.192 \text{ gcm}^{-3}$, $\mu = 14.376 \text{ mm}^{-1}$, Cu-K $_{\alpha 1}$ ($\lambda = 1.5406 \text{ \AA}$, Stoe StadiP), $T = 293 \text{ K}$, 993 observed reflections, 109 parameters, $R_p = 0.035$, $R_{wp} = 0.048$, $R_{exp} = 0.025$, $R_{Bragg} = 0.015$, $GoF = 1.936$. Deposition number 2022941 contains the supplementary crystallographic data for this paper. These data are provided free of charge by the joint Cambridge Crystallographic Data Centre and Fachinformationszentrum Karlsruhe Access Structures service www.ccdc.cam.ac.uk/structures.
- [37] S. D. Kloß, N. Weidmann, R. Niklaus, W. Schnick, "*High-Pressure Synthesis of Melilite-type Rare-Earth Nitridophosphates RE₂P₃N₇ and a Ba₂Cu[Si₂O₇]-type Polymorph*", *Inorg. Chem.* **2016**, *55*, 9400-9409.

10 Summary

The main research objective of this thesis was the fundamental investigation of alkaline earth metal nitridophosphates in terms of their importance as luminescent materials and the development of appropriate application-oriented synthesis strategies. Prior to this work, the multianvil technique has been established as the standard method for nitridophosphate synthesis and only very few P/N-based phosphor materials were reported in literature. This thesis, however, proves nitridophosphates as intriguing and promising host lattices for luminescent materials. The presented results reach from conventional high-pressure high-temperature synthesis and characterization of nitridophosphate-based phosphors to a step-wise simplification of their synthesis and can be divided into three major parts.

The first part of this thesis deals with the high-pressure high-temperature syntheses of novel luminescent (imido)nitridophosphates and is covered by Chapter 2 and 3. Using the conventional multianvil technique, $\text{BaP}_6\text{N}_{10}\text{NH}$ and $\text{AEP}_8\text{N}_{14}$ ($\text{AE} = \text{Ca}, \text{Sr}, \text{Ba}$) are obtained by reaction of alkaline earth metal azides and P_3N_5 . Additional NH_4Cl is used as a hydrogen source for the synthesis of $\text{BaP}_6\text{N}_{10}\text{NH}$. Upon excitation with UV to blue light all Eu^{2+} -doped products show blue emission, with $\text{CaP}_8\text{N}_{14}:\text{Eu}^{2+}$ and $\text{SrP}_8\text{N}_{14}:\text{Eu}^{2+}$ being classified as the first nitridophosphate-based ultra-narrow-band blue-emitters.

Within the second part, covered by Chapters 4, 5, and 6, the ammonothermal method is established as a potent access to (oxo)nitridophosphates in the medium-pressure range. Up to now, only little attention was paid to such autoclave techniques in the context of nitridophosphate syntheses. Herein, the first systematic studies are carried out granting access to a great diversity of nitridophosphates with representatives for group-, chain-, layer-, and framework-type structures. The introduction of red phosphorus as a readily available starting material further simplifies the synthesis of both known and novel P/N compounds. For instance, $\text{Ba}_2\text{PO}_3\text{N}$ and $\text{Sr}_3\text{P}_3\text{N}_7$ are prepared accordingly. Overall, the target compounds span a degree of condensation from 1/4 to 4/7 demonstrating the broad applicability of this approach. Additionally, Eu^{2+} -doped samples of $\text{Ba}_2\text{PO}_3\text{N}$ and $\text{Sr}_3\text{P}_3\text{N}_7$ show green and deep-red to infrared emission, respectively, and prove the availability of phosphor materials at medium-pressure conditions starting from P_{red} .

The third part of the thesis is concerned with hitherto unprecedented synthesis strategies, introducing two separate approaches. The first application-oriented attempt takes up the advantages of ammonothermal synthesis (i.e. medium-pressure conditions and P_{red} as a starting material) and aims to overcome remaining obstacles like scaling issues and the usage of supercritical ammonia. Therefore, hot isostatic presses are employed as powerful devices for an innovative and easy access to P/N chemistry. This approach enables synthesis temperatures far beyond the decomposition point of nitridophosphates and phosphorus nitrides that are practically feasible under medium-pressure conditions, for the first time. Chapter 7 elaborates the benefits and the simplicity of the implemented approach by preparing large-volume samples of the model compound Ca_2PN_3 starting from P_{red} and using significantly reduced reaction times compared to literature known ampoule synthesis. In Chapter 8 the syntheses of zeolite-like $\text{AE}_3\text{P}_5\text{N}_{10}\text{X}$ ($\text{AE} = \text{Sr}, \text{Br}; \text{X} = \text{Cl}, \text{Br}$) demonstrate that the presented access is also applicable to highly-condensed functional nitridophosphates. Here, the synthesis of the respective strontium compounds is particularly remarkable, as they are only accessible under medium pressure. The importance of this technique for potential phosphors is underlined by luminescence investigations on Eu^{2+} -doped samples of the title compounds. An alternative access to nitridophosphates with a more basic character is developed in Chapter 9. Here, pre-synthesized alkaline earth nitridophosphates are reacted in terms of post-synthetic modification with halides of lighter homologues. This reaction principle is applied to compounds with different degrees of condensation representing chain-, layer-, and framework-type structures. The observed various reaction behavior of the starting materials towards used halides serves as a highly potential proof-of-concept.

More details on the publications of this cumulative dissertation are provided below within the summaries of the individual Chapters

- 10.1 BaP₆N₁₀NH:Eu²⁺ as a Case Study – An Imidonitridophosphate Showing Luminescence,
- 10.2 Nitridophosphate-Based Ultra-Narrow-Band Blue-Emitters: Luminescence Properties of AEP₈N₁₄:Eu²⁺ (AE = Ca, Sr, Ba),
- 10.3 Crystalline Nitridophosphates by Ammonothermal Synthesis,
- 10.4 Ammonothermal Synthesis of Ba₂PO₃N – An Oxonitridophosphate with Non-Condensed PO₃N Tetrahedra,
- 10.5 Sr₃P₃N₇: Complementary Approach of Ammonothermal and High-Pressure Methods,
- 10.6 HIP to be Square: Simplifying Nitridophosphate Synthesis in a Hot Isostatic Press,
- 10.7 Synthesis of Nitride Zeolites in a Hot Isostatic Press, and
- 10.8 Post-Synthetic Modification: Systematic Study on a Simple Access to Nitridophosphates

10.1 BaP₆N₁₀NH:Eu²⁺ as a Case Study – An Imidonitridophosphate Showing Luminescence

Published in: **S. Wendl**, L. Eisenburger, M. Zipkat, D. Günther, J. P. Wright, P. J. Schmidt, O. Oeckler, and W. Schnick

Chem. Eur. J. **2020**, 26, 5010–5016.

Access via: DOI: 10.1002/chem.201905082

Reprinted at: Chapter 2, Supporting Information in Chapter A

The preparation and structure elucidation of the imidonitridophosphate BaP₆N₁₀NH is reported. Employing high-pressure high-temperature conditions (5 GPa, 1000 °C), the title compound was synthesized starting from Ba(N₃)₂, P₃N₅, and NH₄Cl. Due to the microcrystalline and heterogeneous character of the initially obtained sample, a synergy of transmission electron microscopy and single-crystal diffraction with microfocused synchrotron radiation was used for structure elucidation (*P*₆3 (no. 173), *a* = 7.5633(11), *c* = 8.512(2) Å, *Z* = 2). EDX, CHNS, FTIR and solid-state MAS NMR measurements (¹H, ³¹P, and ³¹P{¹H}) confirm the assumed sum formula and the presence of NH functionalities. The highly condensed structure of BaP₆N₁₀NH (*κ* ≈ 0.55) is built up from all-side vertex-sharing PN₄ tetrahedra arranged in propeller-like [P₃N₁₀] subunits.

Rietveld refinement of optimized samples confirmed the structure model and phase purity. The thermal stability was investigated by temperature-dependent powder X-ray diffraction experiments. Additionally, diffuse reflectance UV/Vis spectroscopy estimated the band gap to 5.4 eV, while luminescence measurements revealed blue emission ($\lambda_{\text{em}} = 460 \text{ nm}$, $fwhm = 52 \text{ nm}/2423 \text{ cm}^{-1}$) for Eu²⁺-doped samples of BaP₆N₁₀NH. This renders BaP₆N₁₀NH:Eu²⁺ the first luminescent imidonitride.

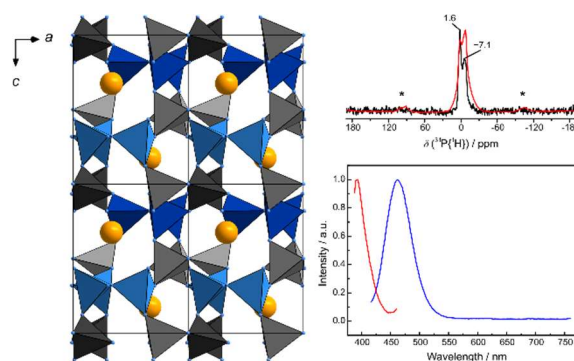


Figure 10.1. Crystal structure of BaP₆N₁₀NH and corresponding solid-state NMR and luminescence spectra. PN₄ tetrahedra: blue and gray, Ba: yellow.

10.2 Nitridophosphate-Based Ultra-Narrow-Band Blue-Emitters: Luminescence Properties of $AEP_8N_{14}:Eu^{2+}$ ($AE = Ca, Sr, Ba$)

Published in: **S. Wendl**, L. Eisenburger, P. Strobel, D. Günther, J. P. Wright, P. J. Schmidt, O. Oeckler, and W. Schnick

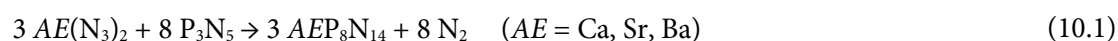
Chem. Eur. J. **2020**, *26*, 7292–7298.

Access via: DOI: 10.1002/chem.202001129

Reprinted at: Chapter 3, Supporting Information in Chapter B

Highly condensed nitridophosphates AEP_8N_{14} ($AE = Ca, Sr, Ba$) were synthesized in a multianvil apparatus starting from P_3N_5 and the respective alkaline earth metal azide (4–5 GPa, 1050–1150 °C, Equation 10.1). The crystal structure of CaP_8N_{14} (*Cmcm* (no. 63), $a = 8.5328(3)$, $b = 5.0794(2)$, $c = 23.9516(8)$ Å, $Z = 4$) was refined from powder X-ray diffraction data using the literature-known

SrP_8N_{14} as starting model. Structure elucidation of BaP_8N_{14} (*Amm2* (no. 38), $a = 12.4862(7)$, $b = 8.6648(3)$, $c = 5.1373(2)$ Å, $Z = 4$) was performed by a combination of transmission electron microscopy and single-crystal diffraction data obtained with microfocused synchrotron radiation.



All title compounds showed a layered structure type with alternating quadruple layers built of PN_4 tetrahedra and alkaline earth metal atoms. Different stacking patterns of the quadruple layers lead to octahedrally coordinated Ca and Sr atoms, while Ba is located in a trigonal-prismatic coordination. Luminescence investigations rendered $CaP_8N_{14}:Eu^{2+}$ ($\lambda_{em} = 470$ nm, $fwhm = 1380$ cm^{-1}) and $SrP_8N_{14}:Eu^{2+}$ ($\lambda_{em} = 440$ nm, $fwhm = 1350$ cm^{-1}) the first nitridophosphate-based ultra-narrow-band blue emitters. $BaP_8N_{14}:Eu^{2+}$ shows two broader emission bands ($\lambda_{em1} = 417$ nm, $fwhm = 2075$ cm^{-1} ; $\lambda_{em2} = 457$ nm, $fwhm = 3350$ cm^{-1} ;

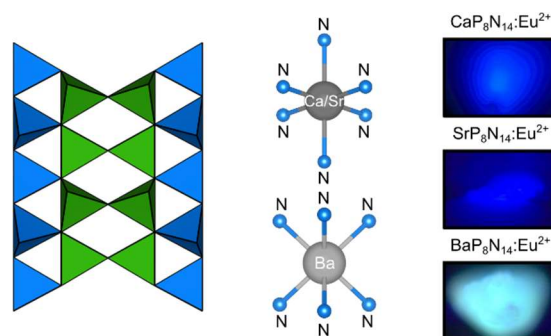


Figure 10.2. Quadruple layers of AEP_8N_{14} ($AE = Ca, Sr, Ba$) built of PN_4 tetrahedra. In addition, sixfold N-coordinated AE sites and photographs of Eu^{2+} -doped particles are shown.

10.3 Crystalline Nitridophosphates by Ammonothermal Synthesis

Published in: M. Mallmann, S. Wendl, and W. Schnick

Chem. Eur. J. **2020**, *26*, 2067–2072.

Access via: DOI: 10.1002/chem.201905227

Reprinted at: Chapter 4, Supporting Information in Chapter C

The preparation of literature-known α -Li₁₀P₄N₁₀, β -Li₁₀P₄N₁₀, Li₁₈P₆N₁₆, Ca₂PN₃, SrP₈N₁₄, and LiPN₂ is presented. Employing ammonobasic reaction conditions (up to 1070 K and 200 MPa), the obtained compounds underline the versatile applicability of this synthesis strategy by covering a wide degree of condensation κ from 1/3 to 4/7. The conducted systematic investigations enabled the formation of

different structural motifs from non-condensed tetrahedra groups to highly condensed frameworks. Therefore, the structural diversity of accessible nitridophosphates by ammonothermal synthesis was extended by far, since previously primarily oxide nitride perovskites and wurtzite-type derivatives were obtained. Moreover, commonly used and specially prepared phosphorus nitride P₃N₅ was replaced by readily available red phosphorus P_{red} as appropriate starting material. Respectively, thinkable reaction mechanisms and plausible intermediates were discussed. Rietveld refinements and energy dispersive X-ray spectroscopy were used to verify all title compounds. Additional Fourier transformed infrared spectroscopy confirmed the absence of NH functionalities in lithium containing samples.

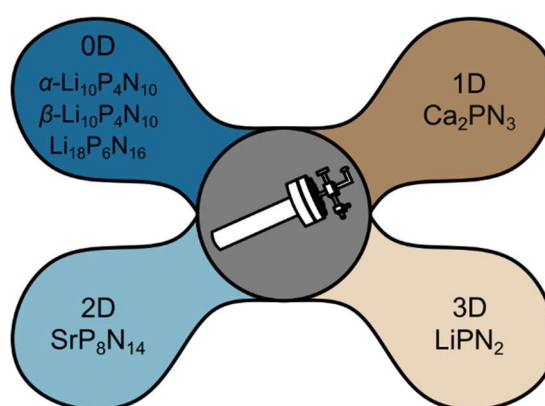


Figure 10.3. Overview of ammonothermally accessible representatives for group-, chain-, layer-, and framework-type nitridophosphates.

10.4 Ammonothermal Synthesis of Ba_2PO_3N – An Oxonitridophosphate with Non-Condensed PO_3N Tetrahedra

Published in: M. Mallmann, S. Wendl, P. Strobel, P. J. Schmidt, and W. Schnick

Eur. J. Inorg. Chem. **2020**, 841–846.

Access via: DOI: 10.1002/ejic.202000041

Reprinted at: Chapter 5, Supporting Information in Chapter D

The oxonitridophosphate Ba_2PO_3N is reported, which was prepared under ammonobasic conditions at 120 MPa and 800 °C. Starting from BaO, P_{red}, NaN₃, and KOH extraordinary large single-crystals (up to 600 μm) formed in the upper part of the liner. Since this part is expected to be the cooler zone, a chemical transport reaction may be assumed.

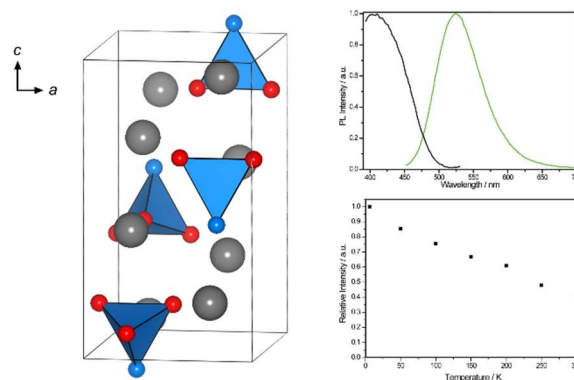


Figure 10.4. Crystal structure of Ba_2PO_3N with respective luminescence spectra and thermal quenching data of Eu^{2+} -doped samples. PO_3N tetrahedra: blue, Ba: gray; O: red; N: blue.

The crystal structure of Ba_2PO_3N was elucidated from single-crystal X-ray diffraction data ($Pnma$ (no. 62), $a = 7.596(2)$, $b = 5.796(1)$, $c = 10.212(3)$ Å, $Z = 4$). With its non-condensed $[PO_3N]^{4-}$ ions (β - K_2SO_4 structure type) the title compound showed isotypic to its lighter homologues and shifted the minimum degree of condensation for ammonothermally accessible nitridophosphates to $\kappa = 1/4$. The structure model was verified by Rietveld refinement and its chemical composition was examined by energy dispersive X-ray spectroscopy. The electrostatic plausibility and the assumed O/N assignment were supported by CHARDI and BVS analyses as well as MAPLE calculations. The band gap was determined to 4.3 eV by diffuse reflectance spectroscopy. Furthermore, luminescence investigations attribute $Ba_2PO_3N:Eu^{2+}$ green luminescence ($\lambda_{em} = 534$ nm, $fwhm = 85$ nm/ 2961 cm^{-1}) under excitation with UV to blue light. Low temperature luminescence measurements revealed a strong thermal quenching at room temperature ($\approx 40\%$).

10.5 $\text{Sr}_3\text{P}_3\text{N}_7$: Complementary Approach by Ammonothermal and High-Pressure Synthesis

Published in: M. Mallmann, S. Wendl, P. Strobel, P. J. Schmidt, and W. Schnick

Chem. Eur. J. **2020**, *26*, 6257–6263.

Access via: DOI: 10.1002/chem.202000297

Reprinted at: Chapter 6, Supporting Information in Chapter E

The preparation and structure elucidation of $\text{Sr}_3\text{P}_3\text{N}_7$ is presented. Therefore, a complementary approach of high-pressure multianvil and medium-pressure autoclave techniques was applied. While single-crystals were obtained under high-pressure high-temperature conditions (5 GPa, 1000 °C; Equation 10.2), phase-pure crystalline powder samples were produced by ammonothermal synthesis (140 MPa, 800 °C) starting from P_3N_5 , SrH_2 , and NaN_3 .



The structure of $\text{Sr}_3\text{P}_3\text{N}_7$ was elucidated by single-crystal X-ray diffraction ($P2/c$ (no. 13), $a = 6.882(8)$, $b = 7.416(9)$, $c = 7.036(8)$ Å, $\beta = 104.96(3)^\circ$, $Z = 2$). The one-dimensional infinite structure of $\text{Sr}_3\text{P}_3\text{N}_7$ features *dreier* double chains built up from *dreier* and *vierer* rings. The title compound complemented the accessible degrees of condensation for ternary alkaline earth nitridophosphates by $\kappa = 3/7$. An additional Rietveld refinement confirmed the presented structure model and the elemental composition was verified by energy dispersive X-ray spectroscopy. Fourier transformed infrared spectroscopy ruled out any NH functionalities. Diffuse reflectance UV/Vis spectroscopy measurements estimated the optical band gap to 4.4 eV. Eu^{2+} -doped samples of $\text{Sr}_3\text{P}_3\text{N}_7$ show deep-red to infrared emission ($\lambda_{\text{em}} = 681$ nm, $\text{fwhm} \approx 3402$ cm^{-1}) due to excitation with UV to blue light and an internal quantum efficiency of 42%.

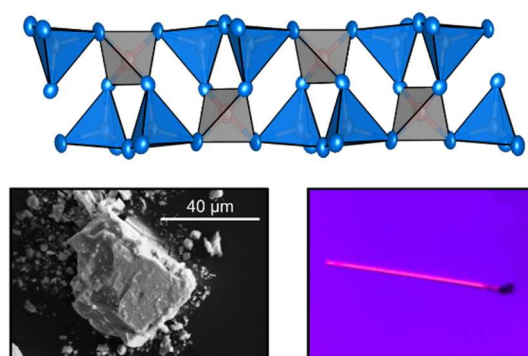


Figure 10.5. Infinite *dreier* double chain of $\text{Sr}_3\text{P}_3\text{N}_7$ with corresponding images of a single crystal and a capillary filled with a Eu^{2+} -doped sample under irradiation.

10.6 HIP to be Square: Simplifying Nitridophosphate Synthesis in a Hot Isostatic Press

Published in: **S. Wendl**, S. Mardazed, P. Strobel, P. J. Schmidt, and W. Schnick

Angew. Chem. Int. Ed. **2020**, 59, 18240–18243;

Angew. Chem. **2020**, 132, 18397–18400.

Access via: DOI: 10.1002/anie.202008570; 10.1002/ange.202008570

Reprinted at: Chapter 7, Supporting Information in Chapter F

Hot isostatic presses are introduced as synthetic tools for the access to nitridophosphates. As model compound Ca_2PN_3 was prepared. After simplification of literature-known protocols, significantly accelerated synthesis was possible under medium-pressure conditions (150 MPa N_2 ; 1200 °C). According to Equation 10.3 P_{red} could be implemented as starting material enabling synthesis of an alkaline earth metal nitridophosphate from exclusively readily available compounds.



The crystal structure of Ca_2PN_3 was refined from single-crystal X-ray diffraction data (*Cmce* (no. 64), $a = 5.1987(4)$, $b = 10.3145(10)$, $c = 11.2834(14)$ Å, $Z = 8$). The obtained results were in good agreement with previous refinements based on powder X-ray diffraction data. Rietveld refinements and energy dispersive X-ray spectroscopy confirmed phase purity and the chemical composition, respectively. Excitation with blue light induced deep-red emission ($\lambda_{\text{em}} = 650$ nm, $\text{fwhm} \approx 84$ nm/ 1972 cm^{-1}) of $\text{Ca}_2\text{PN}_3:\text{Eu}^{2+}$. The internal quantum efficiency was determined to $\approx 32\%$.

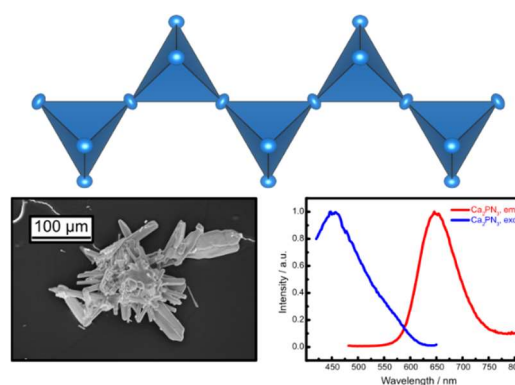


Figure 10.6. Infinite *zweier* single chains of Ca_2PN_3 . A corresponding SEM image and luminescence spectra of a Eu^{2+} -doped sample are displayed.

10.7 Synthesis of Nitride Zeolites in a Hot Isostatic Press

Published in: **S. Wendl**, M. Zipkat, P. Strobel, P. J. Schmidt, and W. Schnick

Angew. Chem. Int. Ed. **2021**, *60*, 4470–4473;

Angew. Chem. **2021**, *133*, 4520–4523.

Access via: DOI: 10.1002/anie.202012722; 10.1002/ange.202012722

Reprinted at: Chapter 8, Supporting Information in Chapter G

The synthesis of nitride zeolites $AE_3P_5N_{10}X$ ($AE = Sr, Ba$; $X = Cl, Br$) in a hot isostatic press is reported. The products were obtained under medium-pressure conditions (150 MPa N_2 , 1000 °C) starting from P_3N_5 or P_{red} and the respective alkaline earth metal azides $AE(N_3)_2$ and halides AEX_2 . The structure of $Sr_3P_5N_{10}Cl$ was refined from single-crystal X-ray diffraction data ($Pnma$

(no. 62), $a = 12.240(3)$, $b = 12.953(3)$, $c = 13.427(3)$ Å, $Z = 8$). The presented structure model was verified by additional Rietveld refinements and further used as starting point for the refinement of $Sr_3P_5N_{10}Br$ based on powder X-ray diffraction data ($Pnma$ (no. 62), $a = 12.297(1)$, $b = 12.990(1)$, $c = 13.458(1)$ Å, $Z = 8$). Phase purity of literature-known barium compounds $Ba_3P_5N_{10}X$ ($X = Cl, Br$) was confirmed by Rietveld refinements. The elemental compositions were verified by energy dispersive X-ray spectroscopy. The successful preparation of the title compounds extended the degree of condensation for accessible nitridophosphates by HIP synthesis to $\kappa = 0.5$. Moreover, hitherto unprecedented $Sr_3P_5N_{10}X$ demonstrates the benefits of a possible fine pressure balancing. Corresponding size effects of alkaline earth metal and halide ions were discussed. Eu^{2+} -doped samples revealed natural-white ($Ba_3P_5N_{10}Br:Eu^{2+}$), orange ($Ba_3P_5N_{10}Cl:Eu^{2+}$), and deep-red ($Sr_3P_5N_{10}X:Eu^{2+}$) emission. The internal quantum efficiencies were determined to 29% ($X = Cl$) and 32% ($X = Br$) for $Sr_3P_5N_{10}X:Eu^{2+}$ as well as 12% for $Ba_3P_5N_{10}X:Eu$.

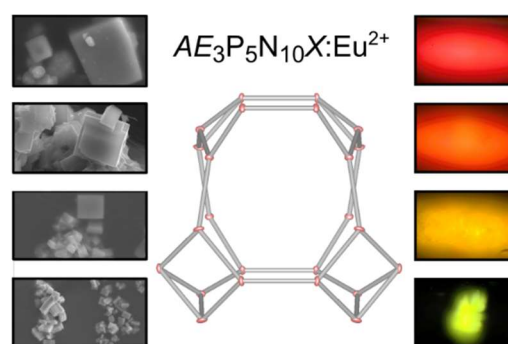


Figure 10.7. Topological illustration of the zeolite cages in $AE_3P_5N_{10}X$ with respective SEM images and photographs of Eu^{2+} -doped particles. AE/X combinations in top-down order: Sr/Cl, Sr/Br, Ba/Cl, and Ba/Br.

10.8 Post-Synthetic Modification: Systematic Study on a Simple Access to Nitridophosphates

Published in: **S. Wendl**, L. Seidl, P. Schüler, and W. Schnick

Angew. Chem. Int. Ed. **2020**, *59*, 23579–23582;

Angew. Chem. **2020**, *132*, 23785–23788.

Access via: DOI: 10.1002/anie.202011835; 10.1002/ange.202011835

Reprinted at: Chapter 9, Supporting Information in Chapter H

Investigations on the reaction behavior of pre-synthesized nitridophosphates towards halides are presented. BaP_2N_4 , $\text{Ba}_3\text{P}_5\text{N}_{10}\text{Br}$, $\text{SrH}_4\text{P}_6\text{N}_{12}$, $\text{CaP}_8\text{N}_{14}$, and Ca_2PN_3 were chosen as model compounds and reacted with alkaline earth metal halides of the lighter homologues under elevated pressures and temperatures (Equation 10.4). The observed multifaceted behavior did not allow the conclusion of a general reaction mechanism. Besides products that were structurally related to the starting materials and suggested some kind of topotactic reactions, even completely unrelated products were observed.

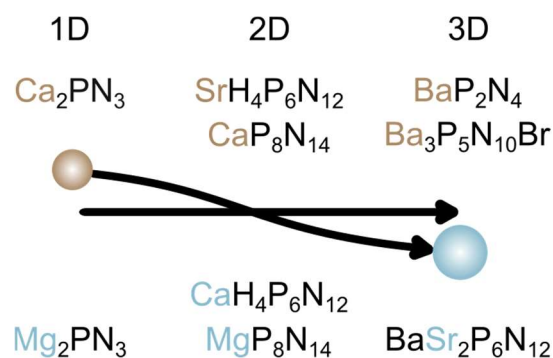


Figure 10.8. Overview of nitridophosphates investigated in terms of their reaction behavior towards halides. 1D: Ca_2PN_3 ; 2D: $\text{SrH}_4\text{P}_6\text{N}_{12}$ and $\text{CaP}_8\text{N}_{14}$; 3D: BaP_2N_4 and $\text{Ba}_3\text{P}_5\text{N}_{10}\text{Br}$. Observed products are given below.



Following this post-synthetic top-down approach, its great potential could be underlined by synthesis of $\text{MgP}_8\text{N}_{14}$ which was hitherto not accessible by conventional syntheses. The structure of $\text{MgP}_8\text{N}_{14}$ was refined on the basis of powder X-ray diffraction data ($Cmc2_1$ (no. 36), $a = 8.3646(1)$, $b = 5.0215(1)$, $c = 23.1963(3)$ Å, $Z = 4$). Rietveld refinements were used to verify all products and energy dispersive X-ray spectroscopy was used for the determination of chemical compositions.

11 Discussion and Outlook

As outlined in the Summary (Chapter 10), this dissertation deals with fundamental investigations on innovative synthesis strategies, the structural chemistry of nitridophosphates, and their promising luminescence properties. To deduce the main insights of this thesis, the key results are condensed into two separate sections below and discussed in their respective scientific context. In addition, the following sections give prospects for future investigations while potential pathways to the industrial application of nitridophosphate-based phosphor materials are highlighted.

11.1 Nitridophosphates as Promising Aspirants for Solid-State Lighting

Despite 30 years of research and the development of various synthetic approaches, ternary alkaline earth metal nitridophosphates have been limited to AE_2PN_3 and AEP_2N_4 due to their sophisticated synthesis prior to this work.^[1-4] Even with the consideration of pseudoternary H and O containing compounds (i.e. imido- and oxonitridophosphates) the compositional diversity has been highly limited (see Figure 1.4).^[5-9]

Applying established high-pressure techniques, as well as hitherto sparsely or even unexplored medium-pressure approaches (Section 11.2), this compound class is extended in the course of this work. Figure 11.1 illustrates the updated status quo of Figure 1.4 and highlights the introduced compounds in blue. Additionally, Ca_2PN_3 and $Ba_3P_5N_{10}X$ ($X = Cl, Br$) are highlighted, since they have been reproduced within this thesis in a significantly simplified way (Section 11.2).

Recapitulating, this thesis doubles the overall number of ternary compositions. $Sr_3P_3N_7$ represents the first formal 1:1 adduct of P_3N_5 and a formal alkaline earth metal nitride AE_3N_2 to be synthesized. All other ternary alkaline earth metal nitridophosphates can be directly derived thereof by variation of the $P_3N_5:AE_3N_2$ ratio, as exemplified in Figure 11.2. AEP_8N_{14} ($AE = Ca, Sr, Ba$) is introduced extending the degree of condensation for ternary compounds to $\kappa = 4/7 \approx 0.57$. Moreover, pseudoternary $BaP_6N_{10}NH$ and Ba_2PO_3N as well as quaternary strontium zeolites $Sr_3P_5N_{10}X$ ($X = Cl, Br$) complement the related compound classes.

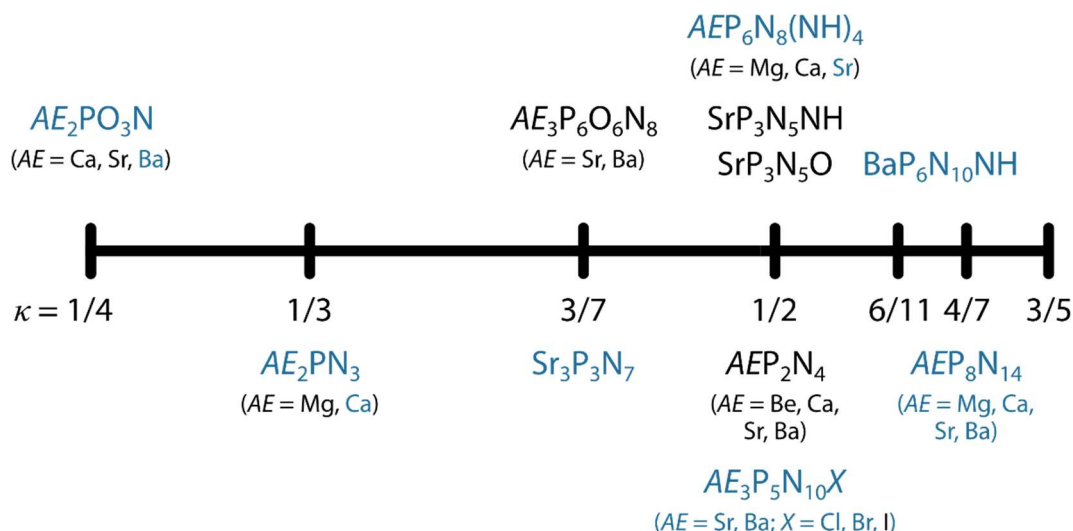


Figure 11.1. Updated range of degree of condensation for (pseudo)ternary (oxo/imido)nitridophosphates. Sum formulas highlighted in blue represent either unprecedented nitridophosphates prior to this work or compounds that were reproduced with significantly simplified approaches. Additionally, zeolite-like $AE_3P_5N_{10}X$ is listed, from which only the barium compounds were previously known. To keep the overview simple, further halide containing nitridophosphates are neglected.



Figure 11.2. Overview of known ternary alkaline earth metal nitridophosphates. Compositional relations of adjacent compounds are indicated by the formal addition of P_3N_5 or AE_3N_2 . Hypothetical “ AEP_5N_9 ” (green) is indicated as stoichiometric void between AEP_2N_4 and AEP_8N_{14} .

Despite a now noticeably larger number of alkaline earth metal (oxo/imido)nitridophosphates, some striking gaps remain within the feasible degree of condensation that could be addressed by future research. First of all, “ AEP_5N_9 ” comes to mind, which represents the stoichiometric void between AEP_2N_4 and AEP_8N_{14} by either adding or removing one equivalent P_3N_5 , respectively (Figure 11.2, green). Moreover, the upper end of the degree of condensation may be pushed by synthesizing even higher-condensed “ $AEP_{11}N_{19}$ ” or “ $AEP_{14}N_{24}$ ”. However, it appears challenging to find appropriate synthesis conditions, since the reaction pathways are unknown, thermodynamic sinkholes have to be avoided, and the desired degrees of condensation do not differ significantly, as shown in the gray area of Figure 11.3.

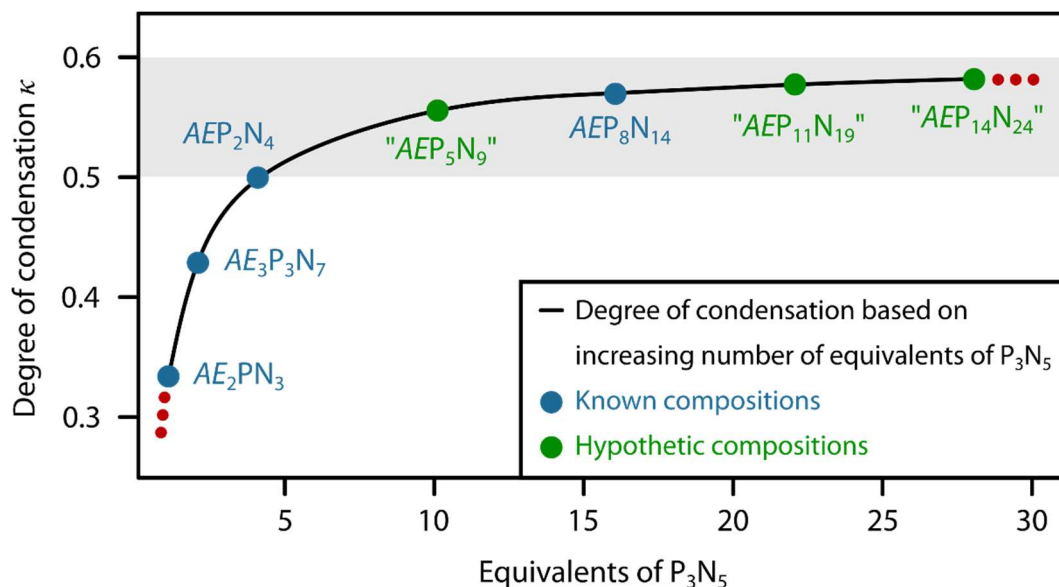


Figure 11.3. Illustration of the degree of condensation κ in dependence on respective equivalents of P_3N_5 . In order to enable a useful comparison, the given sum formulas have been converted into the general form $AE_6P_{3x}N_{5x+4}$ with x giving the respective number of P_3N_5 equivalents. Only this way, accurate conclusion can be drawn, since 6 is the least common multiple of AE for considered compounds. Exemplary, AEP_2N_4 can be formulated as " $AE_6P_{12}N_{24}$ ", which is equal to " $2 AE_3N_2 + 4 P_3N_5$ ". As indicated in gray, the curve flattens significantly in the higher condensed region underlining the only fine nuances in the degree of condensation. By far larger voids remain up to $x = 5$ equivalents of P_3N_5 . Compositions displayed in blue are already known; fictive compositions are colored green.

In contrast, the remaining gaps in the lower-condensed range are noticeably larger. In order to target reasonable values at this point, a comparison of alkaline earth metal compounds with other groups of nitridophosphates may be helpful. Considering all nitridophosphates known so far, it is noticeable that certain degrees of condensation are repeatedly observed and obviously well accessible for this substance class. An illustration of this fact is given in Figure 11.4 referring to alkaline earth metal (vertical black bars),^[1-9] lithium (ochre),^[10-17] rare earth(/lithium) metal (brown/dark blue),^[18-22] and transition metal nitridophosphates (light blue).^[23-26] Strikingly, there are some degrees of condensation that have not yet been observed for alkaline earth metal compounds so far (green).

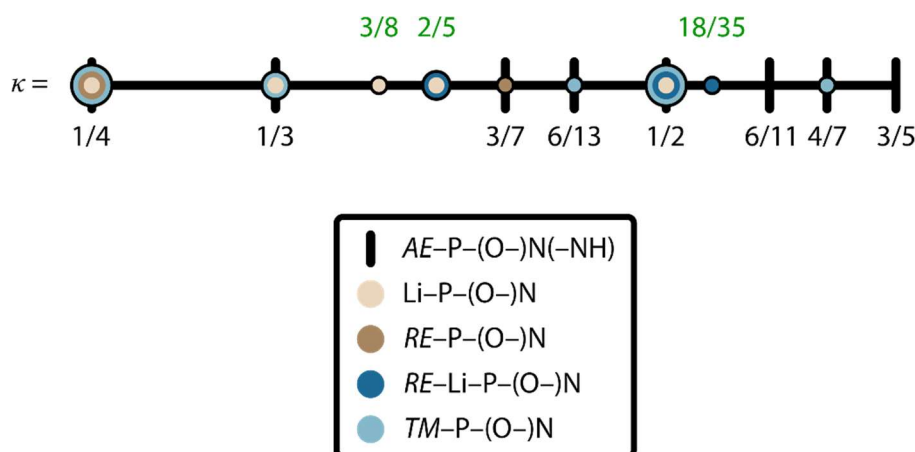


Figure 11.4. Degrees of condensation for selected groups of nitridophosphates. Realized values for κ follow the subsequent color coding: black: alkaline earth metal (oxo/imido)nitridophosphates; ochre: lithium nitridophosphates; brown: rare earth metal nitridophosphates; blue: rare earth metal/lithium nitridophosphates; light blue: transition metal nitridophosphates; green: unrealized degrees of condensation in alkaline earth metal (oxo/imido)nitridophosphates. Strikingly, distinct degrees of condensation (e.g. $\kappa = 1/4$, $1/3$, or $1/2$) are observed for different groups. However, other points (e.g. $\kappa = 3/8$, $2/5$, $3/7$, etc.) are only realized in one or two groups of nitridophosphates and offer inspiration for the synthesis of novel compounds. The upper end of the degree of condensation ($\kappa = 3/5$) is given by binary P_3N_5 .

Consequently, the hypothetical compounds " $AE_5P_4N_{10}$ " or " $AE_9P_6N_{16}$ " seem to be particularly suitable for further lowly-condensed AE-nitridophosphates. Especially the latter seems to be auspicious, since P/N anions with $\kappa = 3/8$, such as $[P_6N_{16}]^{18-}$ in $Li_{18}P_6N_{16}$, have already been observed in a one-dimensional infinite extension in $Sr_3P_3N_7$.^[10]

Next to the ever-growing compositional and structural diversity, hitherto unknown compounds may lead to promising materials for various fields of application. As indicated in Section 1.3, alkaline earth metal nitridophosphates are particularly capable as host lattices for solid-state phosphors. Previously, AE/P/N-based phosphors have been limited to $AEP_2N_4:Eu^{2+}$ ($AE = Ca, Sr, Ba$) and zeolite-like $Ba_3P_5N_{10}X:Eu^{2+}$ ($X = Cl, Br, I$).^[3, 27, 28] Within the presented work, this list is supplemented by investigations on the luminescence properties of obtained products emphasizing the industrial relevance of functional nitridophosphates. Figure 11.5 gives an optical impression of the emissions of Eu^{2+} -doped products under irradiation with UV to blue light. As can be seen, the introduced phosphors cover almost the whole range of the visible spectrum. Moreover, some of them show luminescence characteristics making nitridophosphates competitive with other Eu^{2+} -doped (oxo)nitride materials. For instance, $CaP_8N_{14}:Eu^{2+}$ and $SrP_8N_{14}:Eu^{2+}$ represent the first P/N-based

ultra-narrow-band blue-emitters, and the emission band of red-emitting $\text{Ca}_2\text{PN}_3:\text{Eu}^{2+}$ is comparable to commercial $\text{Sr}_2\text{Si}_5\text{N}_8:\text{Eu}^{2+}$ (2-5-8).^[29]

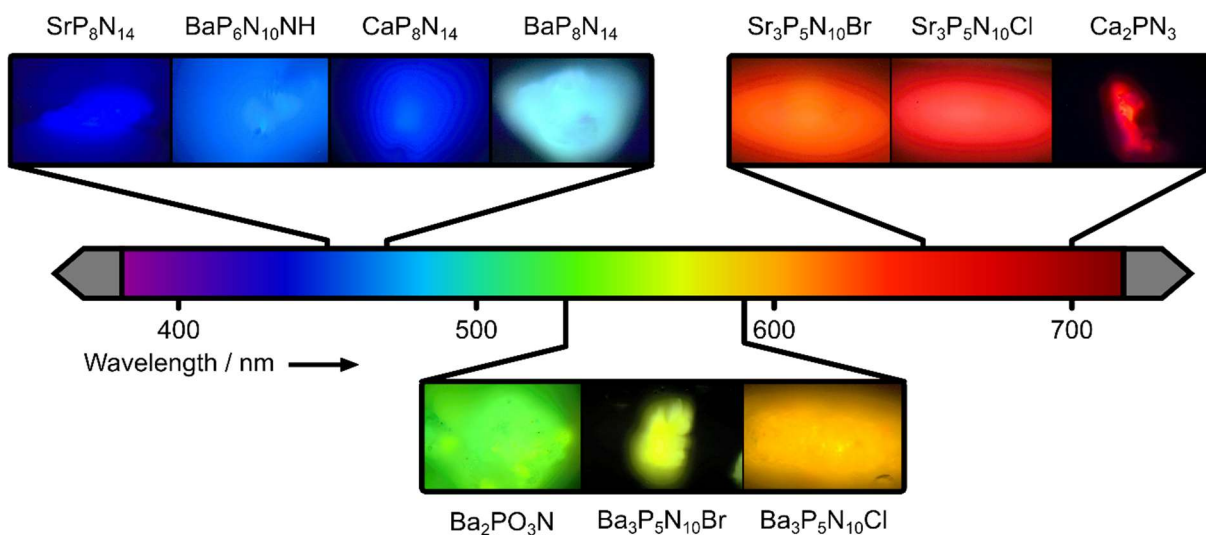


Figure 11.5. Illustration of the obtained Eu^{2+} -doped samples within the presented thesis.

These outstanding properties encourage searching for new nitridophosphates – not only in the interest of basic research, but also in an application-oriented manner. Here, commercial solid-state phosphors from related compound classes can serve scientists as inspiration. Host lattices from applied luminescent materials, such as $\text{Ca}[\text{AlSiN}_3]:\text{Eu}^{2+}$ ($\text{CASN}:\text{Eu}^{2+}$), may be mimicked with P/N structures via the formal substitution of the tetrahedra centers, resulting in possible compounds such as $\text{Ca}[\text{MgPN}_3]:\text{Eu}^{2+}$.^{[30,31]†} The case studies on $\text{BaP}_6\text{N}_{10}\text{NH}:\text{Eu}^{2+}$ and $\text{AE}_2\text{PO}_3\text{N}:\text{Eu}^{2+}$ open up additional options, considering anionic charge balancing by introducing O or NH groups. For instance, $\text{Y}_3\text{Al}_5\text{O}_{12}$ (YAG) analogous garnet-type (oxo/imido)nitridophosphates, such as $\text{Ca}_3[\text{P}_5\text{N}_7(\text{O}/\text{NH})_5]$ or $\text{Y}_3[\text{P}_5\text{N}_{10}(\text{O}/\text{NH})_2]$, may be synthesized.^[32] However, such compounds seem to be accessible exclusively under extreme pressure conditions, since this structures feature sixfold coordinated P sites, which in condensed structures have only been reported at pressures above 40 GPa, as yet. A further far-reaching contribution to mimicking established phosphors could be made by considering other framework forming species allowing for cationic charge balancing. So far, only Mg, Al, Si, B,

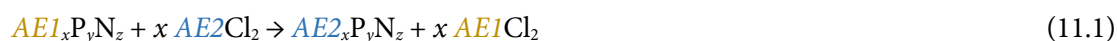
† This notation of the sum formulas is used to indicate the framework-forming units (anionic networks) in the square brackets. The counter cations are prefixed.

and Li have been respectively considered in P/N compounds. Here, especially Li seems promising, since it is already a component in industrially relevant phosphors (e.g. UCr_4C_4 -type $\text{Sr}[\text{LiAl}_3\text{N}_4]:\text{Eu}^{2+}$ (SLA)).^[33] Moreover, the class of ternary lithium nitridophosphates is well studied and Li has already been implemented in quaternary rare earth metal nitridophosphates like LiNdP_4N_8 or $\text{LiPr}_2\text{P}_4\text{N}_7\text{O}_3$.^[19, 20] Consequently, the P/N-based recreation of phosphors like SLA may be eased by using Li containing starting materials. Therefore, " $\text{AE}[\text{Li}_2\text{PO}_2\text{N}_2]:\text{Eu}^{2+}$ " and " $\text{AE}_2[\text{Li}_5\text{P}_3\text{N}_8]:\text{Eu}^{2+}$ " can be named as conceivable sum formulas. Nevertheless, other elements that can partly replace P in tetrahedron centers, such as mentioned Si and B seem promising. Alternatively Al, which has previously only been observed in form of sixfold N-coordinated octahedral, as well as hitherto neglected Be and others, should be the subject of future research. This way, numerous hypothetical CASN, YAG, SLA, or 258 variants may be screened, opening the way to a variety of new P/N-compounds.

11.2 Progress in Nitridophosphate Synthesis

Due to exploratory approaches, fundamental progress in nitridophosphate synthesis has been made within this thesis. In this section, the successfully introduced synthesis strategies are outlined and put into context of their scientific and industrial importance. For this purpose, a simplified reaction concept is briefly outlined below.

While established synthesis routes have been limited to *bottom-up* strategies, in which covalent bonds between P and N are (re-)created, the first *top-down* approach is developed using alkaline earth metal nitridophosphates as model substance class.^[34] The elaborated strategy is best described with the term "post-synthetic modification" and works by re-functionalizing pre-arranged P/N frameworks. The basic idea was initially a formal exchange of the embedded alkaline earth ions in nitridophosphates without changing the existing P/N networks to increase synthesis control. Therefore, compounds should be reacted with alkaline earth metal halide melts under elevated temperatures as exemplified in Equation 11.1.



Although analogous reactions have extensively been studied for structurally related oxosilicates, there are only a few contributions on ion exchange reactions in nitride substance classes.^[35-37] Among nitridophosphates in particular only a deprotonation of $Zn_5H_4[P_{12}N_{24}]Cl_2$ with $ZnCl_2$ has been reported.^[38,39] Moreover, only the nitridosilicates $AE_2Si_5N_8$ ($AE = Ca, Sr$) have been investigated with regard to this *top-down* strategy.^[40-43] The studies on $AE_2Si_5N_8$ have however been focused on the elemental variety of introduced cations. The presented work on nitridophosphates in contrast deals with the applicability of the ion exchange on different nitride-based networks, as there are framework-, layer-, and chain-type structures. Due to the beforehand observed lability of P/N compounds towards halide melts at ambient pressure (see Chapter 9), ion exchange reactions are carried out under elevated pressures utilizing multianvil apparatuses or hot isostatic presses (HIPs, see below). As presented in Chapter 9, the implemented ion exchange reactions, however, do not always follow simple topotactic mechanisms, but an atomic resemblance may be observed, as well, yielding different structure types in some cases. Since there are no systematic studies on ion exchange reactions in other nitride materials, the question for future studies is raised whether the multifaceted reaction behavior of nitridophosphates represents an exception or applies in the same way to other substance classes. Although this reaction behavior impedes the actually intended facilitation of synthesis control, it also underlines the far-reaching possibilities of this approach. To gain insight on the reaction mechanisms, *in situ* investigations at elevated pressures should be subject to future research. Notwithstanding of the reaction behavior, the introduced post-synthetic treatment will basically provide a very powerful tool for the access to P/N chemistry due to its broad applicability. The reason for this is that the reaction products do not have to be built up from starting materials, some of which are specially prepared and prone to thermal decomposition. Instead, known and easily pre-synthesized nitridophosphates are combined with metal halides. If one assumes that the results observed for nitridosilicates also apply in a similar way to nitridophosphates, the halides to be used are not limited to alkaline earth metals opening up access to several other classes of nitridophosphates. Furthermore, this approach might also have a great impact in optimization processes of material properties, since solid solutions no longer have to be synthesized from scratch but from pre-synthesized precursors, for instance.

The fact that application-oriented optimization processes may someday play a role at all is owed to a second novel synthetic access to nitridophosphates introduced within this thesis. Earlier, *AE/P/N*-based phosphors have been considered exotic despite their promising luminescence properties. The reason for this is that established methods and routes are associated with significant drawbacks that intrinsically rule out a broad industrial application. To put this problem into figures, the multianvil technique, which has emerged to the standard synthesis method, serves as a good example. Here, specially prepared starting materials (e.g. P_3N_5 , $LiPN_2$, etc.) are reacted at extreme conditions (1–20 GPa; 800–1500 °C), yielding only small sample quantities (10–150 mg).^[3, 27, 28] Consequently, following obstacles have had to be addressed when thinking about industrial application:

- Reducing synthesis pressure
- Starting from readily available materials
- Upscaling
- Targeting short reaction times

In order to devise a suitable strategy for large-scale production, the synthesis pressure is initially reduced by ammonothermal synthesis that is an established however sparsely used technique.^[44, 45] Working with supercritical ammonia and mineralizers, reactive intermediates are formed to allow reactions starting from P_3N_5 well below its critical decomposition temperature. Extensive studies and the successful synthesis of numerous literature-known nitridophosphates within this thesis show that a great variety of nitridophosphates can certainly be synthesized in a medium-pressure range. For further simplification, specially prepared P_3N_5 is waived by using readily available P_{red} , which has so far only been used for ampoule synthesis of HPN_2 in ammonia.^[46] Despite this great progress in nitridophosphate synthesis, the ammonothermal method does not meet all demands for large-scale production. In addition to long reaction times, there are serious scaling and material-related issues due to necessary operations in supercritical ammonia.

For this reason, hot isostatic presses (HIPs) are presented as a previously neglected access to *P/N* chemistry, since significantly higher synthesis pressures have been assumed to be necessary. However, HIPs have already been used industrially for sintering and annealing processes of ceramics.^[47-52] In *P/N* chemistry, this approach is the first possibility to combine advantages of different established methods. For example, reactions are carried out on the minute to hour scale just

as in high-pressure apparatuses and only moderate pressures are applied just as in ammonothermal autoclaves. Moreover, the HIP approach comes with additional and unique benefits. Preparation procedures are simplified, since neither supercritical ammonia nor high-pressure assemblies are required. Significant larger sample quantities (> 10 g) are available and it is particularly remarkable that red phosphorus could be adapted as starting material, as well. Next to enabled reactions only from commercially available materials, this route can be seen as a far-reaching case study, since P_{red} in absence of ammonia is used as starting material for the first time. Consequently, azide ions (N_3^- , starting material) and/or N_2 (pressure medium) are discussed as redox partners for a stepwise oxidation of elemental phosphorus through intermediate “PN”. The evaluation of this hypothesis could be subject to future *in situ* investigations.

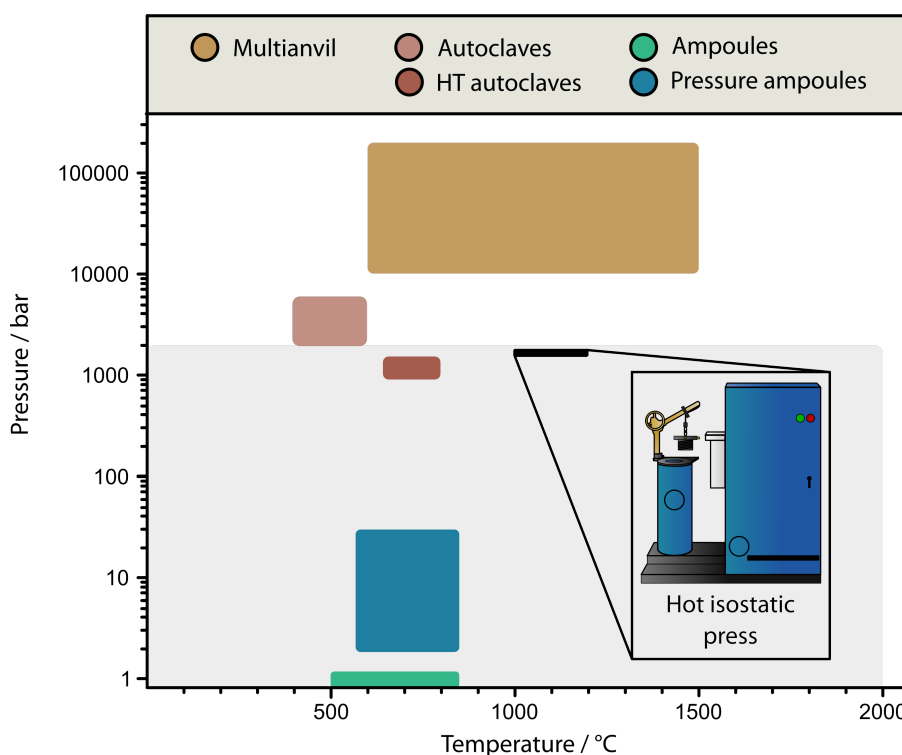


Figure 11.6. Illustration of the feasible p - T range for nitridophosphate/phosphorus nitride syntheses by hot isostatic pressing (gray). Already implemented reaction conditions for (pressure) ampoules (blue/green), (HT) autoclaves (dark/light red), and multianvil techniques (brown) are displayed for comparison. The black range illustrates the used conditions within the presented thesis.

However, in the context of a possible reaction mechanism a prior transformation of P_{red} into highly reactive P_4 has to be taken into account due to the applied reaction conditions. Interestingly, in contrast to other MP methods, HIPs enable high reaction temperatures ($t_{\text{max}} = 2000 \text{ }^\circ\text{C}$). This means that temperatures far beyond the decomposition temperature at ambient pressure of starting materials and products can be practically implemented under MP conditions for the first time (Figure 11.6). Thereby a so far completely unexplored p - T range is opened up for P/N chemistry, which seems to be very promising since numerous solid-state compounds require temperatures above $1000 \text{ }^\circ\text{C}$ for the cleavage and reformation of chemical bonds. The successful syntheses of Ca_2PN_3 and $\text{AE}_3\text{P}_5\text{N}_{10}\text{X}$ ($\text{AE} = \text{Sr, Ba}$; $\text{X} = \text{Cl, Br}$) at 200 MPa and $1200 \text{ }^\circ\text{C}$ demonstrate the applicability of the previously inaccessible reaction conditions for the preparation of nitridophosphates covering a wide degree of condensation.

Recapitulating, the presented results render the HIP approach a milestone in P/N research, since advantages of different approaches are initially combined, enabling a simple and fast preparation of nitridophosphates. HIP synthesis is additionally afflicted with further benefits that concern aspects of applied as well as basic research. For the latter, especially the preparation of the strontium compounds $\text{Sr}_3\text{P}_5\text{N}_{10}\text{X}$ ($\text{X} = \text{Cl, Br}$) is noteworthy. Up to now, such zeolites have not been obtained under high- nor ambient pressure conditions. A reason for this might be the required MP reaction pressure, which has to be high enough to suppress thermal decomposition but low enough to prevent a structural collapse of large cages within the porous structure type. The possibility to balance reaction pressures may lead to further unknown MP phases. To investigate the limits of pressure balancing even more vulnerable compounds may be targeted. For instance, hypothetical “ $\text{Ca}_3\text{P}_5\text{N}_{10}\text{X}$ ” seems an appropriate candidate due to the lower space filling of Ca^{2+} compared to Sr^{2+} . In this context, possible structure effects of incorporated anions may be examined. If fundamental building units collapse when filled with Ca^{2+} and lighter halides ($\text{X} = \text{Cl, Br}$), larger I^- ions may be introduced to stabilize the zeolite framework.

In further experiments, the implemented range of the degree of condensation ($1/3 < \kappa < 1/2$) could be expanded. Therefore, already known highly-condensed $\text{AEP}_8\text{N}_{14}$ ($\kappa \approx 0.57$) appears as an appropriate candidate for initial experiments. In Chapter 4, it has already been shown that in principle MP pressure conditions are adequate for the synthesis of respective $\text{SrP}_8\text{N}_{14}$. The higher feasible synthesis temperatures in HIPs may also allow for better crystallization and reactions started

from P_{red} at this point. Especially concerning the synthesis of higher condensed compounds, the offered technical possibilities of HIPs seem very promising. Since standard conditions of 200 MPa and 1200 °C are used within this thesis and the actually required pressure to suppress the thermal decomposition of P/N compounds is not known, large parts of the recently accessible p - T range by HIP remain unexplored (Figure 11.6).

The simple and straightforward access to alkaline earth metal nitridophosphates following azide and nitride routes encourages to put effort on the syntheses of other P/N-based compound classes, as well. Here, especially lithium nitridophosphates come to mind since they are already accessible in a broad range of conditions.^[10-13, 15-17] Easiest thinkable reactions may start from different ratios of Li_3N and P_{red} to obtain large-volume samples contributing to the solution of two serious issues concerning Li/P/N chemistry. On the one hand, structure elucidation of lithium nitridophosphates might be facilitated. To date, mostly X-ray diffraction have been used for structure solution, although they are of restricted suitability due to the low scattering factor of light elements. A much more appropriate strategy for location of lighter Li atoms is neutron diffraction, for which however established ampoules, autoclaves, and multianvil apparatuses are not capable to provide sufficient amounts from a single batch. That is why several phase-pure samples had to be merged elongating the synthesis process by far. On the other hand, the same applies to the comprehensive characterization of possible lithium ion conductivity, since large sample volumes are required for the preparation of cold-pressed test pellets.

Transferring other established synthesis routes to the HIP approach could be beneficial, as well. While some routes appear easily transferable, others may necessitate modifications of the common HIP setup. The mineralizer route, for instance, makes use of very harsh reaction conditions. Starting from H-containing materials (e.g. NH_4Cl) hydrogen halides (e.g. HCl) are formed that are considered as an activator for inert materials and as an promoter for crystallization.^[53] These *in situ* formed hydrogen halides could likely corrode metal components of the device, which may necessitates protective covers of getter materials. Similar concepts and solutions are already applied as liners used in autoclaves or capsules in HP/HT assemblies.^[54]

As shown in Chapter 9, first investigations on ion exchange reactions demonstrate its applicability at MP conditions. Reminiscent of Section 11.1, more alkaline earth metal nitridophosphates should be examined concerning their reaction behavior towards halides. Of course, next to alkaline earth

compounds, other materials should be considered, as well. While other groups of halides may lead to the preparation of transition (*TM*) or rare earth metal (*RE*) nitridophosphates, for instance, other classes of pre-arranged nitridophosphates are still completely unexplored in terms of post-synthetic modification.

However, ion exchange/post-synthetic modification may be seen as a special form of a much larger group of reactions – the metathesis. This synthesis route has been proven suitable for the preparation of transition and rare earth metal nitridophosphates under HP/HT conditions following the general reaction concept of Equation 11.2 (Chapter 1):^[18-24]



A successful combination of metathesis with HIPs seems extraordinarily promising, at this point. Although metathesis reactions have only been introduced to nitridophosphates using *TM* and *RE* halides, there is no indication for any limitation to these metal groups. The joined approach of both strategies may therefore be seen as a first serious contender for a universal approach to nitridophosphates providing large-volume samples.

11.3 Concluding Remarks

Starting from fundamental studies on nitridophosphates and related compound classes, this thesis further paths the way for near-future application-oriented research. Motivated by multiple intriguing luminescence properties the focus of the work was the elaboration of innovative synthesis strategies that may pave the way to large-scale production of functional nitridophosphates. Especially the introduction of hot isostatic presses as a synthesis tools has pushed P/N chemistry beyond established limitations and therefore made it more relevant for application than ever before. Furthermore, this method offers significant advantages for other aspects such as structure elucidation and the investigation of material properties. The presented results are only considered the tip of the iceberg and therefore serve as a foundation for versatile and deep future research. Even the long-sought-after universal access to large-volume samples of nitridophosphates seems within reach, as outlined by conceivable forecasts and prospects above. Since creativity is an unlimited ability of science, this conclusion does not claim for completeness and only time will tell where exactly the path of nitridophosphates ends.

11.4 References

- [1] W. Schnick, V. Schultz-Coulon, "Ca₂PN₃: A New Phosphorus(V) Nitride with One-Dimensional Infinite Chains of Corner-Sharing PN₄ Tetrahedra", *Angew. Chem. Int. Ed. Engl.* **1993**, 32, 280-281; *Angew. Chem.* **1993**, 105, 308-309.
- [2] V. Schultz-Coulon, W. Schnick, "Mg₂PN₃ and Ca₂PN₃ – Phosphorus(V) Nitrides with Infinite Chains of Corner Sharing PN₄ Tetrahedra", *Z. Anorg. Allg. Chem.* **1997**, 623, 69-74.
- [3] F. J. Pucher, A. Marchuk, P. J. Schmidt, D. Wiechert, W. Schnick, "Luminescent Nitridophosphates CaP₂N₄:Eu²⁺, SrP₂N₄:Eu²⁺, BaP₂N₄:Eu²⁺, and BaSr₂P₆N₁₂:Eu²⁺", *Chem. Eur. J.* **2015**, 21, 6443-6448.
- [4] F. J. Pucher, S. R. Römer, F. W. Karau, W. Schnick, "Phenakite-Type BeP₂N₄ - A Possible Precursor for a New Hard Spinel-Type Material", *Chem. Eur. J.* **2010**, 16, 7208-7214.
- [5] S. J. Sedlmaier, J. Schmedt auf der Günne, W. Schnick, "Sr₃P₆O₆N₈ - a highly condensed layered phosphate", *Dalton Trans.* **2009**, 4081-4084.
- [6] S. J. Sedlmaier, E. Mugnaioli, O. Oeckler, U. Kolb, W. Schnick, "SrP₃N₅O: A Highly Condensed Layer Phosphate Structure Solved from a Nanocrystal by Automated Electron Diffraction Tomography", *Chem. Eur. J.* **2011**, 17, 11258-11265.
- [7] A. Marchuk, V. R. Celinski, J. Schmedt auf der Günne, W. Schnick, "MH₄P₆N₁₂ (M = Mg, Ca): New Imidonitridophosphates with an Unprecedented Layered Network Structure Type", *Chem. Eur. J.* **2015**, 21, 5836-5842.
- [8] A. Marchuk, P. Schultz, C. Hoch, O. Oeckler, W. Schnick, "M₂PO₃N (M = Ca, Sr): ortho-Oxonitridophosphates with β-K₂SO₄ Structure Type", *Inorg. Chem.* **2016**, 55, 974-982.
- [9] S. Vogel, W. Schnick, "SrP₃N₅NH: A Framework-Type Imidonitridophosphate Featuring Structure-Directing Hydrogen Bonds", *Chem. Eur. J.* **2018**, 24, 14275-14281.
- [10] E.-M. Bertschler, C. Dietrich, J. Janek, W. Schnick, "Li₁₈P₆N₁₆ - A Lithium Nitridophosphate with Unprecedented Tricyclic [P₆N₁₆]¹⁸⁻ Ions", *Chem. Eur. J.* **2017**, 23, 2185-2191.
- [11] E.-M. Bertschler, C. Dietrich, T. Leichtweiß, J. Janek, W. Schnick, "Li⁺ Ion Conductors with Adamantane-Type Nitridophosphate Anions β-Li₁₀P₄N₁₀ and Li₁₃P₄N₁₀X₃ with X = Cl, Br", *Chem. Eur. J.* **2018**, 24, 196-205.
- [12] E.-M. Bertschler, R. Niklaus, W. Schnick, "Li₁₂P₃N₉ with Non-Condensed [P₃N₉]¹²⁻-Rings and its High-Pressure Polymorph Li₄PN₃ with Infinite Chains of PN⁴⁻ Tetrahedra", *Chem. Eur. J.* **2017**, 23, 9592-9599.
- [13] E.-M. Bertschler, R. Niklaus, W. Schnick, "Reversible Polymerization of Adamantane-type [P₄N₁₀]¹⁰⁻ Anions to Honeycomb-type [P₂N₅]⁵⁻ Layers under High-Pressure", *Chem. Eur. J.* **2018**, 24, 736-742.

- [14] A. Marchuk, L. Neudert, O. Oeckler, W. Schnick, "*CaMg₂P₆O₃N₁₀ – A Quinary Oxonitridophosphate with an Unprecedented Tetrahedra Network Structure Type*", *Eur. J. Inorg. Chem.* **2014**, 2014, 3427-3434.
- [15] W. Schnick, U. Berger, "*Li₁₀P₄N₁₀ - A Lithium Phosphorus(V) Nitride with the Novel Complex Anion P₄N₁₀¹⁰⁻*", *Angew. Chem. Int. Ed. Engl.* **1991**, 30, 830-831; *Angew. Chem.* **1991**, 103, 857-858.
- [16] W. Schnick, J. Lücke, "*On Lithium Phosphorus Nitride. Preparation and Refinement of the Crystal Structure of LiPN₂*", *Z. Anorg. Allg. Chem.* **1990**, 588, 19-25.
- [17] W. Schnick, J. Luecke, "*Synthesis and crystal structure of lithium phosphorus nitride Li₇PN₄: The first compound containing isolated PN₄-tetrahedra*", *J. Solid State Chem.* **1990**, 87, 101-106.
- [18] S. D. Kloß, L. Neudert, M. Döblinger, M. Nentwig, O. Oeckler, W. Schnick, "*Puzzling Intergrowth in Cerium Nitridophosphate Unraveled by Joint Venture of Aberration-Corrected Scanning Transmission Electron Microscopy and Synchrotron Diffraction*", *J. Am. Chem. Soc.* **2017**, 139, 12724-12735.
- [19] S. D. Kloß, W. Schnick, "*Rare-Earth-Metal Nitridophosphates through High-Pressure Metathesis*", *Angew. Chem. Int. Ed.* **2015**, 54, 11250-11253; *Angew. Chem.* **2015**, 127, 11402-11405.
- [20] S. D. Kloß, W. Schnick, "*LiPr₂P₄N₇O₃: Structural Diversity of Oxonitridophosphates Accessed by High-Pressure Metathesis*", *Inorg. Chem.* **2018**, 57, 4189-4195.
- [21] S. D. Kloß, N. Weidmann, R. Niklaus, W. Schnick, "*High-Pressure Synthesis of Melilite-type Rare-Earth Nitridophosphates RE₂P₃N₇ and a Ba₂Cu[Si₂O₇]-type Polymorph*", *Inorg. Chem.* **2016**, 55, 9400-9409.
- [22] S. D. Kloß, N. Weidmann, W. Schnick, "*Antiperovskite Nitridophosphate Oxide Ho₃[PN₄]O by High-Pressure Metathesis*", *Eur. J. Inorg. Chem.* **2017**, 2017, 1930-1937.
- [23] S. D. Kloß, O. Janka, T. Block, R. Pöttgen, R. Glaum, W. Schnick, "*Open-Shell 3d Transition Metal Nitridophosphates M^{II}P₈N₁₄ (M^{II} = Fe, Co, Ni) by High-Pressure Metathesis*", *Angew. Chem. Int. Ed.* **2019**, 58, 4685-4689; *Angew. Chem.* **2019**, 131, 4733-4737.
- [24] S. D. Kloß, S. Wandelt, A. Weis, W. Schnick, "*Accessing Tetravalent Transition-Metal Nitridophosphates through High-Pressure Metathesis*", *Angew. Chem. Int. Ed.* **2018**, 57, 3192-3195; *Angew. Chem.* **2018**, 130, 3246-3249.
- [25] F. J. Pucher, F. Hummel, W. Schnick, "*CuPN₂: Synthesis, Crystal Structure, and Electronic Properties*", *Eur. J. Inorg. Chem.* **2015**, 2015, 1886-1891.
- [26] F. J. Pucher, F. W. Karau, J. Schmedt auf der Günne, W. Schnick, "*CdP₂N₄ and MnP₂N₄ – Ternary Transition-Metal Nitridophosphates*", *Eur. J. Inorg. Chem.* **2016**, 2016, 1497-1502.

- [27] A. Marchuk, W. Schnick, "*Ba₃P₅N₁₀Br:Eu²⁺: A Natural-White-Light Single Emitter with a Zeolite Structure Type*", *Angew. Chem. Int. Ed.* **2015**, *54*, 2383-2387; *Angew. Chem.* **2015**, *127*, 2413-2417.
- [28] A. Marchuk, S. Wendl, N. Imamovic, F. Tambornino, D. Wiechert, P. J. Schmidt, W. Schnick, "*Nontypical Luminescence Properties and Structural Relation of Ba₃P₅N₁₀X:Eu²⁺ (X = Cl, I): Nitridophosphate Halides with Zeolite-like Structure*", *Chem. Mater.* **2015**, *27*, 6432-6441.
- [29] Y. Q. Li, J. E. J. van Steen, J. W. H. van Krevel, G. Botty, A. C. A. Delsing, F. J. DiSalvo, G. de With, H. T. Hintzen, "*Luminescence properties of red-emitting M₂Si₅N₈:Eu²⁺ (M = Ca, Sr, Ba) LED conversion phosphors*", *J. Alloys Compd.* **2006**, *417*, 273-279.
- [30] H. S. Kim, K.-i. Machida, T. Horikawa, H. Hanzawa, "*Luminescence properties of CaAlSiN₃:Eu²⁺ phosphor prepared by direct-nitriding method using fine metal hydride powders*", *J. Alloys Compd.* **2015**, *633*, 97-103.
- [31] K. Uhedaa, N. Hirotsaki, Y. Yamamoto, A. Naito, T. Nakajima, H. Yamamoto, "*Luminescence Properties of a Red Phosphor, CaAlSiN₃:Eu²⁺, for White Light-Emitting Diodes*", *Electrochem. Solid-State Lett.* **2006**, *9*, H22-H25.
- [32] G. Blasse, A. Bril, "*A New Phosphor for Flying-Spot Cathode-Ray Tubes for Color Television: Yellow-Emitting Y₃Al₅O₁₂-Ce³⁺*", *Appl. Phys. Lett.* **1967**, *11*, 53-55.
- [33] P. Pust, V. Weiler, C. Hecht, A. Tücks, A. S. Wochnik, A.-K. Henß, D. Wiechert, C. Scheu, P. J. Schmidt, W. Schnick, "*Narrow-band red-emitting Sr[LiAl₃N₄]:Eu²⁺ as a next-generation LED-phosphor material*", *Nat. Mater.* **2014**, *13*, 891-896.
- [34] S. D. Kloß, W. Schnick, "*Nitridophosphates – A Success Story of Nitride Synthesis*", *Angew. Chem. Int. Ed.* **2019**, *58*, 7933-7944; *Angew. Chem.* **2019**, *131*, 8015-8027.
- [35] G. Lagaly, K. Beneke, "*Intercalation and exchange reactions of clay minerals and non-clay layer compounds*", *Colloid. Polym. Sci.* **1991**, *269*, 1198-1211.
- [36] A. Weiss, "*Über das Kationenaustauschvermögen der Tonminerale. II. Der Kationenaustausch bei den Mineralen der Glimmer-, Vermikulit- und Montmorillonitgruppe*", *Z. Anorg. Allg. Chem.* **1958**, *297*, 257-286.
- [37] A. Weiss, "*Über das Kationenaustauschvermögen der Tonminerale. III. Der Kationenaustausch bei Kaolinit*", *Z. Anorg. Allg. Chem.* **1959**, *299*, 92-120.
- [38] W. Schnick, J. Lücke, "*Zn₇[P₁₂N₂₄]Cl₂ - A Sodalite with a Phosphorus Nitrogen Framework*", *Angew. Chem. Int. Ed. Engl.* **1992**, *31*, 213-215; *Angew. Chem.* **1992**, *104*, 208-209.
- [39] W. Schnick, J. Lücke, "*Nitrido-Sodalithe. I Synthesis, Crystal Structure, and Properties of Zn_{7-x}H_{2x}[P₁₂N₂₄]Cl, with 0 ≤ x ≤ 3*", *Z. Anorg. Allg. Chem.* **1994**, *620*, 2014-2019.
- [40] P. Bielec, L. Eisenburger, H. L. Deubner, D. Günther, F. Kraus, O. Oeckler, W. Schnick, "*Targeting Vacancies in Nitridosilicates: Aliovalent Substitution of M²⁺ (M = Ca, Sr) by Sc³⁺ and U³⁺*", *Angew. Chem. Int. Ed.* **2019**, *58*, 840-843; *Angew. Chem.* **2019**, *131*, 850-853.

- [41] P. Bielec, O. Janka, T. Block, R. Pöttgen, W. Schnick, "*Fe₂Si₅N₈: Access to Open-Shell Transition-Metal Nitridosilicates*", *Angew. Chem. Int. Ed.* **2018**, *57*, 2409-2412; *Angew. Chem.* **2018**, *130*, 2433-2436.
- [42] P. Bielec, R. Nelson, R. P. Stoffel, L. Eisenburger, D. Günther, A.-K. Henß, J. P. Wright, O. Oeckler, R. Dronskowski, W. Schnick, "*Cationic Pb₂ Dumbbells Stabilized in the Highly Covalent Lead Nitridosilicate Pb₂Si₅N₈*", *Angew. Chem. Int. Ed.* **2019**, *58*, 1432-1436; *Angew. Chem.* **2019**, *131*, 1446-1450.
- [43] P. Bielec, W. Schnick, "*Increased Synthetic Control - Gaining Access to Predicted Mg₂Si₅N₈ and β-Ca₂Si₅N₈*", *Angew. Chem. Int. Ed.* **2017**, *56*, 4810-4813; *Angew. Chem.* **2017**, *129*, 4888-4891.
- [44] H. Jacobs, R. Nymwegen, "*Synthesis and Crystal Structure of a Potassium Nitridophosphate, K₃P₆N₁₁*", *Z. Anorg. Allg. Chem.* **1997**, *623*, 429-433.
- [45] M. Mallmann, C. Maak, R. Niklaus, W. Schnick, "*Ammonothermal Synthesis, Optical Properties, and DFT Calculations of Mg₂PN₃ and Zn₂PN₃*", *Chem. Eur. J.* **2018**, *24*, 13963-13970.
- [46] J. M. Sullivan, "*Ammoniated phosphonitrilic amides, imides, and nitrides. I. The equilibrium 4 NH₃(g) + 2 P(r) = 2 PN₂H(s) + 5 H₂(g)*", *Inorg. Chem.* **1976**, *15*, 1055-1059.
- [47] A. G. Padalko, V. A. Baklan, "*Transformation in Metal Materials during Hot Isostatic Pressing*", *Inorg. Mater.* **2012**, *48*, 1226-1242.
- [48] K. Tsukuma, "*Transparent MgAl₂O₄ Spinel Ceramics Produced by HIP Post-Sintering*", *J. Ceram. Soc. Jpn.* **2006**, *114*, 802-806.
- [49] K. Tsukuma, I. Yamashita, T. Kusunose, "*Transparent 8 mol% Y₂O₃-ZrO₂ (8Y) Ceramics*", *J. Am. Ceram. Soc.* **2008**, *91*, 813-818.
- [50] H. Watanabe, M. Imai, N. Kijima, "*Nitridation of AEAlSi for Production of AEAlSiN₃:Eu²⁺ Nitride Phosphors (AE = Ca, Sr)*", *J. Am. Ceram. Soc.* **2009**, *92*, 641-648.
- [51] H. Watanabe, N. Kijima, "*Synthesis of Sr_{0.99}Eu_{0.01}AlSiN₃ from intermetallic precursor*", *J. Ceram. Soc. Jpn.* **2009**, *117*, 115-119.
- [52] Z. Xiao, S. Yu, Y. Li, S. Ruan, L. B. Kong, Q. Huang, Z. Huang, K. Zhou, H. Su, Z. Yao, W. Que, Y. Liu, T. Zhang, J. Wang, P. Liu, D. Shen, M. Allix, J. Zhang, D. Tang, "*Materials development and potential applications of transparent ceramics: A review*", *Mater. Sci. Eng. R Rep.* **2020**, *139*, 100518.
- [53] S. Vogel, A. T. Buda, W. Schnick, "*United in Nitride: The Highly Condensed Boron Phosphorus Nitride BP₃N₆*", *Angew. Chem. Int. Ed.* **2018**, *57*, 13202-13202; *Angew. Chem.* **2018**, *130*, 13386-13389.
- [54] J. Häusler, W. Schnick, "*Ammonothermal Synthesis of Nitrides: Recent Developments and Future Perspectives*", *Chem. Eur. J.* **2018**, *24*, 11864-11879.

A Supporting Information for Chapter 2

A.1 Results and Discussions

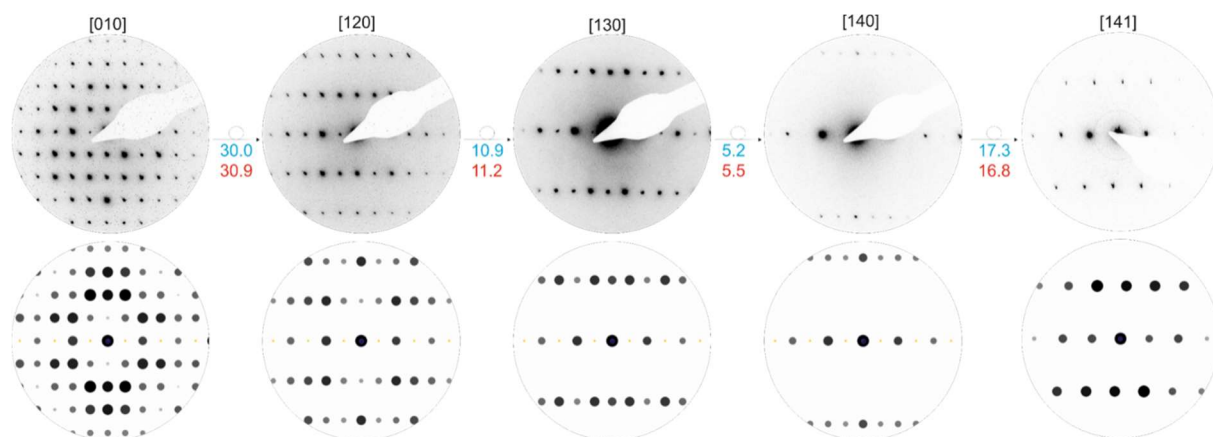


Figure A1. Measured (top) and simulated (bottom) selected area electron diffraction (SAED) patterns of the investigated crystallite.

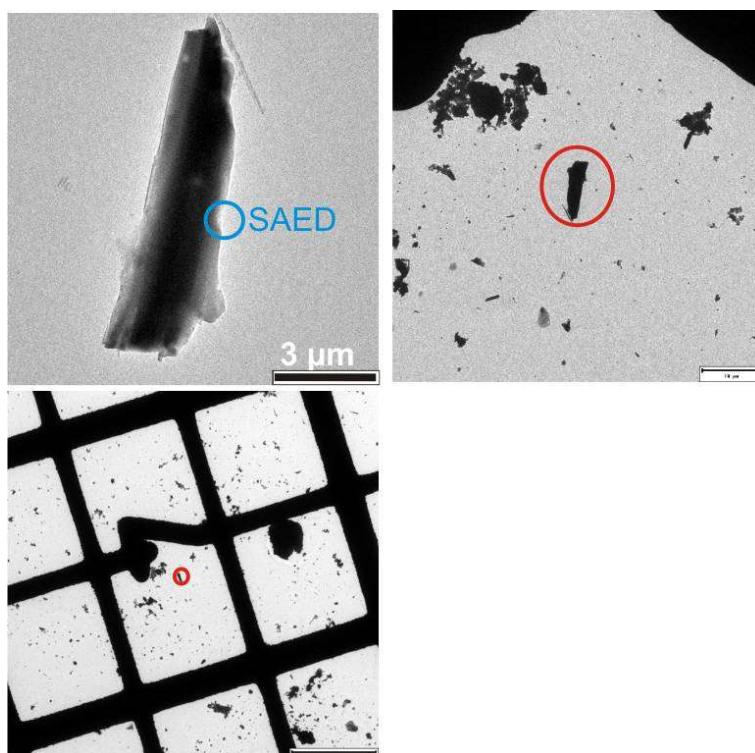


Figure A2. Position of the investigated crystallite on the finder grid.

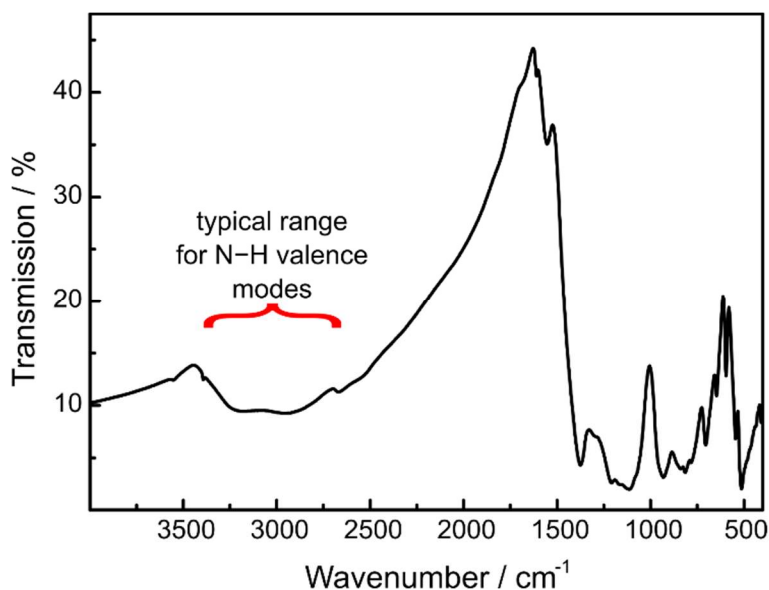


Figure A3. FTIR spectrum of BaP₆N₁₀NH, measured using the KBr pellet method. A significant vibration attributed to the N–H valence mode can be seen between 2700 and 3400 cm⁻¹.

Table A1. Crystallographic data of the single-crystal refinement of BaP₆N₁₀NH.

Formula	BaP ₆ N ₁₀ NH
Formula weight / g·mol ⁻¹	478.28
Crystal system; space group	hexagonal; <i>P</i> 6 ₃ (no. 173)
Lattice parameters / Å ^[a,b]	<i>a</i> = 7.5585(1) <i>c</i> = 8.5106(1)
Cell volume / Å ^{3[a]}	421.08(1)
Formula units per unit cell	2
Density / g·cm ⁻³	3.764
μ / mm ⁻¹	2.808
Diffractometer	ESRF beamline ID11
Radiation	synchrotron, $\lambda = 0.30996$ Å
2 θ -range / °	1.712 ≤ θ ≤ 14.966
Total number of reflections	3929
No. of independent reflections	1264
Observed reflections ($F^2 > 2\sigma(F^2)$)	1246
R_{int} , R_{σ}	0.032; 0.056
Refined parameters	56
Goodness of fit (χ^2)	0.927
$R1$ (all data); $R1$ ($F^2 > 2\sigma(F^2)$)	0.023; 0.023
$wR2$ (all data); $wR2$ ($F^2 > 2\sigma(F^2)$)	0.056; 0.056
$\Delta\rho_{\text{max}}$; $\Delta\rho_{\text{min}}$ / e·Å ⁻³	1.526; -0.869

Table A2. Atomic coordinates, crystallographic positions, and equivalent isotropic displacement parameters (\AA^2) of $\text{BaP}_6\text{N}_{10}\text{NH}$.

Atom	Wyckoff	<i>x</i>	<i>y</i>	<i>z</i>	U_{eq}
Ba1	2b	1/3	2/3	0.32488(5)	0.01877(10)
P1	6c	0.15059(10)	0.26065(9)	0.02807(7)	0.00817(12)
P2	6c	0.40609(9)	0.17513(10)	0.20595(6)	0.00695(12)
N1	6c	0.2929(3)	0.3026(3)	0.1813(2)	0.0092(3)
N2	6c	0.3467(3)	0.0088(3)	0.0655(2)	0.0091(3)
N3	6c	0.3734(3)	0.0801(3)	0.3791(2)	0.0095(3)
N4	2b	1/3	2/3	0.6784(5)	0.0078(5)
N5	2a	0	0	0.0000(4)	0.0093(5)

Table A3. Anisotropic displacement parameters of $\text{BaP}_6\text{N}_{10}\text{NH}$ (\AA^2).

Atom	U_{11}	U_{22}	U_{33}	U_{12}	U_{13}	U_{23}
Ba1	0.01962(11)	0.01962(11)	0.01706(12)	0.00981(6)	0.00000	0.00000
P1	0.0084(2)	0.0081(2)	0.0079(2)	0.0040(2)	-0.0009(2)	-0.0000(2)
P2	0.0067(2)	0.0073(2)	0.0068(2)	0.0034(2)	-0.0002(2)	0.0001(2)
N1	0.0099(7)	0.0104(7)	0.0085(5)	0.0060(6)	-0.0017(6)	-0.0009(5)
N2	0.0072(7)	0.0099(7)	0.0086(5)	0.0030(6)	-0.0005(5)	-0.0026(6)
N3	0.0120(7)	0.0118(7)	0.0069(6)	0.0076(6)	0.0028(6)	0.0021(6)
N4	0.0065(7)	0.0065(7)	0.0106(11)	0.0032(4)	0.00000	0.00000
N5	0.0076(7)	0.0076(7)	0.0129(12)	0.0038(3)	0.00000	0.00000

Table A4. Crystallographic data of the Rietveld refinement of BaP₆N₁₀NH.

Formula	BaP₆N₁₀NH
Formula weight / g·mol ⁻¹	478.28
Crystal system; space group	hexagonal; <i>P</i> 6 ₃ (no. 173)
Lattice parameters / Å ^[a]	<i>a</i> = 7.5585(1) <i>c</i> = 8.5106(1)
Cell volume / Å ³ [a]	421.07(1)
Formula units per unit cell	2
Density / g·cm ⁻³	3.764
μ / mm ⁻¹	4.999
Diffractometer	Stoe Stadi P
Radiation	Mo _{Kα} (λ = 0.71073 Å)
Detector	Mythen 1K
Monochromator	Ge(111)
2 θ -range / °	3.0 ≤ 2 θ ≤ 56.3
Step width / °	0.015
Data points	3552
Total number of reflections	281
Refined parameters	47
Background function	Shifted Chebyshev
Number of background parameters	14
Goodness of fit (χ^2)	1.979
<i>R</i> _p ; <i>R</i> _{wp}	0.038; 0.051
<i>R</i> _{exp} ; <i>R</i> _{Bragg}	0.026; 0.015

Table A5. EDX measurements of BaP₆N₁₀NH.

EDX point / atom %	Ba	P	N	O
1	5.9	35.9	58.2	-
2	6.4	36.3	57.3	-
3	4.7	28.8	64.5	2.0
4	6.7	38.0	53.6	1.7
5	4.5	25.8	66.3	3.4
6	6.5	28.3	62.9	2.3
7	5.6	33.5	60.9	-
8	6.0	34.0	60.0	-
9	5.0	33.1	59.1	2.8
10	6.2	35.9	57.9	-
Measured atom %	5.7	33.0	60.1	1.2
Calculated atom %	5.6	33.3	61.1	-

Table A6. CHNS analysis of BaP₆N₁₀NH.

Element	C	H	N	S
Measured weight %	-	0.37	32.07	-
Calculated weight %	-	0.20	32.22	-

Table A7. Interatomic distances (Å) and bond angles (°) in the structure of BaP₆N₁₀NH.

Ba1-	N1	2.884(3)	N3	-P1-	N2	112.9(1)
Ba1-	N1	2.884(2)	N3	-P1-	N1	109.2(1)
Ba1-	N1	2.884(2)	N3	-P1-	N5	112.4(1)
Ba1-	N4	3.009(4)	N2	-P1-	N1	108.3(1)
Ba1-	N3	3.021(2)	N2	-P1-	N5	104.7(1)
Ba1-	N3	3.021(2)	N1	-P1-	N5	109.2(1)
Ba1-	N3	3.021(3)	N1	-P2-	N3	112.6(1)
Ba1-	N2	3.182(2)	N1	-P2-	N2	110.3(1)
Ba1-	N2	3.182(2)	N1	-P2-	N4	109.5(1)
Ba1-	N2	3.182(2)	N3	-P2-	N2	114.1(1)
Ba1-	N2	3.363(2)	N3	-P2-	N4	107.5(1)
Ba1-	N2	3.363(2)	N2	-P2-	N4	102.3(1)
Ba1-	N2	3.363(2)	P2	-N1-	P1	119.6(1)
P1-	N3	1.606(2)	P1	-N2-	P2	119.8(1)
P1-	N2	1.612(3)	P2	-N3-	P1	129.5(1)
P1-	N1	1.618(2)	P2	-N4-	P2	118.2(1)
P1-	N5	1.730(1)	P1	-N5-	P1	118.1(1)
P2-	N1	1.590(3)				
P2-	N3	1.603(2)				
P2-	N2	1.627(2)				
P2-	N4	1.735(1)				

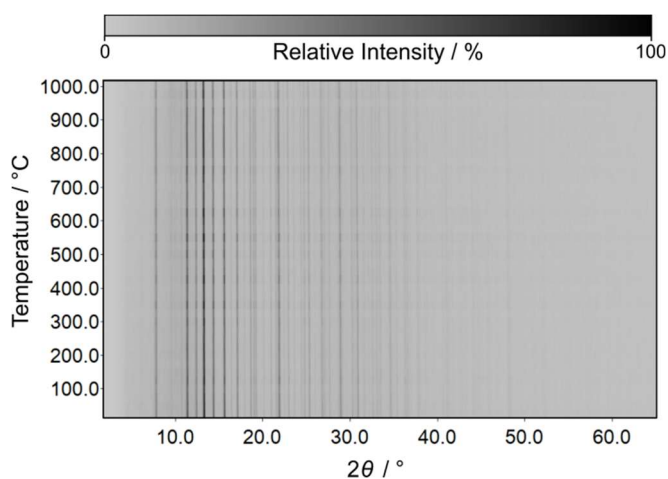


Figure A4. Temperature-dependent powder X-ray diffraction pattern (Mo-K α radiation, $\lambda = 0.71073 \text{ \AA}$) of BaP₆N₁₀NH measured under Ar atmosphere showing a liminal thermal expansion with increasing temperature.

Table A8. Determined values for a , c , and V from Rietveld refinements of BaP₆N₁₀NH at selected temperatures.

Temperature / °C	$a / \text{\AA}$	$c / \text{\AA}$	$V / \text{\AA}^3$
25	7.5821(3)	8.5378(4)	425.06(4)
250	7.5930(3)	8.5453(5)	426.66(4)
500	7.6062(3)	8.5576(5)	428.77(4)
750	7.6221(3)	8.5719(5)	431.27(4)
1000	7.6398(6)	8.5909(7)	434.24(7)

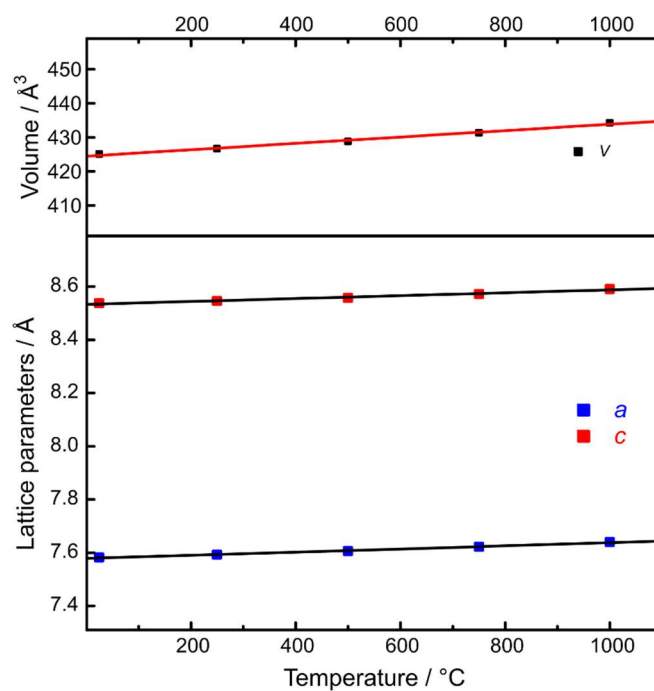


Figure A5. Temperature-dependent evolution of lattice parameters and volume of BaP₆N₁₀NH.

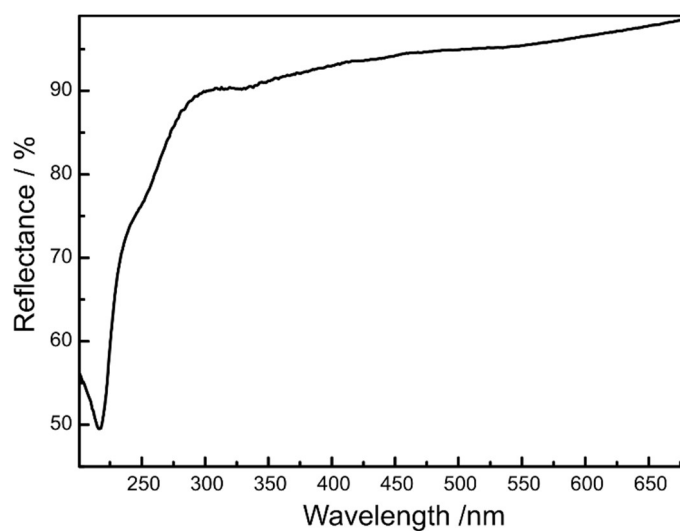


Figure A6. Diffuse reflectance spectrum of BaP₆N₁₀NH.

Table A9. Weighed portions of the starting materials used for the synthesis of BaP₆N₁₀NH.

Compound	Starting material	Amount
BaP ₆ N ₁₀ NH	P ₃ N ₅	23.85 mg
	NH ₄ Cl	3.91 mg
	Ba(N ₃) ₂	21.87 mg

A.2 Author Contributions

S.W.: Conceptualization: Lead; Formal analysis: Lead; Investigation: Lead; Validation: Lead; Visualization: Lead; Writing - Original Draft: Lead; Writing - Review & Editing: Lead

L.E.: Formal analysis: Supporting ; Investigation: Supporting; Validation: Supporting ; Visualization: Supporting ; Writing - Original Draft: Supporting ; Writing - Review & Editing: Supporting

M.Z.: Formal analysis: Supporting; Investigation: Supporting

D.G.: Investigation: Supporting; Writing - Review & Editing: Supporting

J.W.: Investigation: Supporting; Methodology: Supporting

P.S.: Investigation: Supporting; Methodology: Supporting ; Supervision: Supporting; Validation: Supporting; Writing -Review & Editing: Supporting

O.O.: Conceptualization: Supporting; Formal analysis: Supporting ; Funding acquisition : Supporting; Investigation: Supporting; Methodology: Supporting; Project administration: Supporting; Resources: Supporting; Supervision: Support-ing; Validation: Supporting; Writing - Review & Editing: Supporting

W.S.: Conceptualization: Lead; Funding acquisition: Lead; Project administration: Lead; Resources: Lead; Supervi-sion: Lead; Validation: Equal; Writing - Review & Editing: Equal

B Supporting Information for Chapter 3

B.1 Results and Discussions

Table B1. Wyckoff positions, atomic coordinates, and isotropic displacement parameters (\AA^2) of $\text{CaP}_8\text{N}_{14}$ obtained from Rietveld refinement.

Atom	Wyckoff	x	y	z	U_{iso}
Ca1	4a	0	0	0	1.09(6)
P1	16h	0.3267(2)	0.0141(4)	0.08576(6)	1.00(3)
P2	16h	0.1656(2)	0.2052(4)	0.18838(6)	$= U_{\text{iso}}(\text{P1})$
N1	16h	0.2027(4)	0.4998(9)	0.15745(17)	0.20(5)
N2	8f	0	0.0917(9)	0.1714(2)	$= U_{\text{iso}}(\text{N1})$
N3	8f	0	0.6218(10)	0.0707(2)	$= U_{\text{iso}}(\text{N1})$
N4	16h	0.1986(4)	0.2211(10)	0.0630(1)	$= U_{\text{iso}}(\text{N1})$
N5	8g	0.2146(5)	0.242(1)	1/4	$= U_{\text{iso}}(\text{N1})$

Table B2. Wyckoff positions, atomic coordinates, and isotropic displacement parameters (\AA^2) of $\text{SrP}_8\text{N}_{14}$ obtained from Rietveld refinement.

Atom	Wyckoff	x	y	z	U_{iso}
Sr1	4a	0	0	0	1.27(8)
P1	16h	0.3266(4)	0.0241(8)	0.0891(2)	1.06(7)
P2	16h	0.1663(4)	0.2172(7)	0.1886(2)	$= U_{\text{iso}}(\text{P1})$
N1	16h	0.2930(9)	0.011(3)	0.1587(4)	0.39(12)
N2	8f	0	0.128(3)	0.1719(5)	$= U_{\text{iso}}(\text{N1})$
N3	8f	0	0.622(3)	0.0766(5)	$= U_{\text{iso}}(\text{N1})$
N4	16h	0.208(1)	0.238(3)	0.0664(4)	$= U_{\text{iso}}(\text{N1})$
N5	8g	0.208(1)	0.256(4)	1/4	$= U_{\text{iso}}(\text{N1})$

Table B3. Crystallographic data of the Rietveld refinement for AEP_8N_{14} ($AE = Ca, Sr$).

Formula	CaP_8N_{14}	SrP_8N_{14}
Formula weight / $g \cdot mol^{-1}$	483.96	531.50
Crystal system; space group	orthorhombic; $Cmcm$ (no. 63)	
Lattice parameters / Å	$a = 8.5328(3)$	$a = 8.5979(3)$
	$b = 5.0794(2)$	$b = 5.1129(2)$
	$c = 23.9516(8)$	$c = 24.4073(8)$
Cell volume / Å ³	1038.10(6)	1072.95(7)
Formula units per unit cell	4	
Density / $g \cdot cm^{-3}$	3.096	3.290
μ / mm^{-1}	17.221	18.566
Diffractometer	Stoe Stadi P	
Radiation	Cu- $K_{\alpha 1}$ ($\lambda = 1.5406$ Å)	
Detector	Mythen 1K	
Monochromator	Ge(111)	
θ -range / °	$2.5 \leq \theta \leq 46.2$	$2.5 \leq \theta \leq 46.2$
Data points	5829	5829
Total number of reflections	257	266
Refined parameters	67	51
Background function	Shifted Chebyshev	
Number of background parameters	24	12
Goodness of fit (χ^2)	1.618	0.889
$R_p; R_{wp}$	0.026; 0.035	0.105; 0.142
$R_{exp}; R_{Bragg}$	0.022; 0.012	0.160; 0.023

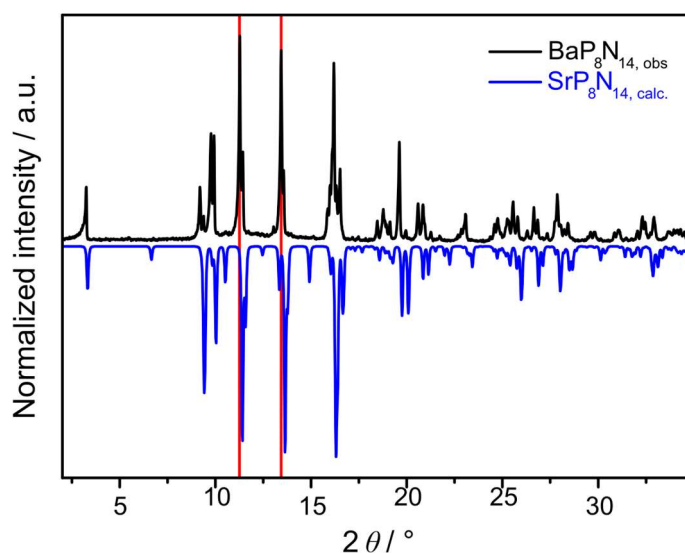


Figure B1. Observed powder X-ray diffraction pattern of BaP_8N_{14} (top, black) and simulated powder X-ray diffraction pattern of SrP_8N_{14} (bottom, blue). A shift to lower diffraction angles, is indicated for BaP_8N_{14} by vertical red lines. At first glance, the X-ray diffraction patterns show some similarities; however, a Rietveld refinement based on the structure model of SrP_8N_{14} was not successful for the pattern of BaP_8N_{14} .

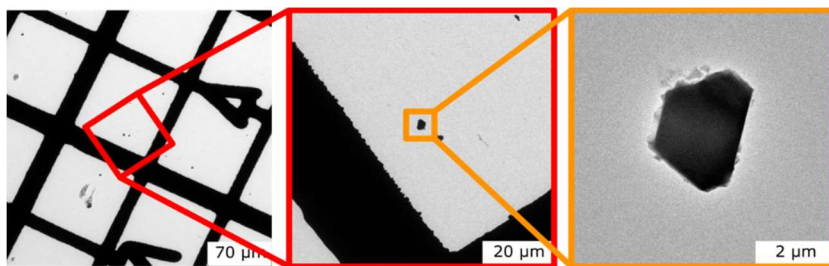


Figure B2. Investigated crystallite of BaP₈N₁₄ and its location on a TEM finder grid.

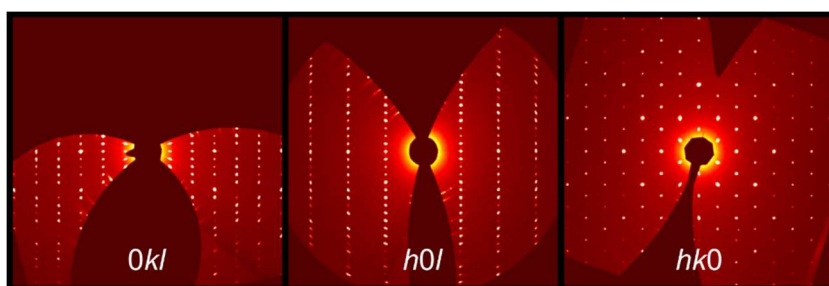


Figure B3. Reconstructed reciprocal layer sections for BaP₈N₁₄.

Table B4. Crystallographic data of the single-crystal refinement of BaP₈N₁₄.

Formula	BaP ₈ N ₁₄
Formula weight / g·mol ⁻¹	581.24
Crystal system; space group	orthorhombic; <i>Amm</i> 2 (no. 38)
Lattice parameters / Å ^[a]	$a = 12.4862(7)$ $b = 8.6648(3)$ $c = 5.1373(2)$
Cell volume / Å ³	555.81(4)
Formula units per unit cell	2
Density / g·cm ⁻³	3.473
μ / mm ⁻¹	2.163
Data collection	ESRF beamline ID11
Radiation	synchrotron, $\lambda = 0.30996$ Å
θ -range / °	$2.009 \leq \theta \leq 18.057$
Total number of reflections	2677
No. of independent reflections	1020
Observed reflections ($F^2 > 2\sigma(F^2)$)	1002
R_{int} , R_{σ}	0.0239, 0.0422
Refined parameters	60
Goodness of fit (χ^2)	1.068
$R1$ (all data); $R1$ ($F^2 > 2\sigma(F^2)$)	0.0228; 0.0224
$wR2$ (all data); $wR2$ ($F^2 > 2\sigma(F^2)$)	0.0560; 0.0559
$\Delta\rho_{\text{max}}$; $\Delta\rho_{\text{min}}$ / e·Å ⁻³	0.994; -1.285

[a] The lattice parameters were used as determined from powder data (Table B7).

Table B5. Atomic coordinates, crystallographic positions, and equivalent displacement parameters (in Å²) of BaP₈N₁₄.

Atom	Wyckoff	x	y	z	$U_{eq.}$
Ba1	2a	0	0	0.00000(7)	0.01038(12)
P1	8f	0.18634(9)	0.32695(9)	0.02530(18)	0.0068(2)
P2	8f	0.38048(9)	0.16545(10)	0.21888(17)	0.0071(2)
N1	8f	0.3213(2)	0.2915(3)	0.0065(8)	0.0077(5)
N2	4c	0.3437(5)	0	0.1286(8)	0.0107(9)
N3	4e	1/2	0.2056(6)	0.2487(9)	0.0124(8)
N4	4c	0.1599(5)	0	0.6089(8)	0.0089(8)
N5	8f	0.1384(3)	0.2127(3)	0.2437(6)	0.0090(5)

Table B6. Anisotropic displacement parameters of BaP₈N₁₄ (in Å²).

Atom	U_{11}	U_{22}	U_{33}	U_{12}	U_{13}	U_{23}
Ba1	0.0133(2)	0.0085(2)	0.0094(2)	0.00000	0.00000	0.00000
P1	0.0099(5)	0.0042(3)	0.0062(4)	0.0004(2)	0.0001(3)	0.0002(3)
P2	0.0103(5)	0.0056(3)	0.0053(3)	0.0004(3)	0.0006(3)	0.0001(2)
N1	0.010(2)	0.0075(9)	0.0055(9)	0.0010(8)	-0.001(1)	0.0008(12)
N2	0.019(3)	0.005(2)	0.009(2)	0.00000	-0.002(1)	0.00000
N3	0.009(2)	0.018(2)	0.010(2)	0.00000	0.00000	0.001(2)
N4	0.013(3)	0.007(2)	0.007(2)	0.00000	0.001(1)	0.00000
N5	0.013(2)	0.0079(12)	0.0057(11)	-0.0024(9)	-0.0003(9)	0.0017(10)

Table B7. Crystallographic data of the Rietveld refinement of BaP₈N₁₄.

Formula	BaP ₈ N ₁₄
Formula weight / g·mol ⁻¹	581.24
Crystal system; space group	orthorhombic; <i>Amm</i> 2 (no. 38)
Lattice parameters / Å	<i>a</i> = 12.4841(3) <i>b</i> = 8.6678(2) <i>c</i> = 5.1389(1)
Cell volume / Å ³	556.08(2)
Formula units per unit cell	2
Density / g·cm ⁻³	3.471
μ / mm ⁻¹	4.108
Diffractometer	Stoe Stadi P
Radiation	Mo-K α 1 (λ = 0.71073 Å)
Detector	Mythen 1K
Monochromator	Ge(111)
2 θ -range / °	2.0 \leq 2 θ \leq 56.3
Data points	3618
Total number of reflections	430
Refined parameters	60
Background function	Shifted Chebyshev
Number of background parameters	21
Goodness of fit (χ^2)	1.030
R_p ; R_{wp}	0.052; 0.068
R_{exp} ; R_{Bragg}	0.066; 0.020

Table B8. EDX (SEM) measurements of CaP₈N₁₄:Eu²⁺ (in atom-%).

Point	Ca	P	N	O	Eu
1	4	35	57	5	> 1
2	5	38	56	1	> 1
3	5	40	53	1	> 1
Average	5(1)	38(3)	55(2)	2(2)	-
Calculated for CaP ₈ N ₁₄	4.3	34.8	60.9	-	-

Table B9. EDX (SEM) measurements of $\text{SrP}_8\text{N}_{14}:\text{Eu}^{2+}$ (in atom-%).

Point	Sr	P	N	O	Eu
1	4	37	57	1	> 1
2	5	36	53	6	> 1
3	4	31	57	8	> 1
Average	4(1)	35(3)	56(2)	5(4)	-
Calculated	4.3	34.8	60.9	-	-

Table B10. EDX (SEM) measurements of $\text{BaP}_8\text{N}_{14}:\text{Eu}^{2+}$ (in atom-%).

Point	Ba	P	N	O	Eu
1	5	38	57	-	> 1
2	4	34	58	5	> 1
3	4	36	57	4	> 1
Average	4(1)	36(2)	57(1)	3(3)	-
Calculated	4.3	34.8	60.9	-	-

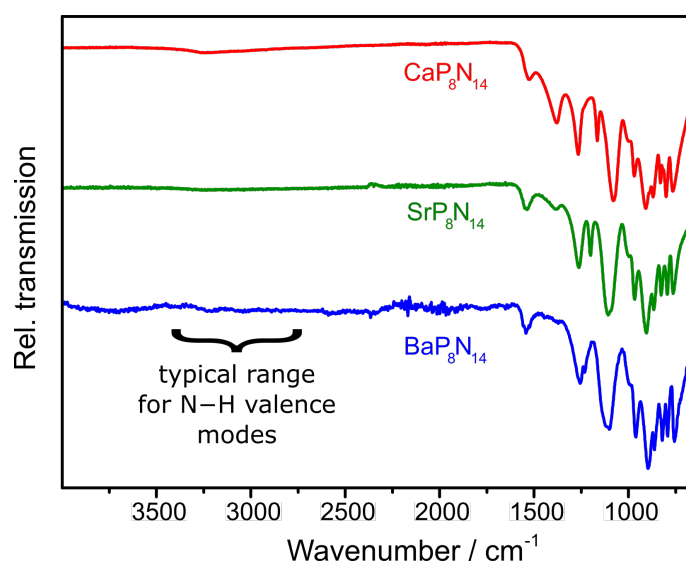


Figure B4. FTIR spectra of $\text{AEP}_8\text{N}_{14}$; $\text{CaP}_8\text{N}_{14}$ is displayed in red, $\text{SrP}_8\text{N}_{14}$ in green, and $\text{BaP}_8\text{N}_{14}$ in blue: no significant vibrations attributable to N–H valence modes can be seen between 2700 and 3400 cm^{-1} . The fingerprint region (600 to 1500 cm^{-1}) shows similar absorption bands for all compounds. These are typical for symmetric and asymmetric P–N–P stretching modes.

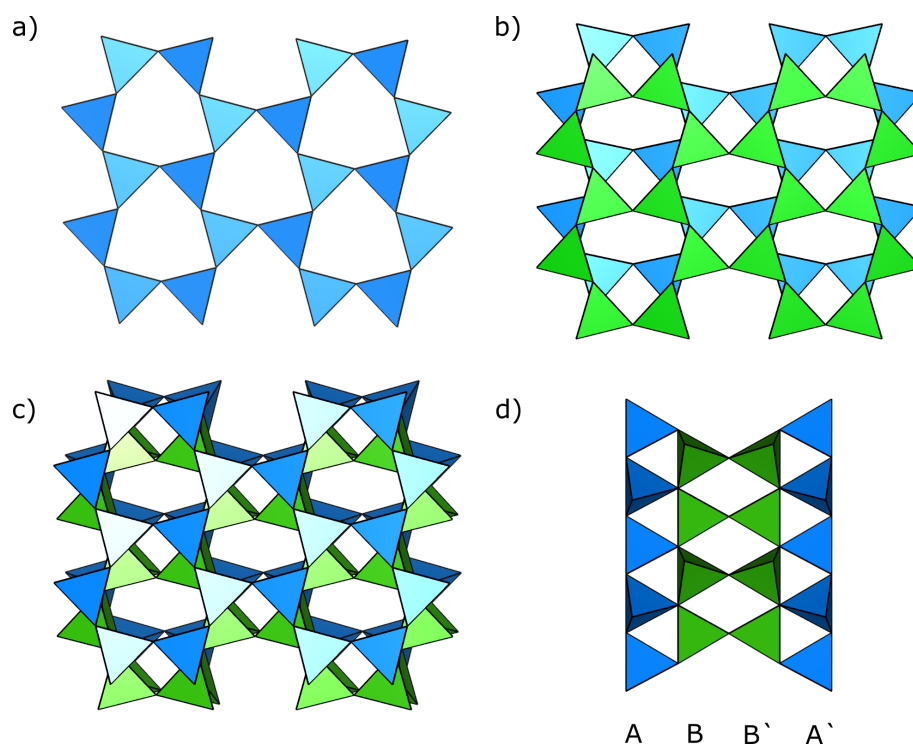


Figure B5. Illustration of the quadruple layers in AEP_8N_{14} ($AE = Ca, Sr, Ba$) formed by Q^4 -type (i.e. all-side vertex-sharing) PN_4 tetrahedra. These formally consist of four tetrahedra-layers, as shown for SrP_8N_{14} .^[1] The single layers consist of sechser rings forming honeycomb-like nets. The outer (blue) and inner (green) layers are related by a mirror plane according to the space groups $Cmcm$ and $Amm2$ ($ABB'A'$ stacking) **a)** projection of a single honeycomb-like layer formed by sechser rings; **b)** projection of two shifted layers; **c)** projection of a quadruple layer; **d)** illustration of the $ABB'A'$ stacking order.

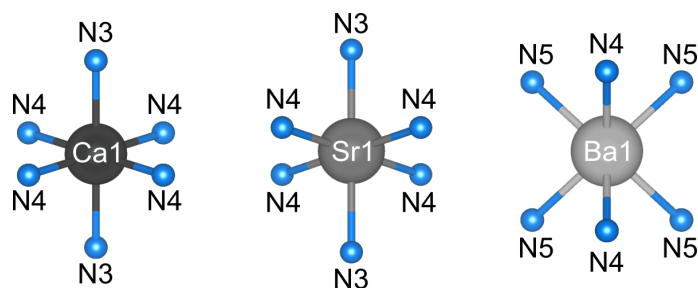


Figure B6. Coordination spheres of the alkaline earth cations. Ca^{2+} and Sr^{2+} are coordinated in form of a distorted octahedron; Ba^{2+} is located in the center of a distorted trigonal prism.

Table B11. Interatomic distances (Å) and bond angles (°) in the structure of CaP₈N₁₄.^[a]

Ca1–	N4	(4x)	2.532(4)	N4	-P1-	N4	113.6(3)
	N3	(2x)	2.561(5)	N4		N3	111.2(2)
P1–	N4		1.600(5)	N4		N1	106.2(2)
	N4		1.612(4)	N4		N3	108.9(1)
	N3		1.618(3)	N4		N1	105.3(2)
	N1		1.737(4)	N3		N1	111.5(1)
P2–	N5		1.546(2)	N5	-P2-	N2	122.2(1)
	N2		1.580(3)	N5		N1	105.0(2)
	N1		1.700(5)	N5		N1	108.2(2)
	N1		1.703(4)	N2		N1	112.0(1)
				N2		N1	104.7(1)
				N1		N1	103.1(2)
				P2	-N1-	P2	118.2(2)
				P2		P1	116.2(2)
				P2		P1	120.0(2)
				P2	-N2-	P2	126.9(1)
				P1	-N3-	P1	132.2(1)
				P1	-N4-	P1	125.7(3)
				P2	-N5-	P2	145.5(1)

[a] Standard deviations from Rietveld refinement are systematically underestimated, which is most likely due to the small step width (0.015°) during measurements.

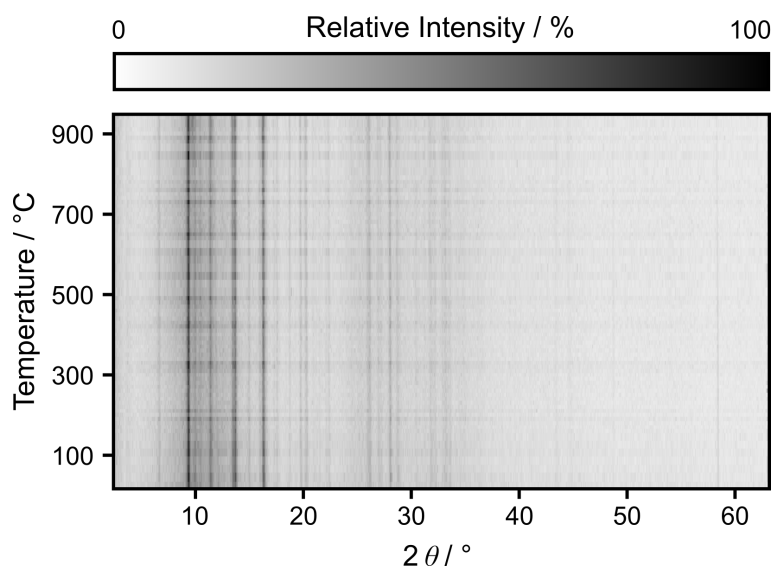
Table B12. Interatomic distances (Å) and bond angles (°) in the structure of SrP₈N₁₄.^[a]

Sr1–	N3	(2x)	2.689(1)	N4	-P1-	N4	113.0(7)
	N4	(4x)	2.705(1)	N4		N3	113.4(4)
P1–	N4		1.592(2)	N4		N1	106.0(5)
	N4		1.593(1)	N4		N3	108.3(4)
	N3		1.602(1)	N4		N1	105.2(5)
	N1		1.726(8)	N3		N1	110.8(3)
P2–	N5		1.553(5)	N5	-P2-	N2	120.2(2)
	N2		1.555(7)	N5		N1	110.5(3)
	N1		1.683(11)	N5		N1	104.7(3)
	N1		1.707(12)	N2		N1	107.3(3)
				N2		N1	109.5(4)
				N1		N1	103.5(6)
				P2	-N1-	P2	119.9(7)
				P2		P1	120.8(5)
				P2		P1	114.9(5)
				P2	-N2-	P2	133.6(2)
				P1	-N3-	P1	137.1(2)
				P1	-N4-	P1	129.1(8)
				P2	-N5-	P2	149.5(2)

[a] Standard deviations from Rietveld refinement are systematically underestimated, which is most likely due to the small step width (0.015°) during measurements.

Table B13. Interatomic distances (Å) and bond angles (°) in the structure of BaP₈N₁₄.

Ba1-	N5	(4x)	2.820(3)	N4	-P1-	N5	111.6(1)
	N4	(2x)	2.833(5)	N4		N5	108.3(1)
P1-	N4		1.594(2)	N4		N1	112.8(1)
	N5		1.603(3)	N5		N5	111.0(2)
	N5		1.612(3)	N5		N1	106.1(2)
	N1		1.716(3)	N5		N1	107.1(2)
P2-	N3		1.540(2)	N3	-P2-	N2	121.2(1)
	N2		1.575(2)	N3		N1	106.6(1)
	N1		1.694(4)	N3		N1	109.7(1)
	N1		1.712(3)	N2		N1	109.3(1)
				N2		N1	105.5(1)
				N1		N1	103.1(2)
				P2	-N1-	P2	120.6(2)
				P2		P1	116.0(2)
				P2		P1	120.2(2)
				P2	-N2-	P2	131.0(1)
				P2	-N3-	P2	151.4(1)
				P1	-N4-	P1	140.3(1)
				P1	-N5-	P1	128.4(2)

**Figure B7.** Temperature-dependent powder X-ray diffraction pattern of CaP₈N₁₄. The measurement was carried out under Ar atmosphere with Mo-K_{α1} radiation ($\lambda = 0.71073$).

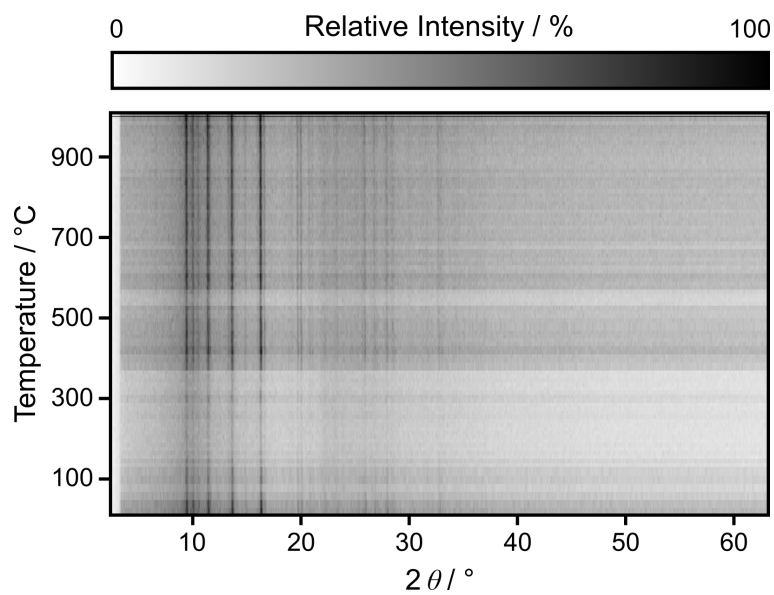


Figure B8. Temperature-dependent powder X-ray diffraction pattern of SrP₈N₁₄. The measurement was carried out under Ar atmosphere with Mo-K_{α1} radiation ($\lambda = 0.71073$).

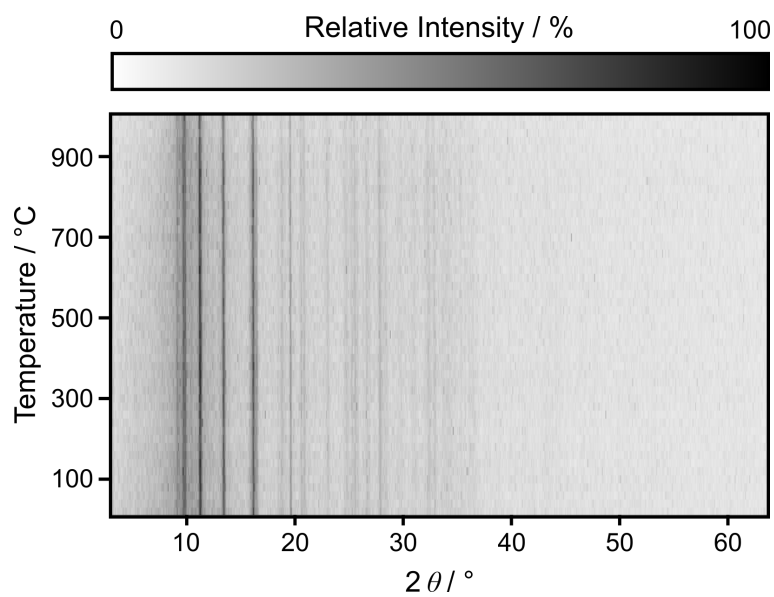


Figure B9. Temperature-dependent powder X-ray diffraction pattern of BaP₈N₁₄. The measurement was carried out under Ar atmosphere with Mo-K_{α1} radiation ($\lambda = 0.71073$).

Table B14. Determined lattice parameters from Rietveld refinements for $\text{AEP}_8\text{N}_{14}$ (AE = Ca, Sr, Ba) at selected temperatures.

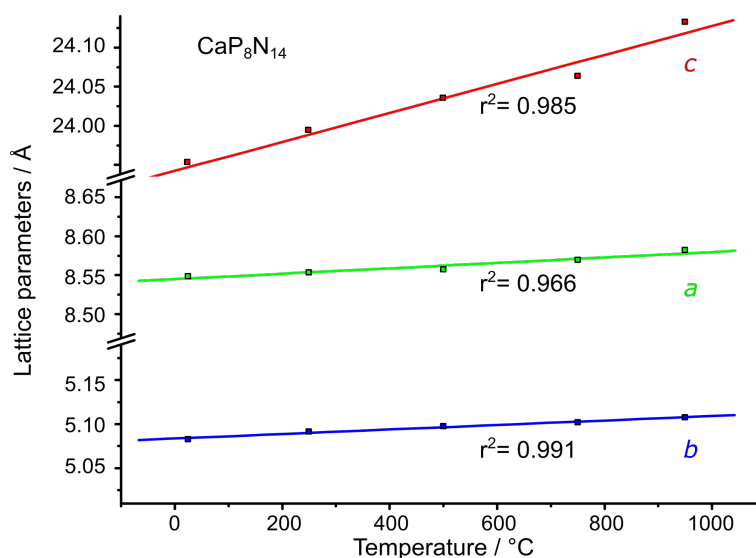
$T / ^\circ\text{C}$	$\text{CaP}_8\text{N}_{14}$			$\text{SrP}_8\text{N}_{14}$			$\text{BaP}_8\text{N}_{14}$		
	$a / \text{\AA}$	$b / \text{\AA}$	$c / \text{\AA}$	$a / \text{\AA}$	$b / \text{\AA}$	$c / \text{\AA}$	$a / \text{\AA}$	$b / \text{\AA}$	$c / \text{\AA}$
RT	8.550(3)	5.083(1)	23.953(6)	8.643(4)	5.140(2)	24.537(9)	12.427(9)	8.636(5)	5.113(3)
250	8.555(6)	5.091(3)	23.994(16)	*1	*1	*1	12.439(5)	8.640(5)	5.115(3)
500	8.559(2)	5.098(1)	24.036(6)	8.667(3)	5.153(2)	24.638(7)	12.450(6)	8.651(3)	5.124(2)
750	8.571(4)	5.102(3)	24.064(16)	8.683(2)	5.161(1)	24.685(6)	12.463(5)	8.657(3)	5.127(2)
950	8.583(3)	5.107(1)	24.133(7)	8.690(3)	5.172(1)	24.692(7)	12.464(8)	8.661(4)	5.133(3)

*1 values for $\text{SrP}_8\text{N}_{14}$ could not be determined in a range from $\sim 100^\circ\text{C}$ up to $\sim 400^\circ\text{C}$ due to the insufficient quality of the collected high-temperature X-ray diffraction patterns

Table B15. Unit-cell volumes from Rietveld refinements for $\text{AEP}_8\text{N}_{14}$ (AE = Ca, Sr, Ba) at selected temperatures.

$T / ^\circ\text{C}$	$\text{CaP}_8\text{N}_{14}$		$\text{SrP}_8\text{N}_{14}$		$\text{BaP}_8\text{N}_{14}$	
	$V / \text{\AA}^3$	$V/V_0 / \%$	$V / \text{\AA}^3$	V/V_0	$V / \text{\AA}^3$	V/V_0
RT	1040.9(5)		1089.9(8)		548.8(6)	
250	1045.1(12)	+ 0.4%	*1		549.7(5)	+ 0.2%
500	1048.6(4)	+ 0.7%	1100.4(6)	+ 1.0%	551.8(4)	+ 0.6%
750	1052.2(10)	+ 1.1%	1106.2(5)	+ 1.5%	553.5(4)	+ 0.9%
950	1057.9(5)	+ 1.6%	1109.8(5)	+ 1.8%	554.2(5)	+ 1.0%

*1 values for $\text{SrP}_8\text{N}_{14}$ could not be determined in a range from $\sim 100^\circ\text{C}$ up to $\sim 400^\circ\text{C}$ due to the bad quality of the collected high-temperature X-ray diffraction patterns

**Figure B10.** Lattice parameters of $\text{CaP}_8\text{N}_{14}$ as a function of temperature (cf. Table B14). Thermal expansion is remarkably small.

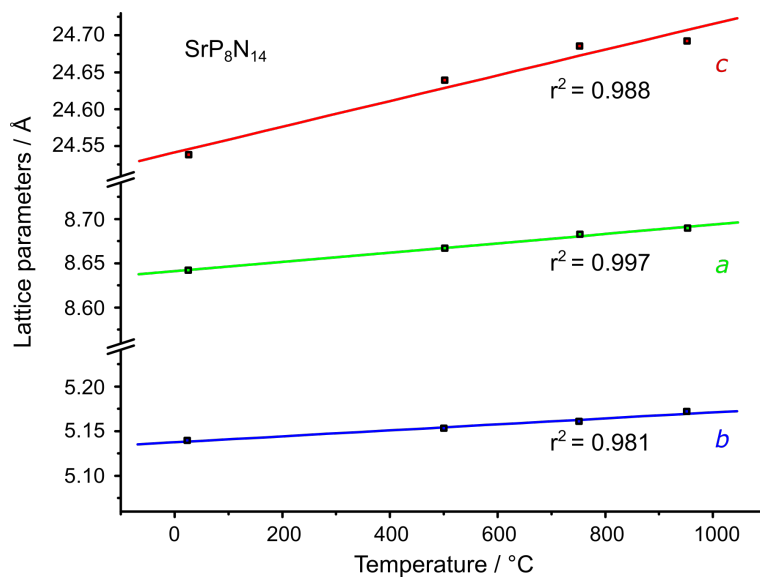


Figure B11. Lattice parameters of $\text{SrP}_8\text{N}_{14}$ as a function of temperature (cf. Table B14). Thermal expansion is remarkably small.

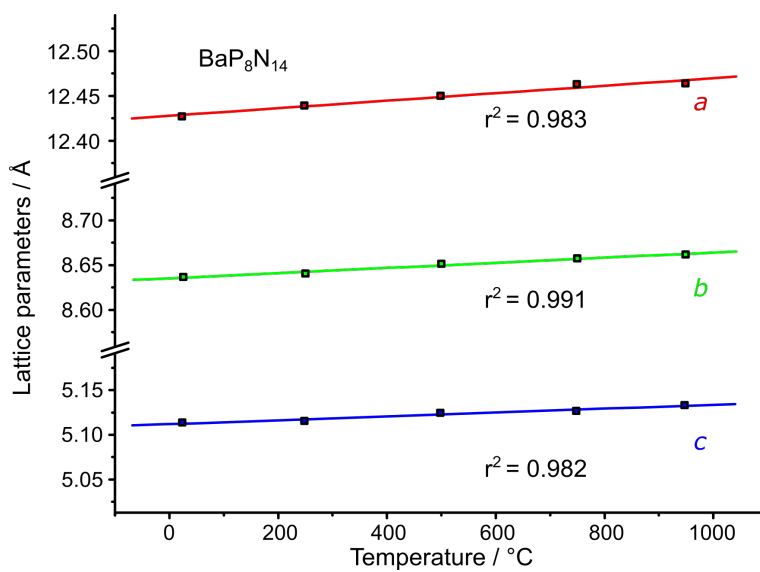


Figure B12. Lattice parameters of $\text{BaP}_8\text{N}_{14}$ as a function of temperature (cf. Table B14). Thermal expansion is remarkably small.

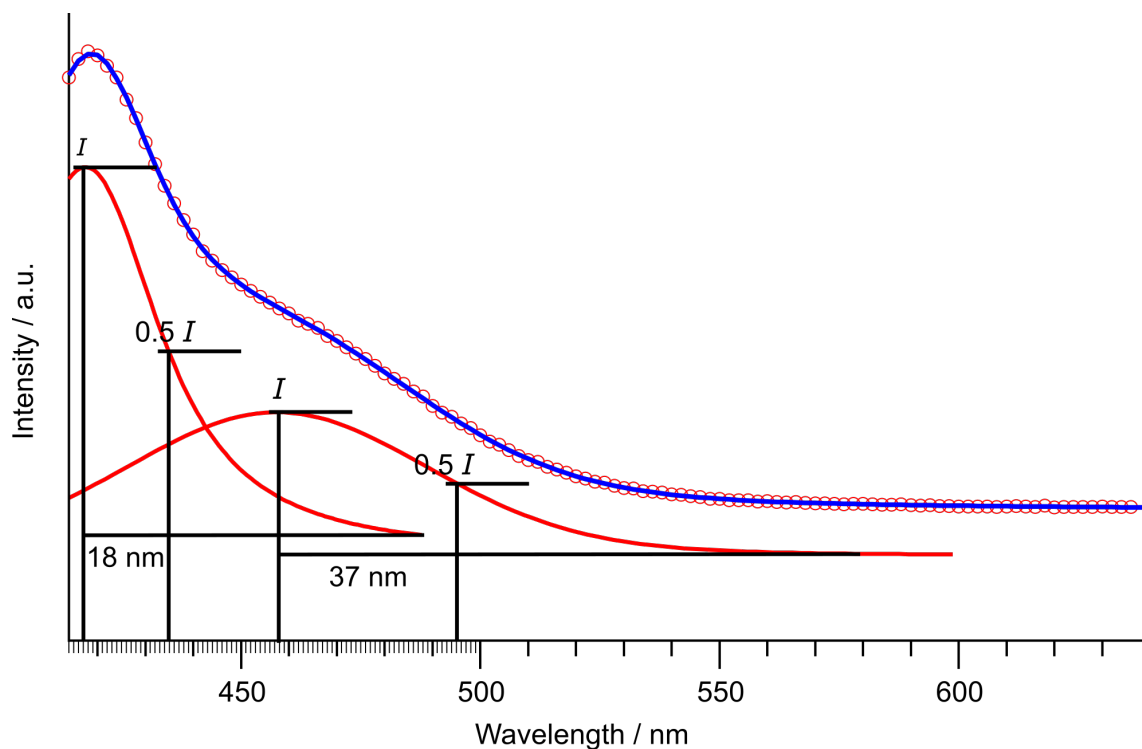


Figure B13. Observed emission spectrum of $\text{BaP}_8\text{N}_{14}:\text{Eu}^{2+}$ (red circles) fitted (blue line) by two pseudo-Voigt functions (red lines) using IgorPro7 (WaveMetrics Inc.) to determine the maxima and fwhm values.

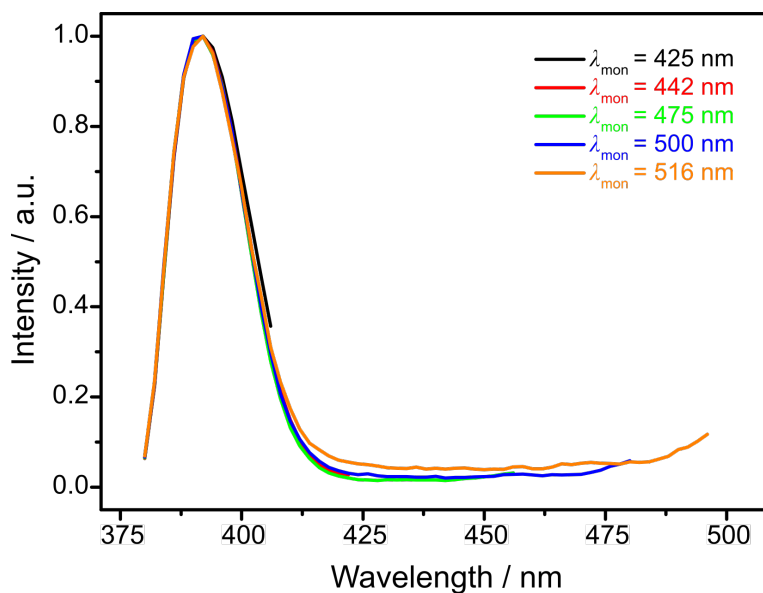


Figure B14. Comparison of the excitation spectra of $\text{BaP}_8\text{N}_{14}:\text{Eu}^{2+}$ with a nominal doping concentration of 3 %, monitored at different wavelengths λ_{mon} .

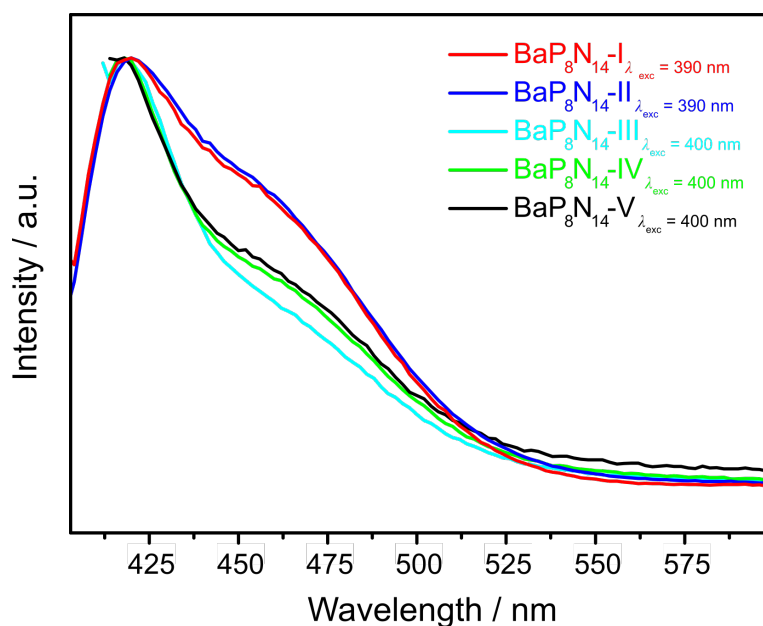


Figure B15. Comparison of the emission spectra of different samples of $\text{BaP}_8\text{N}_{14}:\text{Eu}^{2+}$ with a nominal doping concentration of 3 %; $\lambda_{\text{exc}}(\text{I, II}) = 390 \text{ nm}$; $\lambda_{\text{exc}}(\text{III-V}) = 400 \text{ nm}$.

Table B16. Weighed portions of starting materials for the syntheses of $\text{AEP}_8\text{N}_{14}:\text{Eu}^{2+}$ ($\text{AE} = \text{Ca, Sr, Ba}$).

Title compounds	Starting materials / mg		
$\text{CaP}_8\text{N}_{14}(:\text{Eu}^{2+})$	$\text{Ca}(\text{N}_3)_2$	P_3N_5	EuCl_2
	10.77	37.71	~0.6
$\text{SrP}_8\text{N}_{14}(:\text{Eu}^{2+})$	$\text{Sr}(\text{N}_3)_2$	P_3N_5	EuCl_2
	13.56	34.34	~0.5
$\text{BaP}_8\text{N}_{14}(:\text{Eu}^{2+})$	$\text{Ba}(\text{N}_3)_2$	P_3N_5	EuCl_2
	15.23	29.91	~0.5

Table B17. Temperature and pressure programs for the syntheses of $\text{AEP}_8\text{N}_{14}:\text{Eu}^{2+}$ ($\text{AE} = \text{Ca, Sr, Ba}$). Segment 1: pressure build-up; Segment 2: heat up phase; segment 3: plateau phase; segment 4: cooling phase; segment 5: pressure release.

Segme	$\text{CaP}_8\text{N}_{14}$			$\text{SrP}_8\text{N}_{14}$			$\text{BaP}_8\text{N}_{14}$		
	p / bar	t / min	$P / \%$	p / bar	t / min	$P / \%$	p / bar	t / min	$P / \%$
1	0 → 138	115	-	0 → 138	115	-	0 → 110	100	-
2	138	60	0 → 26	138	60	0 → 26	110	60	0 → 24
3	138	60	26	138	60	26	110	180	24
4	138	60	26 → 0	138	60	26 → 0	110	180	24 → 0
5	138 → 0	330	-	138 → 0	330	-	110 → 0	300	-

B.2 Author Contributions

S.W.: Conceptualization: Equal; Formal analysis: Lead; Investigation : Lead; Validation: Lead; Visualization: Lead; Writing - Original Draft: Lead; Writing - Review & Editing: Equal

L.E.: Formal analysis: Supporting; Investigation: Supporting; Validation: Supporting; Writing - Review & Editing: Supporting

P.S.: Formal analysis: Supporting; Investigation: Supporting ; Validation: Supporting; Writing - Review & Editing: Supporting

D.G.: Formal analysis: Supporting; Investigation: Supporting ; Validation: Supporting; Writing - Review & Editing: Supporting

J.W.: Investigation: Supporting; Methodology: Supporting ; Supervision: Supporting

P.S.: Formal analysis: Supporting; Funding acquisition: Lead; Project administration: Supporting; Supervision: Supporting; Validation: Supporting; Writing - Review & Editing: Supporting

O.O.: Formal analysis: Supporting; Funding acquisition: Equal; Investigation: Supporting; Project administration: Equal; Resources: Supporting; Supervision: Equal; Validation: Supporting; Writing - Review & Editing: Supporting

W.S.: Conceptualization: Equal; Funding acquisition: Lead; Project administration: Lead; Resources: Lead; Supervision: Lead; Validation: Equal; Writing - Original Draft: Supporting; Writing - Review & Editing: Supporting

B.3 References

- [1] S. Wendl, W. Schnick, "*SrH₄P₆N₁₂ and SrP₈N₁₄: Insights into the Condensation Mechanism of Nitridophosphates under High Pressure*", *Chem. Eur. J.* **2018**, *24*, 15889-15896.

C Supporting Information for Chapter 4

C.1 Results and Discussions

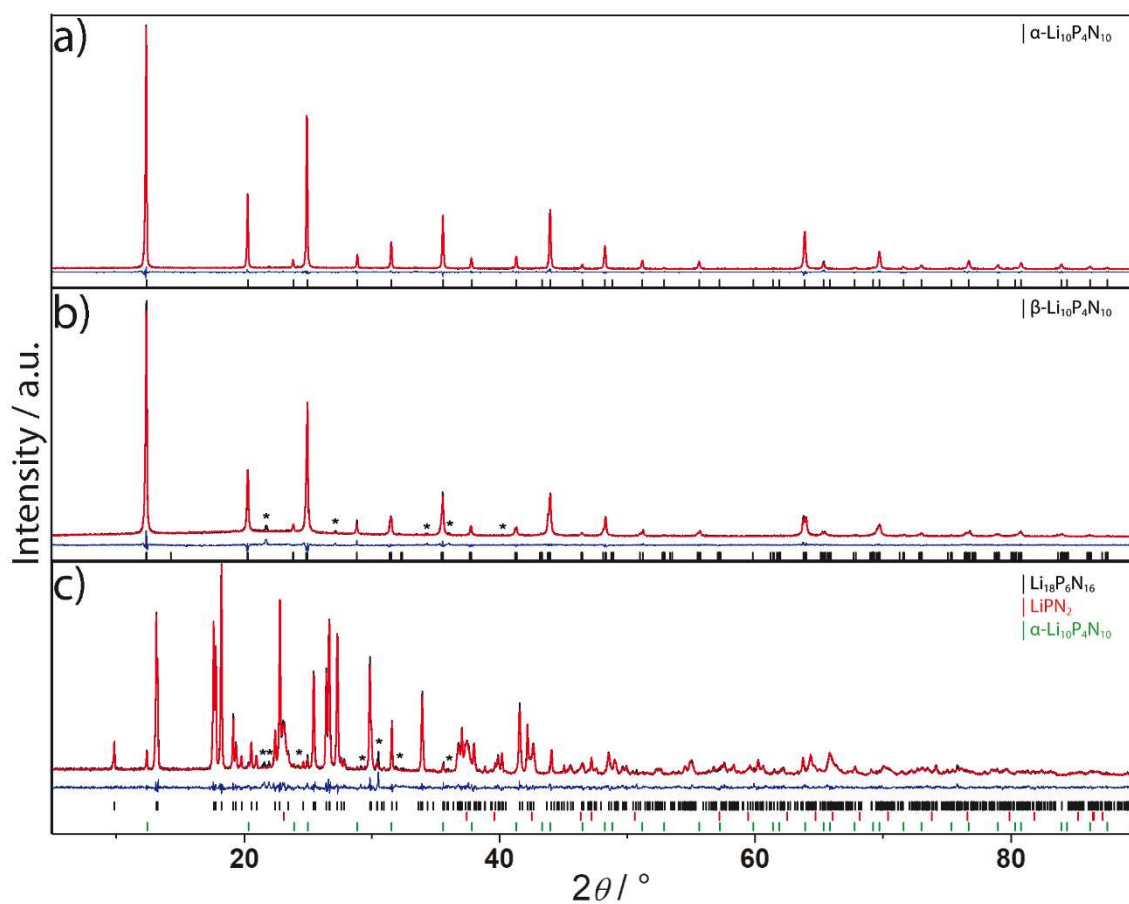
 α -Li₁₀P₄N₁₀, β -Li₁₀P₄N₁₀ and Li₁₈P₆N₁₆

Figure C.1. Rietveld refinements of α -Li₁₀P₄N₁₀ (a), β -Li₁₀P₄N₁₀ (b) and Li₁₈P₆N₁₆ (c). Experimental and calculated data are displayed in black and red lines, and difference profiles are shown as blue lines. Vertical bars mark Bragg reflections of the refined phases. Unknown side phases are marked with asterisks. Start values for Rietveld refinement were taken from literature.^[1-3]

Table C.1. Crystallographic data of α -Li₁₀P₄N₁₀, β -Li₁₀P₄N₁₀ and Li₁₈P₆N₁₆ obtained by Rietveld refinement, standard deviations in parentheses. Li sites were not refined for all three compounds.

Formula	α -Li ₁₀ P ₄ N ₁₀	β -Li ₁₀ P ₄ N ₁₀	Li ₁₈ P ₆ N ₁₆
Crystal system	cubic	trigonal	triclinic
Space group	$Fd\bar{3}m$ (no. 227)	$R3$ (no. 146)	$P\bar{1}$ (no. 2)
$a / \text{\AA}$	12.35331(8)	8.72293(2)	5.3986(1)
$b / \text{\AA}$			7.4837(2)
$c / \text{\AA}$		21.4622(7)	9.8333(2)
$\alpha / ^\circ$			108.933(1)
$\beta / ^\circ$			99.118(1)
$\gamma / ^\circ$			104.942(1)
Cell volume / \AA^3	1885.17(4)	1414.26(7)	350.11(1)
Density / $\text{g}\cdot\text{cm}^{-3}$	2.34922(4)	2.34922(4)	2.53625(10)
Formula units / cell	8	6	1
T / K	293(2)		
Diffractionmeter	STOE STADI P		
Radiation / \AA	Cu- $K_{\alpha 1}$ ($\lambda = 1.5406$)		
2θ range / $^\circ$	$5.0 \leq 2\theta \leq 90$		
Profile function	fundamental parameters model		
Background function	Shifted Chebyshev		
Data points	5668		
Number of reflections	51	249	569
Refined parameters	25	60	139
R values	$R_p = 0.0608$ $R_{wp} = 0.0865$ $R_{\text{Bragg}} = 0.0173$	$R_p = 0.0716$ $R_{wp} = 0.0941$ $R_{\text{Bragg}} = 0.0299$	$R_p = 0.0548$ $R_{wp} = 0.0755$ $R_{\text{Bragg}} = 0.0133$
Goodness of fit	0.977	1.252	1.218

Table C.2. Wyckoff positions and atomic coordinates of α -Li₁₀P₄N₁₀ obtained from Rietveld refinement, standard deviations in parentheses.

Atom	Wyckoff	x	y	z	SOF	U_{iso}
Li1	16d	1/2	1/2	1/2	1	0.0089
Li2	8a	1/8	1/8	1/8	1	0.0089
Li3	48f	0.3154	1/8	1/8	0.96	0.0089
Li4	32e	0.9628	0.9628	0.9628	0.31	0.0089
P1	32e	0.29376(6)	0.29376(6)	0.29376(6)	1	0.0089
N1	48f	0.47223(19)	1/8	1/8	1	0.0089
N2	32e	0.21844(12)	0.21844(12)	0.21844(12)	1	0.0089

Table C.3. Wyckoff positions and atomic coordinates of β -Li₁₀P₄N₁₀ obtained from Rietveld refinement, standard deviations in parentheses.

Atom	Wyckoff	x	y	z	SOF	U_{iso}
Li1	9b	0.905	0.159	0.4168	1	0.0089
Li2	9b	0.850	0.173	0.2720	1	0.0089
Li3	3a	1/3	2/3	0.140	1	0.0089
Li4	9b	0.785	0.211	0.1305	1	0.0089
Li5	9b	0.155	0.805	0.3556	1	0.0089
Li6	9b	0.787	0.191	0.8688	1	0.0089
Li7	3a	0	0	0.7137	1	0.0089
Li8	3a	0	0	0.101	1	0.0089
Li9	9b	0.212	1.018	0.6158	2/3	0.0089
P1	3a	0	0	0.9062(16)	1	0.0089
P2	9b	0.885(2)	0.0448(2)	0.3490(10)	1	0.0089
P3	3a	0	0	0.3153(18)	1	0.0089
P4	9b	0.121(2)	0.559(2)	0.8766(11)	1	0.0089
N1	9b	0.129(6)	0.575(7)	0.705(3)	1	0.0089
N2	9b	0.882(5)	0.439(5)	0.2645(17)	1	0.0089
N3	3a	0	0	0.833(3)	1	0.0089
N4	9b	0.888(6)	0.791(6)	0.186(3)	1	0.0089
N5	9b	0.735(4)	0.200(5)	0.620(2)	1	0.0089
N6	3a	2/3	1/3	0.724(4)	1	0.0089
N7	9b	0.885(6)	0.138(7)	0.518(3)	1	0.0089
N8	9b	0.121(6)	0.871(6)	0.707(2)	1	0.0089

Table C.4. Wyckoff positions and atomic coordinates of $\text{Li}_{18}\text{P}_6\text{N}_{16}$ obtained from Rietveld refinement, standard deviations in parentheses.

Atom	Wyckoff	x	y	z	SOF	U_{iso}
Li1	2i	0.1297	0.0264	0.4033	1	0.0117
Li2	2i	0.202	0.2786	0.7920	1	0.0183
Li3	2i	0.0785	0.1228	0.1450	1	0.0219
Li4	2i	0.3342	0.3953	0.3881	1	0.0188
Li5	2i	0.3710	0.0989	0.9653	1	0.0247
Li6	2i	0.6624	0.3295	0.1917	1	0.0271
Li7	2i	0.0638	0.4199	0.5862	1	0.0328
Li8	2i	0.392	0.4440	0.0551	0.6	0.039
Li9	2i	0.268	0.4588	0.0951	0.5	0.030
Li10	2i	0.130	0.465	0.113	0.35	0.036
Li11	2i	0.022	0.429	0.152	0.54	0.066
P1	2i	0.5435(11)	0.2598(7)	0.6374(5)	1	0.0098
P2	2i	0.2168(13)	0.8143(8)	0.1188(5)	1	0.0220
P3	2i	0.6871(11)	0.1306(7)	0.3461(5)	1	0.0108
N1	2i	0.546(3)	0.5268(17)	0.2702(13)	1	0.0089
N2	2i	0.193(3)	0.746(2)	0.2672(14)	1	0.0089
N3	2i	0.055(3)	0.2098(19)	0.9829(15)	1	0.0089
N4	2i	0.576(3)	0.269(2)	0.4832(14)	1	0.0089
N5	2i	0.063(2)	0.7343(18)	0.6664(12)	1	0.0089
N6	2i	0.326(3)	0.6745(16)	0.0186(15)	1	0.0089
N7	2i	0.430(2)	0.035(2)	0.1862(11)	1	0.0089
N8	2i	0.278(3)	0.0591(18)	0.6218(12)	1	0.0089

Table C.5. SEM EDX measurements of α -Li₁₀P₄N₁₀, β -Li₁₀P₄N₁₀ and Li₁₈P₆N₁₆. Oxygen impurities could be due to hydrolysis during sample preparation.

α -Li ₁₀ P ₄ N ₁₀	P	O	N
measurement 1:	25.1	17.6	57.3
measurement 2:	23.1	19.6	57.3
measurement 3:	22.7	9.5	67.8
\emptyset	24(1)	16(5)	60(6)
ratio	4	2.7	10
ideal	4	0	10
β -Li ₁₀ P ₄ N ₁₀	P	O	N
measurement 1:	24.2	5.0	70.8
measurement 2:	31.4	6.8	61.8
measurement 3:	25.2	6.2	68.6
\emptyset	27(4)	6(1)	67(5)
ratio	4	0.9	9.9
ideal	4	0	10
Li ₁₈ P ₆ N ₁₆	P	O	N
measurement 1:	25.5	17.3	57.2
measurement 2:	22.7	18.6	58.7
measurement 3:	23.2	17.6	59.2
\emptyset	24(1)	18(1)	58(1)
ratio	6	4.5	14.5
ideal	6	0	16

The vibration bands below 1400 cm^{-1} are attributed to P–N framework vibrations. There are no significant stretching vibrations in the region around 3000 cm^{-1} where N–H vibrations would be expected.^[4–6] Weak signals can be explained by surface hydrolysis of the product during washing treatment.

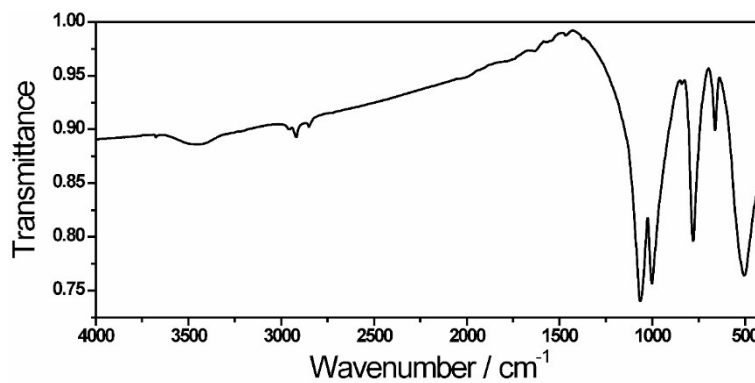


Figure C.2. FTIR spectrum of $\alpha\text{-Li}_{10}\text{P}_4\text{N}_{10}$.

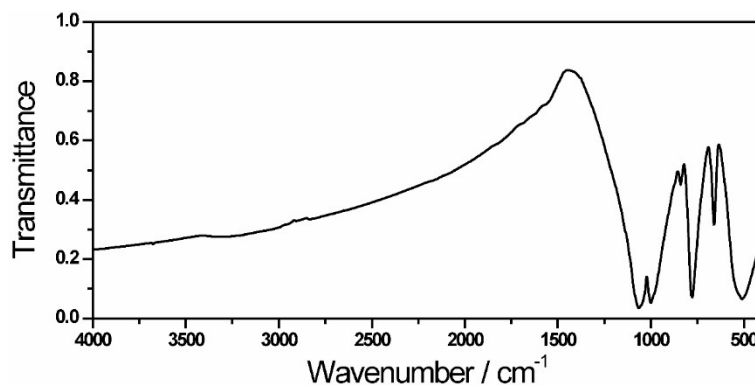


Figure C.3. FTIR spectrum of $\beta\text{-Li}_{10}\text{P}_4\text{N}_{10}$.

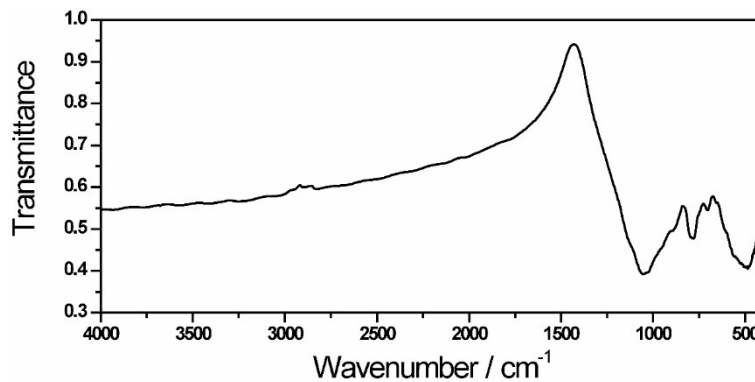


Figure C.4. FTIR spectrum of $\text{Li}_{18}\text{P}_6\text{N}_{16}$.

Ca_2PN_3 **Table C.6.** Crystallographic data of Ca_2PN_3 obtained from Rietveld refinement, standard deviations in parentheses.

Formula	Ca_2PN_3
Crystal system	orthorhombic
Space group	$Cmce$ (no. 64)
$a / \text{\AA}$	5.18798(6)
$b / \text{\AA}$	10.31927(14)
$c / \text{\AA}$	11.28164(12)
Cell volume / \AA^3	603.976(12)
Density / $\text{g}\cdot\text{cm}^{-3}$	3.36847(7)
Formula units / cell	8
T / K	293(2)
Diffractometer	STOE STADI P
Radiation / \AA	$\text{Cu-K}\alpha_1$ ($\lambda = 1.5406$)
2θ range / $^\circ$	$10 \leq 2\theta \leq 90$
Profile function	fundamental parameters model
Background function	Shifted Chebyshev
Data points	5332
Number of reflections	146
Refined parameters	57
R values	$R_p = 0.0407$ $R_{wp} = 0.0540$ $R_{\text{Bragg}} = 0.0160$
Goodness of fit	0.707

Table C.7. Wyckoff positions and atomic coordinates of Ca_2PN_3 obtained from powder X-ray diffraction, standard deviations in parentheses.

Atom	Wyckoff	x	y	z	SOF	U_{iso}
Ca1	$8f$	0	0.05150(13)	0.14303(11)	1	0.0190(5)
Ca2	$8f$	0	0.36211(10)	0.07499(10)	1	0.0089(4)
P1	$8f$	0	0.24233(17)	0.33300(15)	1	0.0092(5)
N1	$8f$	0	0.3371(4)	0.4484(3)	1	0.0060(6)
N2	$8f$	0	0.0889(4)	0.3583(4)	1	0.0060(6)
N3	$8e$	1/4	0.2865(4)	1/4	1	0.0060(6)

Table C.8. SEM EDX measurements of Ca_2PN_3 . All EDX measurements showed amounts of impurities (O, Na) which originate from washing treatment, residual mineralizer and hydrolysis during sample preparation. For the quantification of the composition of the compounds, Na was not taken into account.

Ca_2PN_3	Ca	P	O	N
measurement 1:	15.9	9.6	46.3	28.1
measurement 2:	15.5	10.0	44.8	29.7
measurement 3:	17.2	11.3	44.8	26.7
\emptyset	17(1)	10(1)	45(1)	28(2)
ratio	1.7	1	4.5	2.8
ideal	2	1	0	3

$\text{SrP}_8\text{N}_{14}$

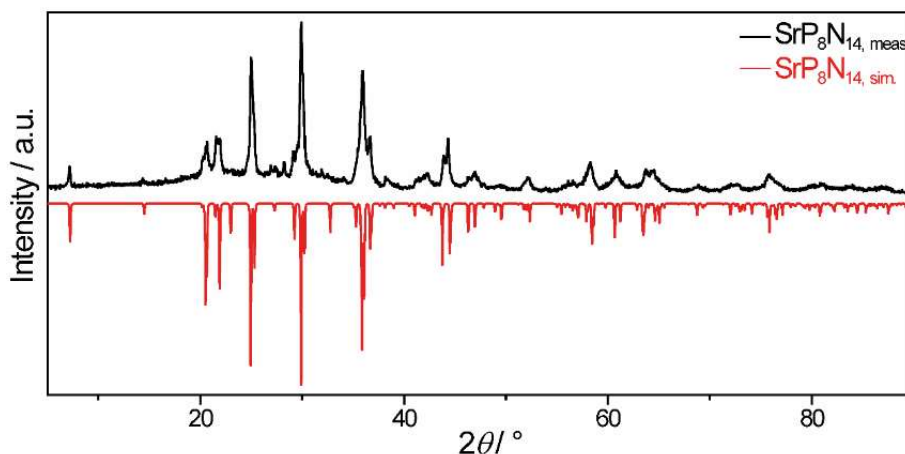


Figure C.5. Experimental PXR D pattern of $\text{SrP}_8\text{N}_{14}$ (black) and simulated pattern (red) taken from literature.^[5]

Table C.9. SEM EDX measurements of $\text{SrP}_8\text{N}_{14}$. The atomic ratios deviate from calculated ones, possibly due to an amorphous side phase (see PXR D). Traces of oxygen may originate from washing treatment with H_2O and HCl .

$\text{SrP}_8\text{N}_{14}$	Sr	P	O	N
measurement 1:	7.4	31.4	6.9	54.3
measurement 2:	5.7	20.1	19.1	55.1
measurement 3:	7.8	23.4	16.6	52.2
\emptyset	7(1)	25(6)	14(6)	54(2)
ratio	2.2	8	4.5	17.3
ideal	1	8	0	14

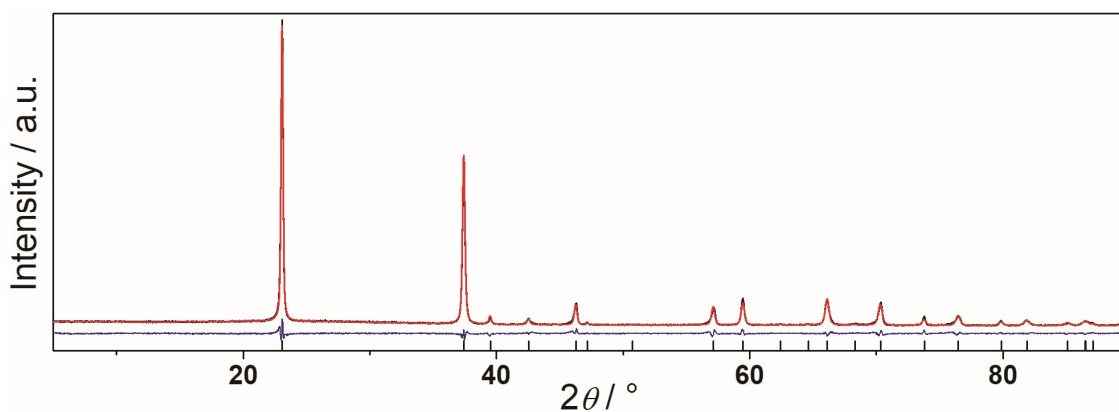
LiPN₂

Figure C.6. Rietveld refinement of PXRD pattern of LiPN₂ with experimental data (black line), calculated data (red line), difference profile (blue line) and reflection positions (black bars). Start values were taken from literature.^[6]

Table C.10. Crystallographic data of LiPN₂ obtained by Rietveld refinement, standard deviations in parentheses.

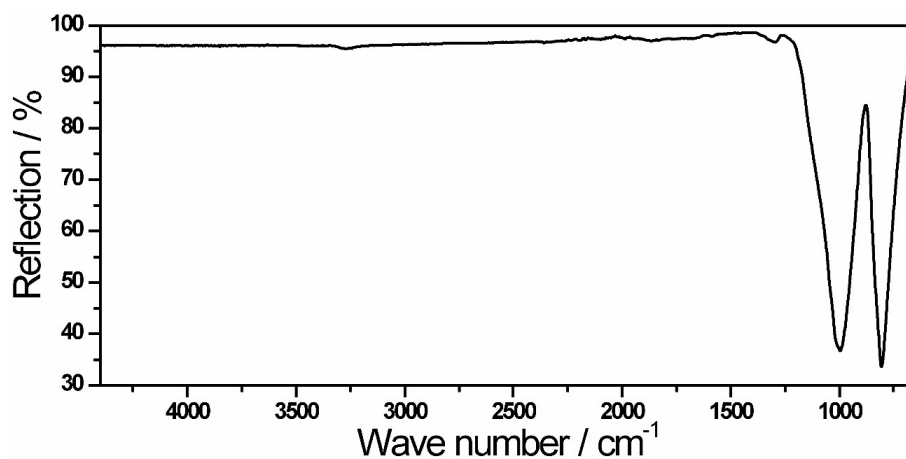
Formula	LiPN ₂
Crystal system	tetragonal
Space group	$I\bar{4}2d$ (no. 122)
$a / \text{\AA}$	4.55609(10)
$c / \text{\AA}$	7.1945(2)
Cell volume / \AA^3	149.343(8)
Density / $\text{g}\cdot\text{cm}^{-3}$	2.93214(16)
Formula units / cell	4
T / K	293(2)
Diffractometer	STOE STADI P
Radiation / \AA	Cu- $K_{\alpha 1}$ ($\lambda = 1.5406$)
2θ range / $^\circ$	$5.0 \leq 2\theta \leq 90$
Profile function	fundamental parameters model
Background function	Shifted Chebyshev
Data points	5668
Number of reflections	24
Refined parameters	26
R values	$R_p = 0.0692$ $R_{wp} = 0.0942$ $R_{\text{Bragg}} = 0.0270$
Goodness of fit	1.283

Table C.11. Wyckoff positions and atomic coordinates of LiPN₂ obtained from powder X-ray diffraction, standard deviations in parentheses.

Atom	Wyckoff	x	y	z	SOF	U_{iso}
Li1	4b	0	0	1/2	1	0.0127
P1	4a	0	0	0	1	0.0084(5)
N1	8d	0.1637(6)	1/4	1/8	1	0.0089

Table C.12. SEM EDX measurements of LiPN₂. All EDX measurements showed small amounts of impurities (O, Cl) which originate from washing treatment with HCl. For the quantification of the composition of the compounds, Cl was not taken into account.

LiPN ₂	P	O	N
measurement 1:	34.4	7.1	58.5
measurement 2:	36.2	1.7	62.1
measurement 3:	35.4	2.2	62.4
∅	35(1)	4(3)	61(2)
ratio	1	0.1	1.7
ideal	1	0	2

**Figure C.7.** FTIR (ATR) spectrum of LiPN₂. The two vibration bands at 998 and 808 cm⁻¹ are attributable to PN framework vibrations. There is no significant valance vibration in the region around 3000 cm⁻¹ where N-H-vibrations would be expected.^[4, 5] A weak signal can be explained by surface hydrolysis of the product during washing treatment.

C.2 Author Contributions

M.M.: Conceptualization: Equal; Formal analysis: Lead; Investigation: Lead; Validation: Lead; Visualization: Lead; Writing - Original Draft: Lead; Writing - Review & Editing: Lead

S.W.: Formal analysis: Supporting; Investigation: Supporting; Validation: Supporting; Writing - Original Draft: Supporting; Writing - Review & Editing: Supporting

W.S.: Conceptualization: Equal; Funding acquisition: Lead; Methodology: Equal; Project administration: Lead; Resources: Lead; Supervision: Lead; Validation: Equal; Writing - Original Draft: Supporting; Writing - Review & Editing: Supporting

C.3 References

- [1] E. M. Bertschler, C. Dietrich, T. Leichtweiß, J. Janek, W. Schnick, "Li⁺ Ion Conductors with Adamantane-Type Nitridophosphate Anions β -Li₁₀P₄N₁₀ and Li₁₃P₄N₁₀X₃ with X = Cl, Br", *Chem. Eur. J.* **2018**, *24*, 196-205.
- [2] W. Schnick, U. Berger, "Li₁₀P₄N₁₀ - A Lithium Phosphorus(V) Nitride with the Novel Complex Anion P₄N₁₀¹⁰⁻", *Angew. Chem. Int. Ed. Engl.* **1992**, *31*, 213-214; *Angew. Chem.* **1991**, *103*, 857-858.
- [3] E. M. Bertschler, C. Dietrich, J. Janek, W. Schnick, "Li₁₈P₆N₁₆—A Lithium Nitridophosphate with Unprecedented Tricyclic [P₆N₁₆]¹⁸⁻ Ions", *Chem. Eur. J.* **2017**, *23*, 2185-2191.
- [4] A. Marchuk, V. R. Celinski, J. Schmedt auf der Günne, W. Schnick, "MH₄P₆N₁₂ (M = Mg, Ca): New Imidonitridophosphates with an Unprecedented Layered Network Structure Type", *Chem. Eur. J.* **2015**, *21*, 5836-5842.
- [5] S. Wendl, W. Schnick, "SrH₄P₆N₁₂ and SrP₈N₁₄: Insights into the Condensation Mechanism of Nitridophosphates under High Pressure", *Chem. Eur. J.* **2018**, *24*, 15889-15896.
- [6] W. Schnick, J. Lücke, "On Lithium Phosphorus Nitride. Preparation and Refinement of the Crystal Structure of LiPN₂", *Z. Anorg. Allg. Chem.* **1990**, *588*, 19-25.

D Supporting Information for Chapter 5

D.1 Results and Discussions

Additional crystallographic data

Table D.1. Wyckoff positions and atomic coordinates of Ba₂PO₃N obtained from single-crystal X-ray diffraction, standard deviations in parentheses.

Atom	Wyckoff	x	y	z	U_{eq} [Å ²]
Ba1	4c	0.15869(3)	3/4	0.58252(2)	0.01504(5)
Ba2	4c	0.49595(2)	3/4	0.30557(2)	0.01158(4)
P1	4c	0.73340(10)	3/4	0.58127(8)	0.0087(1)
O1	8d	0.7994(3)	0.5307(3)	0.6576(2)	0.0201(4)
O2	4c	0.5226(3)	3/4	0.5847(3)	0.0213(5)
N1	4c	0.8089(4)	3/4	0.4373(2)	0.0117(5)

Table D.2. Anisotropic displacement parameters [Å²] of Ba₂PO₃N, standard deviations in parentheses.

Atom	U ₁₁	U ₂₂	U ₃₃	U ₂₃	U ₁₃	U ₁₂
Ba1	0.01388(8)	0.01275(8)	0.01849(9)	0	0.00218(7)	0
Ba2	0.00967(7)	0.01371(8)	0.01135(8)	0	0.00015(6)	0
P1	0.0085(3)	0.0085(3)	0.0092(3)	0	0.0002(2)	0
O1	0.0219(9)	0.0160(8)	0.0224(8)	0.0074(7)	-0.0031(7)	0.0011(7)
O2	0.0126(10)	0.029(2)	0.0223(12)	0	0.0003(9)	0
N1	0.0126(10)	0.0150(12)	0.0074(10)	0	0.0025(8)	0

Table D.3. Selected interatomic distances [Å] and angles [°] occurring in Ba₂PO₃N obtained from single-crystal X-ray diffraction, standard deviations in parentheses.

Ba1 – O2	2.764(2)	Ba2 – O1	2.711(2)	P1 – O1	1.573(2)
Ba1 – N1	2.9156(8)	Ba2 – O1	2.711(2)	P1 – O1	1.573(2)
Ba1 – N1	2.9156(8)	Ba2 – N1	2.731(3)	P1 – N1	1.578(2)
Ba1 – O1	2.960(2)	Ba2 – O1	2.797(2)	P1 – O2	1.602(2)
Ba1 – O1	2.960(2)	Ba2 – O1	2.797(2)		
Ba1 – N1	3.043(3)	Ba2 – O2	2.858(3)	O1 – P1 – O1	107.81(9)
Ba1 – O1	3.107(2)	Ba2 – N1	2.858(2)	O1 – P1 – N1	110.23(7)
Ba1 – O1	3.107(2)	Ba2 – O2	3.110(1)	O1 – P1 – O2	107.93(8)
Ba1 – O1	3.131(2)	Ba2 – O2	3.110(1)	N1 – P1 – O2	112.6(2)
Ba1 – O1	3.131(2)				

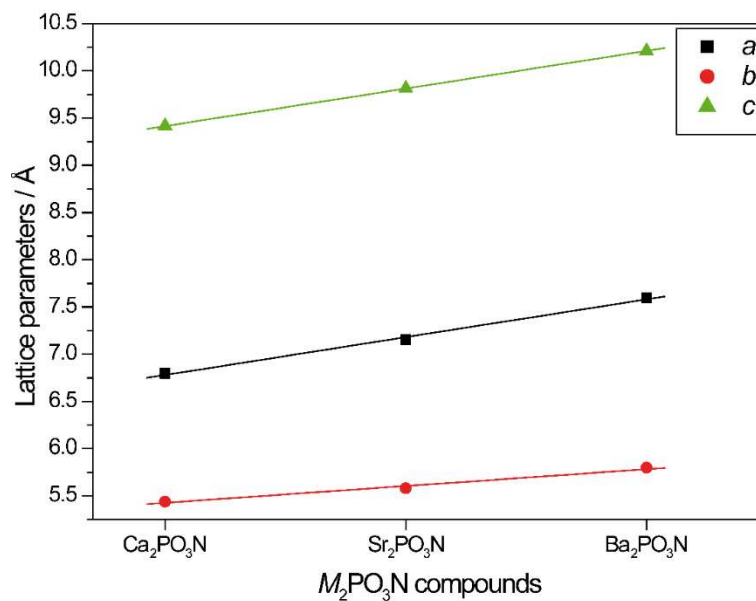


Figure D.1. Comparison of lattice parameters of M_2PO_3N ($M = Ca, Sr, Ba$) compounds.

Table D.4. Results of MAPLE calculations [kJ/mol] for Ba_2PO_3N . Partial MAPLE values, total MAPLE value and deviation to sum of total MAPLE values of binary ionic compounds, forming Ba_2PO_3N in a hypothetical reaction (structural data were taken from literature).^[1, 2]

Ba1 ²⁺	Ba2 ²⁺	P1 ⁵⁺	O1 ^{[1]2-}	O2 ^{[1]2-}	N1 ^{[1]3-}	total MAPLE
1685	1912	14550	2606	2588	5036	30983
2 · BaO + PON _(cristobalite)						
2 · 3519 + 24142						31180
						$\Delta \approx 0.63\%$

Typical partial MAPLE values [kJ/mol]:^[3]

Ba²⁺: 1500-2000

P⁵⁺: 14422-15580

N^{[1]3-}: 4300-5000

O^{[1]2-}: 2000-2800

Table D.5. Bond-valance sums for Ba₂PO₃N.

	Ba1	Ba2	P	O1	O2	N1
	1.876	2.407	4.686	2.064	1.781	3.063
oxidation state	2	2	5	2	2	3

Table D.6. Results of CHARDI calculations for Ba₂PO₃N.

Ba1	Ba2	P	O1	O2	N1
2.022	1.985	4.993	-2.350	-1.880	-2.420

Table D.7. Crystallographic data of Ba₂PO₃N obtained by Rietveld refinement, standard deviations in parentheses.

Formula	Ba ₂ PO ₃ N
Crystal system	orthorhombic
Space group	<i>Pnma</i> (no. 62)
<i>a</i> / Å	7.5896(2)
<i>b</i> / Å	5.78984(9)
<i>c</i> / Å	10.1969(2)
Cell volume / Å ³	448.08(1)
Formula units / cell	4
Density / g·cm ⁻³	5.4496(2)
<i>T</i> / K	293
Diffractometer	Stoe STADI P
Radiation / Å	Mo-K _{α1} (0.71073)
Detector	Mythen 1K
Monochromator	Ge(111)
2θ range / °	2.5 ≤ 2θ ≤ 56.26
Profile function	fundamental parameters approach
Background function	Shifted Chebyshev
Data points	3584
Number of reflections	618
Refined parameters	44
<i>R</i> _p	0.0426
<i>R</i> _{wp}	0.0699
<i>R</i> _{Bragg}	0.0190
Goodness of Fit	2.66

Table D.8. Wyckoff positions and atomic coordinates of Ba₂PO₃N obtained from Rietveld refinement, standard deviations in parentheses. Isotropic displacement parameters of P, O and N were taken from single-crystal XRD measurement.

Atom	Wyckoff	x	y	z	U_{iso} [Å ²]
Ba1	4c	0.1598(2)	3/4	0.58443(12)	0.0138(4)
Ba2	4c	0.4959(2)	3/4	0.30508(11)	0.0073(3)
P1	4c	0.7335(6)	3/4	0.5777(7)	0.00872
O1	8d	0.7986(10)	0.537(1)	0.6562(9)	0.0201
O2	4c	0.526(1)	3/4	0.5883(11)	0.0213
N1	4c	0.809(1)	3/4	0.440(1)	0.0117

Detailed information on scanning electron microscopy

Table D.9. SEM EDX measurements of Ba₂PO₃N:Eu²⁺.

Ba ₂ PO ₃ N:Eu ²⁺	Ba	P	O	N	Eu
measurement 1:	31.7	15.1	38.1	14.5	0.6
measurement 2:	32.3	15.4	38.1	13.7	0.5
measurement 3:	32.0	15.1	38.3	14.1	0.5
measurement 4:	31.6	15.6	37.5	14.9	0.4
∅	31.9	15.3	38.0	14.3	0.5
calculated	28.3	14.3	42.8	14.3	0.3

Detailed information on IR spectroscopy

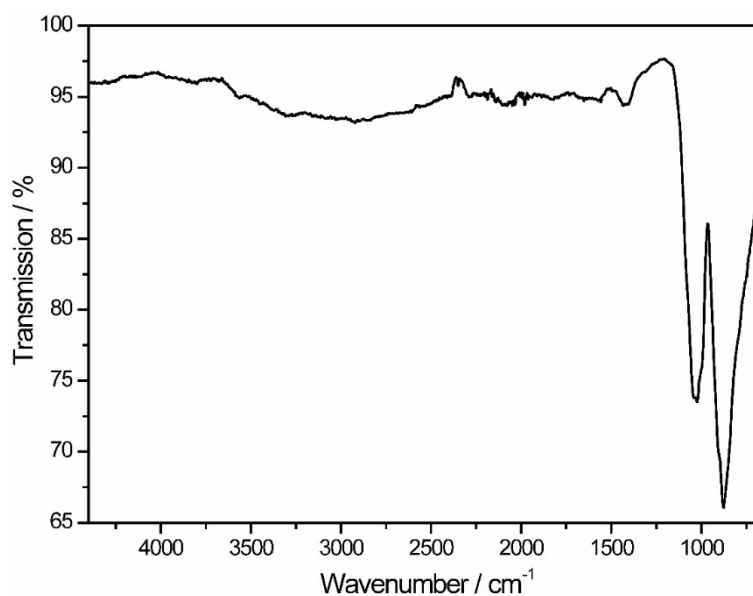


Figure D.2. FTIR (ATR) spectrum of Ba₂PO₃N.

Detailed information on UV/Vis spectroscopy

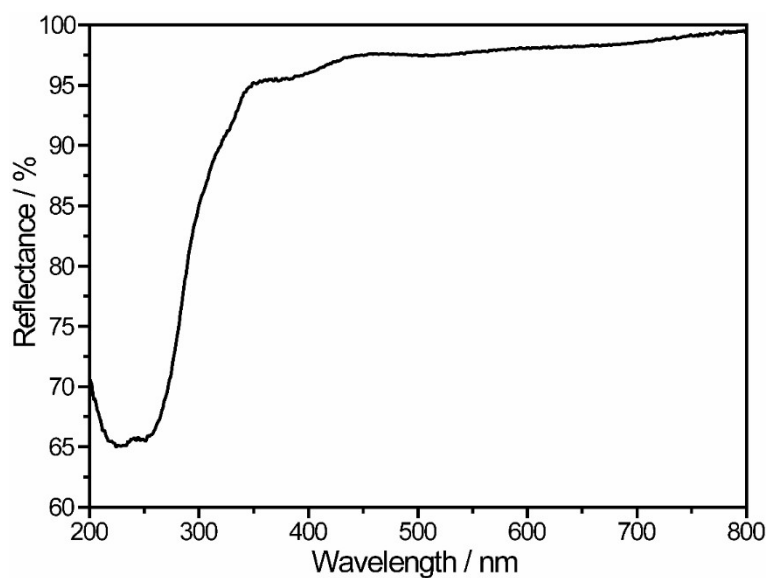


Figure D.3. Diffuse reflectance spectrum of Ba₂PO₃N. The lamp switch causes the artifact around 340 nm.

Luminescence properties

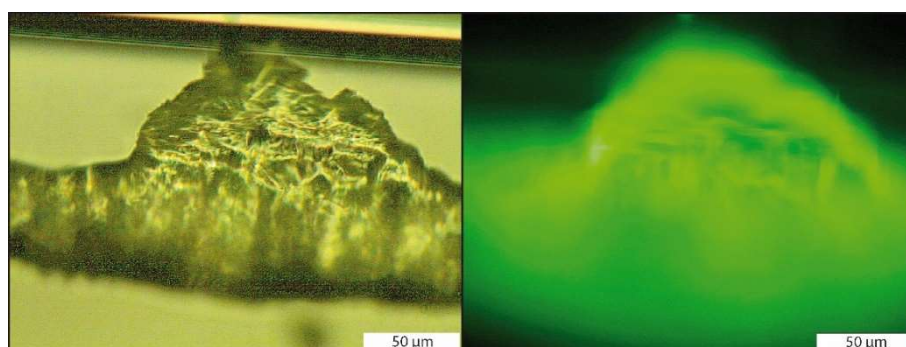


Figure D.4. Comparison of a Ba₂PO₃N:Eu²⁺ single-crystal irradiated with white light (left) and UV light (right).

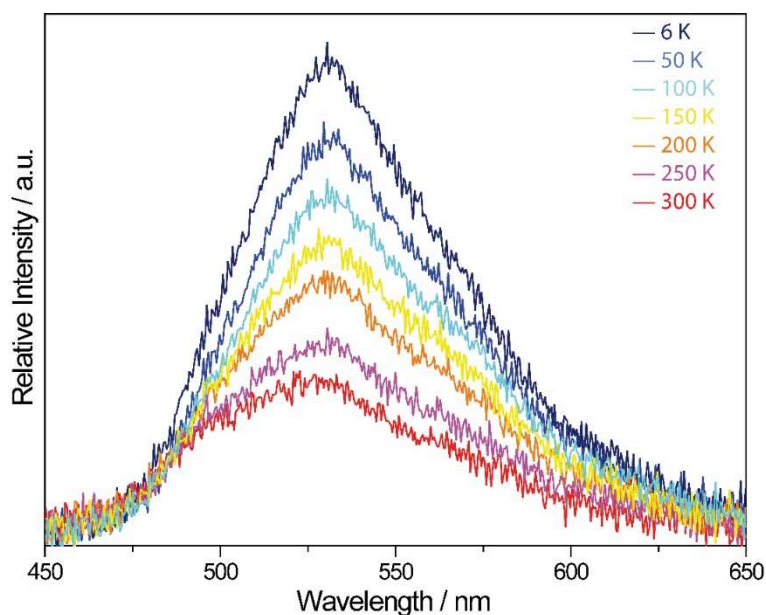


Figure D.5. Luminescence spectra of $\text{Ba}_2\text{PO}_3\text{N}:\text{Eu}^{2+}$ powder at temperatures ranging from 6 to 300 K.

D.2 Author Contributions

S.W.: Formal analysis: Lead; Investigation: Lead; Validation: Lead; Visualization: Lead; Writing – Original Draft: Lead; Writing – Review & Editing: Equal

M.M.: Conceptualization: Equal; Formal analysis: Equal; Investigation: Equal; Validation: Equal; Writing – Original Draft: Equal; Writing – Review & Editing: Equal

P.S.: Formal analysis: Supporting; Investigation: Supporting; Validation: Supporting; Writing – Original Draft: Supporting; Writing – Review & Editing: Supporting

P.S.: Conceptualization: Supporting; Formal analysis: Supporting; Funding acquisition: Supporting; Investigation: Supporting; Project administration: Supporting; Supervision: Supporting; Validation: Supporting; Writing – Original Draft: Supporting; Writing – Review & Editing: Supporting

W.S.: Conceptualization: Lead; Funding acquisition: Lead; Project administration: Lead; Resources: Lead; Supervision: Lead; Validation: Supporting; Writing – Original Draft: Supporting; Writing – Review & Editing: Equal

D.3 References

- [1] W. Gerlach, "Die Gitterstruktur der Erdalkalioxyde", *Z. Phys.* **1922**, 9, 184-192.
- [2] J. M. Léger, J. Haines, C. Chateau, G. Bocquillon, M. W. Schmidt, S. Hull, F. Gorelli, A. Lesauze, R. Marchand, "Phosphorus oxynitride PON, a silica analogue: structure and compression of the cristobalite-like phase; P-T phase diagram", *Phys. Chem. Miner.* **2001**, 28, 388-398.
- [3] M. Zeuner, S. Pagano, W. Schnick, "Nitridosilicates and Oxonitridosilicates: From Ceramic Materials to Structural and Functional Diversity", *Angew. Chem. Int. Ed.* **2011**, 50, 7754-7775; *Angew. Chem.* **2011**, 123, 7898-7920.

E Supporting Information for Chapter 6

E.1 Results and Discussions

Additional crystallographic data

Table E.1. Wyckoff positions and atomic coordinates of Sr₃P₃N₇ obtained from single-crystal X-ray diffraction, standard deviations in parentheses.

Atom	Wyckoff	x	y	z	U_{eq} [Å ²]
Sr1	2f	1/2	0.46228(16)	1/4	0.0188(3)
Sr2	4g	0.73739(16)	0.89636(11)	0.45130(11)	0.01718(19)
P1	4g	0.1749(3)	0.7068(3)	0.4251(3)	0.0158(4)
P2	2e	0	0.3684(4)	1/4	0.0165(6)
N1	2e	0	0.8006(13)	1/4	0.0177(19)
N2	4g	0.1711(9)	0.4873(9)	0.4010(9)	0.0147(13)
N3	4g	0.3899(9)	0.7822(10)	0.4302(9)	0.0190(14)
N4	4g	0.1178(10)	0.2307(10)	0.1330(9)	0.0198(14)

Table E.2. Anisotropic displacement parameters [Å²] of Sr₃P₃N₇, standard deviations in parentheses.

Atom	U_{11}	U_{22}	U_{33}	U_{23}	U_{13}	U_{12}
Sr1	0.0172(5)	0.0269(6)	0.0145(5)	0	0.0081(4)	0
Sr2	0.0154(3)	0.0225(4)	0.0159(3)	-0.0013(3)	0.0081(3)	-0.0009(3)
P1	0.0157(9)	0.0208(11)	0.0131(9)	-0.0010(8)	0.0080(8)	0.0000(8)
P2	0.0161(13)	0.0224(17)	0.0138(12)	0	0.0088(11)	0
N1	0.022(5)	0.021(5)	0.010(4)	0	0.005(4)	0
N2	0.007(3)	0.024(4)	0.011(3)	-0.002(2)	0.000(2)	0.000(2)
N3	0.018(3)	0.026(4)	0.015(3)	-0.002(3)	0.008(3)	0.001(3)
N4	0.022(3)	0.024(4)	0.017(3)	0.002(3)	0.013(3)	0.001(3)

Table E.3. Selected interatomic distances [Å] and angles [°] occurring in $\text{Sr}_3\text{P}_3\text{N}_7$ obtained from single-crystal X-ray diffraction, standard deviations in parentheses.

Sr1 – N1	2.740(9)	P1 – N1	1.631(8)	N1 – P1 – N1	115.0(4)
Sr1 – N1	2.740(9)	P1 – N1	1.575(10)	N1 – P1 – N3	112.3(5)
Sr1 – N2	2.846(9)	P1 – N3	1.646(10)	N1 – P1 – N3	106.7(5)
Sr1 – N2	2.846(9)	P1 – N3	1.646(10)	N1 – P1 – N3	106.7(5)
Sr1 – N2	2.883(10)	P2 – N2	1.575(10)	N1 – P1 – N3	112.3(5)
Sr1 – N2	2.883(10)	P2 – N4	1.638(6)	N3 – P1 – N3	103.3(5)
Sr1 – N1	2.895(7)	P2 – N1	1.642(9)	N2 – P2 – N4	111.4(5)
Sr1 – N1	2.895(7)	P2 – N3	1.683(10)	N2 – P2 – N1	110.2(5)
Sr1 – N3	3.068(10)			N2 – P2 – N3	108.2(5)
Sr1 – N3	3.068(10)			N4 – P2 – N1	111.1(5)
Sr2 – N2	2.504(10)			N4 – P2 – N3	104.5(5)
Sr2 – N4	2.665(4)			N1 – P2 – N3	111.3(5)
Sr2 – N2	2.726(9)				
Sr2 – N2	2.740(10)				
Sr2 – N3	2.772(9)				
Sr2 – N3	2.793(10)				
Sr2 – N3	2.978(9)				
Sr2 – N1	3.030(9)				
Sr2 – N4	3.283(10)				

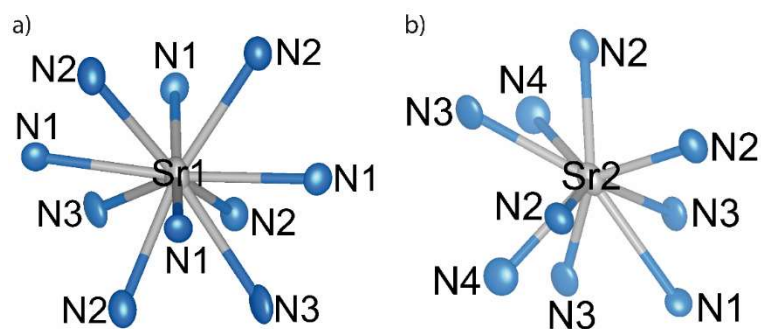
**Figure E.1.** Coordination polyhedra of Sr atoms (Sr1 (a) and Sr2 (b)) in $\text{Sr}_3\text{P}_3\text{N}_7$. Sr atoms are depicted in gray, nitrogen atoms in blue. Thermal ellipsoids are depicted at 90% probability.

Table E.4. Crystallographic data of ammonothermally synthesized $\text{Sr}_3\text{P}_3\text{N}_7$ obtained by Rietveld refinement, standard deviations in parentheses.

Formula	$\text{Sr}_3\text{P}_3\text{N}_7$
Crystal system	monoclinic
Space group	$P2/c$ (no. 13)
$a / \text{\AA}$	6.8970(4)
$b / \text{\AA}$	7.4289(4)
$c / \text{\AA}$	7.0693(4)
$\beta / ^\circ$	104.9555(11)
Cell volume / \AA^3	349.94(3)
Formula units / cell	2
Density / $\text{g}\cdot\text{cm}^{-3}$	4.3070(4)
T / K	293
Diffractometer	Stoe STADI P
Detector	Mythen 1K
Monochromator	Ge(111)
Radiation / \AA	$\text{Cu}\text{-}K_{\alpha 1}$ (1.5406)
2θ range / $^\circ$	$5.0 \leq 2\theta \leq 109.5$
Profile function	fundamental parameters approach
Background function	Shifted Chebyshev
Data points	6968
Number of reflections	442
Refined parameters	97
R_p	0.056
R_{wp}	0.073
R_{Bragg}	0.021
Goodness of Fit	1.19

Table E.5. Wyckoff positions and atomic coordinates of $\text{Sr}_3\text{P}_3\text{N}_7$ obtained from Rietveld refinement, standard deviations in parentheses.

Atom	Wyckoff	x	y	z	$U_{iso} [\text{\AA}^2]$
Sr1	2f	1/2	0.4601(3)	1/4	0.0191(11)
Sr2	4g	0.7372(2)	0.8960(2)	0.4557(2)	0.0191(11)
P1	4g	0.1729(5)	0.7081(5)	0.4218(7)	0.0184(14)
P2	2e	0	0.3709(8)	1/4	0.0184(14)
N1	2e	0	0.814(2)	1/4	0.017(2)
N2	4g	0.1646(17)	0.4822(13)	0.400(2)	0.017(2)
N3	4g	0.3883(16)	0.7946(17)	0.4309(17)	0.017(2)
N4	4g	0.1128(16)	0.2332(15)	0.1242(18)	0.017(2)

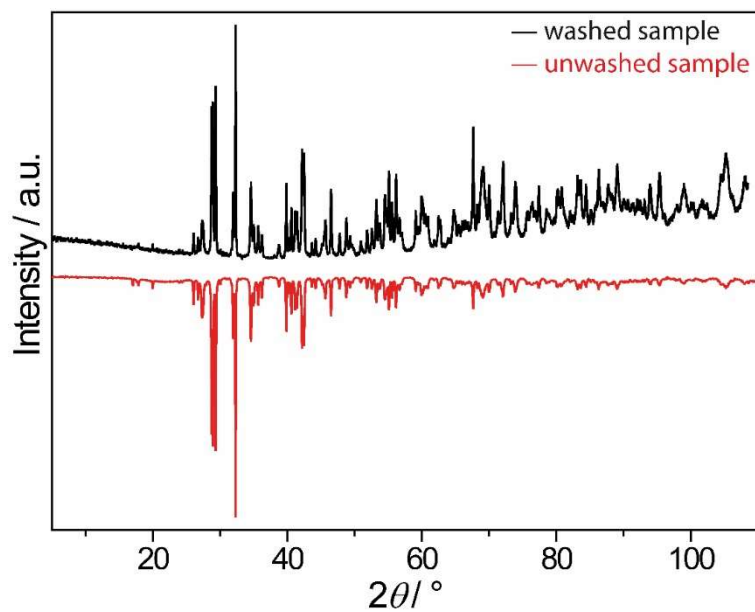


Figure E.2. Comparison of PXRD data of washed (black line) and unwashed (red line) $\text{Sr}_3\text{P}_3\text{N}_7$ samples synthesized ammonothermally.

Detailed Information on scanning electron microscopy

Table E.6. SEM EDX measurements of $\text{Sr}_3\text{P}_3\text{N}_7:\text{Eu}^{2+}$.

$\text{Sr}_3\text{P}_3\text{N}_7:\text{Eu}^{2+}$	Sr	P	N	Eu	O
measurement 1:	20.8	19.9	58.5	0.8	-
measurement 2:	24.2	24.4	47.2	0.7	3.5
measurement 3:	19.9	21.0	50.9	0.7	7.5
measurement 4:	19.5	23.3	56.7	0.5	-
∅	21.1	22.1	53.3	0.7	2.8
calculated	22.6	23.1	53.8	0.5	-

Detailed information on IR spectroscopy

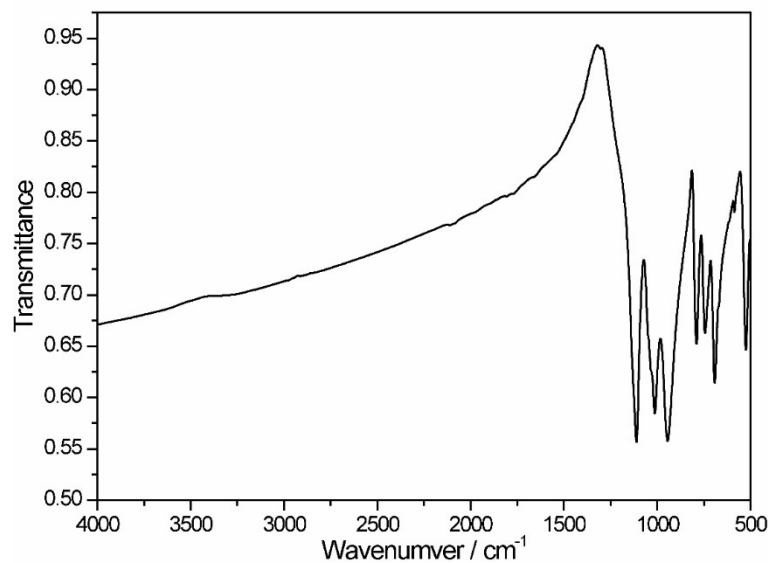


Figure E.3. FTIR spectrum of ammonothermally synthesized $\text{Sr}_3\text{P}_3\text{N}_7$, measured using the KBr pellet method.

Detailed information on UV/Vis spectroscopy

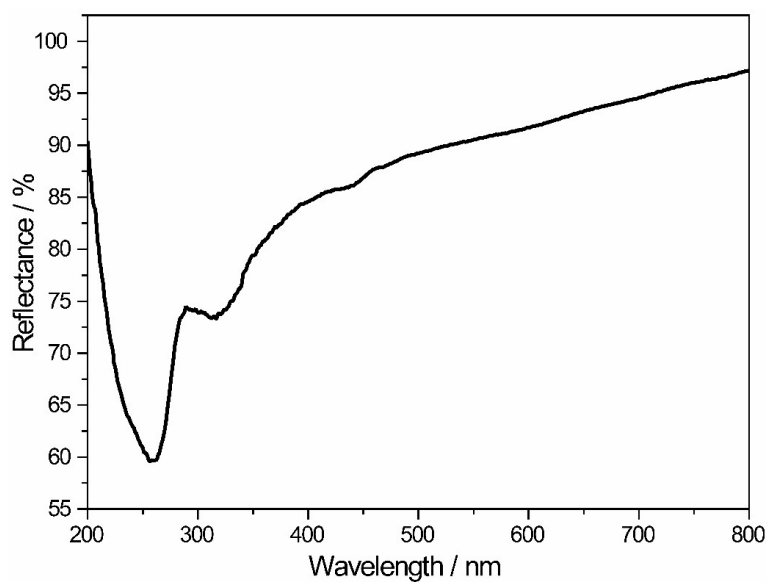


Figure E.4. Diffuse reflectance spectrum of ammonothermally synthesized $\text{Sr}_3\text{P}_3\text{N}_7$. The lamp switch causes the artifact around 340 nm.

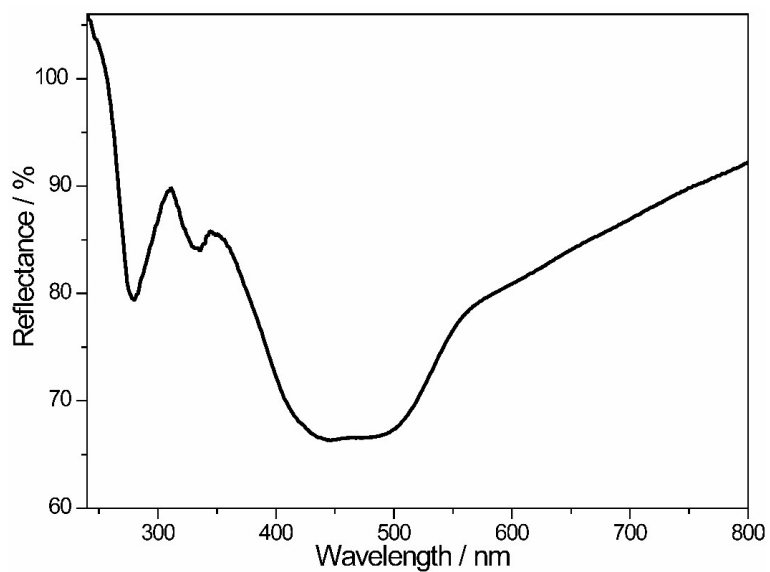


Figure E.5. Diffuse reflectance spectrum of ammonothermally synthesized $\text{Sr}_3\text{P}_3\text{N}_7:\text{Eu}^{2+}$. The lamp switch causes the artifact around 340 nm.

Luminescence properties



Figure E.6. Photograph of ammonothermally synthesized red luminescence $\text{Sr}_3\text{P}_3\text{N}_7:\text{Eu}^{2+}$ powder in a glass capillary when irradiated with UV light.

E.2 Author Contributions

M.M.: Conceptualization: Equal; Formal analysis: Equal; Investigation: Equal; Validation: Equal; Visualization: Equal; Writing - Original Draft: Equal; Writing - Review & Editing: Equal

S.W.: Conceptualization: Equal; Formal analysis: Equal; Investigation: Equal; Validation: Equal; Writing - OriginalDraft: Equal; Writing - Review & Editing: Equal

P.S.: Formal analysis: Supporting; Investigation: Supporting; Validation: Supporting; Writing - Original Draft: Supporting; Writing - Review & Editing: Supporting

P.S.: Formal analysis: Supporting; Funding acquisition: Supporting; Project administration: Supporting; Resources: Supporting; Supervision: Supporting; Validation: Supporting; Writing - Original Draft: Supporting; Writing - Review & Editing: Supporting

W.S.: Conceptualization: Equal; Funding acquisition: Lead; Project administration: Lead; Resources: Lead; Supervision: Lead; Validation: Equal; Writing - Original Draft: Supporting; Writing - Review & Editing: Equal.

F Supporting Information for Chapter 7

F.1 Experimental

Inert conditions

All manipulations were carried out in an Ar filled glovebox (MBraun, H₂O, O₂ < 1 ppm), in order to prevent starting materials from oxidation and hydrolysis.

Preparation of starting materials

Phosphorus nitride P₃N₅ was prepared by ammonolysis starting from P₄S₁₀ (ca. 7.0 g, Acros Organics, > 98%) in a tube furnace.^[1,2] After heating the silica reaction tube (4 h, 1000 °C, ≤ 10–3 mbar), P₄S₁₀ was loaded and saturated in a flow of dry ammonia (≈ 3.6 L h⁻¹, Air Liquide, 5.0) at room temperature. The reaction mixture was heated to 850 °C (rate: 5 °C min⁻¹) for 4 h in a constant flow of ammonia. The product was obtained in form of orange grains, which were purified by treatment with water, ethanol, and acetone. Purity was confirmed by X-ray diffraction, FTIR spectroscopy, and CHNS analysis.

Calcium azide Ca(N₃)₂ was prepared according to the instructions of Suhrmann and modified by Karau.^[3,4] Therefore, a diluted solution of HN₃, which is formed in situ by passing an aqueous solution of NaN₃ through a cation exchanger (Amberlyst 15), is dropped into a stirring aqueous suspension of CaCO₃ (Alfa Aesar, 99.5%). When the eluate shows a neutral pH value and the solution turns clear, residues of CaCO₃ are filtered off and the solvent is removed with a rotary evaporator (50 mbar, 40 °C). The product yielded as colorless and fine powder. After recrystallization from acetone, phase purity was confirmed by X-ray diffraction and FTIR spectroscopy.

Caution: Special care is absolute necessary as gaseous HN₃ is potentially explosive and highly poisonous.

Synthesis with a hot isostatic press

Ca₂PN₃ was synthesized under N₂ atmosphere (99.9%) in a hot isostatic press (HIP, AIP6-30H, American Isostatic Presses, Inc., Columbus, Ohio, USA) starting from stoichiometric amounts of Ca₃N₂ (ABCR, 99%) or Ca(N₃)₂, and P₃N₅ or P_{red} (Chempur, ≥ 99.999%). Small amounts of EuCl₂ (~ 3 mol% with respect to Ca) were added for the syntheses of Eu²⁺-doped samples. The starting materials were ground in an agate mortar and given into a tungsten crucible. This crucible was closed with a lid made out of tungsten and placed in a second one made out of corundum. This assembly was closed with a

corundum plate and transferred into the pressure module and placed between the heating elements of the carbon fiber reinforced carbon furnace ($T_{\max} = 2000$ °C, $\phi = 70$ mm, $h = 125$ mm). After rinsing the atmosphere in the pressure vessel ($p_{\max} = 207$ MPa) with Ar for 10 times, a pressure booster (Maximator, DLE-5-30-2, $p_{\max} = 60$ MPa) was used to build up the necessary pressure to operate the main compressor. Following, the pressure was constantly increased to 70 MPa. Subsequently, the sample was heated to 1200 °C within 4 h while ending up with a pressure of 150 MPa. After maintaining these conditions for 10 h, the mixture was cooled down to 20 °C and the pressure was released. The detailed pressure and temperature curves are plotted in Figures F1 and F2. The products were obtained as colorless to light beige sinter cakes, which show a high sensitivity towards air and moisture.

Single-crystal X-ray diffraction (SC-XRD)

Selected single crystals were transferred into glass capillaries (ϕ 0.5 mm, Hilgenberg, Malsfeld, Germany) filled with dried paraffin oil. The collection of single crystal X-ray diffraction data was carried out with a Bruker D8 Quest diffractometer (Mo- K_{α} radiation). Received data were indexed and integrated with the APEX3 software package.^[5, 6] Semi-empirical absorption correction and determination of the space group were conducted with APEX3, as well.^[7-9] The structure was solved using the SHELXT algorithm and refined by full-matrix least-squares methods applying WinGX with implemented SHELXL.^[10, 11]

Powder X-ray diffraction (PXRD)

Samples of Ca_2PN_3 were ground and sealed in glass capillaries (ϕ 0.5 mm, Hilgenberg, Malsfeld, Germany). A Stoe Stadi P device (Cu- $K_{\alpha 1}$ ($\lambda = 1.5406$ Å) radiation, Stoe & Cie GmbH, Darmstadt, Germany, Ge(111) monochromator) in parafocusing Debye-Scherrer geometry, equipped with a Mythen 1K Si strip detector (Dectris, Baden, Switzerland) was used to collect powder X-ray diffraction data. Phase purity of the samples was confirmed by Rietveld refinements using the Topas Academic software.^[12, 13] Peak profiles were modeled by the fundamental parameter approach, while the background was fitted by a shifted Chebyshev polynomial.^[14, 15] A fourth order spherical harmonics function accounted for any possible preferred orientation.

Scanning electron microscopy (SEM) and energy dispersive X-ray spectroscopy (EDX)

Examination of the morphology and the chemical composition was carried out with a Dualbeam Helios Nanolab G3 UC (FEI) microscope with attached X-Max 80 SSD EDX detector (Oxford Instruments). Samples were coated with a thin film of carbon by an electron beam evaporator (BAL-TEC MED 020, Bal Tec AG) prior to measurements in order to provide electrical conductivity. EDX measurements were carried out with an accelerating voltage of 20 kV.

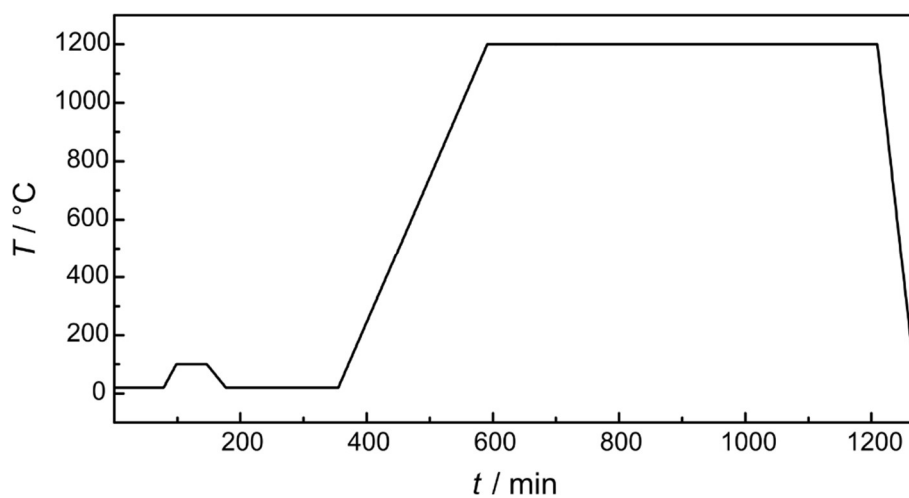
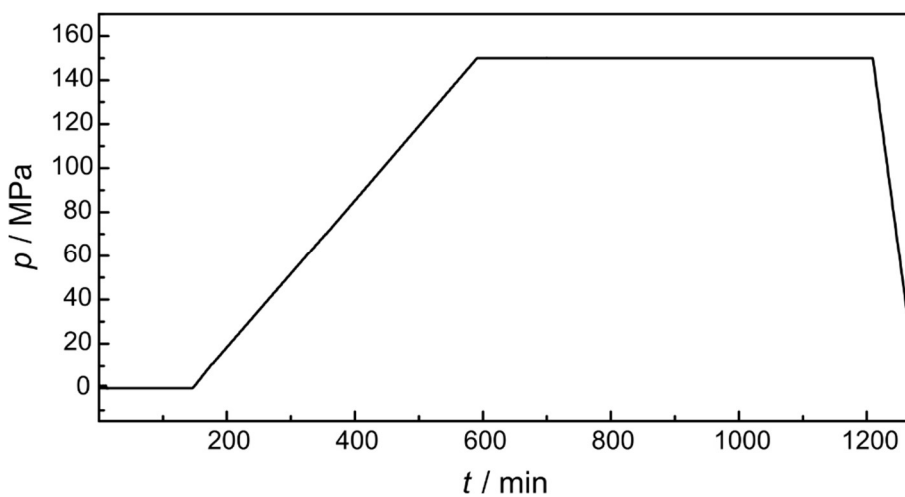
Luminescence

Small Eu²⁺-doped (3 mol%) particles of Ca₂PN₃ were sealed in fused silica capillaries and investigated with a Horiba Fluoromax4 spectrofluorimeter system and an Olympus BX51 microscope attached by optical fibers. Within a spectral range from 400 to 800 nm emission spectra were recorded at room temperature with a step width of 2 nm and an excitation wavelength of $\lambda_{\text{exc}} = 440$ nm.

An in-house-built system was used to investigate thick-bed powder samples of Eu²⁺-doped (3 mol%) Ca₂PN₃. The system is based on a spectrofluorimeter with 5.3" integration sphere. The spectrofluorimeter is equipped with a 150 W Xe lamp and two Czerny-Turner monochromators, providing a focal length of 500 mm (grating: 1800 g mm⁻¹, blazed at 250/500 nm). The spectral range reaches from 230 up to 820 nm. Internal quantum efficiency (IQE) was determined by comparing integrated emission and absorption intensities to reference samples (BaSO₄ (white standard), SrSi₂O₂N₂:Eu²⁺).

Visualization

The software packages Origin 6.1 and VESTA were used for the illustration of powder X-ray diffraction data and crystal structures, respectively.^[16]

Plots of the used temperature and pressure programs**Figure F1.** Plot of the used temperature program for the synthesis of Ca_2PN_3 .**Figure F2.** Plot of the used pressure program for the synthesis of Ca_2PN_3 .

F.2 Results and Discussion

Single-crystal X-ray diffraction of Ca_2PN_3 **Table F1.** Crystallographic data of Ca_2PN_3 (synthesized by HIP approach) obtained from single-crystal X-ray diffraction compared to values obtained from powder X-ray diffraction in literature.^[17, 18]

Formula	Ca_2PN_3 , SC	Ca_2PN_3 , PXRD ^[17, 18]
Formula weight / $\text{g}\cdot\text{mol}^{-1}$	153.15	
Crystal system; space group	orthorhombic; $Cmce$ (no. 64)	
Lattice parameters / Å	$a = 5.1987(4)$	$a = 5.1914(4)$
	$b = 10.3145(10)$	$b = 10.3163(8)$
	$c = 11.283(1)$	$c = 11.288(1)$
Cell volume / Å ³	605.04(1)	604.60(6)
Formula units per unit cell	8	
Density / $\text{g}\cdot\text{cm}^{-3}$	3.363	-
μ / mm^{-1}	4.031	-
Diffractometer	Bruker D8 Quest	Stoe Stadi P
Radiation	Mo- K_α ($\lambda = 0.71073$)	Cu- $K_{\alpha 1}$ ($\lambda = 1.5406$ Å)
θ -range / °	$3.6 < \theta < 35.6$	$5.0 < \theta < 45.0$
Data points	-	4001
Total number of reflections	11096	138
No. of independent reflections	755	-
Observed Reflections ($F^2 > 2\sigma(F^2)$)	690	-
$R_{\text{int}}; R_\sigma$	0.055; 0.024	-
Structure solution	SHELXT	Patterson-Method
Structure refinement	SHELXL	Rietveld
Refined parameters	36	31
Profile function	-	Pseudo-Voigt
Goodness of fit (χ^2)	1.085	1.35
$R1$ (all data); $R1$ ($F^2 > 2\sigma(F^2)$)	0.020; 0.017	-
$wR2$ (all data); $wR2$ ($F^2 > 2\sigma(F^2)$)	0.045; 0.043	-
$\Delta\rho_{\text{max}}; \Delta\rho_{\text{min}}$ / $\text{e}\cdot\text{Å}^{-3}$	0.358; -0.603	-
$R_p; R_{\text{wp}}$	-	0.0497; 0.0636

The determined cell parameters are in good agreement with a maximal difference of 9σ (a : 9σ ; b : 2σ ; c : 3σ ; V : 6σ). The actual matching of the lattice parameters is likely to be even better, since standard deviations from Rietveld refinements are systematically underestimated for small step width (here: 0.01°).

Table F2. Atomic coordinates, crystallographic positions, and equivalent displacement parameters (in Å²) of Ca₂PN₃.

Atom	Wyckoff	X	y	z	U _{eq.}
Ca1	8f	0	0.05239(3)	0.35715(3)	0.00805(7)
Ca2	8f	0	0.36240(3)	0.42593(3)	0.00703(7)
P1	8f	0	0.24405(3)	0.16524(3)	0.00472(8)
N1	8f	0	0.33923(12)	0.05050(11)	0.0072(2)
N2	8f	0	0.08840(11)	0.13966(11)	0.0078(2)
N3	8e	1/4	0.28775(12)	1/4	0.0085(2)

Table F3. Anisotropic displacement parameters of Ca₂PN₃ (in Å²).

Atom	U ₁₁	U ₂₂	U ₃₃	U ₁₂	U ₁₃	U ₂₃
Ca1	0.00907(12)	0.00804(12)	0.00702(12)	0.00000	0.00000	0.00112(8)
Ca2	0.00798(12)	0.00681(12)	0.00629(12)	0.00000	0.00000	-0.00044(8)
P1	0.00486(14)	0.00470(14)	0.00460(15)	0.00000	0.00000	0.00018(10)
N1	0.00850(5)	0.00670(4)	0.00650(5)	0.00000	0.00000	0.00100(4)
N2	0.00990(5)	0.00530(4)	0.00810(5)	0.00000	0.00000	0.00070(4)
N3	0.00630(4)	0.01070(5)	0.00860(5)	0.00000	-0.00230(4)	0.00000

Table F4. Interatomic distances (Å) and bond angles (°) of Ca₂PN₃.

Ca1–	N1	2.4331(13)	N1 –P1–	N2	116.98(6)
	N1	2.4514(13)		N3	106.99(2)
	N2	2.4820(13)	N2	N3	111.46(2)
	N2 (2x)	2.6260(3)	N3	N3	101.74(1)
	N3 (2x)	3.0074(11)			
Ca2–	N2	2.4457(12)			
	N2	2.4644(13)			
	N3 (2x)	2.4945(5)			
	N1	2.5101(13)			
	N1 (2x)	2.6238(3)			
P1–	N1	1.6248(13)			
	N2	1.6312(12)			
	N3 (2x)	1.6754(4)			

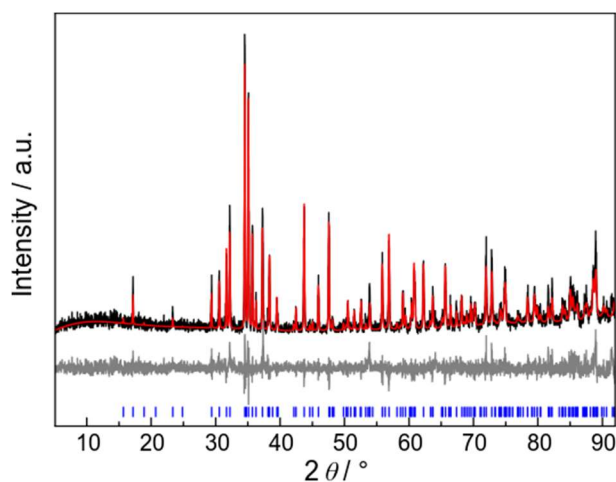
Rietveld refinement of Ca_2PN_3 

Figure F3. Rietveld refinement for Ca_2PN_3 ; observed (black, Cu- $K_{\alpha 1}$) and refined (red) diffraction pattern. The difference profile is displayed in gray. Positions of Bragg reflections of Ca_2PN_3 are marked with vertical blue bars. Deviations in intensity might be caused by hydrolysis of the product and a poor signal-to-noise ratio.

Table F5. Crystallographic data of the Rietveld refinement of Ca_2PN_3 .

Formula	Ca_2PN_3
Formula weight / $\text{g}\cdot\text{mol}^{-1}$	153.15
Crystal system; space group	orthorhombic; $Cmce$ no. 64
Lattice parameters / Å	$a = 5.1885(4)$ $b = 10.3085(9)$ $c = 11.2842(9)$
Cell volume / Å^3	603.54(8)
Formula units per unit cell	8
Density / $\text{g}\cdot\text{cm}^{-3}$	3.371
μ / mm^{-1}	35.738
Diffractometer	Stoe Stadi P
Radiation	Cu- $K_{\alpha 1}$ ($\lambda = 0.15406 \text{ Å}$)
Detector	Mythen 1K
Monochromator	Ge(111)
2θ -range / $^\circ$	$5.0 \leq 2\theta \leq 90.0$
Data points	5876
Total number of reflections	155
Refined parameters	30
Background function	Shifted Chebyshev
Number of background parameters	12
Goodness of fit (χ^2)	0.962
R_p ; R_{wp}	0.216; 0.289
R_{exp} ; R_{Bragg}	0.301; 0.081

Discussion of the Rietveld refinement and additional powder X-ray diffraction data

The observed deviations in intensity might have different reasons. First, the sensitivity of Ca_2PN_3 towards moisture has to be mentioned. Even shortest reaction time with atmosphere after reaction (transfer into glovebox) seems to be sufficient for the beginning of hydrolysis. This assumption is illustrated in Figures F4 and F5 in which two diffractograms of the identical sample (immediately after sealing and 1 h after sealing) are compared in terms of absolute and relative intensity. It is noticeable that the absolute intensity of reflections decreases significantly after only one hour. Comparing relative intensities of the measured diffractograms, it can be observed that the amorphous amount increases, while the most intense reflections lose intensity faster than weaker ones. A second reason for the observed deviations is the poor signal-to-noise ratio. This issue is due to short measuring time and is a consequence of the above-mentioned hydrolysis. The most likely formed hydrolysis product $\text{Ca}(\text{OH})_2$ chemically corrodes the SiO_2 capillaries and makes longer measurements impossible. Already after one hour, the capillaries become brittle and are no longer suitable for measurements. Within a few days the capillaries are eroded completely and the remaining solid residue can be identified as $\text{Ca}(\text{OH})_2$ and calcium oxosilicate (Figure F6).

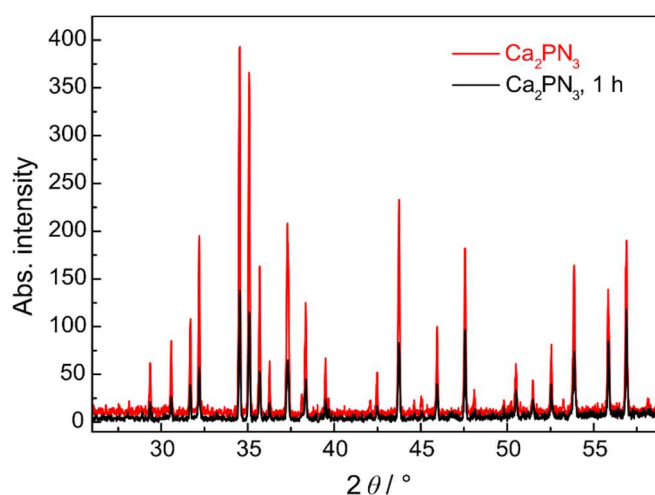


Figure F4. Comparison of the absolute intensities of measured diffractograms of Ca_2PN_3 immediately after sealing (red) and 1 h after sealing (black). A remarkable loss of absolute intensity can be observed.

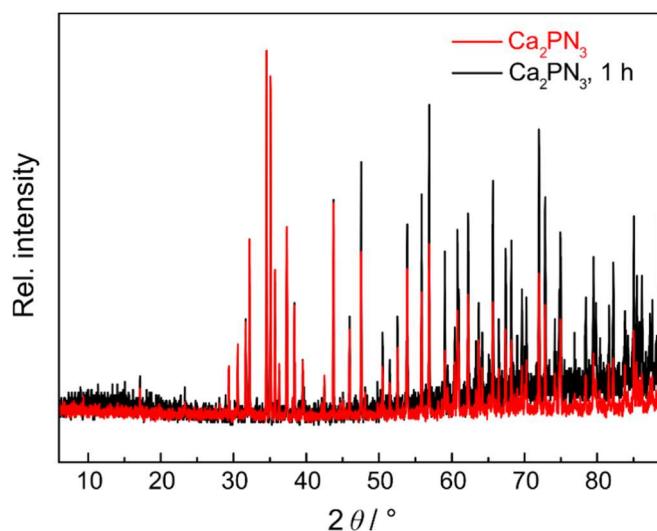


Figure F5. Comparison of the relative intensities of measured diffractograms of Ca_2PN_3 immediately after sealing (red) and 1 h after sealing (black). The amorphous amount increases, while the most intense reflections lose intensity faster than weaker ones.

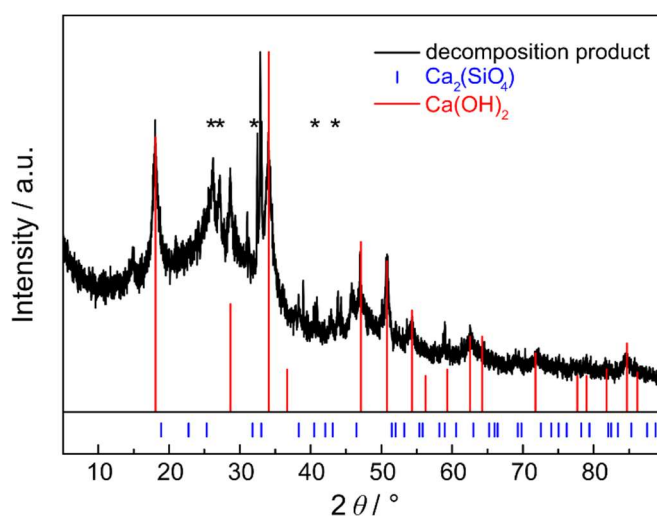


Figure F6. Powder X-ray diffraction pattern (black) of the observed decomposition product after eroding the capillaries. $\text{Ca}(\text{OH})_2$ and Ca_2SiO_4 can be identified. Unidentified reflections are tagged with asterisks.

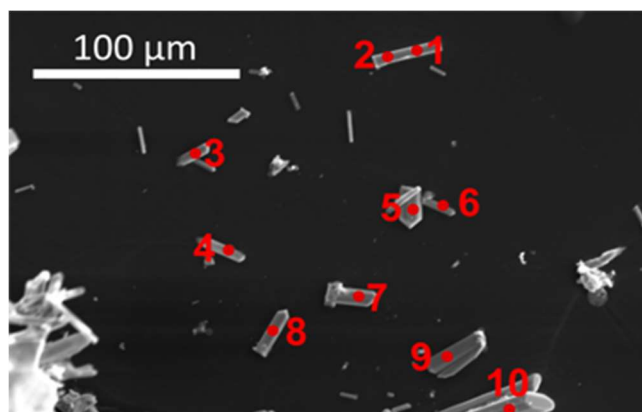
EDX (SEM) measurements of Ca_2PN_3 

Figure F7. SEM image of Ca_2PN_3 obtained by hot isostatic pressing. Ten different EDX measuring points on selected single crystals are tagged with red dots.

Table F6. EDX measurements (at%) of the selected points of Ca_2PN_3 (20.0 kV acceleration voltage). For normalized values only Ca, P, and N are taken into account. Standard deviations are given in parentheses.

	Ca	P	N	O	Cl
1	27	15	51	5	2
2	28	16	49	6	1
3	33	16	42	7	2
4	23	13	58	5	1
5	26	14	56	3	1
6	25	14	54	6	1
7	29	16	49	4	2
8	28	15	52	4	1
9	30	16	47	5	2
10	30	15	51	3	1
Average	28(3)	15(1)	51(5)	5(1)	1(1)
Normalized	1.9(2)	1.0(1)	3.4(3)	-	-

F.3 Author Contributions

S.W.: Formal analysis: Lead; Investigation: Lead; Validation: Equal; Visualization: Lead; Writing - Original Draft: Lead; Writing - Review & Editing: Lead

S.M.: Investigation: Supporting; Writing - Review & Editing: Supporting

P.S.: Formal analysis: Supporting; Investigation: Supporting; Validation: Supporting; Writing - Original Draft: Supporting; Writing - Review & Editing: Supporting

P.S.: Conceptualization: Equal; Formal analysis: Supporting; Investigation: Supporting; Methodology: Supporting; Project administration: Equal; Resources: Equal; Supervision: Equal; Validation: Supporting; Writing - Original Draft :Supporting; Writing - Review & Editing: Supporting

W.S.: Conceptualization: Equal; Funding acquisition: Equal; Project administration: Equal; Resources: Equal; Supervision: Equal; Validation: Equal; Writing - Original Draft: Supporting; Writing - Review & Editing: Supporting

F.4 References

- [1] A. Stock, B. Hoffmann, "Die Einwirkung von Ammoniak auf Phosphorpentasulfid und der Phosphorstickstoff, P_3N_5 ", *Ber. Dtsch. Chem. Ges.* **1903**, 36, 314-319.
- [2] A. Stock, H. Grüneberg, "Über den Phosphorstickstoff", *Ber. Dtsch. Chem. Ges.* **1907**, 40, 2573-2578.
- [3] R. Suhrmann, K. Clusius, "Über die Reindarstellung der Alkalimetalle", *Z. Anorg. Allg. Chem.* **1926**, 152, 52-58.
- [4] F. W. Karau, Dissertation, Ludwig-Maximilians-Universität München (Germany) **2007**.
- [5] Data Integration Software, *SAINT*, Madison, Wisconsin, USA, **1997**.
- [6] Bruker AXS, Inc., *APEX3*, Karlsruhe, Germany, **2016**.
- [7] Bruker AXS, Inc., *SADABS*, Madison, Wisconsin, USA, **2001**.
- [8] G. M. Sheldrick, "A short history of *SHELX*", *Acta Crystallogr. Sect. A* **2008**, 64, 112-122.
- [9] Bruker AXS, Inc., *XPREP Reciprocal Space Exploration*, Karlsruhe, Germany, **2001**.
- [10] G. M. Sheldrick, "*SHELXT - Integrated space-group and crystal-structure determination*", *Acta Crystallogr. Sect. A* **2015**, 71, 3-8.
- [11] G. M. Sheldrick, "*Crystal structure refinement with SHELXL*", *Acta Crystallogr. Sect. C* **2015**, 71, 3-8.
- [12] A. A. Coelho, *TOPAS Academic*, Version 6, Coelho Software, Brisbane, Australia, **2016**.
- [13] H. Rietveld, "A profile refinement method for nuclear and magnetic structures", *J. Appl. Crystallogr.* **1969**, 2, 65-71.
- [14] R. W. Cheary, A. Coelho, "A fundamental parameters approach to X-ray line-profile fitting", *J. Appl. Crystallogr.* **1992**, 25, 109-121.
- [15] R. W. Cheary, A. A. Coelho, J. P. Cline, "Fundamental Parameters Line Profile Fitting in Laboratory Diffractometers", *J. Res. Natl. Inst. Stand. Technol.* **2004**, 109, 1-25.
- [16] K. Momma, F. Izumi, "VESTA 3 for three-dimensional visualization of crystal, volumetric and morphology data", *J. Appl. Crystallogr.* **2011**, 44, 1272-1276.
- [17] W. Schnick, V. Schultz-Coulon, "*Ca₂PN₃: A New Phosphorus(V) Nitride with One-Dimensional Infinite Chains of Corner-Sharing PN₄ Tetrahedra*", *Angew. Chem. Int. Ed. Engl.* **1993**, 32, 280-281; *Angew. Chem.* **1993**, 105, 308-309.

- [18] V. Schultz-Coulon, W. Schnick, "*Mg₂PN₃ and Ca₂PN₃ – Phosphorus(V) Nitrides with Infinite Chains of Corner Sharing PN₄ Tetrahedra*", *Z. Anorg. Allg. Chem.* **1997**, 623, 69-74.

G Supporting Information for Chapter 8

G.1 Experimental

Inert conditions

All starting materials were handled in Ar filled gloveboxes (MBraun, H₂O, O₂ < 1 ppm), in order to prevent oxidation and hydrolysis.

Synthesis with a hot isostatic press

The synthesis of $AE_3P_5N_{10}X$ ($AE = Sr, Ba$; $X = Cl, Br$) was carried out under N₂ (99.9%) atmosphere in a hot isostatic press (HIP, AIP6-30H, American Isostatic Presses, Inc., Columbus, Ohio, USA) at 150 MPa and 1200 °C. Reactions were started from stoichiometric amounts of the respective azides $AE(N_3)_2$ ($AE = Sr, Ba$), halides AEX_2 ($AE = Sr, Ba$; $X = Cl, Br$), and P₃N₅ or P_{red.} Additional EuCl₂ (~ 3 mole% with respect to AE^{2+}) was used for the syntheses of Eu²⁺-doped samples. After grinding the starting materials thoroughly in an agate mortar, the mixture was filled into a W crucible. The latter was closed with a W lid and put into an Al₂O₃ vessel. The closed assembly was placed between the graphite heating elements ($T_{max} = 2000$ °C, $\phi = 70$ mm, $h = 125$ mm) of the furnace in the pressure module ($p_{max} = 207$ MPa). Before reaction, the reactor was rinsed with Ar for ten times. Afterwards, a pressure booster (Maximator, DLE-5-30-2, $p_{max} = 60$ MPa) was used to build up the necessary pressure to operate the main compressor. The pressure was increased to 70 MPa at 20 °C, followed by heating the sample up to 1000 °C within 4 h (rate: ≈ 250 °C·min⁻¹), ending up at a synthesis pressure of 150 MPa. Synthesis conditions were maintained for 10 h. The system was allowed to cool down to 20 °C before releasing the pressure. Figures G1 and G2 show the detailed temperature and pressure programs. Undoped products were isolated as colorless solids, while Eu²⁺-doped samples show yellow (Ba compounds) to orange body colors (Sr compounds). All compounds are insensitive towards oxidation and were washed with deionized water after reaction.

Powder X-ray diffraction (PXRD)

After sealing ground samples in glass capillaries (ϕ 0.5 mm, Hilgenberg, Malsfeld, Germany) Stoe Stadi P devices (Stoe & Cie GmbH, Darmstadt, Germany, Ge(111) monochromator) with Cu-K α_1 ($\lambda = 1.5406$ Å) or Mo-K α_1 ($\lambda = 0.71073$ Å) radiation were used for measurements in parafocusing Debye-Scherrer geometry. Data collection was carried out with a Mythen 1K Si strip detector (Dectris,

Baden, Switzerland). The Rietveld method was applied to refine the structure model of $\text{Sr}_3\text{P}_5\text{N}_{10}\text{Br}$ (more details follow below), as well as to confirm the phase purity of all samples. In this context the Topas Academic software was used.^[1,2] During refinements a shifted Chebyshev polynomial was used to fit the background and peak profiles were modeled applying a fundamental parameters approach.^[3,4] Possible preferred orientation was handled taking a fourth order spherical harmonics function into account.

Single crystal X-ray diffraction (SC-XRD)

Suitable single crystals of $\text{Sr}_3\text{P}_5\text{N}_{10}\text{Cl}$ were selected with a optical microscope (MZ 12, Leica, Wetzlar, Germany) and fixed on MicroMounts (20 μm , MiTeGen, Ithaca, New York, USA). The data collection was performed with a Bruker D8 Venture diffractometer (Mo- K_α radiation). The software package APEX 3 was used for indexing, integration, semi-empirical absorption correction and determination of the space group.^[5-9] WinGX with its implemented tools SHELXT and SHELXL was used for structure solution and refinement by full-matrix least-squares method.^[10,11]

Scanning electron microscopy (SEM) and energy dispersive X-ray spectroscopy (EDX)

Imaging of the samples in a nanoscale was carried out with a Dualbeam Helios Nanolab G3 UC (FEI) microscope. An additionally attached X-Max 80 SSD EDX detector (Oxford Instruments) allowed for the determination of the chemical compositions of the title compounds at an accelerating voltage of 20 kV. Prior to measurements, a thin film of carbon was put on by an electron beam evaporator (BAL-TEC MED 020, Bal Tec AG) to ensure electrical conductivity of the samples.

Luminescence

Luminescence measurements of small Eu^{2+} -doped (3 mol%) particles, which were sealed in fused silica capillaries, were carried out with a Horiba Fluoromax4 spectrofluorimeter system. An Olympus BX51 microscope was attached by optical fibers. Emission spectra were recorded at room temperature in a range from 400 to 800 nm with a step width of 2 nm and an excitation wavelength of $\lambda_{\text{exc}} = 420$ nm.

Thick-bed powder samples of Eu^{2+} -doped (3 mol%) samples were examined with an in-house-built system. This is based on a 5.3" integration sphere and a spectrofluorimeter, which is equipped with a 150 W Xe lamp and two Czerny-Turner monochromators. The respective focal length is 500 mm (grating: 1800 g mm^{-1} , blazed at 250/500 nm) and the spectral range reaches from 230 up to 820 nm.

The determination of internal quantum efficiencies (IQE) was carried out by comparing integrated emission and absorption intensities with reference samples (BaSO_4 (white standard), $\text{SrSi}_2\text{O}_2\text{N}_2:\text{Eu}^{2+}$).

Visualization

Origin 6.1 was used to plot the collected data. VESTA was used to illustrate crystal structures.^[12]

Weighed portions

Table G1. Weighed portions of starting materials for the syntheses of $\text{AE}_3\text{P}_5\text{N}_{10}\text{X}:\text{Eu}^{2+}$ ($\text{AE} = \text{Sr}, \text{Ba}; \text{X} = \text{Cl}, \text{Br}$)

Title compound	Starting materials / mg			
$\text{Sr}_3\text{P}_5\text{N}_{10}\text{Cl}:\text{Eu}^{2+}$	$\text{Sr}(\text{N}_3)_2$	SrCl_2	P_3N_5	EuCl_2
	120.00	22.16	75.94	5.61
$\text{Sr}_3\text{P}_5\text{N}_{10}\text{Cl}:\text{Eu}^{2+}$	$\text{Sr}(\text{N}_3)_2$	SrCl_2	P_{red}	EuCl_2
	140.00	25.86	12.63	6.54
$\text{Sr}_3\text{P}_5\text{N}_{10}\text{Br}:\text{Eu}^{2+}$	$\text{Sr}(\text{N}_3)_2$	SrBr_2	P_3N_5	EuCl_2
	115.00	33.15	72.78	5.38
$\text{Sr}_3\text{P}_5\text{N}_{10}\text{Br}:\text{Eu}^{2+}$	$\text{Sr}(\text{N}_3)_2$	SrBr_2	P_{red}	EuCl_2
	140.00	40.36	12.63	6.54
$\text{Ba}_3\text{P}_5\text{N}_{10}\text{Cl}:\text{Eu}^{2+}$	$\text{Ba}(\text{N}_3)_2$	BaCl_2	P_3N_5	EuCl_2
	140.00	26.34	68.70	5.07
$\text{Ba}_3\text{P}_5\text{N}_{10}\text{Cl}:\text{Eu}^{2+}$	$\text{Ba}(\text{N}_3)_2$	BaCl_2	P_{red}	EuCl_2
	200.00	37.63	14.00	7.25
$\text{Ba}_3\text{P}_5\text{N}_{10}\text{Br}:\text{Eu}^{2+}$	$\text{Ba}(\text{N}_3)_2$	BaBr_2	P_3N_5	EuCl_2
	150.00	40.27	73.61	5.44
$\text{Ba}_3\text{P}_5\text{N}_{10}\text{Br}:\text{Eu}^{2+}$	$\text{Ba}(\text{N}_3)_2$	BaBr_2	P_{red}	EuCl_2
	190.00	51.01	13.29	6.89

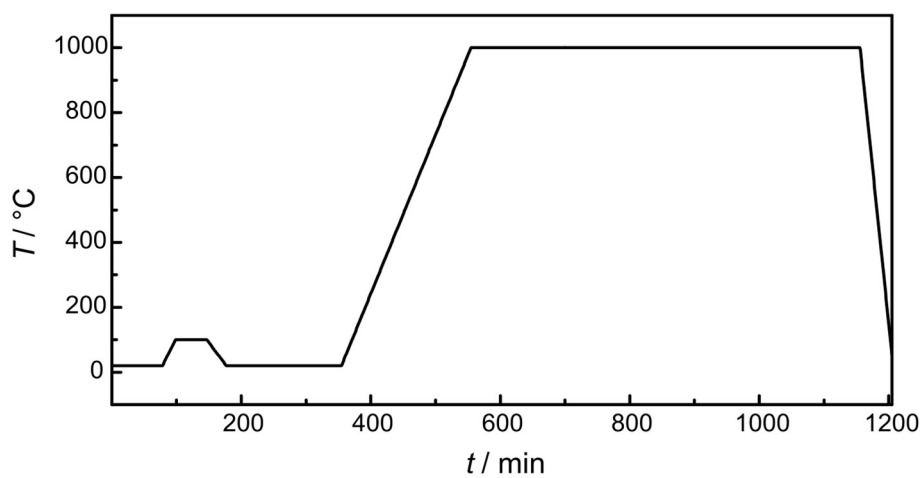
Plots of the used temperature and pressure programs

Figure G1. Plot of the used temperature program for the synthesis of $AE_3P_5N_{10}X$ ($AE = Sr, Ba; Cl, Br$). The first temperature increase ($\approx 100\text{ }^\circ\text{C}$) serves to heat the graphite elements.

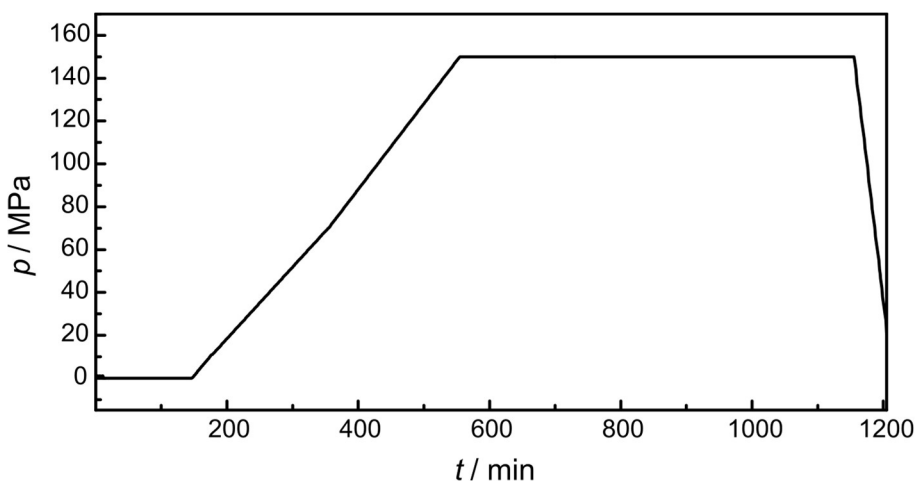


Figure G2. Plot of the used pressure program for the synthesis of $AE_3P_5N_{10}X$ ($AE = Sr, Ba; Cl, Br$).

G.2 Results and Discussion

Rietveld refinement of $\text{Ba}_3\text{P}_5\text{N}_{10}\text{X}$ ($\text{X} = \text{Cl}, \text{Br}$)

Rietveld refinements of $\text{Ba}_3\text{P}_5\text{N}_{10}\text{X}$ ($\text{X} = \text{Cl}, \text{Br}$) were carried out using the structure models of the corresponding single-crystal refinements as starting point.^[13, 14] During refinements the as-refined site parameters from the structure models obtained from single-crystal X-ray diffraction were fixed. Next to lattice and device specific parameters, only background and profile parameters were refined.

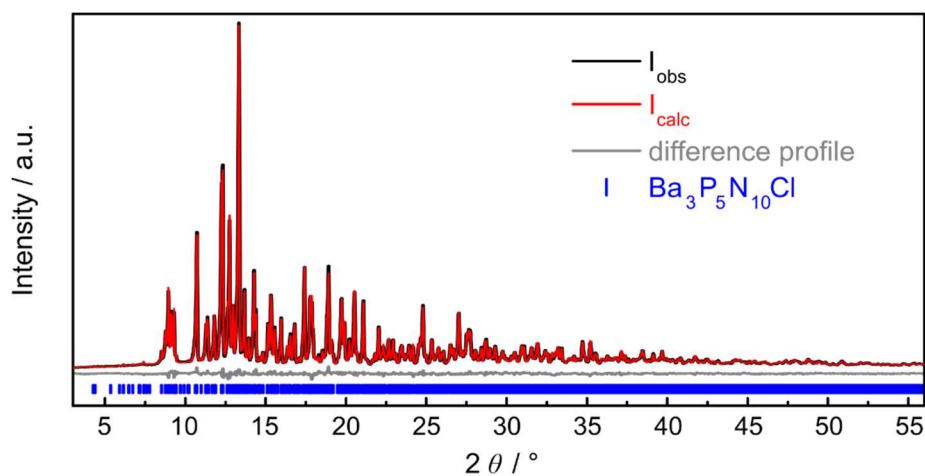


Figure G3. Rietveld refinement for $\text{Ba}_3\text{P}_5\text{N}_{10}\text{Cl}$; black: observed diffraction pattern ($\text{Mo-K}\alpha_1$), red: refined diffraction pattern, gray: difference profile, blue: positions of Bragg reflections of $\text{Ba}_3\text{P}_5\text{N}_{10}\text{Cl}$.

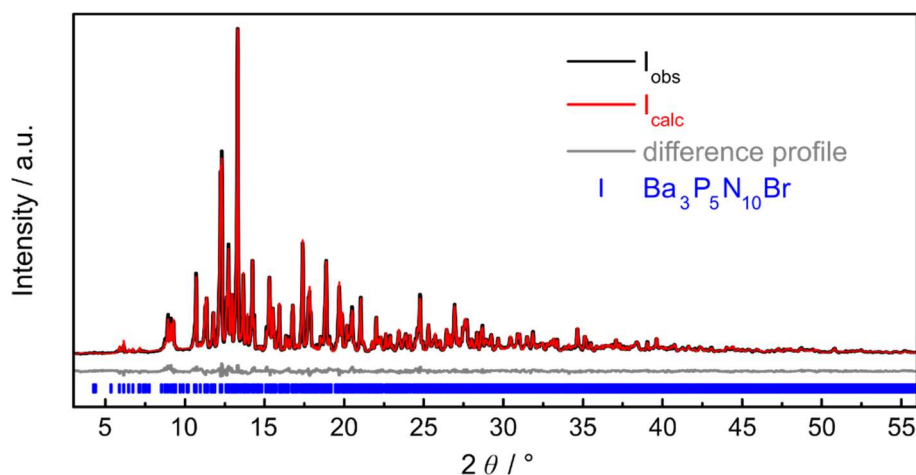


Figure G4. Rietveld refinement for $\text{Ba}_3\text{P}_5\text{N}_{10}\text{Br}$; black: observed diffraction pattern ($\text{Mo-K}\alpha_1$), red: refined diffraction pattern, gray: difference profile, blue: positions of Bragg reflections of $\text{Ba}_3\text{P}_5\text{N}_{10}\text{Br}$.

Table G2. Crystallographic data of the Rietveld refinement for Ba₃P₅N₁₀X (X = Cl, Br).

Formula	Ba₃P₅N₁₀Cl	Ba₃P₅N₁₀Br
Formula weight / g·mol ⁻¹	742.36	786.88
Crystal system; space group	orthorhombic; <i>Pnma</i> (no. 62)	
Lattice parameters / Å	<i>a</i> = 12.5452(2)	<i>a</i> = 12.5841(2)
	<i>b</i> = 13.2136(2)	<i>b</i> = 13.2287(2)
	<i>c</i> = 13.7850(3)	<i>c</i> = 13.8102(3)
Cell volume / Å ³	2285.09(7)	2299.01(7)
Formula units per unit cell	8	
Density / g·cm ⁻³	4.316	4.546
μ / mm ⁻¹	9.229	12.333
Diffractometer	Stoe Stadi P	
Radiation	Mo-K α_1 (λ = 0.71073 Å)	
Detector	Mythen 1K	
Monochromator	Ge(111)	
θ -range / °	1.5 ≤ θ ≤ 28.5	1.5 ≤ θ ≤ 28.5
Data points	3552	3552
Total number of reflections	2999	3019
Refined parameters	28	28
Background function	Shifted Chebyshev	
Number of background parameters	14	14
Goodness of fit (χ^2)	2.726	2.288
R_p ; R_{wp}	0.050; 0.063	0.035; 0.045
R_{exp} ; R_{Bragg}	0.023; 0.035	0.020; 0.026

Structure elucidation of $\text{Sr}_3\text{P}_5\text{N}_{10}\text{Cl}$ **Table G3.** Crystallographic data of the single-crystal refinement of $\text{Sr}_3\text{P}_5\text{N}_{10}\text{Cl}$.

Formula	$\text{Sr}_3\text{P}_5\text{N}_{10}\text{Cl}$
Formula weight / $\text{g}\cdot\text{mol}^{-1}$	593.26
Crystal system; space group	orthorhombic; <i>Pnma</i> (no. 62)
Lattice parameters / \AA	$a = 12.241(2)$ $b = 12.953(3)$ $c = 13.427(3)$
Cell volume / \AA^3	2128.9(8)
Formula units per unit cell	8
Density / $\text{g}\cdot\text{cm}^{-3}$	3.702
μ / mm^{-1}	15.980
Diffractometer	Bruker D8 Venture
Radiation	Mo- K_α (0.71073)
θ -range / $^\circ$	$2.2 \leq \theta \leq 31.0$
Total number of reflections	33698
No. of independent reflections	3522
Observed reflections ($F^2 > 2\sigma(F^2)$)	2921
R_{int}, R_σ	0.036; 0.072
Structure solution	SHELXT
Structure refinement	SHELXL
Refined parameters	192
Goodness of fit (χ^2)	1.077
$R1$ (all data); $R1$ ($F^2 > 2\sigma(F^2)$)	0.046; 0.033
$wR2$ (all data); $wR2$ ($F^2 > 2\sigma(F^2)$)	0.070, 0.066
$\Delta\rho_{\text{max}}; \Delta\rho_{\text{min}}$ / $\text{e}\cdot\text{\AA}^{-3}$	3.360; -1.277

Table G4. Atomic coordinates, crystallographic positions, and equivalent displacement parameters (in Å²) of Sr₃P₅N₁₀Cl.

Atom	Wyckoff	x	y	z	<i>U</i> _{eq}	occ
Sr1	8 <i>d</i>	0.28054(3)	0.01905(3)	0.32357(3)	0.01690(9)	1.00
Sr2	4 <i>c</i>	0.03822(7)	1/4	0.73015(6)	0.03513(19)	1.00
Sr3	4 <i>c</i>	0.04467(4)	1/4	0.24282(4)	0.01423(11)	1.00
Sr4	4 <i>c</i>	0.33171(5)	1/4	0.02204(4)	0.01646(11)	1.00
Sr5a	4 <i>c</i>	0.33170(6)	1/4	0.58680(6)	0.0129(2)	0.72(1)
Sr5b	4 <i>c</i>	0.35423(15)	1/4	0.49125(16)	0.0145(6)	0.28(1)
Cl1	4 <i>c</i>	0.27301(15)	1/4	0.80319(12)	0.0288(3)	1.00
Cl2	4 <i>c</i>	0.29612(13)	1/4	0.26353(12)	0.0218(3)	1.00
P1	8 <i>d</i>	0.02673(7)	0.01215(7)	0.63734(7)	0.00709(16)	1.00
P2	8 <i>d</i>	0.03886(7)	0.53424(7)	0.15046(7)	0.00760(16)	1.00
P3	8 <i>d</i>	0.07191(7)	0.13266(7)	0.01782(7)	0.00785(17)	1.00
P4	8 <i>d</i>	0.09579(7)	0.13385(7)	0.47286(7)	0.00755(16)	1.00
P5	8 <i>d</i>	0.24936(8)	0.50605(7)	0.07219(7)	0.00811(16)	1.00
N1	8 <i>d</i>	0.0048(3)	0.0805(2)	0.1118(2)	0.0110(6)	1.00
N2	8 <i>d</i>	0.0134(3)	0.1154(2)	0.5666(2)	0.0093(6)	1.00
N3	8 <i>d</i>	0.0291(2)	0.0581(2)	0.7498(2)	0.0085(5)	1.00
N4	8 <i>d</i>	0.0737(2)	0.0680(2)	0.3701(2)	0.0096(6)	1.00
N5	8 <i>d</i>	0.1704(2)	0.5417(3)	0.1652(2)	0.0109(6)	1.00
N6	8 <i>d</i>	0.3100(2)	0.5769(2)	0.4988(2)	0.0099(6)	1.00
N7	8 <i>d</i>	0.2219(3)	0.1090(2)	0.5046(2)	0.0107(6)	1.00
N8	8 <i>d</i>	0.3582(2)	0.0479(2)	0.1174(2)	0.0105(6)	1.00
N9	8 <i>d</i>	0.0017(3)	0.6333(2)	0.0822(2)	0.0107(6)	1.00
N10	4 <i>c</i>	0.0953(4)	1/4	0.0528(3)	0.0131(9)	1.00
N11	4 <i>c</i>	0.0790(4)	1/4	0.4335(3)	0.0104(8)	1.00

Table G5. Anisotropic displacement parameters (in Å²) of Sr₃P₅N₁₀Cl.

Atom	U_{11}	U_{22}	U_{33}	U_{23}	U_{13}	U_{12}
Sr1	0.01170(16)	0.0289(2)	0.01012(16)	-0.00075(14)	0.00016(13)	0.00596(15)
Sr2	0.0653(5)	0.0079(2)	0.0322(4)	0.000	-0.0131(3)	0.000
Sr3	0.0173(2)	0.0158(2)	0.0095(2)	0.000	0.00077(18)	0.000
Sr4	0.0148(2)	0.0151(2)	0.0195(3)	0.000	-0.0026(2)	0.000
Sr5a	0.0099(3)	0.0077(3)	0.0212(4)	0.000	-0.0030(3)	0.000
Sr5b	0.0085(9)	0.0085(9)	0.0264(11)	0.000	-0.0021(7)	0.000
Cl1	0.0328(9)	0.0313(8)	0.0224(8)	0.000	-0.0006(6)	0.000
Cl2	0.0210(7)	0.0170(6)	0.0273(8)	0.000	0.0035(6)	0.000
P1	0.0075(4)	0.0066(4)	0.0072(4)	-0.0002(3)	0.0003(3)	-0.0007(3)
P2	0.0080(4)	0.0072(4)	0.0077(4)	-0.0002(3)	0.0003(3)	-0.0005(3)
P3	0.0091(4)	0.0067(4)	0.0078(4)	0.0004(3)	-0.0002(3)	0.0002(3)
P4	0.0082(4)	0.0066(4)	0.0079(4)	-0.0002(3)	-0.0002(3)	-0.0003(3)
P5	0.0074(4)	0.0080(4)	0.0089(4)	-0.0003(3)	0.0001(3)	0.0000(3)
N1	0.0092(14)	0.0104(14)	0.0135(15)	0.0013(11)	0.0020(11)	0.0006(11)
N2	0.0116(14)	0.0072(13)	0.0092(14)	0.0013(11)	0.0013(11)	0.0006(11)
N3	0.0096(13)	0.0096(13)	0.0063(13)	-0.0010(11)	0.0002(10)	-0.0013(11)
N4	0.0089(13)	0.0100(14)	0.0098(14)	-0.0030(11)	0.0019(11)	-0.0015(11)
N5	0.0075(13)	0.0145(15)	0.0107(14)	-0.0022(11)	0.0009(11)	0.0001(11)
N6	0.0062(13)	0.0118(14)	0.0118(14)	0.0033(11)	-0.0003(10)	-0.0021(11)
N7	0.0102(14)	0.0117(14)	0.0102(14)	0.0026(11)	-0.0004(11)	-0.0013(11)
N8	0.0081(13)	0.0097(14)	0.0139(15)	-0.0011(11)	-0.0008(11)	0.0007(11)
N9	0.0136(14)	0.0088(13)	0.0096(14)	0.0030(11)	-0.0018(11)	-0.0005(11)
N10	0.022(2)	0.0046(18)	0.012(2)	0.000	-0.0019(18)	0.000
N11	0.018(2)	0.0047(18)	0.009(2)	0.000	-0.0011(16)	0.000

Structure elucidation of $\text{Sr}_3\text{P}_5\text{N}_{10}\text{Br}$

The structure refinement of $\text{Sr}_3\text{P}_5\text{N}_{10}\text{Br}$ was carried out using the Rietveld method based on single-crystal X-ray diffraction data of $\text{Sr}_3\text{P}_5\text{N}_{10}\text{Cl}$ after substitution of Cl by Br. During refinement Sr and Br atoms were refined with isotropic displacement parameters using equal values for all atoms of a kind. Displacement parameters of P and N were fixed to reasonable values. The collected powder X-ray diffraction data were not sufficient for any anisotropic refinement.

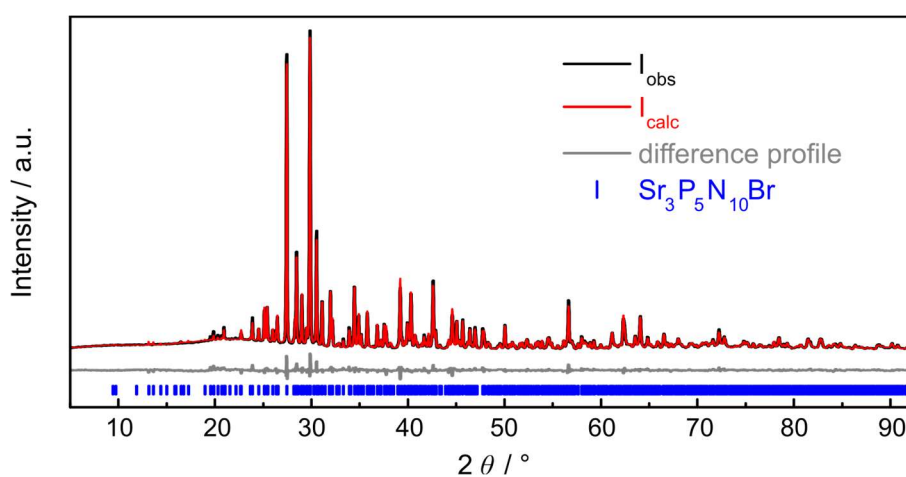


Figure G5. Rietveld refinement for $\text{Sr}_3\text{P}_5\text{N}_{10}\text{Br}$; black: observed diffraction pattern ($\text{Cu-K}\alpha_1$), red: refined diffraction pattern, gray: difference profile, blue: positions of Bragg reflections of $\text{Sr}_3\text{P}_5\text{N}_{10}\text{Br}$.

Table G6. Atomic coordinates, crystallographic positions, and equivalent displacement parameters (in Å²) of Sr₃P₅N₁₀Br.

Atom	Wyckoff	x	y	z	U _{eq}	occ
Sr1	8d	0.27817(16)	0.01364(17)	0.32455(15)	1.20(4)	1.00
Sr2	4c	0.0346(3)	1/4	0.7301(2)	= Uiso(Sr1)	1.00
Sr3	4c	0.0451(2)	1/4	0.2443(3)	= Uiso(Sr1)	1.00
Sr4	4c	0.3332(3)	1/4	0.0260(3)	= Uiso(Sr1)	1.00
Sr5a	4c	0.3336(4)	1/4	0.5726(4)	= Uiso(Sr1)	0.66
Sr5b	4c	0.3489(7)	1/4	0.4927(9)	= Uiso(Sr1)	0.34
Br1	4c	0.2736(4)	1/4	0.8039(4)	5.11(9)	1.00
Br2	4c	0.2963(4)	1/4	0.2647(3)	= Uiso(Cl1)	1.00
P1	8d	0.0273(5)	0.0095(6)	0.6369(4)	0.7	1.00
P2	8d	0.0335(5)	0.5337(5)	0.1481(5)	0.7	1.00
P3	8d	0.0744(5)	0.1306(5)	0.0188(4)	0.7	1.00
P4	8d	0.0957(6)	0.1360(5)	0.4745(5)	0.7	1.00
P5	8d	0.2533(6)	0.5061(6)	0.0762(4)	0.7	1.00
N1	8d	0.0091(12)	0.0811(14)	0.1086(11)	0.7	1.00
N2	8d	0.0162(14)	0.1161(13)	0.5678(13)	0.7	1.00
N3	8d	0.0243(11)	0.0621(10)	0.7515(15)	0.7	1.00
N4	8d	0.0651(14)	0.0684(12)	0.3768(11)	0.7	1.00
N5	8d	0.1739(12)	0.5391(12)	0.1647(11)	0.7	1.00
N6	8d	0.2008(13)	0.0831(12)	0.0030(12)	0.7	1.00
N7	8d	0.2116(15)	0.1050(12)	0.5035(12)	0.7	1.00
N8	8d	0.3560(12)	0.0473(14)	0.1314(11)	0.7	1.00
N9	8d	0.5010(12)	0.1273(13)	0.5737(13)	0.7	1.00
N10	4c	0.0897(18)	1/4	0.0541(15)	0.7	1.00
N11	4c	0.0834(19)	1/4	0.4325(17)	0.7	1.00

Rietveld refinement of $\text{Sr}_3\text{P}_5\text{N}_{10}\text{X}$ ($\text{X} = \text{Cl}, \text{Br}$)

Rietveld refinement of $\text{Sr}_3\text{P}_5\text{N}_{10}\text{Cl}$ was performed based on the as-refined structure. During refinement all site parameters obtained from single-crystal X-ray diffraction stayed unchanged. Next to lattice and device specific parameters, only background and profile parameters were refined.

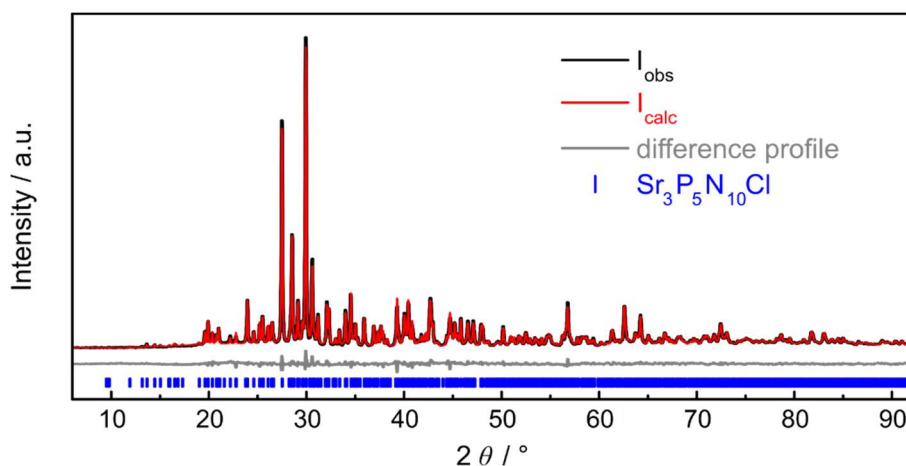


Figure G6. Rietveld refinement for $\text{Sr}_3\text{P}_5\text{N}_{10}\text{Cl}$; black: observed diffraction pattern (Cu- $K_{\alpha 1}$), red: refined diffraction pattern, gray: difference profile, blue: positions of Bragg reflections of $\text{Sr}_3\text{P}_5\text{N}_{10}\text{Cl}$.

Table G7. Crystallographic data of the Rietveld refinement for $\text{Sr}_3\text{P}_5\text{N}_{10}\text{X}$ ($\text{X} = \text{Cl}, \text{Br}$).

Formula	$\text{Sr}_3\text{P}_5\text{N}_{10}\text{Cl}$	$\text{Sr}_3\text{P}_5\text{N}_{10}\text{Br}$
Formula weight / $\text{g}\cdot\text{mol}^{-1}$	593.26	637.70
Crystal system; space group	orthorhombic; $Pnma$ (no. 62)	
Lattice parameters / Å	$a = 12.2472(1)$ $b = 12.9629(2)$ $c = 13.4365(2)$	$a = 12.2970(2)$ $b = 12.9896(2)$ $c = 13.4585(2)$
Cell volume / Å^3	2133.17(4)	2149.76(5)
Formula units per unit cell	8	
Density / $\text{g}\cdot\text{cm}^{-3}$	3.694	3.942
μ / mm^{-1}	28.681	30.520
Diffractometer	Stoe Stadi P	
Radiation	Cu- $K_{\alpha 1}$ ($\lambda = 1.5406 \text{ Å}$)	
Detector	Mythen 1K	
Monochromator	Ge(111)	
θ -range / $^\circ$	$2.5 \leq \theta \leq 55.3$	$2.5 \leq \theta \leq 46.2$
Data points	7035	5829
Total number of reflections	1431	993
Refined parameters	38	101
Background function	Shifted Chebyshev	
Number of background parameters	24	18
Goodness of fit (χ^2)	2.018	2.257
R_p ; R_{wp}	0.033; 0.046	0.035; 0.046
R_{exp} ; R_{Bragg}	0.023; 0.023	0.020; 0.022

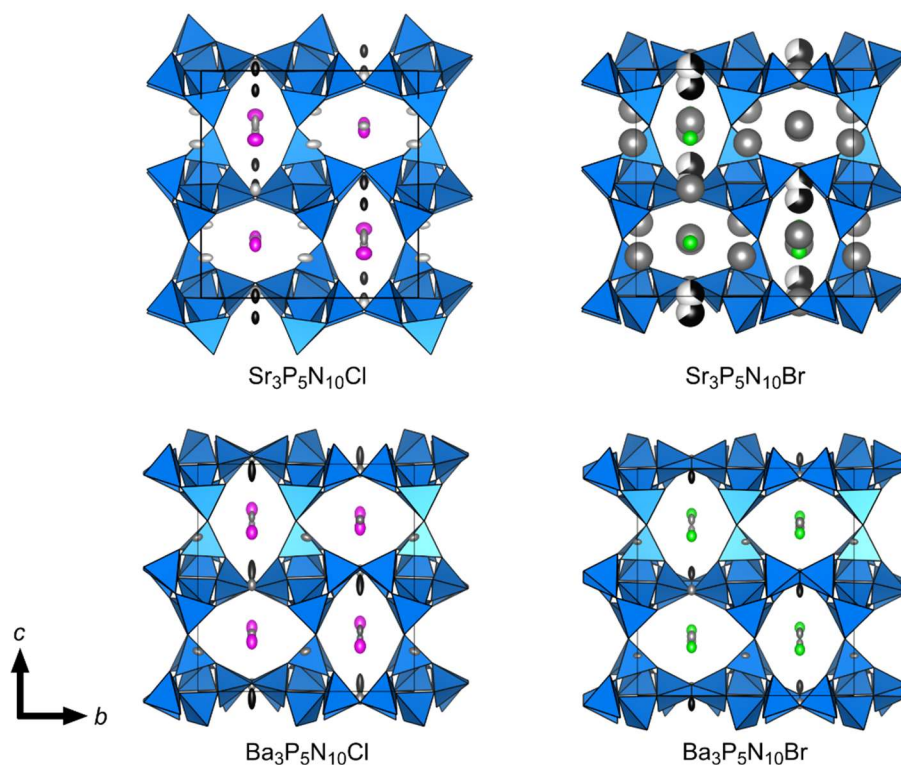
Crystal structure of $AE_3P_5N_{10}X$ ($AE = Sr, Ba; X = Cl, Br$)

Figure G7. Projections of the crystal structures of $AE_3P_5N_{10}X$ ($AE = Sr, Ba; X = Cl, Br$) along [100] for the different element combinations AE/X . Illustrations of $AE = Ba$ and $Sr_3P_5N_{10}Cl$ are based on single-crystal data and all atoms are displayed with 95% probability.^[13,14] The illustration of $Sr_3P_5N_{10}Br$ is based on a Rietveld refinement using the structure model of $Sr_3P_5N_{10}Cl$ as starting model. Color coding: PN_4 tetrahedra blue, $AE1$ – $AE4$ atoms gray, $AE5$ atoms black, Cl atoms pink, Br atoms green.

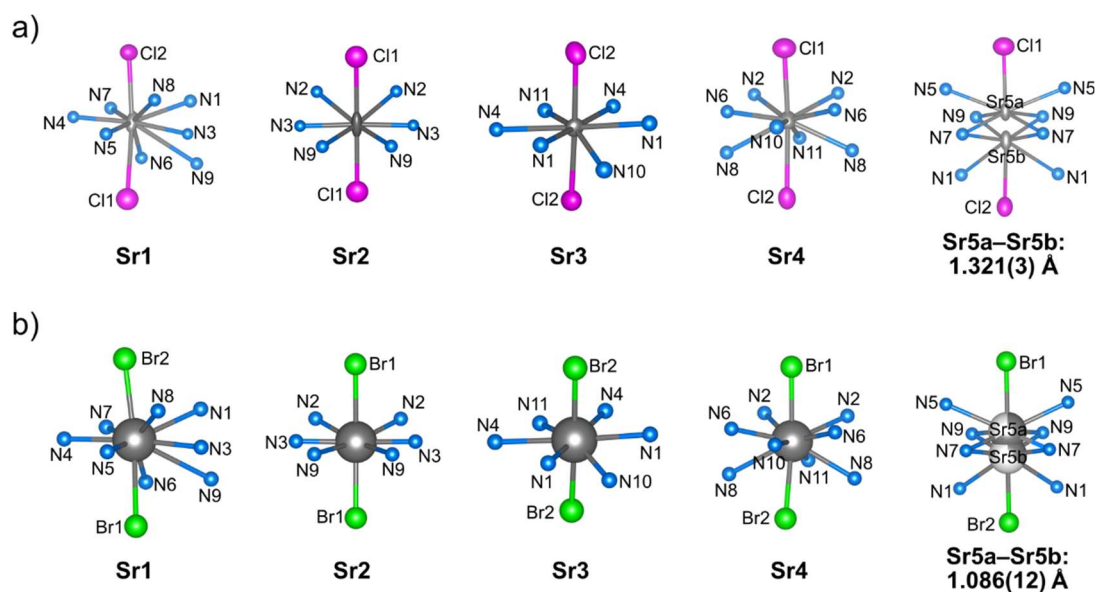


Figure G8. Coordination spheres of Sr^{2+} in $Sr_3P_5N_{10}X$ for $X = Cl$ (a) and $X = Br$ (b). Atoms are displayed with a probability of 95% for $Sr_3P_5N_{10}Cl$. For $X = Br$ all atoms are display isotropically, as powder X-ray diffraction data were not sufficient for anisotropic refinements. A decrease of the interatomic Sr5a–Sr5b distance is observed from $X = Cl$ to $X = Br$.

Table G8. Coordination numbers (CN) and interatomic Sr–N/X distances (Å) of Sr₃P₅N₁₀X (X = Cl, Br).

CN		X = Cl	∅ Sr–N/Cl	X = Br	∅ Sr–N/Br	
Sr1	10	Sr–N	2.638(4)–3.580(5)	2.880	2.575(16)–3.549(17)	2.896
		Sr–X	3.104(1)–3.557(1)	3.331	3.183(3)–3.494(3)	3.339
Sr2	8	Sr–N	2.502(3)–2.979(3)	2.768	2.462(14)–3.111(18)	2.792
		Sr–X	3.037(3)–3.277(3)	3.157	3.101(7)–3.243(7)	3.172
Sr3	8	Sr–N	2.595(6)–2.933(3)	2.800	2.58(3)–2.97(2)	2.817
		Sr–X	3.044(2)–3.090(2)	3.067	3.062(6)–3.101(6)	3.082
Sr4	10	Sr–N	2.854(4)–3.086(5)	2.964	2.739(17)–3.113(18)	2.981
		Sr–X	3.025(2)–3.272(2)	3.149	3.079(8)–3.243(8)	3.161
Sr5 a/b	10	Sr–N	2.523(4)–3.182(5)	2.921	2.520(19)–3.251(19)	2.949
		Sr–X	2.993(2)–3.139(3)	3.066	3.147(12)–3.194(8)	3.171

Table G9. Interatomic distances (Å) and bond angles (°) of Sr₃P₅N₁₀X (X = Cl, Br).

		Sr ₃ P ₅ N ₁₀ Cl	Sr ₃ P ₅ N ₁₀ Br			Sr ₃ P ₅ N ₁₀ Cl	Sr ₃ P ₅ N ₁₀ Br
P1–	N4	1.612(3)	1.533(18)	N4 –P1–	N3	107.9(1)	111.2(8)
	N3	1.623(3)	1.687(20)	N4	N8	109.9(2)	110.6(9)
	N8	1.632(4)	1.615(17)	N4	N2	114.3(1)	114.8(9)
	N2	1.648(3)	1.674(19)	N3	N8	108.3(1)	104.3(8)
P2–	N3	1.606(3)	1.571(20)	N3	N2	104.0(1)	99.9(8)
	N5	1.625(4)	1.742(16)	N8	N2	112.1(2)	115.1(9)
	N1	1.629(4)	1.611(19)	N3 –P2–	N5	113.5(2)	109.2(8)
	N9	1.642(3)	1.631(18)	N3	N1	108.0(1)	114.6(9)
P3–	N9	1.616(3)	1.538(18)	N3	N9	99.9(1)	103.6(9)
	N1	1.617(2)	1.587(16)	N5	N1	110.3(2)	105.3(8)
	N6	1.636(4)	1.686(17)	N5	N9	107.3(2)	107.8(8)
	N1	1.649(3)	1.633(9)	N1	N9	117.6(2)	116.0(9)
P4–	N1	1.608(2)	1.592(11)	N9 –P3–	N10	109.6(1)	109.2(7)
	N2	1.630(3)	1.612(19)	N9	N6	111.4(2)	115.4(9)
	N7	1.632(4)	1.532(20)	N9	N1	111.1(1)	107.9(9)
	N4	1.645(3)	1.625(17)	N10	N6	107.7(1)	106.1(6)
P5–	N8	1.622(4)	1.621(17)	N10	N1	104.5(1)	102.8(7)
	N6	1.629(3)	1.652(17)	N6	N1	112.2(2)	114.5(8)
	N5	1.646(3)	1.599(16)	N11 –P4–	N2	108.2(1)	111.6(7)
	N7	1.651(3)	1.672(18)	N11	N7	113.0(1)	115.0(7)
				N11	N4	100.9(1)	101.1(7)
				N2	N7	110.8(2)	108.9(10)
				N2	N4	118.0(1)	113.8(9)
			N7	N4	105.8(2)	106.2(9)	
			N8 –P5–	N6	108.0(2)	106.1(9)	
			N8	N5	108.7(2)	104.4(9)	
			N8	N7	112.2(2)	113.3(9)	
			N6	N5	112.4(1)	113.2(9)	
			N6	N7	107.2(1)	106.9(9)	
			N5	N7	108.4(1)	112.8(9)	

EDX measurements

Besides the expected elements, all measurements show an elevated oxygen content, which might be caused by surface hydrolysis or water intercalation during water treatment. Neglecting the oxygen content, and trace amounts of europium (EuCl_2 as dopant), the measured atomic ratios are in good accordance with expected sum formulas.

Table G10. EDX (SEM) measurements (at%) of $\text{AE}_3\text{P}_5\text{N}_{10}\text{X}:\text{Eu}^{2+}$ (AE = Sr, Ba, X = Cl, Br) with an acceleration voltage of 20 kV. O and Eu contents are neglected for the calculations of normalized sum formulas. Standard deviations are given in parentheses.

	EA	P	N	X	Eu	O
$\text{Sr}_3\text{P}_5\text{N}_{10}\text{Cl}$						
1	14	24	47	6	< 1	9
2	14	26	47	5	< 1	8
3	13	20	54	4	< 1	9
Average	14(1)	23(3)	49(4)	5(1)	-	9(1)
Normalized	2.7(1)	4.7(6)	9.9(8)	1.0(2)	-	-
$\text{Sr}_3\text{P}_5\text{N}_{10}\text{Br}$						
1	14	28	46	5	< 1	7
2	17	24	47	4	< 1	8
3	17	28	42	7	1	5
Average	16(2)	27(2)	45(3)	5(2)	-	7(2)
Normalized	3.2(3)	5.4(4)	9.0(5)	1.0(3)	-	-
$\text{Ba}_3\text{P}_5\text{N}_{10}\text{Cl}$						
1	16	26	44	5	< 1	9
2	15	25	47	6	< 1	7
3	15	27	48	5	< 1	5
Average	15(1)	26(1)	46(2)	5(1)	-	7(2)
Normalized	3.0(1)	5.2(2)	9.2(4)	1.0(1)	-	-
$\text{Ba}_3\text{P}_5\text{N}_{10}\text{Br}$						
1	16	26	45	5	< 1	8
2	16	25	45	5	1	8
3	19	28	42	6	< 1	5
Average	17(2)	26(2)	44(2)	5(1)	-	7(2)
Normalized	3.4(3)	5.2(3)	8.8(3)	1.0(1)	-	-

Luminescence properties of $AE_3P_5N_{10}X$ ($AE = Sr, Ba; X = Cl, Br$)

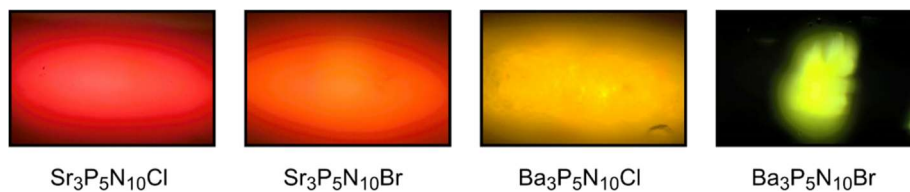


Figure G9. Photographs of Eu^{2+} -doped particles of $AE_3P_5N_{10}X$ ($AE = Sr, Ba; X = Cl, Br$) under irradiation with blue to UV-light ($\lambda_{exc} = 420$ nm).

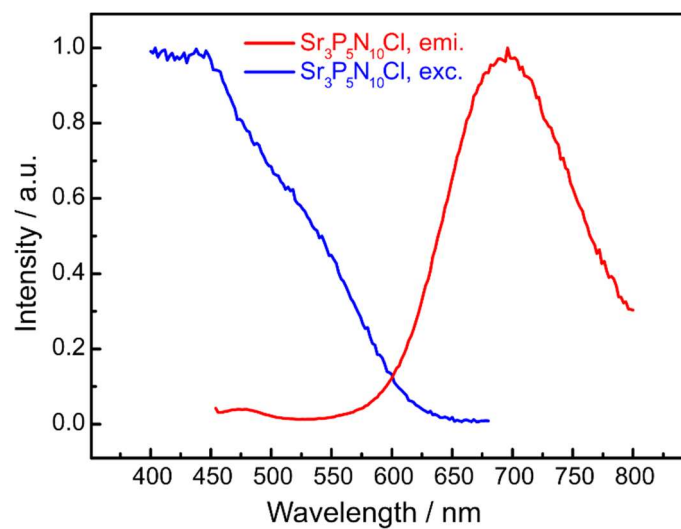


Figure G10. Normalized excitation (blue) and emission spectra (red) of $Sr_3P_5N_{10}Cl:Eu^{2+}$ measured at room temperature.

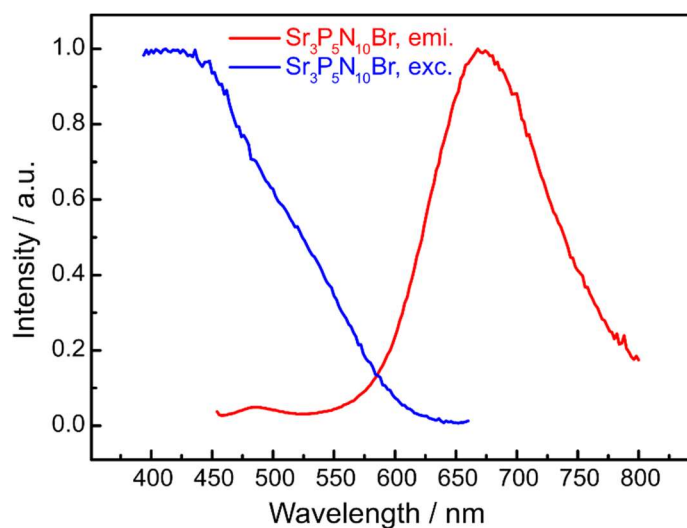


Figure G11. Normalized excitation (blue) and emission spectra (red) of $Sr_3P_5N_{10}Br:Eu^{2+}$ measured at room temperature.

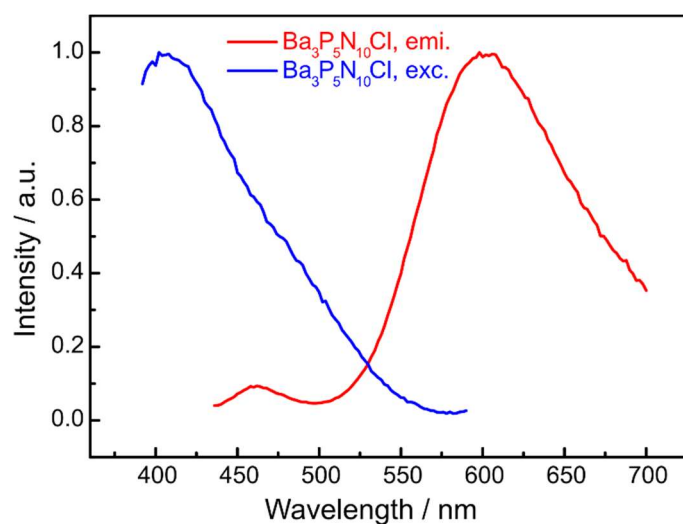


Figure G12. Normalized excitation (blue) and emission spectra (red) of $\text{Ba}_3\text{P}_5\text{N}_{10}\text{Cl}:\text{Eu}^{2+}$ measured at room temperature.

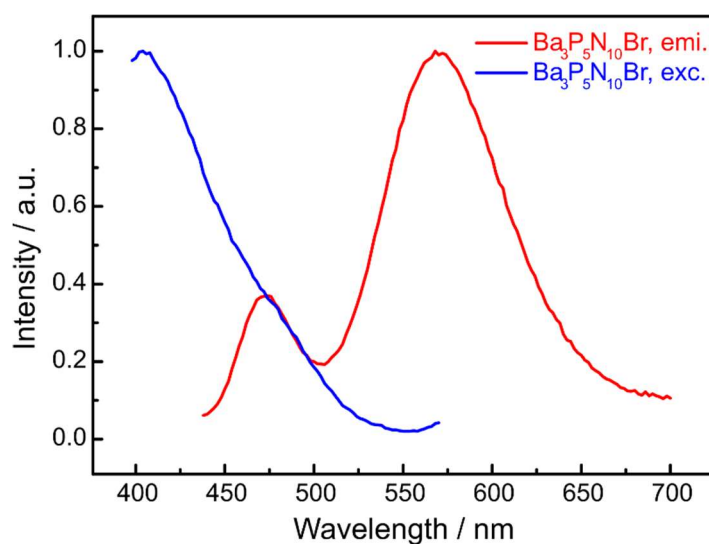


Figure G13. Normalized excitation (blue) and emission spectra (red) of $\text{Ba}_3\text{P}_5\text{N}_{10}\text{Br}:\text{Eu}^{2+}$ measured at room temperature.

Table G11. Values of the measured luminescence properties of $\text{AE}_3\text{P}_5\text{N}_{10}\text{X}:\text{Eu}^{2+}$ ($\text{AE} = \text{Sr}, \text{Ba}; \text{X} = \text{Cl}, \text{Br}$) at room temperature with a nominal doping level of 3 mol% Eu^{2+} referred to AE^{2+} ($\lambda_{\text{exc}} = 420 \text{ nm}$).

compound	λ_{emi}	fwhm / nm	fwhm / cm^{-1}	IQE / %
$\text{Sr}_3\text{P}_5\text{N}_{10}\text{Cl}:\text{Eu}^{2+}$	478	≈ 41	≈ 1772	29
	695	126	2577	
$\text{Sr}_3\text{P}_5\text{N}_{10}\text{Br}:\text{Eu}^{2+}$	488	≈ 60	≈ 2530	32
	668	116	2520	
$\text{Ba}_3\text{P}_5\text{N}_{10}\text{Cl}:\text{Eu}^{2+}$	462	≈ 53	≈ 2330	12
	602	107	2874	
$\text{Ba}_3\text{P}_5\text{N}_{10}\text{Br}:\text{Eu}^{2+}$	474	≈ 40	≈ 1776	12
	568	83	2528	

Discussion of luminescence spectra

As can be seen from the luminescence spectra, each one exhibits two emission bands. An explanation therefore is provided in the manuscript. But in addition there are further interesting observations when comparing the emission spectra, meaning the influence of different ions AE^{2+} and X^- . Thereby the influence of AE^{2+} is most striking, as the emission bands of $AE_3P_5N_{10}Cl$ and $AE_3P_5N_{10}Br$ are red-shifted from $AE = Ba$ to $AE = Sr$. This effect is attributable to the different AE^{2+} radii and the associated distances $AE-N/X$ and the corresponding activator–ligand distances $Eu^{2+}-N/X$. Decreased activator–ligand distances, in turn, lead to a stronger crystal field for $AE = Sr$, lowering the $5d^1$ energy level and causing the as-observed red shift. These results are in accordance with previous investigations on nitridophosphates and related compounds. Another observation describes the influence of the halide ions on the position of the emission maxima. While the higher energetic emission bands are shifted red with increasing size of X , lower energetic emission bands are shifted blue. This effect has already been described for $Ba_3P_5N_{10}X$ and can be explained with the crystal field and the nephelauxetic effect. Thereby, it must be estimated for the individual groups of emission bands ($CN = 8/10$) which of the above-mentioned effects has the greater influence and which shift is caused by it. In principle, the larger the activator–ligand distances are, the smaller is the influence of the crystal field, but the larger is the nephelauxetic effect. Consequently, the nephelauxetic effect, which depends on the covalent character of a chemical bond, is used to explain the behavior of the emission bands at higher energies, assigned to $CN = 10$. As expected, corresponding $AE-N$ distances are significantly elongated due to the higher coordination number, causing only a weak crystal field. But interestingly, the $AE-N$ distances differ only marginally in $AE_3P_5N_{10}Cl$ and $AE_3P_5N_{10}Br$, despite of the different radii of Cl^- and Br^- (Table G8). Even the $AE-Cl$ and $AE-Br$ distances are roughly equal (Table G8). Therefore, the nephelauxetic effect exceeds crystal field effects, which can be neglected in this case. Considering the electronegativity of Cl and Br, a higher covalency of the $AE-Br$ bond ($AE = Sr, Ba$) and thus $Eu-Br$ is assumed. Due to the higher covalence a red shift from $X = Cl$ to $X = Br$ is observed. The contrary shift of the lower energetic emission bands, assigned to $CN = 8$ with shorter $AE-N$ distances, can be explained by a predominant influence of the crystal field, neglecting weaker nephelauxetic effects. With increasing radius of X , the mean interatomic $AE-N$ distances increase, as well (Table G8). As a consequence, a weaker crystal field is induced by larger Br^- ions, leading to blue shift of the emission band compared to $X = Cl$.

G.3 Author Contributions

S.W.: Conceptualization: Equal; Formal analysis: Lead; Investigation : Lead; Validation: Lead; Visualization: Lead; Writing - Original Draft: Lead; Writing - Review & Editing: Equal

M.Z.: Formal analysis: Supporting; Investigation: Supporting

P.S.: Conceptualization: Supporting; Formal analysis: Supporting ; Investigation: Supporting; Validation: Supporting ; Writing - Original Draft: Supporting

P.S.: Conceptualization: Supporting; Formal analysis: Supporting ; Investigation: Supporting; Project administration: Supporting; Resources: Supporting; Supervision: Supporting; Validation: Supporting; Writing - Review & Editing: Supporting

W.S.: Conceptualization: Equal; Funding acquisition: Lead; Project administration: Lead; Supervision: Lead; Writing - Review & Editing: Supporting.

G.4 References

- [1] A. A. Coelho, *TOPAS Academic*, Version 6, Coelho Software, Brisbane, Australia, **2016**.
- [2] H. Rietveld, "A profile refinement method for nuclear and magnetic structures", *J. Appl. Crystallogr.* **1969**, 2, 65-71.
- [3] R. W. Cheary, A. Coelho, "A fundamental parameters approach to X-ray line-profile fitting", *J. Appl. Crystallogr.* **1992**, 25, 109-121.
- [4] R. W. Cheary, A. A. Coelho, J. P. Cline, "Fundamental Parameters Line Profile Fitting in Laboratory Diffractometers", *J. Res. Natl. Inst. Stand. Technol.* **2004**, 109, 1-25.
- [5] Data Integration Software, *SAINTE*, Madison, Wisconsin, USA, **1997**.
- [6] Bruker AXS, Inc., *APEX3*, Karlsruhe, Germany, **2016**.
- [7] Bruker AXS, Inc., *SADABS*, Madison, Wisconsin, USA, **2001**.
- [8] G. M. Sheldrick, "A short history of SHELX", *Acta Crystallogr. Sect. A* **2008**, 64, 112-122.
- [9] Bruker AXS, Inc., *XPREP Reciprocal Space Exploration*, Karlsruhe, Germany, **2001**.
- [10] G. M. Sheldrick, "SHELXT - Integrated space-group and crystal-structure determination", *Acta Crystallogr. Sect. A* **2015**, 71, 3-8.
- [11] G. M. Sheldrick, "Crystal structure refinement with SHELXL", *Acta Crystallogr. Sect. C* **2015**, 71, 3-8.
- [12] K. Momma, F. Izumi, "VESTA 3 for three-dimensional visualization of crystal, volumetric and morphology data", *J. Appl. Crystallogr.* **2011**, 44, 1272-1276.
- [13] A. Marchuk, W. Schnick, " $Ba_3P_5N_{10}Br:Eu^{2+}$: A Natural-White-Light Single Emitter with a Zeolite Structure Type", *Angew. Chem. Int. Ed.* **2015**, 54, 2383-2387; *Angew. Chem.* **2015**, 127, 2413-2417.
- [14] A. Marchuk, S. Wendl, N. Imamovic, F. Tambornino, D. Wiechert, P. J. Schmidt, W. Schnick, "Nontypical Luminescence Properties and Structural Relation of $Ba_3P_5N_{10}X:Eu^{2+}$ ($X = Cl, I$): Nitridophosphate Halides with Zeolite-like Structure", *Chem. Mater.* **2015**, 27, 6432-6441.

H Supporting Information for Chapter 9

H.1 Experimental

Inert conditions

In order to prevent starting materials from oxidation and hydrolysis, all preparations were carried out in an Ar filled glovebox (MBraun, H₂O, O₂ < 1 ppm).

Powder X-ray diffraction (PXRD)

Powder X-ray diffraction patterns were collected on two Stoe Stadi P devices (Stoe & Cie GmbH, Darmstadt, Germany, Ge(111) monochromator) in parafocusing Debye-Scherrer geometry, using either Cu-K_{α1} ($\lambda = 1.5406 \text{ \AA}$) or Mo-K_α ($\lambda = 0.71073 \text{ \AA}$) radiation. Both diffractometers were equipped with a Mythen 1K Si strip detector (Dectris, Baden, Switzerland). All samples were ground thoroughly and sealed in glass capillaries ($\varnothing 0.3 \text{ mm}$, Hilgenberg, Malsfeld, Germany).

Rietveld refinements

The Topas Academic software was used for Rietveld refinements.^[1, 2] While the fundamental parameter approach served to model the peak profiles, a shifted Chebyshev polynomial was used to fit the background.^[3, 4] Potential preferred crystal orientation was handled using a fourth order spherical harmonics model.

Scanning electron microscopy (SEM) and energy dispersive X-ray spectroscopy (EDX)

A Dualbeam Helios Nanolab G3 UC (FEI) microscope with additional X-Max 80 SSD EDX detector (Oxford Instruments) was used for SEM and EDX analysis. Electrical conductivity was provided by coating samples with carbon by an electron beam evaporator (BAL-TEC MED 020, Bal Tec AG).

Visualization

The software packages Origin 6.1 and VESTA were used for the illustration of powder X-ray diffraction data and crystal structures, respectively.^[5]

Preparation of starting materials

All nitridophosphates used as starting materials were prepared according to the respective instructions in literature under medium- (MP) or high-pressure high-temperature conditions (HP/HT).^[6-9] A hot isostatic press (HIP, AIP6-30H, American Isostatic Presses, Inc., Columbus, Ohio, USA) was used for MP experiments, while HP/HT investigations were carried out using a 1000 t press (Voggenreiter GmbH, Mainleus, Germany). General instructions for both methods, which also apply to the syntheses of the products, are provided below.

Medium-pressure (MP) synthesis

Medium-pressure syntheses were carried out under N₂ (99.9%) atmosphere in a hot isostatic press (HIP, AIP6-30H, American Isostatic Presses, Inc., Columbus, Ohio, USA). The starting materials (Table H1) were ground and filled into a tungsten crucible. Subsequently, the crucible was transferred into a corundum vessel and the assembly was placed between the graphite heating elements ($T_{\max} = 2000\text{ °C}$, $\phi = 70\text{ mm}$, $h = 125\text{ mm}$) in the pressure module of the HIP ($p_{\max} = 207\text{ MPa}$). The reactor was rinsed with Ar for ten times before the necessary pressure to operate the main compressor was built up with a pressure booster (Maximator, DLE-5-30-2, $p_{\max} = 60\text{ MPa}$). Subsequently, the pressure was constantly increased to 70 MPa at 20 °C. Within 4 h the sample was then heated to 1000 °C (rate: 250 °C min⁻¹) ending up with a synthesis pressure of 150 MPa. After a reaction time of 10 h, temperature was cooled down to 20 °C and the pressure was released. The product Mg₂PN₃ was yielded as light beige sinter cake, which was sensitive towards air and moisture.

High-pressure high-temperature (HP/HT) synthesis

The syntheses under high-pressure high-temperature conditions were performed with a hydraulic 1000 t press applying the multianvil technique with a modified Walker module.^[10-12] The starting materials (Table H1) were thoroughly ground in an agate mortar and filled into a capsule made out of *h*-BN (Henze, Kempten). **Notation:** Standard 18/11 *h*-BN crucibles were used for the syntheses of the ternary/quaternary starting materials, while modified 18/11 *h*-BN crucibles (14/8 borehole) were used for the syntheses of the final products (Figure H4, Table H2). After compressing the mixture, the crucible was transferred into a specially prepared octahedron (MgO, doped with Cr₂O₃ (5 %), edge length 18 mm, Ceramic Substrates & Components, Isle of Wight, UK), which was pierced in the center and loaded with a ZrO₂ sleeve (Cesima Ceramics, Wust-Fischbeck, Germany). The ZrO₂ sleeve was

sealed on one side with a Mo plate, which served as electrical contact to the inner resistance furnace tube consisting of two (a longer and a shorter) graphite tubes (Schunk Kohlenstofftechnik GmbH, Gießen, Germany). The shorter tube was centered in the longer by a MgO spacer (Cesima Ceramics, Wust-Fischbeck, Germany). After inserting the h-BN crucible, it was capped with a h-BN disc and additional MgO and Mo plates to ensure a symmetrical setup. The thus prepared assembly was transferred to the Walker module, surrounded by eight Co-doped (7%) WC cubes (Hawedia, Marklkofen, Germany) with truncated edges (11 mm edge length). The WC cubes were laminated with pyrophyllite gaskets, Bristol board (369 g·m²), and PTFE film (Vitaflon Technische Produkte GmbH, Bad Kreuznach, Germany). More detailed information on the preparation of the WC cubes and the Walker module is provided in literature.^[10] During the experiments, the assembly was cold compressed up to 5 GPa within 115 min and heated under pressure to ~ 1000 °C within 60 min. These conditions were upheld for 60 min prior to cooling the assembly down to room temperature within 60 min under pressure. Finally, the pressure was released within 330 min. All samples were recovered as colorless powders after washing with de-ionized water, in order to remove residual halides.

Weighed portions

Table H1. Weighed portions of starting materials for post-synthetic modification experiments.

Target compounds	Technique	Starting materials / mg	
"β-SrP₂N₄"	HP/HT	BaP ₂ N ₄ 17.80	SrCl ₂ 16.58
"Sr₃P₅N₁₀Br"	HP/HT	Ba ₃ P ₅ N ₁₀ Br 15.00	SrBr ₂ 21.23
CaH₄P₆N₁₂	HP/HT	SrH ₄ P ₆ N ₁₂ 25.00	CaCl ₂ 9.34
MgP₈N₁₄	HP/HT	CaP ₈ N ₁₄ 25.00	MgCl ₂ 7.34
Mg₂PN₃	MP	Ca ₂ PN ₃ 150.00	MgCl ₂ 139.88

H.2 Results and Discussion

Pretests for ion-exchange reactions under ambient pressure

Two model compounds were selected to investigate the transferability of the conditions used for ion exchange experiments on nitridosilicates to nitridophosphates. Based on the reported results for sodalite-like $\text{Zn}_5\text{H}_4[\text{P}_{12}\text{N}_{24}]\text{Cl}_2$, $\beta\text{-HPN}_2$ was reacted with ZnCl_2 in a fused silica ampoule at $850\text{ }^\circ\text{C}$ under Ar atmosphere targeting “ ZnP_2N_4 ”.^[13] As can be seen in Figure H1 the observed PXRD pattern of the product (black) shows no similarity to the simulated one for $\beta\text{-HPN}_2$ (red). Therefore, a topotactic reaction can be excluded under the given conditions. Furthermore, the second model compound $\text{SrH}_4\text{P}_6\text{N}_{12}$ was reacted with CaCl_2 under identical reaction conditions. The respective PXRD patterns of the observed product (black) and of $\text{CaH}_4\text{P}_6\text{N}_{12}$ (red) show significant differences, as well (Figure H2). Moreover, when comparing the PXRD diffraction patterns of used starting materials to those of observed products (exemplary shown for $\beta\text{-HPN}_2$ and “ ZnP_2N_4 ” in Figure H3) a substantial increase of amorphous components is observed, which might indicate a potential lability of nitridophosphates towards halide melts under ambient pressure.

In conclusion to these findings, we modified the synthesis conditions applying medium- and high-pressure methods.

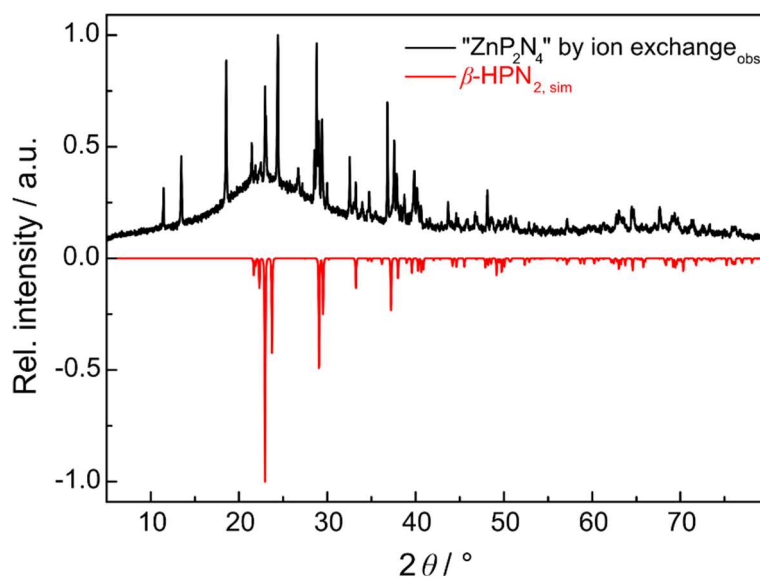


Figure H1. PXRD pattern ($\text{Cu-K}\alpha_1$, $\lambda = 1.5406\text{ \AA}$) of the product obtained by reaction of $\beta\text{-HPN}_2$ with ZnCl_2 . The observed (black) reflection pattern does not show any similarity to the simulated one for $\beta\text{-HPN}_2$ (red), which might be expected for topotactic reactions forming isotypic compounds.^[14]

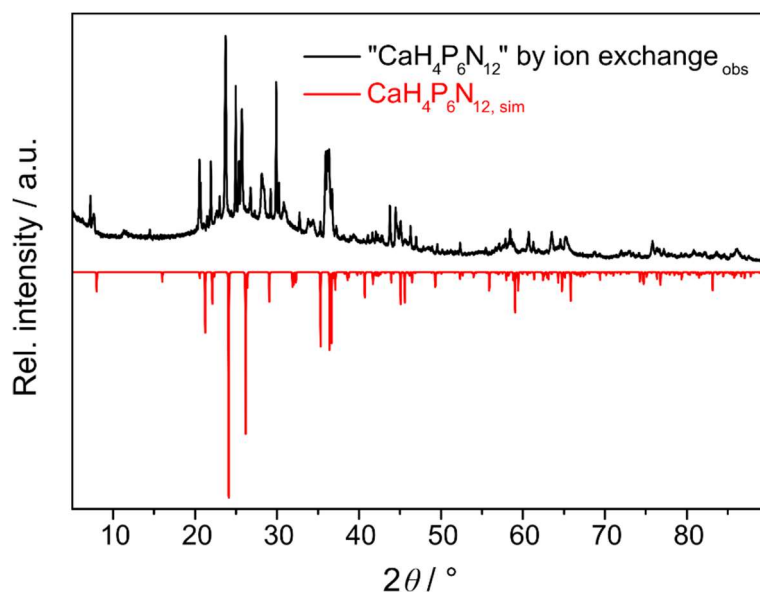


Figure H2. PXRD pattern (Cu- $K_{\alpha 1}$, $\lambda = 1.5406 \text{ \AA}$) of the product obtained by ion exchange experiments of $\text{SrH}_4\text{P}_6\text{N}_{12}$ reacting with CaCl_2 . The observed (black) reflection pattern shows significant differences to the simulated pattern for $\text{CaH}_4\text{P}_6\text{N}_{12}$ and does not indicate a successful ion exchange.^[8]

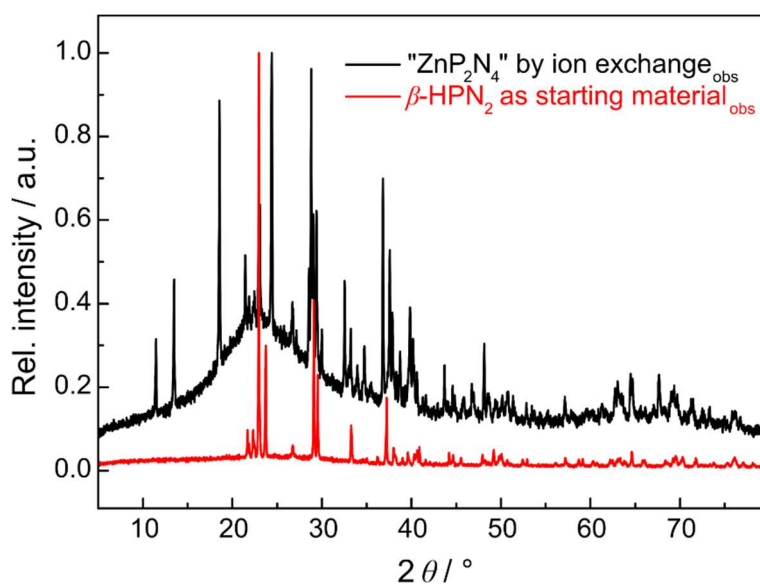


Figure H3. Comparison of the PXRD patterns (Cu- $K_{\alpha 1}$, $\lambda = 1.5406 \text{ \AA}$) of the used starting material (red) and the obtained product (black) for ion exchange experiments of β -HPN₂ reacting with ZnCl_2 . A significant increase of amorphous components is observed for the product.

Modified 18/11 assembly

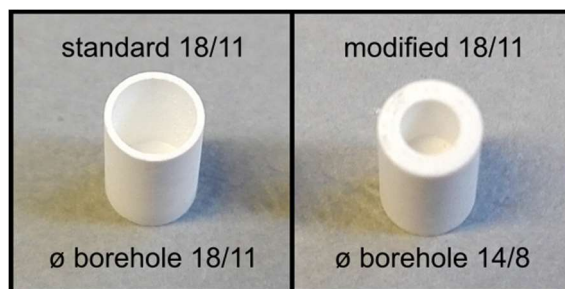


Figure H4. Graphical comparison of a standard 18/11 assembly with a modified assembly (14/8 borehole).

Table H2. Comparison of the respective dimensions for the standard 18/11 and modified 18/11 assembly.

Atom	Standard 18/11	Modified 18/11
Edge length MgO octahedron	18 mm	18 mm
Truncated edge length of WC cube	11 mm	11 mm
Max. synthesis pressure	10 GPa	10 GPa
Borehole radius r	1.5 mm	1 mm
Borehole depth h	5 mm	5 mm
Sample volume	~ 35 mm ³	~ 16 mm ³
Sample quantities	~30–50 mg	~15–30 mg

EDX measurements

Besides the expected elements, most measurements show small contents of oxygen, which might be caused by surface hydrolysis or water intercalation during washing treatment. At a single measuring point of $\text{MgP}_8\text{N}_{14}$, traces of Cl were observed. These may originate from starting materials or in situ formed by-products. Additionally, EDX measurements of Mg_2PN_3 reveal small amounts of Ca and Cl. The measured atomic ratio of 1:2 suggests the presence of in situ formed CaCl_2 , which is in accordance with powder X-ray diffraction. This cannot be prevented by washing the product due to the sensitivity of Mg_2PN_3 towards water treatment. Neglecting CaCl_2 for Mg_2PN_3 and oxygen contents the measured atomic ratios are in very good accordance with expected sum formulas (SF).

Table H3. EDX (SEM) measurements (at%) of the obtained reaction products with an acceleration voltage of 20 kV. Standard deviations are given in parentheses.

	EA1	EA2	P	N	O	X
	Ba	Sr	BaSr₂P₆N₁₂ starting from BaP₂N₄			
1	4	9	29	55	3	-
2	5	10	30	53	2	-
3	5	10	30	54	1	-
Average	5(1)	10(1)	30(1)	54(1)	2(1)	-
Norm. SF	Ba _{1.0(1)} Sr _{2.1(1)} P _{6.4(1)} N _{11.6(2)}					
	Ba	Sr	BaSr₂P₆N₁₂ starting from Ba₃P₅N₁₀Br			
1	4	10	28	56	2	-
2	6	9	31	53	1	-
3	5	10	31	54	-	-
Average	5(1)	10(1)	30(2)	54(2)	1(1)	-
Norm. SF	Ba _{1.0(2)} Sr _{1.9(1)} P _{6.0(4)} N _{10.9(3)}					
	Ca		CaH₄P₆N₁₂			
1	5	-	32	61	2	-
2	5	-	29	63	3	-
3	6	-	29	62	3	-
Average	5(1)	-	30(2)	62(1)	3(1)	-
Norm. SF	Ca _{1.0(1)} P _{5.6(3)} N _{11.6(2)}					
	Mg		MgP₈N₁₄			
1	5	-	36	56	2	1
2	5	-	34	61	-	-
3	4	-	37	57	2	-
Average	5(1)	-	36(2)	58(3)	1(1)	0(1)
Norm. SF	Mg _{1.0(1)} P _{7.6(3)} N _{12.4(6)}					
	Mg	Ca	Mg₂PN₃			
1	29	1	14	51	3	2
2	28	2	15	47	4	4
3	30	-	16	47	7	-
Average	29(1)	1(1)	15(1)	48(2)	5(2)	2(2)
Norm. SF	Mg _{1.9(1)} P _{1.0(1)} N _{3.2(2)}					

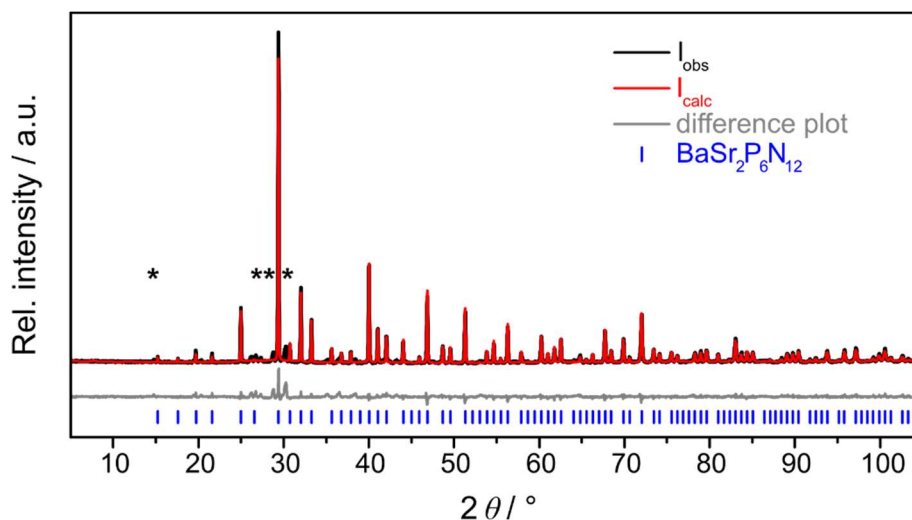
Rietveld refinements for framework-type $\text{BaSr}_2\text{P}_6\text{N}_{12}$ 

Figure H5. Rietveld refinement for $\text{BaSr}_2\text{P}_6\text{N}_{12}$ (Cu- $K_{\alpha 1}$) starting from BaP_2N_4 and SrCl_2 . The observed and calculated powder X-ray diffraction patterns are displayed in black and red. The gray curve represents the difference profile. Vertical bars in blue show the positions of the Bragg reflections of $\text{BaSr}_2\text{P}_6\text{N}_{12}$. Unidentified reflections are tagged with asterisks.

Table H4. Crystallographic data of the Rietveld refinement of $\text{BaSr}_2\text{P}_6\text{N}_{12}$.

Formula	$\text{BaSr}_2\text{P}_6\text{N}_{12}$
Crystal system; space group	cubic; $P\bar{a}3$ (no. 205)
Lattice parameters / \AA ^[a]	$a = 10.0639(2)$
Cell volume / \AA^3 ^[a]	1019.3(1)
Formula units per unit cell	4
Density / $\text{g}\cdot\text{cm}^{-3}$	4.343
Diffractometer	Stoe Stadi P
Radiation	Cu- $K_{\alpha 1}$ ($\lambda = 1.5406 \text{ \AA}$)
Detector	Mythen 1K
Monochromator	Ge(111)
2θ -range / $^\circ$	$5.0 \leq 2\theta \leq 105.5$
Step width / $^\circ$	0.015
Data points	6700
Total number of reflections	201
Refined parameters	38
Background function	Shifted Chebyshev
Number of background parameters	12
Goodness of fit (χ^2)	2.486
R_p ; R_{wp}	0.092; 0.134
R_{exp} ; R_{Bragg}	0.054; 0.051

[a] Estimated standard deviations are given in parentheses.

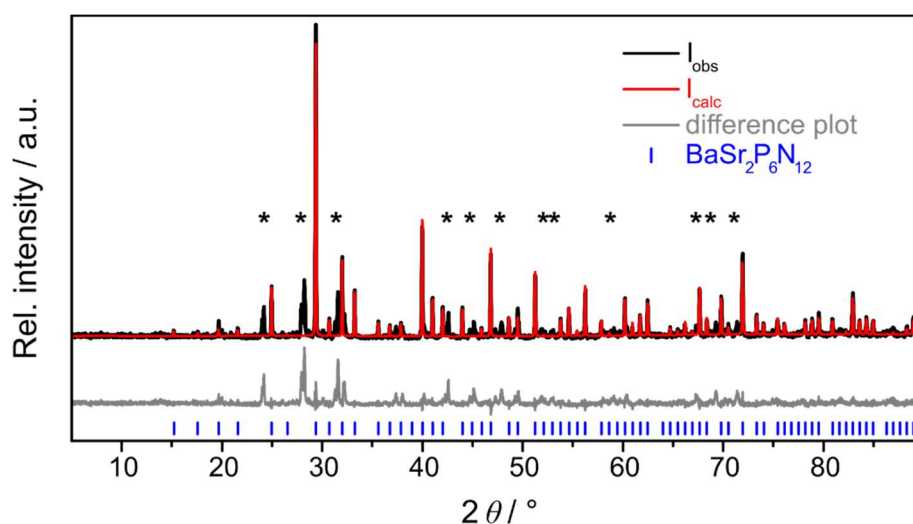


Figure H6. Rietveld refinement for $\text{BaSr}_2\text{P}_6\text{N}_{12}$ (Cu- $K_{\alpha 1}$) starting from $\text{Ba}_3\text{P}_5\text{N}_{10}\text{Br}$ and SrBr_2 . Black, red, and gray curves illustrate the observed and calculated powder X-ray diffraction patterns and the corresponding difference plot, respectively. Positions of the Bragg reflections of $\text{BaSr}_2\text{P}_6\text{N}_{12}$ are indicated by blue bars. Reflections of unknown side phases with small to medium intensity could not be assigned and are tagged with asterisks.

Table H5. Crystallographic data of the Rietveld refinement of $\text{BaSr}_2\text{P}_6\text{N}_{12}$.

Formula	$\text{BaSr}_2\text{P}_6\text{N}_{12}$
Crystal system; space group	cubic; $P\bar{a}3$ (no. 205)
Lattice parameters / \AA [a]	$a = 10.0730(9)$
Cell volume / \AA^3 [a]	1022.1(3)
Formula units per unit cell	4
Density / $\text{g}\cdot\text{cm}^{-3}$	4.331
Diffractometer	Stoe Stadi P
Radiation	Cu- $K_{\alpha 1}$ ($\lambda = 1.5406 \text{ \AA}$)
Detector	Mythen 1K
Monochromator	Ge(111)
2θ -range / $^\circ$	$5.0 \leq 2\theta \leq 92.4$
Step width / $^\circ$	0.015
Data points	5829
Total number of reflections	152
Refined parameters	36
Background function	Shifted Chebyshev
Number of background parameters	12
Goodness of fit (χ^2)	1.775
R_p ; R_{wp}	0.228; 0.310
R_{exp} ; R_{Bragg}	0.175; 0.060

[a] Estimated standard deviations are given in parentheses.

Rietveld refinements for layered structure type $\text{CaH}_4\text{P}_6\text{N}_{12}$ and $\text{MgP}_8\text{N}_{14}$

Impurities, which can be assigned to parts of the used assembly, are observed by powder X-ray diffraction. During Rietveld refinement phase quantities of 1 wt% and 78 wt% are observed for MgO (spacer) and *h*-BN (crucible), respectively. The amount of *h*-BN could not be reduced as it was almost inseparable from the sample.

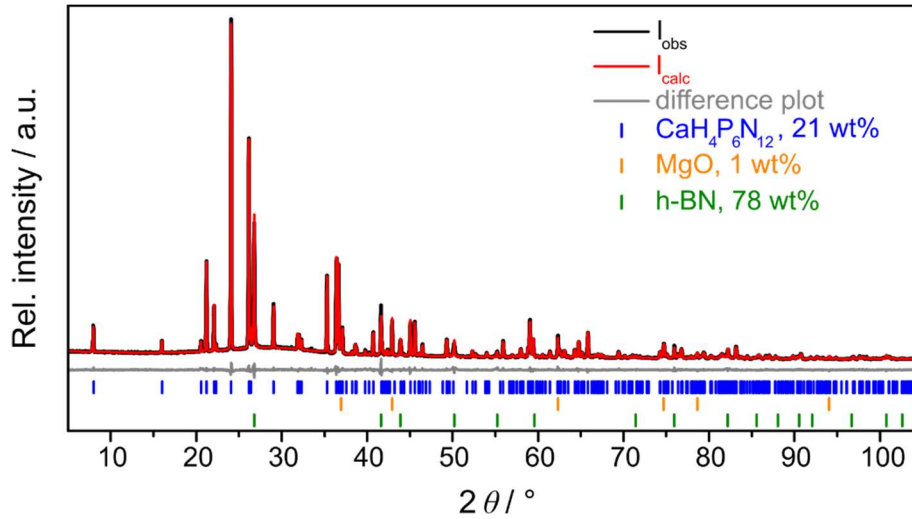


Figure H7. Rietveld refinement for $\text{CaH}_4\text{P}_6\text{N}_{12}$ (Cu- $K\alpha_1$). The black and red curves show the observed and calculated powder X-ray diffraction patterns, respectively. The difference profile is plotted in gray. Vertical bars indicate the positions of the Bragg reflections of the identified phases ($\text{CaH}_4\text{P}_6\text{N}_{12}$: blue; MgO: orange (residual parts of the assembly spacers); *h*-BN: green (crucible material)).

Table H6. Crystallographic data of the Rietveld refinement of $\text{CaH}_4\text{P}_6\text{N}_{12}$.

Formula	$\text{CaH}_4\text{P}_6\text{N}_{12}$
Crystal system; space group	orthorhombic; <i>Cmcm</i> (no. 63)
	$a = 8.6317(1)$
Lattice parameters / Å ^[a]	$b = 4.9003(1)$
	$c = 22.1442(2)$
Cell volume / Å ³ ^[a]	936.6(1)
Formula units per unit cell	4
Density / g·cm ⁻³	2.823
Diffractometer	Stoe Stadi P
Radiation	Cu- $K_{\alpha 1}$ ($\lambda = 1.5406$ Å)
Detector	Mythen 1K
Monochromator	Ge(111)
2θ -range / °	$5.0 \leq 2\theta \leq 105.5$
Step width / °	0.015
Data points	6700
Total number of reflections	298
Refined parameters	83
Background function	Shifted Chebyshev
Number of background parameters	24
Goodness of fit (χ^2)	1.672
R_p ; R_{wp}	0.030; 0.042
R_{exp} ; R_{Bragg}	0.025; 0.013

[a] Estimated standard deviations are given in parentheses.

Structure refinement of $\text{MgP}_8\text{N}_{14}$ Discussion of the structure refinement of $\text{MgP}_8\text{N}_{14}$:

Initially, the observed powder X-ray diffraction data of $\text{MgP}_8\text{N}_{14}$ were refined in space group $Cmcm$ using the structure model of $\text{CaP}_8\text{N}_{14}$ as starting point. Although the refinement showed reasonable R values and a good fitting of measured and calculated data after substituting Ca by Mg, the intensity of the [002] Bragg reflection deviated significantly (Figure H8, Table H7). For this reason a distortion of the PN_4 tetralayers was taken into account ending up in a *translationsgleiche* symmetry reduction (t_2) and space group $Cmc2_1$. The corresponding Rietveld refinement shows a significant better refinement of the [002] Bragg reflection, suggesting the lower symmetry as correct (Figure H9). Detailed information on the Rietveld refinements are given in Table H7. CSD-2022941 contains supplementary crystallographic data for $\text{MgP}_8\text{N}_{14}$ and can be obtained free of charge by the Cambridge Crystallographic Data Center through the CCDC/FIZ Karlsruhe joint deposition service.^[15] P_{black} (50 wt%) and h-BN (crucible, 3 wt%) impurities were detected during Rietveld refinements.

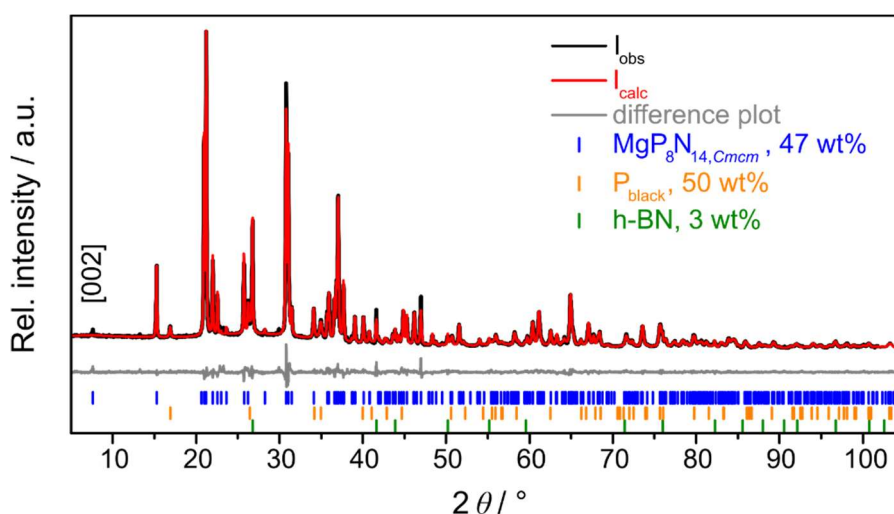


Figure H8. Rietveld refinement for $\text{MgP}_8\text{N}_{14}$ in space group $Cmcm$ ($\text{Cu-K}\alpha_1$). The observed (black) and the calculated (red) powder X-ray diffraction patterns are displayed with corresponding difference profile (gray). The positions of the Bragg reflections of $\text{MgP}_8\text{N}_{14}$ (blue), P_{black} (orange, decomposition product), and h-BN (green; crucible material) are indicated by vertical bars.

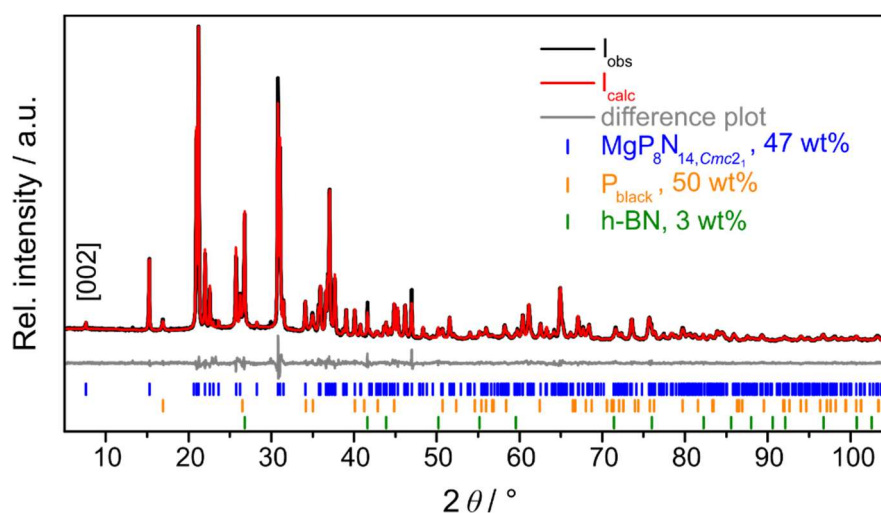


Figure H9. Rietveld refinement for $\text{MgP}_8\text{N}_{14}$ in space group $Cmc2_1$ (Cu- $K_{\alpha 1}$). Observed (black) and calculated (red) powder X-ray diffraction patterns are illustrated with corresponding difference profile (gray). Bragg reflections of $\text{MgP}_8\text{N}_{14}$ (blue), P_{black} (orange, decomposition product), and $h\text{-BN}$ (green; crucible material) are indicated by vertical bars.

Table H7. Crystallographic data of the Rietveld refinements of $\text{MgP}_8\text{N}_{14}$ in space groups $Cmcm$ and $Cmc2_1$.

Formula	$\text{MgP}_8\text{N}_{14}$, $Cmcm$	$\text{MgP}_8\text{N}_{14}$, $Cmc2_1$
Crystal system; space group	orthorhombic; $Cmcm$ (no. 63)	orthorhombic; $Cmc2_1$ (no. 36)
Lattice parameters / Å [a]	$a = 8.3647(2)$ $b = 5.0215(1)$ $c = 23.1966(5)$	$a = 8.3646(1)$ $b = 5.0215(1)$ $c = 23.1963(3)$
Cell volume / Å ³ [a]	974.3(1)	974.3(1)
Formula units per unit cell		4
Density / g·cm ⁻³	3.192	3.192
Diffractometer		Stoe Stadi P
Radiation		Cu- $K_{\alpha 1}$ ($\lambda = 1.5406$ Å)
Detector		Mythen 1K
Monochromator		Ge(111)
2θ -range / °		$5.0 \leq 2\theta \leq 108$
Step width / °		0.015
Data points		6873
Total number of reflections		331
Refined parameters		83
Background function		Shifted Chebyshev
Number of background parameters	24	24
Goodness of fit (χ^2)	1.981	1.936
R_p ; R_{wp}	0.036; 0.049	0.035; 0.048
R_{exp} ; R_{Bragg}	0.025; 0.016	0.025; 0.015

[a] Estimated standard deviations are given in parentheses.

Illustration of the observed recrystallization effect during ion exchange reactions

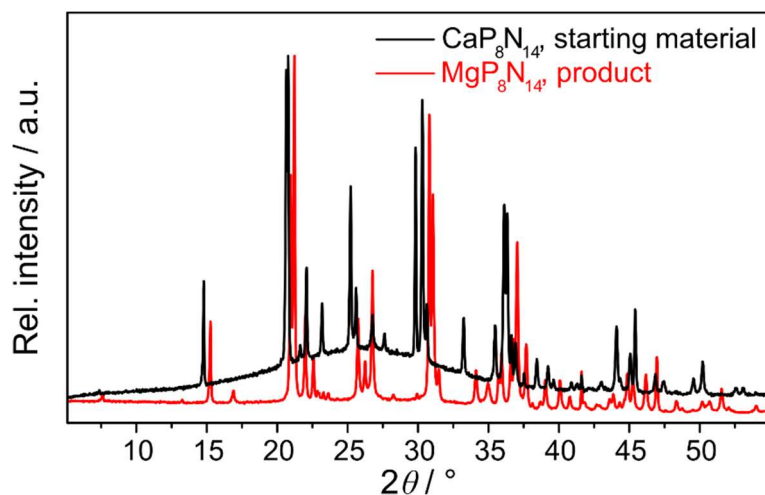


Figure H10. Comparison of the powder X-ray diffraction data of the starting material $\text{CaP}_8\text{N}_{14}$ (black) and the product $\text{MgP}_8\text{N}_{14}$ (red). The initially observed amorphous parts are no longer present after reaction.

Rietveld refinements for chain-like Mg_2PN_3

Powder X-ray diffraction data reveal the presence of MgO (6.5 wt%) and CaCl_2 (68.9 wt%). MgO is supposed to be an oxidation product, which might be caused by short contact time after reaction during the transport, as Mg_2PN_3 shows to be very sensitive towards air and moisture. CaCl_2 is the expected by-product, which is formed in situ during the reaction of Ca_2PN_3 with MgCl_2 .

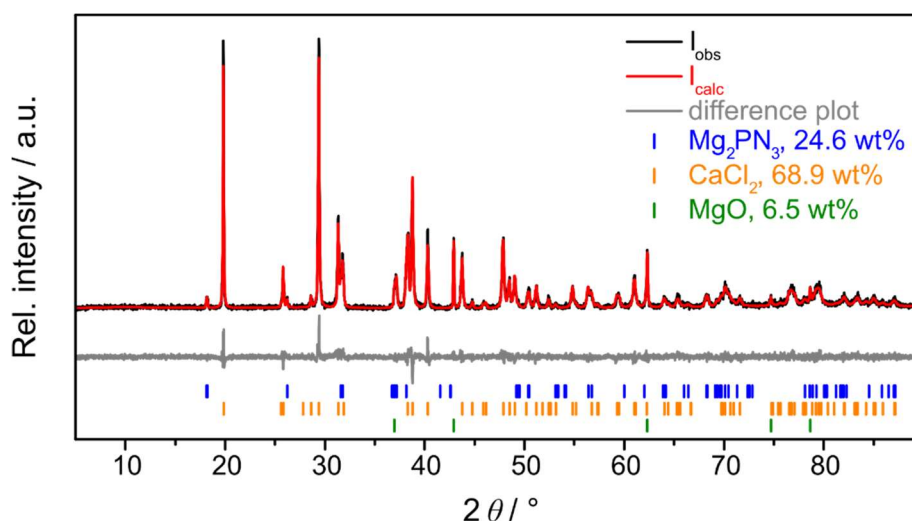


Figure H11. Rietveld refinement for Mg_2PN_3 (Cu- $K_{\alpha 1}$). The black and red curves show the observed and calculated powder X-ray diffraction patterns, respectively. The difference profile is plotted in gray. Vertical bars indicate the positions of Bragg reflections of the identified phases (Mg_2PN_3 : blue; CaCl_2 : orange; MgO : green).

Table H8. Crystallographic data of the Rietveld refinement of Mg₂PN₃.

Formula	Mg₂PN₃
Crystal system; space group	orthorhombic; <i>Cmc</i> 2 ₁ (no. 36)
	$a = 9.7277(9)$
Lattice parameters / Å ^[a]	$b = 5.6579(6)$
	$c = 4.7127(4)$
Cell volume / Å ³ ^[a]	259.4(1)
Formula units per unit cell	4
Density / g·cm ⁻³	3.114
Diffractometer	Stoe Stadi P
Radiation	Cu-K _{α1} ($\lambda = 1.5406$ Å)
Detector	Mythen 1K
Monochromator	Ge(111)
2 θ -range / °	$5.0 \leq 2\theta \leq 93.1$
Step width / °	0.015
Data points	5876
Total number of reflections	75
Refined parameters	59
Background function	Shifted Chebyshev
Number of background parameters	12
Goodness of fit (χ^2)	0.923
R_p ; R_{wp}	0.109; 0.141
R_{exp} ; R_{Bragg}	0.152; 0.035

[a] Estimated standard deviations are given in parentheses.

H.3 Author Contributions

S.W.: Conceptualization: Equal; Formal analysis: Lead; Investigation : Lead; Validation: Equal; Visualization: Lead; Writing - Original Draft: Lead; Writing - Review & Editing: Equal

L.S.: Formal analysis: Supporting; Investigation: Supporting; Writing - Review & Editing: Supporting

P.S.: Formal analysis: Supporting; Investigation: Supporting ; Writing - Review & Editing: Supporting

W.S.: Conceptualization: Equal; Funding acquisition: Lead; Methodology: Equal ; Project Administration: Lead; Resources: Lead; Supervision: Lead; Validation: Equal; Writing - Original Draft: Supporting; Writing - Review & Editing: Equal.

H.4 References

- [1] A. A. Coelho, *TOPAS Academic*, Version 6, Coelho Software, Brisbane, Australia, **2016**.
- [2] H. Rietveld, *J. Appl. Crystallogr.* **1969**, *2*, 65-71.
- [3] R. W. Cheary, A. Coelho, *J. Appl. Crystallogr.* **1992**, *25*, 109-121.
- [4] R. W. Cheary, A. A. Coelho, J. P. Cline, *J. Res. Natl. Inst. Stand. Technol.* **2004**, *109*, 1-25.
- [5] K. Momma, F. Izumi, *J. Appl. Crystallogr.* **2011**, *44*, 1272-1276.
- [6] F. W. Karau, W. Schnick, *J. Solid State Chem.* **2005**, *178*, 135-141.
- [7] A. Marchuk, S. Wendl, N. Imamovic, F. Tambornino, D. Wiechert, P. J. Schmidt, W. Schnick, *Chem. Mater.* **2015**, *27*, 6432-6441.
- [8] S. Wendl, W. Schnick, *Chem. Eur. J.* **2018**, *24*, 15889-15896.
- [9] S. Wendl, S. Mardazad, P. Strobel, P. J. Schmidt, W. Schnick; *Angew. Chem. Int. Ed.* **2020**, *59*, 18240-18243; *Angew. Chem.* **2020**, *132*, 18397-18400.
- [10] H. Huppertz, *Z. Kristallogr.* **2004**, *219*, 330-338.
- [11] D. Walker, *Am. Mineral.* **1991**, *76*, 1092-1100.
- [12] D. Walker, M. A. Carpenter, C. M. Hitch, *Am. Mineral.* **1990**, *75*, 1020-1028.
- [13] W. Schnick, J. Lücke, *Angew. Chem. Int. Ed. Engl.* **1992**, *31*, 213-215; *Angew. Chem.* **1992**, *104*, 208-209.
- [14] A. Marchuk, F. J. Pucher, F. W. Karau, W. Schnick, *Angew. Chem. Int. Ed.* **2014**, *53*, 2469-2472; *Angew. Chem.* **2014**, *126*, 2501-2504.
- [15] Crystal data of $\text{MgP}_8\text{N}_{14}$ from powder X-ray diffraction and Rietveld refinement:
 $M = 468.19 \text{ gmol}^{-1}$, orthorhombic, $Cmc2_1$ (no. 36), $a = 8.3646(1)$, $b = 5.0215(1)$ and $c = 23.1963(3) \text{ \AA}$, $V = 974.3(1) \text{ \AA}^3$, $Z = 4$, $\rho = 3.192 \text{ gcm}^{-3}$, $\mu = 14.376 \text{ mm}^{-1}$, Cu- $K_{\alpha 1}$ ($\lambda = 1.5406 \text{ \AA}$, Stoe StadiP), $T = 293 \text{ K}$, 993 observed reflections, 109 parameters, $R_p = 0.035$, $R_{wp} = 0.048$, $R_{exp} = 0.025$, $R_{Bragg} = 0.015$, $GoF = 1.936$. Deposition number 2022941 contains the supplementary crystallographic data for this paper. These data are provided free of charge by the joint Cambridge Crystallographic Data Centre and Fachinformationszentrum Karlsruhe Access Structures service www.ccdc.cam.ac.uk/structures.

I Miscellaneous

I.1 List of Publications

The following list contains all publications of this thesis in chronological order, including authors, citation, and author contributions.

1. BaP₆N₁₀NH:Eu²⁺ as a Case Study – An Imidoniridophosphate Showing Luminescence

Sebastian Wendl, Lucien Eisenburger, Mirjam Zipkat, Daniel Günther, Jonathan P. Wright, Peter J. Schmidt, Oliver Oeckler, and Wolfgang Schnick

Chem. Eur. J. **2020**, 26, 5010–5016.

DOI: 10.1002/chem.201905082

Synthesis and formal analyses were performed by Sebastian Wendl and Mirjam Zipkat over the course of her Bachelor thesis that was supervised by Sebastian Wendl and Wolfgang Schnick. Preparation and postprocessing of the microfocused X-ray analysis were done by Lucien Eisenburger, supported by Daniel Günther. Jonathan P. Wright supported experiments at ESRF beamline ID 11. Oliver Oeckler supervised the microfocused X-ray analysis. The investigation of luminescence properties was supervised by Peter J. Schmidt. Wolfgang Schnick supervised the project. Sebastian Wendl wrote the manuscript and all authors contributed to the discussion of the results and revised the manuscript.

2. Crystalline Nitridophosphates by Ammonothermal Synthesis

Mathias Mallmann, **Sebastian Wendl**, and Wolfgang Schnick

Chem. Eur. J. **2020**, 26, 2067–2072.

DOI: 10.1002/chem.201905227

Syntheses, formal analyses, as well as the preparation of the manuscript were performed by Mathias Mallmann and supported by Sebastian Wendl. Wolfgang Schnick supervised the project. All authors contributed to the discussion of the results and revised the manuscript.

3. Ammonothermal Synthesis of $\text{Ba}_2\text{PO}_3\text{N}$ – An Oxonitridophosphate with Non-Condensed PO_3N Tetrahedra

Sebastian Wendl, *Mathias Mallmann*, *Philipp Strobel*, *Peter J. Schmidt*, and *Wolfgang Schnick*

Eur. J. Inorg. Chem. **2020**, 2020, 841–846.

DOI: 10.1002/ejic.202000041

Syntheses and formal analyses were performed equally by Sebastian Wendl and Mathias Mallmann. Philipp Strobel carried out the measurements of luminescence properties. Philipp Strobel and Peter J. Schmidt helped with the interpretation of luminescence data. The manuscript was prepared by Sebastian Wendl and Mathias Mallmann. Wolfgang Schnick supervised the project. All authors contributed to the discussion of the results and revised the manuscript.

4. $\text{Sr}_3\text{P}_3\text{N}_7$: Complementary Approach of Ammonothermal and High-Pressure Methods

Mathias Mallmann, **Sebastian Wendl**, *Philipp Strobel*, *Peter J. Schmidt*, and *Wolfgang Schnick*

Chem. Eur. J. **2020**, 26, 6257–6263.

DOI: 10.1002/chem.202000297.

Mathias Mallmann and Sebastian Wendl contributed equally to this manuscript and carried out syntheses and formal analyses. Philipp Strobel measured luminescence properties. Philipp Strobel and Peter J. Schmidt helped with the interpretation of luminescence data. Mathias Mallmann and Sebastian Wendl wrote the manuscript. Wolfgang Schnick supervised the project. All authors contributed to the discussion of the results and revised the manuscript.

5. Nitridophosphate-Based Ultra-Narrow-Band Blue-Emitters: Luminescence Properties of AEP_8N_{14} ($AE = Ca, Sr, Ba$)

Sebastian Wendl, Lucien Eisenburger, Philipp Strobel, Daniel Günther, Jonathan P. Wright, Peter J. Schmidt, Oliver Oeckler, and Wolfgang Schnick

Chem. Eur. J. **2020**, *26*, 7292–7298.

DOI: 10.1002/chem.202001129

Synthesis and formal analyses were performed by Sebastian Wendl. Preparation and postprocessing of the microfocused X-ray analysis were done by Lucien Eisenburger, supported by Daniel Günther. Jonathan P. Wright supported experiments at ESRF beamline ID 11. Oliver Oeckler supervised the microfocused X-ray analysis. Measurements of luminescence properties were carried out by Philipp Strobel. The interpretation of luminescence data was supported by Philipp Strobel and Peter J. Schmidt. Wolfgang Schnick supervised the project. Sebastian Wendl wrote the manuscript and all authors contributed to the discussion of the results and revised the manuscript.

6. HIP to be Square: Simplifying Nitridophosphate Synthesis in a Hot Isostatic Press

Sebastian Wendl, Sara Mardazad, Philipp Strobel, Peter J. Schmidt, and Wolfgang Schnick

Angew. Chem. Int. Ed. **2020**, *59*, 18240–18243;

Angew. Chem. **2020**, *132*, 18397–18400.

DOI: 10.1002/anie.202008570; 10.1002/ange.202008570.

Syntheses and formal analyses were performed by Sebastian Wendl and Sara Mardazad over the course of her Bachelor thesis that was supervised by Sebastian Wendl and Wolfgang Schnick. Structural analysis and data evaluation was performed by Sebastian Wendl. Philipp Strobel carried out measurements of the luminescence properties. The investigation of luminescence properties was supervised by Peter J. Schmidt. Sebastian Wendl wrote the manuscript and Wolfgang Schnick supervised the project. All authors contributed to the discussion of the results and revised the manuscript.

7. Post-Synthetic Modification: Systematic Study on a Simple Access to Nitridophosphates

Sebastian Wendl, Lisa Seidl, Patrick Schüler, and Wolfgang Schnick

Angew. Chem. Int. Ed. **2020**, *59*, 23579–23582;

Angew. Chem. **2020**, *132*, 23785–23788.

DOI: 10.1002/anie.202011835; 10.1002/ange.202011835.

Syntheses and formal analyses were performed by Sebastian Wendl, Lisa Seidl, and Patrick Schüler. Lisa Seidl and Patrick Schüler took part over the course of their Bachelor theses that were supervised by Sebastian Wendl and Wolfgang Schnick. Data evaluation, structural analysis as well as the preparation of the manuscript were performed by Sebastian Wendl. Wolfgang Schnick supervised the project and all authors contributed to the discussion of the results and revised the manuscript.

8. Synthesis of Nitride Zeolites in a Hot Isostatic Press

Sebastian Wendl, Mirjam Zipkat, Philipp Strobel, Peter J. Schmidt, and Wolfgang Schnick

Angew. Chem. Int. Ed. **2021**, *60*, 4470–4473;

Angew. Chem. **2021**, *133*, 4520–4523.

DOI: 10.1002/anie.202012722; 10.1002/ange.202012722.

Synthesis and formal analyses were performed by Sebastian Wendl and Mirjam Zipkat over the course of her Bachelor thesis that was supervised by Sebastian Wendl and Wolfgang Schnick. Philipp Strobel carried out measurements of the luminescence properties. The interpretation of luminescence data was supported by Philipp Strobel and Peter J. Schmidt. The investigation of luminescence properties was supervised by Peter J. Schmidt. Wolfgang Schnick supervised the project. Sebastian Wendl wrote the manuscript and all authors contributed to the discussion of the results and revised the manuscript.

I.2 List of Publications beyond this Thesis

The following list contains the publications beyond this thesis in chronological order.

1. Nontypical Luminescence Properties and Structural Relation of $\text{Ba}_3\text{P}_5\text{N}_{10}\text{X}:\text{Eu}^{2+}$ ($\text{X} = \text{Cl}, \text{I}$): Nitridophosphate Halides with Zeolite-like Structure

Alexey Marchuk, **Sebastian Wendl**, Nedzada Imamovic, Frank Tambornino, Detlef Wiechert, Peter J. Schmidt, and Wolfgang Schnick

Chem. Mater. **2015**, 27, 6432–6441.

DOI: 10.1021/acs.chemmater.5b02668

2. $\text{SrH}_4\text{P}_6\text{N}_{12}$ and $\text{SrP}_8\text{N}_{14}$: Insights into the Condensation Mechanism of Nitridophosphates under High Pressure

Sebastian Wendl, and Wolfgang Schnick

Chem. Eur. J. **2018**, 24, 15889–15896.

DOI: 10.1002/chem.201803125

3. Boron Phosphorus Nitride at Extremes: PN_6 Octahedra in the High-Pressure Polymorph $\beta\text{-BP}_3\text{N}_6$

Sebastian Vogel, Maxim Bykov, Elena Bykova, **Sebastian Wendl**, Simon D. Klob, Anna Pakhomova, Stella Chariton, Egor Koemets, Natalia Dubrovinskaia, Leonid Dubrovinsky, and Wolfgang Schnick

Angew. Chem. Int. Ed. **2019**, 58, 9060–9063;

Angew. Chem. **2019**, 131, 9158–9161.

DOI: 10.1002/anie.201902845

4. Nitride Spinel: An Ultracompressible High-Pressure Form of BeP_2N_4

*Sebastian Vogel, Maxim Bykov, Elena Bykova, **Sebastian Wendl**, Simon D. Kloß, Anna Pakhomova, Natalia Dubrovinskaia, Leonid Dubrovinsky, and Wolfgang Schnick*

Angew. Chem. Int. Ed. **2020**, 59, 2730–2734;

Angew. Chem. **2020**, 132, 2752–2756.

DOI: 10.1002/anie.201910998

1.3 Fundings

Research projects presented in this thesis and related work were funded by the Deutsche Forschungsgemeinschaft (DFG; SCHN 377/18-1; Projekt Nitridische Phosphat-Netzwerke), the European Synchrotron Radiation Facility (ESRF; project CH-5149) and the Ludwig-Maximilians-Universität München (LMU). Travel awards by the Gesellschaft Deutscher Chemiker e.V. are gratefully appreciated.

I.4 Conference Contributions and Presentations

Breaking The Rules – Nitridophosphate neu beleuchtet

Sebastian Wendl, and Wolfgang Schnick

Talk, Seminar Schnick Group, 2020, Munich, Germany

Crystal structure determination of microcrystalline compounds by the combination of TEM and microfocused synchrotron radiation

Daniel Günther, Jonathan P. Wright, Gavin Vaughan, **Sebastian Wendl**, Lucien Eisenburger, Wolfgang Schnick, and Oliver Oeckler

Poster, Microscopy Conference, 2019, Berlin, Germany

Die kleine große Welt der EA/P/N-Verbindungen

Sebastian Wendl, and Wolfgang Schnick

Talk, Seminar Schnick Group, 2019, Munich, Germany

Von treulosen Netzwerken und kleinen Unfällen – Arbeiten unter Hochdruck

Sebastian Wendl, and Wolfgang Schnick

Talk, Seminar Schnick Group, 2018, Munich, Germany

Neuartige (Imido-)Nitridophosphat-Schichtverbindungen

Sebastian Wendl, and Wolfgang Schnick

Talk, 43. Hirschegg-Seminar Festkörperchemie, 2017, Hirschegg, Austria

Neuartige (Imido-)Nitridophosphat-Schichtverbindungen

Sebastian Wendl, and *Wolfgang Schnick*

Talk, Seminar Schnick Group, **2017**, Munich, Germany

1.5 Deposited Crystallographic Data

The CIFs (Crystallographic Information Files) of the compounds discussed in this thesis are deposited at the Fachinformationszentrum (FIZ) Karlsruhe, Germany and/or Cambridge Crystallographic Data Centre (CDCC), Cambridge, United Kingdom. All data can be obtained free of charge upon quoting the corresponding depository number.

Table I.1. List of the compounds that are introduced within this thesis with respective depository numbers.

Compound	CSD
BaP ₆ N ₁₀ NH	1942108
CaP ₈ N ₁₄	1979592
BaP ₈ N ₁₄	1980141
Ba ₂ PO ₃ N	1975933
Sr ₃ P ₃ N ₇	1975990
Sr ₃ P ₅ N ₁₀ Cl	2011982
Sr ₃ P ₅ N ₁₀ Br	2012398
MgP ₈ N ₁₄	2022941

I.6 Curriculum Vitae

Sebastian Wendl

08. September 1990

Bad Kötzting, Germany

Education:

- 03/2022 **PhD thesis:** “Paving Nitridophosphate-Based Phosphors’ Way to Industrial Application”, Ludwig-Maximilians-Universität München, Germany (Prof. Dr. W. Schnick)
- Since 12/2016 PhD studies and research assistant, Ludwig-Maximilians-Universität München, Germany (Prof. Dr. W. Schnick)
- 11/2016 **Master thesis:** “Hochdruck-Hochtemperatur-Synthese und Charakterisierung der neuartigen Nitridophosphat-Schichtverbindungen $\text{SrH}_4\text{P}_6\text{N}_{12}$ und MP_8N_{14} ($M = \text{Mg, Ca, Sr}$)”, Ludwig-Maximilians-Universität München, Germany (Prof. Dr. W. Schnick)
- 04/2015-11/2016 Master of Science, Chemistry, Ludwig-Maximilians-Universität München, Germany
- 08/2014 **Bachelor thesis:** “Synthese und Charakterisierung von lumineszierenden Nitridophosphat-Zeolithen $\text{Ba}_3\text{P}_5\text{N}_{10}\text{X}$ ($X = \text{Cl, Br, I}$)“, Ludwig-Maximilians-Universität München, Germany (Prof. Dr. W. Schnick)
- 09/2011-03/2015 Bachelor of Science, Chemistry and Biochemistry, Ludwig-Maximilians-Universität München, Germany
- 07/2010-06/2011 Community Service, Fachklinik Furth im Wald, Furth im Wald, Germany
- 06/2010 Allgemeine Hochschulreife, Benedikt-Stattler-Gymnasium, Bad Kötzting, Germany